THE EFFECT OF THE INLET BOUNDARY LAYER ON THE SECONDARY FLOW IN AN ANNULAR CASCADE

By

S. A. ELSHAMMAA B.Sc. (Eng.), M.Eng.

A Thesis

Submitted to the School of Graduate Studies

in Partial Fulfilment of the Requirements

for the Degree

Doctor of Philosophy

McMaster University

October 1978

THE EFFECT OF THE INLET BOUNDARY LAYER ON THE SECONDARY FLOW IN AN ANNULAR CASCADE

DOCTOR OF PHILOSOPHY (1978)
(Mechanical Engineering)

McMASTER UNIVERSITY
Hamilton, Ontario

TITLE: The Effect of the Inlet Boundary Layer on the Secondary Flow in an Annular Cascade

AUTHOR: S. A. El Shammaa, B.Sc. (Cairo University)
M.Eng. (McMaster University)

SUPERVISOR: Dr. J. H. T. Wade

NUMBER OF PAGES: xvix, 245

ABSTRACT

The development of small gas turbine units with high specific output calls for the design and testing of rotor cascades with high turning blades. A major portion of the losses that occur in such cascades are associated with the secondary flow. The need for experimental data of highly loaded annular cascades can be readily seen from a review of the available literature.

The objective of this study was to construct and test an annular test rig of special configuration particularly suited for high turning blades. The rig was an open circuit wind tunnel with inlet and exit ducts of hyperboloidal shape. The test facility provided a means for adjusting the inlet flow in the circumferential direction (to ensure periodicity) as well as controlling the inlet endwall boundary layers. The cascade tests were conducted at a Reynolds number of 4.73×10^5 based on the blade chord. Extensive flow measurements were taken at the inlet and the exit from the cascade both in the main stream and the endwall boundary layers. The passage walls static pressure distribution was also measured. Maps of the exit flow parameters were presented for the total pressure loss coefficient, static pressure coefficient and the secondary flow velocity vectors. The averaged flow parameters were analysed and the losses were compared with several predictive correlations.

The measured losses were found comparatively lower than the predicted.

A flow visualization study was carried out using smoke in the air stream and oil film (lamp-black and kerosene) on the passage walls. The results thus obtained were consistent with the general flow picture depicted from the analysis of the measured data.

ACKNOWLEDGEMENTS

The author wishes to express his sincere gratitude and appreciation to his supervisor Dr. J. H. T. Wade for his guidance and encouragement throughout the course of this study and other endeavours.

The author wishes to acknowledge the cooperation of Mr. S. H. Moustapha in the construction of the cascade rig.

Thanks are also due to the staff of the McMaster University Engineering Workshop and the Instrument Machine Shop for their cooperation in the construction of the apparatus and its instrumentation.

The willing cooperation and competent assistance of Mr. E. Peters and Mr. G. Paron are gratefully acknowledged.

The author wishes to express his appreciation to Ms. B. A. Bedell for her rapid and accurate typing of the manuscript.

The financial support provided by the National Sciences and Engineering Research Council through operating grant A1585 is acknowledged.

The two Ontario Graduate Scholarship grants offered by the Ontario Ministry of Colleges and Universities are also gratefully acknowledged.

TABLE OF CONTENTS

LIST OF FIGURES

LIST OF TABLES

NOMENCLATURE

Symbols	Description
a	Speed of sound
C	Blade chord
C_L	Lift coefficient (Eqn. (9.18))
C_{ps}	Static pressure loss coefficient (Eqn. (9.2))
C_{po}	Total pressure loss coefficient (Eqn. (9.1))
E	Voltage
H	Blade span
H_{12}	Shape factor
M	Mach number
$\mathbf{M}$	Molecular weight
N	Blade passage area ratio (Eqn. (3.11))
P	Static pressure
P_o	Stagnation pressure
r	Radial coordinate
R	Reference radial direction
R_N	Reynolds number
s	Streamline direction
S	Blade pitch
V	Absolute flow velocity
V_a	Axial flow velocity
Y_T	Overall loss coefficient (Eqn. (9.11))
Y_p	Blade profile loss coefficient

Sybmols	Description
Y_s	Blade secondary loss coefficient (Eqn. (9.15))
Y'_s	Net secondary loss coefficient (Eqn. (9.16))
Y_I	Inlet boundary layer losses
s,n,z	Streamwise perpendicular coordinates (Fig. 3.2)
u,v,w	Secondary velocities in x, y and z directions
Z	Blade loading parameter (Eqn. (9.17))
z	Spanwise distance measured from the inner wall
α	Flow yaw angle measured from the axial direction
β	Blade angle with respect to the axial direction
Γ	Circulation.
Γ_{tf}	Trailing filament circulation (Eqn. (3.15))
Γ_{ts}	Trailing shed circulation (Eqn. (3.16))
γ	Flow pitch angle
Δ	Increment
δ	Boundary layer thickness at which the absolute velocity is equal to 99% of the free stream velocity
δ^*	Boundary layer displacement thickness
δ_p	Pressure parameter for boundary layer control (Eqn. (7.1))
η	Vorticity normal to the streamline
θ	Tangental direction
μ	Fluid viscosity
ξ	Streamwise vorticity

Symbols	Description
π	Constant = 3.14159
ρ	Fluid density
Σ	Summation
ϕ	Angle between the normal to the Bernoulli surface and the principal normal to the streamlines (Fig. 3.1)
ψ	Secondary flow stream function
$\bar{\omega}$	Vorticity vector
L.E.	Leading edge
T.E.	Trailing edge
B.H.P.	Brake horsepower
c.f.m.	Cubic feet per minute
m/s	meters per second
p.s.i.	Pounds per square inch
r.p.m.	Revolutions per minute
r.m.s.	Root mean square

Subscripts	
0	Stagnation
1	Passage inlet
2	Passage exit
a	Axial
av	Average
i	Inner
o	Outer
m	Arithmetic mean
s	Static
T	Total

CHAPTER 1

INTRODUCTION

The prediction of the three-dimensional characters of the flow in airfoil cascades to date is a challenging problem to the designer of turbomachines. An efficient design of a turbomachine requires a realistic prediction of the losses and exit flow angles from a blade row. Studies conducted in this field were aimed at finding the deviations of the real flow from the ideal (potential) flow field. These deviations are manifested as distortions in the velocity field and as a total pressure drop which is a measure of the losses within the cascade. Apart from the skin friction losses on the blade surface (profile losses) the remainder of the total pressure losses are generally termed "Secondary Losses". Unlike what the name may imply the secondary losses, particularly in high turning cascades, constitute a major portion of the losses in turbomachines. The distortion in the velocity field results in changes of the exit flow angles from the blade row which, in turn, results in incidence variation in a following blade row.

The recent trend of developing small gas turbine units with high specific output and accordingly large stage

loading focused more attention on the design and testing of turbine cascades with high turning angles. The understanding of the complex flow situation in turbomachines required, in the past, testing of simplified models whereby several meaningful observations have been made and considerable amount of data have been accumulated. However there is a limited amount of data available for annular cascades with high turning angles. The lack of such data projects some doubt on the accuracy of many of the available prediction correlations for the losses in such turbine cascades.

The characteristics of the inlet flow boundary layer is thought to be an important parameter which influences the secondary losses in airfoil cascades. In the present study the effect of this parameter is investigated.

A unique annular cascade rig was constructed and tested for different inlet boundary layer displacement thicknesses on both the inner and outer endwalls at the inlet of the cascade. The test facility is an open circuit wind tunnel with an inlet and an outlet ducts of hyperboloidal configuration. The cascade consists of three flow passages formed by four blades of identical shape. The blades - of flat back type - have an axial chord of 188.5 mm, a span of 190.5 mm and a turning angle of $128^{o}30'$. The annular walls of the cascade are made of clear acrylic plastic to facilitate flow visualization studies. The inner radius of the annular cascade is 381 mm, the outer radius is 571.5 mm.

The inlet and outlet sections were designed to provide straight streamlines with an inlet angle of 64° and an exit angle of $64^{\circ}30'$.

Details of the apparatus description are given in Chapter 4. The instrumentation and geometric considerations pertaining to the particular shape of the inlet and exit ducts are given in Chapter 5. The establishment of the inlet flow conditions with various boundary layer displacement thicknesses is presented in Chapter 7. In Chapter 8 the static pressure distribution on the passage surfaces is studied. The corresponding exit flow characteristics and losses contour maps are given in Chapter 9.

CHAPTER 2

DESCRIPTION OF SECONDARY FLOW

The secondary flow in axial flow turbomachines is generally defined as the difference between the actual and the idealized axisymmetric flow. It arises mainly from the cross channel pressure gradients, radial pressure gradients, centrifugal force effects, tip clearance, and the relative motion between the blade tip and the annular walls. Secondary flows result in the displacement and accumulation of low energy boundary layer flow. The influences of such flows are usually indistinguishable and the losses associated with such a complex flow situation are, in many cases, difficult to isolate. An overall picture of the secondary flow phenomena has resulted from several qualitative investigations utilizing flow visualization techniques.

The vortices commonly found in a rotating blade row rotating blade row (see Figure 2.1) can be classified as follows:

1. The Passage Vortex

In annular cascades both circumferential and radial pressure gradients exist. The deflection of the streamlines within the passage gives rise to cross-channel (circumferential) pressure gradient. In the main flow this pressure

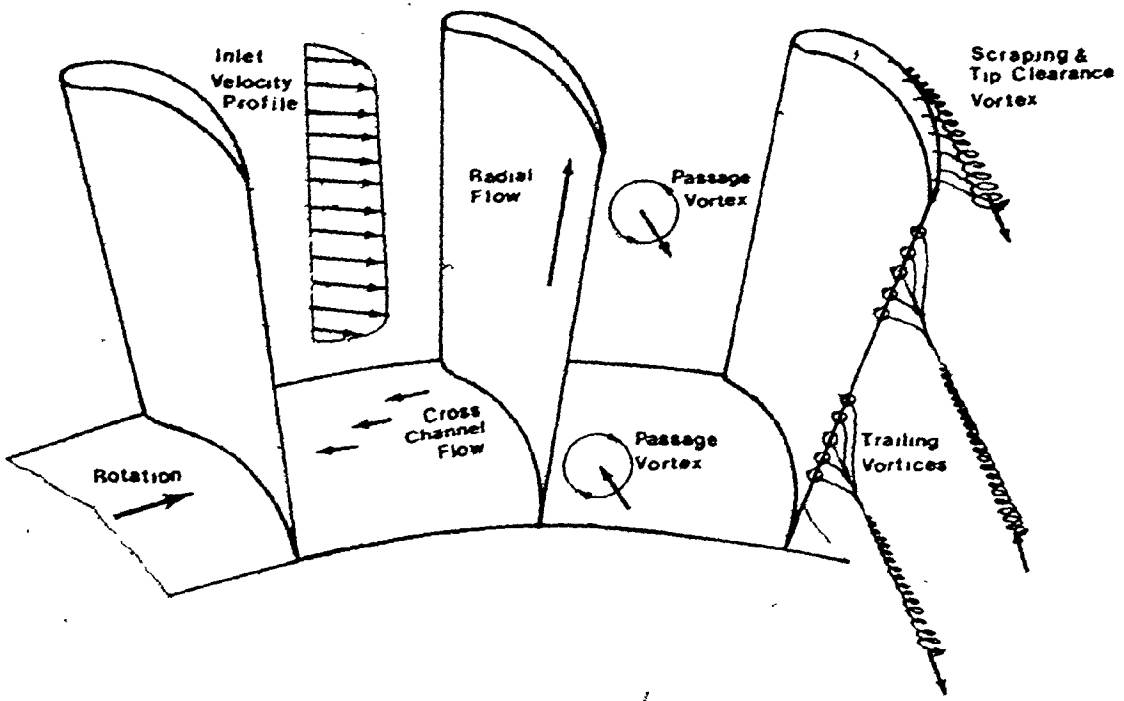

Figure 2.1 Secondary Flow and Vortices in Rotating Turbine Blade Row.

gradient is balanced by the inertia (centrifugal) forces on the fluid particles. According to the boundary layer hypothesis the endwall boundary layers (at the hub and casing) are subjected to the pressure gradient imposed by the inviscid core, however, the flow in the boundary layer being slower than the main flow has less inertia force to balance the cross-channel pressure gradient. Thus, near the annular walls the flow undergoes overturning which sweeps the low energy fluid towards the suction side of the blade. Streamlines near the walls roll up into a vortex termed the 'Passage Vortex' which gives rise to a streamwise vorticity at the exit from the blade passage. The passage vortex is normally located near the corners formed by the endwalls and the suction side of the blade.

2. The Trailing Shed Vortex

The change in the blade circulation (gradient of the bound circulation along each airfoil) results in a streamwise vorticity at the trailing edge. This type of vortex appears even in the case of uniform oncoming flow.

3. The Trailing Filament Vortex

Vortex filaments in the approaching flow are stretched around the blades resulting in another streamwise component of vorticity called 'Trailing Filament Vorticity'.

The trailing shed vortex and the trailing filament vortex combine to form a vortex sheet which rolls up into

a discrete vortex of opposite direction to the passage vortex.

4. Tip Clearance Vortex

Due to the pressure difference between the pressure side of the blade and the suction side a flow is induced in the clearance between the blade tip and the casing in a rotor stage. The motion of the blade also induces mass flow across the gap as shown in Figure 2.1.

5. Scraping Vortex

In a rotating row the blade tip scrapes part of the annular boundary layer on the casing and rolls it up into a vortex called the 'Scraping Vortex'. At the tip region there can be partial cancellation of secondary flow effects. An optimum tip clearance, for minimum losses, has been observed.

6. Horse-Shoe Vortex

The 'Horse-shoe Vortex' is a vortex positioned around the leading edge of the blade near the passage end-walls. It strengthens the secondary flow near the pressure side of the blade and weakens it on the suction side. Such an effect is thought to be dependent on the flow incidence and leading edge shape.

7. Corner Vortices

Due to the accumulation of low momentum flow on the

endwalls a vortex is formed at the corner of the passage at the blade suction side. This vortex is a self-induced, rolled-up vortex sheet from the endwall boundary layers.

The tip clearance vortex and scraping vortex are designated as 'Clearance Flow'.

The trailing filament vortex and the trailing shed vortex are referred to as 'Main Stream Secondary Flow', while the passage vortex is known as the 'Cascade Secondary Flow'. The mainstream secondary flow and the cascade secondary flow are known as the 'Circulatory Flow'.

Radial Flows

In annular cascades, for radial equilibrium, centrifugal forces are balanced by the radial pressure gradient in the main stream. In the boundary layers on the blade surfaces the low energy fluid is subjected to the same pressure gradient. Therefore a radial flow component is established in the blade boundary layers. Radial flows are generally inwards for stators and outwards for rotors.

Secondary Losses in Airfoil Cascades

For incompressible flow through a cascade, the overall mean stagnation pressure loss is a function of both geometric and flow parameters:

ΔP_o = f (blade geometry, incidence, spacing, chord, length, fluid density, thickness of trailing edge, velocity, viscosity, entry

boundary layer thickness and turbulence level).

For the compressible flow of a perfect gas some other parameters allowing for compressibility must be taken into account such as the exit Mach number, specific heat ratio, molecular weight or the gas constant. The losses can be divided into:

1. The profile loss associated with the boundary layer development on the blade surface.

2. The annular wall loss associated with the boundary layer on the hub and casing.

3. The secondary loss associated with the turning of the boundary layer on the endwalls and the resulting separation.

4. Tip clearance losses associated with tip clearance flow.

Figures 2.2 and 2.3 (taken from references [37] and [34] respectively) describe the order of magnitude of the main losses in a pictorial fashion.

It is difficult to separate the annulus wall loss from the secondary loss, thus it is customary to lump these two losses together and they are usually called 'Secondary Loss'.

It is clear that the prediction of the secondary loss, due to the many parameters involved, is best determined through correlations from carefully conducted experiments.

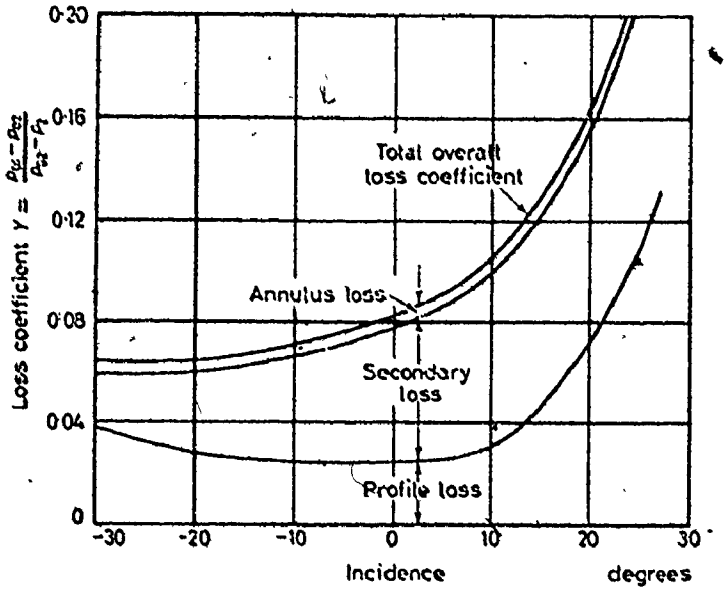

Figure 2.2 Example of Loss Analysis for a Turbine Blade Row. (Taken from Ref. [37])

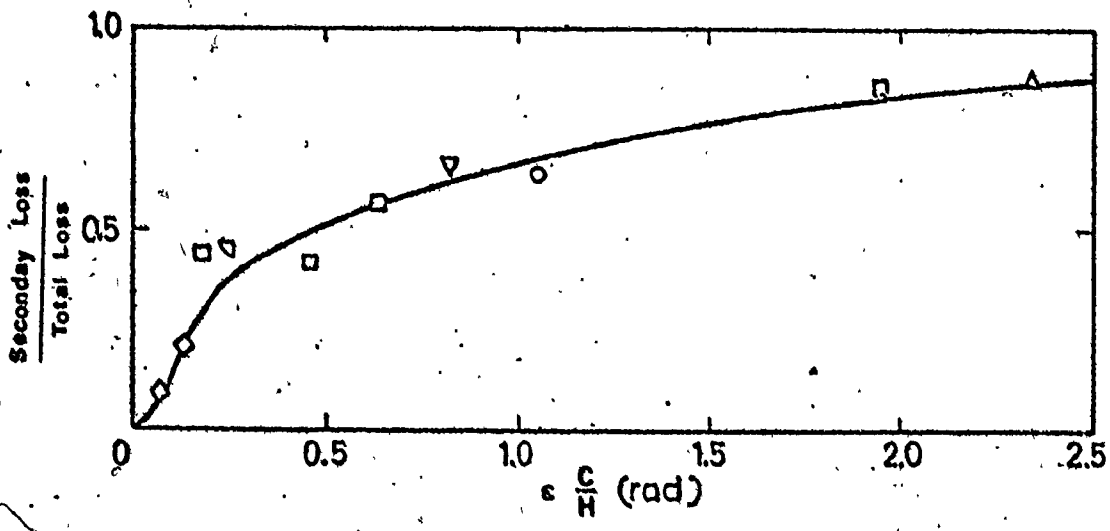

Figure 2.3 Correlation of Secondary Loss Versus Turning. (Taken from Ref. [34])

Most of the correlations have a general pattern of being a product of two terms:

i. Loading term representing the effect of blade loading or deflection.

ii. Length ratio term, being;

$$\lambda = \left(\frac{\text{a length associated with secondary loss}}{\text{annulus height}}\right)$$

Recently there have been several attempts to adequately include the inlet boundary layer characteristics in the length term to obtain more accurate correlations. This subject will be discussed in more detail in the following chapter.

CHAPTER 3

LITERATURE REVIEW

From the study of the flow patterns associated with the secondary flow phenomenon it becomes evident that a complete theoretical solution of the problem is still beyond the reach of the available mathematical techniques. The problem has been treated with simplified mathematical formulations and extensive experimental studies. The common approach to the problem thus falls into two main categories; theoretical analysis and experimental studies.

1. Theoretical Analysis

a) Inviscid rotational flow approximation.

This approach deals mainly with the passage vortex and is known in the literature as the 'Secondary Flow Theory' and/or the 'Secondary Flow Approximation'.

b) Endwall boundary layer analysis, also referred to in the literature as 'Annulus Wall Boundary Layers', 'The Skewed Boundary Layer' and the 'Three Dimensional Boundary Layer'.

2. Experimental Studies

a) Experiments conducted to verify the Secondary

Flow Theory predictions (e.g., exit angle deviations).

b) Experiments devised to study the endwall boundary layer behaviour.

c) Experiments conducted to derive predictive correlations for the secondary flow losses.

d) Qualitative study of the flow behaviour using flow visualization techniques.

Several review papers have been published over the past two decades of which References [1], [2], [3] and [4] are prime examples. Many of the studies reported in the literature included both theory and experiment and therefore may not fall into one of the classifications mentioned above. In the present review an attempt has been made to follow the main lines of the classifications as outlined.

3.1.1 The Secondary Flow Theory

The main objective of the secondary flow theory is to determine:

1) The streamwise vorticity at the exit from the cascade.

2) The secondary flow (velocity normal to the main stream) and the secondary flow streamlines.

3) The deviation in the exit flow angle from the main stream (overturning and underturning).

4) The secondary flow kinetic energy.

A presentation of the general equation of vorticity for compressible viscous flow is given in Reference [5],

$$(\overline{V}.\overline{\nabla})\overline{\omega} = (\overline{\omega}.\overline{\nabla})\overline{V} - \overline{\omega}(\overline{\nabla}.\overline{V}) - \overline{\nabla} \times (\frac{\overline{\nabla}p}{\rho}) - \overline{\nabla} \times [\frac{\mu}{\rho} \overline{\nabla} \times \overline{\omega} - \frac{4}{3} \frac{\mu}{\rho} \overline{\nabla} (\nabla.\overline{V})] \quad (3.1)$$

where,

$$\overline{\omega} = \overline{\nabla} \times \overline{V}$$

Several simplifying assumptions must be made before attempting to solve the problem. The secondary flow approach is based on the main assumptions that the flow is steady, inviscid, rotational, incompressible and with no body forces. The authors of Reference [5] list several cases where a simplified form of Equation (3.1) can be solved. On the other hand several investigators have derived simplified expressions for the vorticity instead of starting from the general form (see References [2], [3], [4], [5], [6], [7], [8]). Hawthorne's paper [6] is one of the earliest attempts to use simple derivation technique to establish the fundamental model of the secondary vorticity. The vorticity $\overline{\omega}$ can be resolved into two components as shown in Figure 3.1.

1) A streamwise component given by:

$$\overline{\xi} = (\frac{\overline{\omega}.\overline{V}}{\overline{V}.\overline{V}}) \overline{V} = \frac{\xi}{V} \overline{V} \quad (3.2)$$

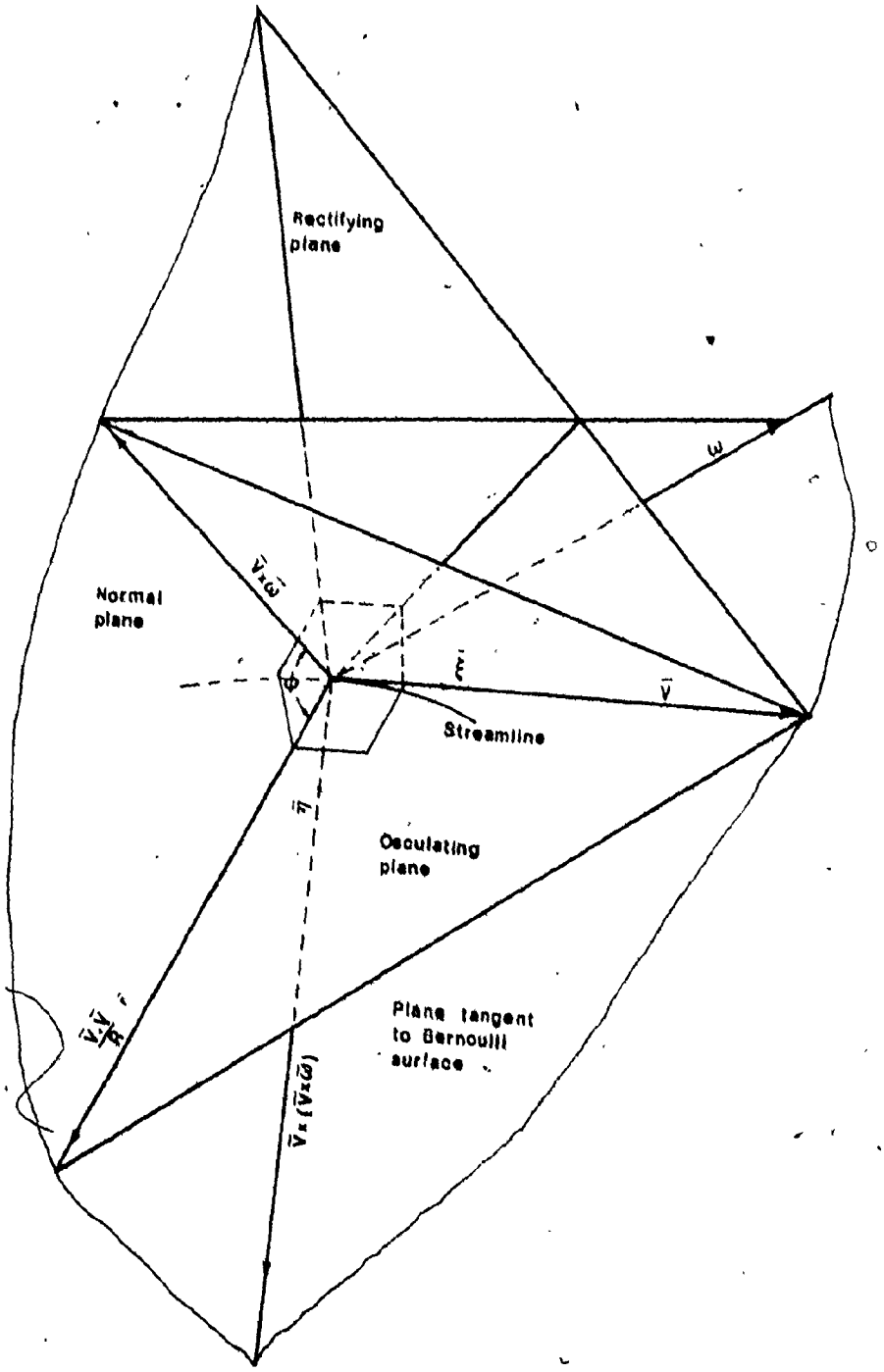

Figure 3.1 Components of Vorticity and Bernoulli Surface Angle ϕ.

2) A component normal to the streamline given by:

$$\bar{n} = \frac{(\nabla \times \bar{\omega}) \times \bar{V}}{\bar{V} \cdot \bar{V}} \qquad (3.3)$$

Taking the divergence of $\bar{\omega}$ (where div $\bar{\omega} = 0$) in terms of its components (3.2) and (3.3):

$$\text{div } \left(\frac{\bar{\omega} \cdot \bar{V}}{\bar{V} \cdot \bar{V}}\right) \bar{V} - \text{div } \frac{\bar{V} \times (\bar{V} \times \bar{\omega})}{\bar{V} \cdot \bar{V}} = 0 \qquad (3.4)$$

or

$$\text{div } \left(\frac{\xi \bar{V}}{V}\right) - \text{div } \frac{\bar{V} \times (\bar{V} \times \bar{\omega})}{\bar{V} \cdot \bar{V}} = 0 \qquad (3.5)$$

which is a purely kinematical relation between $\bar{\omega}$, $\bar{V}$ and $\bar{\xi}$. Using Euler's equation in conjunction with equation (3.5) — the following equation can be obtained,

$$\left(\frac{\xi}{V}\right)_2 - \left(\frac{\xi}{V}\right)_1 = -2 \int_1^2 \text{grad } \left(\frac{p_o}{\rho}\right) \frac{\sin\phi}{V^2} d\epsilon \qquad (3.6)$$

The above equation cannot be solved without further assumptions and/or simplifications. For example, Squire and Winter [7] have given a simple expression for ξ_2 for cascades with small deflection:

$$\xi_2 = 2\, \epsilon \frac{dV_1}{dz}$$

$$= 2\, \eta_1\, \epsilon \qquad (3.7)$$

In Hawthorne's equation (3.6) the term [grad $\frac{p_o}{\rho}$] is considered constant along a streamline. For incompressible flow it can be expessed as:

$$\bar{\nabla} \frac{p_o}{\rho} = \bar{\nabla} \frac{p}{\rho} + \nabla . \bar{\nabla} \nabla$$

$$= V_1 \frac{dV_1}{dz} \qquad (3.8)$$

Hence Hawthorne's equation (3.6) for the case where $\xi_1 = 0$ and $\phi = \frac{\pi}{2}$ reduced to

$$\xi_2 = - 2 V_1 V_2 \frac{dV_1}{dz} \int_{\varepsilon_1}^{\varepsilon_2} \frac{1}{V^2} d\varepsilon \qquad (3.9)$$

Equation (3.9) has been also derived by Hawthorne [8] through the use of vector analysis. Preston [9] followed a simple approach to derive the expression given by Squire and Winter.

Loo's [10] integrated equation (3.9) assuming the axial velocity to remain constant along the streamline and obtained the expression:

$$\xi_2 = \frac{\eta_1}{\cos\alpha_1 \cos\alpha_2} \left[\alpha_2 - \alpha_1 + \frac{\sin 2\alpha_2 - \sin 2\alpha_1}{2}\right] \qquad (3.10)$$

In order to take into account the convergence or divergence of the passage he suggested the following expression for vorticity

$$\xi_2 = - \frac{(N-1/N)}{\ln N} \eta_1 \varepsilon_{12} \qquad (3.11)$$

where N is the divergence ratio $(\frac{\text{exit area}}{\text{inlet area}})$, both measured normal to the main flow.

In order to take the Bernoulli surface rotation into account Lakshminarayana and Horlock [11] showed that

for moderate turning angles,

$$\phi = \frac{\pi}{2} - \eta_1 \frac{(\Delta\epsilon)^2 C}{2V_1 \epsilon_{12}} \qquad (3.12)$$

Equation (3.6) was used with equation (3.12) together with the assumption of constant axial velocity ($V_1\cos\alpha_1 = V_2\cos\alpha_2 = V\cos\alpha$) and a solution was obtained for the secondary flow stream function. Bardon et al. [12] assumed the Bernoulli surface angle to vary linearly with t for small turning angles and estimated the secondary flow effects on flow outlet angles in rectilinear cascades with moderate turning.

Further studies attempted to take more effects into account. Louis [13] considered the effect of viscosity while Morris [14] proved the validity of the basic secondary vorticity equations in a rotating system.

3.1.2 Secondary Flow Approximation

In order to determine the secondary flow velocities and exit angle changes in a cascade, the secondary flow is regarded as perturbations from the shear flow transverse to the main flow. With the assumptions $\frac{\partial v}{\partial n} >> \frac{\partial u}{\partial s}$ and $\frac{\partial w}{\partial z} >> \frac{\partial u}{\partial s}$, the continuity equation for the secondary flow can be written as:

$$\frac{\partial v}{\partial n} + \frac{\partial w}{\partial z} = 0 \qquad (3.13)$$

A stream function is defined by

$$w = -\frac{\partial \omega}{\partial n}, \quad v = \frac{\partial \psi}{\partial z}$$

thus,

$$-\xi = \nabla^2 \psi$$

$$= \frac{\partial v}{\partial z} - \frac{\partial w}{\partial n} \qquad (3.14)$$

Once the streamwise vorticity ξ is obtained the secondary flow stream function ψ and the secondary flow velocities v, w can be determined by solving Poisson's equation (3.14) at any section in the passage.

Hawthorne [15] obtained a series solution for ψ in a rectangular channel for the Squire and Winter solution. Erich [16] obtained a solution for a cascade with twisted blades and Hawthorne and Novak [2] and Dixon [17] presented solutions for annular cascades.

3.1.3 The Trailing Vortices

The trailing vortices exist at the trailing edge of the blades. Lighthill [18] approached the problem by introducing a drift function to trace the path of the vortex filaments carried through the cascade. Hawthorne and Armstrong [19] and Smith [20] followed a similar procedure.

The trailing filament circulation is given by:

$$\Gamma_{tf} = \frac{dV}{dz} V \oint \frac{ds}{V} \qquad (3.15)$$

and the trailing shed circulation is given by:

$$\Gamma_{ts} = - S \cos \alpha_1 \frac{dV}{dz} (\tan \alpha_2 - \tan \alpha_1) \qquad (3.16)$$

The averaged secondary circulation within the passage is the difference between the total circulation far downstream and the trailing vortex circulation.

3.1.4 Limitations of the Secondary Flow Theory

The secondary flow approximation loses validity for large turning cascades with steep inlet velocity profiles. Radial flows, Bernoulli surface distortions and viscous effects are generally not taken into account. The theory can predict with reasonable accuracy the secondary vorticity for low turning angles where separation does not occur. The development of the secondary vorticity in rotating channels can also be assessed. The Secondary Flow Theory, however, fails to predict the flow near the endwalls and the losses associated with the complex flow situation in cascades and multi-stage machines.

3.2.1 Endwall Boundary Layers

The endwall boundary layer presents a difficult problem for analysis because of its highly three-dimensional nature which casts some doubts on the applicability of some of the basic boundary layer assumptions such an negligible pressure gradient normal to the wall and the identification of the boundary layer thickness. The

analytical approach to the problem is based on integral schemes and axisymmetric flow approximations. Experimental investigations into the problem have yielded some simple endwall loss correlations employing only a few flow parameters.

For the case of a bounded boundary layer, where S and δ are of the same order of magnitude so that $\frac{\partial v}{\partial z}$ and $\frac{\partial w}{\partial n}$ (see Figure 3.2) are comparable, the secondary flow approach yields an "S" shaped cross-flow velocity profile. Overturning occurs closer to the wall and underturning in the outer portion. For the case of an unbounded boundary layer (where $\frac{S}{\delta} \to \infty$ and $\frac{\partial w}{\partial n} >> \frac{\partial v}{\partial z}$), from equation (3.7)

$$\xi = -\frac{\partial v}{\partial z}$$

$$= -2\,\varepsilon\,\frac{\partial u}{\partial z} \qquad (3.17)$$

Integrating the above equation with $v = 0$ when $u = V$ gives

$$\frac{v}{V} = -2\,\varepsilon\left(1-\frac{u}{V}\right). \qquad (3.18)$$

This velocity profile is the outer portion of Johnston's [21] triangular polar plot developed for the three-dimensional unbounded boundary layer analysis.

While the secondary flow theory does not predict the crossover in the velocity profile for unbounded boundary layers, experiments [4] have shown that the crossover exists at the outlet of the blade cascades. With the exception of

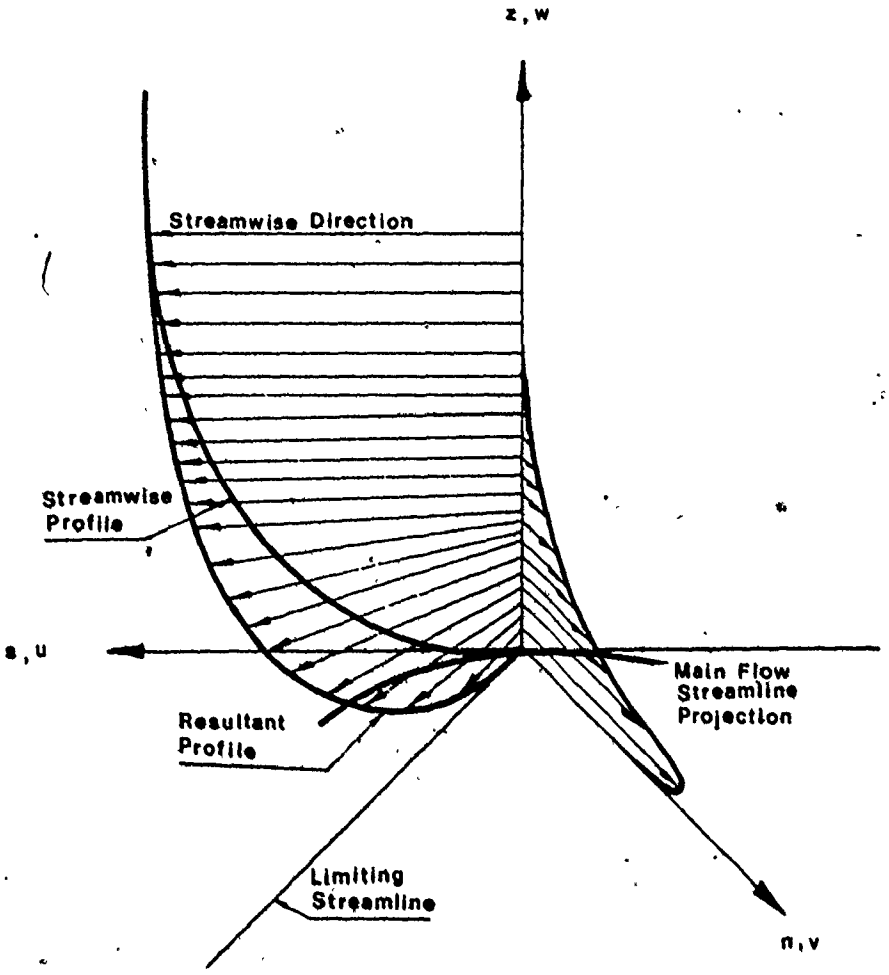

Figure 3.2 Endwall Boundary Layer Basic Notation.

the region near the wall, where viscous effects dominate, the measured and calculated profiles are in good agreement over much of the boundary layer thickness for small flow turning ($<30^{o}$).

A summary of the calculation schemes has been given by Sjolander [22]. Mager [23] derived the momentum integral equations in the streamwise and the crossflow direction. This quasi three-dimensional analysis is limited to application along one particular streamline. In Reference [24] a calculation method was developed for the endwall boundary layer using a flat plate expression for the wall shear stress (with one-seventh power law mean velocity profile).

Jansen [25] and Stratford [26] developed simple methods for predicting the blockage due to the boundary layer displacement thickness.

Further calculation methods were introduced by Mellor and Wood [27] where pitchwise averaged equations were used. A similar scheme was introduced by Horlock and Hoadley [28] and an improvement to the Mellor and Wood method was suggested by Herisch [29].

A comparison of the calculation schemes with two sets of experimental data was published by Marsh and Horlock [30]. Horlock [31] studied the cross flow in the three-dimensional turbulent boundary layer and compared the derived profiles with experimental data. Sjolander [22]

conducted a detailed experimental study on turbine nozzle guide vanes of 50^{o} turning. The results of the tests revealed the presence of some local areas of adverse pressure gradient that can lead to boundary layer separation.

Anand and Lakshminarayana [32] reported an analytical and experimental investigation of the characteristics of a three-dimensional turbulent boundary layer in a rotating helical channel. The authors developed expressions for the velocity profile in both the inner and outer portions of the boundary layer. The analysis was restricted to incompressible flow through a rotor blade with small camber. The measurements showed good agreement with the predicted values.

Recently, Railly and Sharma [33] presented a more rigorous analysis for the annulus wall boundary layer problem using secondary flow hypothesis, taking into account terms in the governing equations that were disregarded by Mellor and Wood.

3.2.2 Three-Dimensional Separation

According to reference [34], Eichelbrenner, illustrated two types of three-dimensional separation:

1) Envelope (or clash) separation, which results from inertial effects arising from the clash of two flows having opposing directions meeting at the separation line, "showing a herring pattern in surface flow visualization".

This type of separation occurs on the suction surface of the blade and does not cause severe flow problems.

2) Asymptotic Separation, which is pressure induced. The separation on the endwall may be of this type and often represents catastrophic failure of the flow in the blade passage. It is thus important to secondary flow studies.

3.2.3 Limitations of the Endwall Boundary Layer Analysis

The integral boundary layer calculation schemes used in conjunction with through flow calculation methods are restricted to small flow turning and therefore they cannot predict the performance of turbine cascades. The analysis is also limited to boundary layers that are originally collateral with simple main stream flow conditions which is seldom the case in the actual machine flow situation. The boundary conditions are difficult to define because of the interaction effects at the corners. The prediction of three-dimensional separation is still unresolved particularly the envelope type separation. It is doubtful that the calculation methods, while not taking separation into account, can predict the boundary layer behaviour beyond the separation region.

The losses associated with the endwall boundary layer cannot be predicted by the available calculation schemes and the designer is, therefore largely dependent on

correlations derived from experimental data.

3.3 Experiments, Losses and Correlations

It is evident, from the discussions in the previous sections, that due to the difficulties associated with analysis of the secondary flow phenomena, the problem cannot be dealt with solely on an analytical basis. Experimental data and predictive correlations are indespensible to the designer of turbomachines. Due to the large number of parameters involved in the problem, there is not a complete set of data resulting from one experimental study that takes all relevant factors into account and yields consistent prediction correlations. In fact there is a large amount of experimental data available (particularly for compressor cascades) but only a few were presented in detail with relevant parameters specified, particularly the inlet boundary layer, with reasonable reliability.

The experimental approach has proceeded in parallel with the theory to check the Secondary Flow Theory, to provide more physical understanding of the phenomenon (e.g., flow visualization) and to study the effect of geometric and flow parameters on cascade losses.

3.3.1 Comparison with Theory

Several experiments have been conducted on ducts, cascades of guide vanes, rotor and stator rows to compare

the performance with the related theoretical models. Hawthorne [6] compared his mathematical formulation with tests on circular and rectangular bends. Squire and Winter [7] compared their simple model with experiments on a cascade of turning vanes 94.8° and found satisfactory agreement between the predicted and measured secondary flows. Hawthorne and Armstrong [19] measured the pressure distribution on a cascade of impulse turbine blades (space to chord ratio of unity, an aspect ratio of 3, with $\alpha_1 = 35$, and $\alpha_2 = -37^\circ$) and compared the local lift coefficient with Hawthorne's small-shear, large-deflection analysis. The results confirmed the variation of the lift and circulation predicted by the theory. The comprehensive analysis of Lakshminarayana and Horlock [11] was compared with experimental results obtained by Louis [35], Soderberg [36] and Lakshminarayana [37]. The comparison included the change in outlet angles and the kinetic energy of the secondary flow. It was concluded that the strength of secondary vorticity was reduced substantially by viscous effects and to a lesser extent by Bernoulli surface rotation and therefore inviscid secondary flow theories tend to overestimate the spanwise variation in the outlet angle. Further experimental data is reported in [1], [16] and [12].

3.3.2 Losses and Correlations

Losses in turbomachines are expressed in several forms

[37], the most common being the total pressure loss coefficient and the enthalpy loss coefficient. For incompressible flow through a cascade the overall mean stagnation pressure loss is a function of inlet flow conditions, cascade geometry and flow geometry:

$$\Delta P_o = P_{o1} - P_{o2} \qquad (3.19)$$

$$= f \text{ (blade geometry, incidence, spacing S, chord C, length H, fluid density } \rho\text{, thickness t, velocity v, viscosity } \mu\text{, boundary layer thickness } \delta\text{, entry boundary layer parameters and turbulence level).}$$

In a dimensionless form,

$$\frac{\Delta P_o}{\frac{1}{2}\rho V_1^2} = f \text{ } (R_N, i, \text{ blade geometry, } \delta/C, \delta_1/C, \text{ inlet boundary layer parameters and turbulence level}). \qquad (3.20)$$

For compressible flow other parameters allowing for compressibility are introduced, thus

$$Y = f \text{ } (R_N, \text{ blade geometry, } S/C, t/C, \delta_1/C, \text{ inlet boundary layer parameters and turbulence level, } M_2, \gamma, R \text{ or } M). \qquad (3.21)$$

There are generally two methods of correlating the losses to the non-dimensional parameters, either the overall

loss is correlated to all parameters or the separate losses (profile and secondary) are correlated with the relevant parameters. Soderberg [36] followed the first method while Ainley and Mathieson [38] followed the second method.

A comprehensive review of the profile losses in turbine cascades was given in Reference [37]. Recently Denton [39] reviewed seven prediction schemes for the profile losses and compared them to seventy-nine sets of cascade data. The author concludes that, while none of the available correlations predicted the losses accurately, some progress could be achieved by obtaining the losses from calculations of the velocity distribution and the boundary layer growth on the surfaces of the blades and in the wake.

It is worth mentioning that the effects of the relevant parameters on the secondary losses was not clear until recently. "Dunham (1970) has made a comprehensive attempt to clear up some of the chaos that exists on the effect of the blade and flow parameters on losses in cascades."* In his review paper, Dunham [3] presented a correlation for secondary loss including a tentative expression for the inlet boundary layer effect. Based on experimental data the correlation derived for Y_s is given by an expression of the form

$$Y_s = \frac{C}{H} \frac{\cos\alpha_2}{\cos\beta_1} \frac{C_L^2}{(S/C)^2} \frac{\cos^2\alpha_2}{\cos^3\alpha_m}\left(0.0055 + 0.078 \sqrt{\frac{\delta^*}{C}}\right) \quad (3.22)$$

* Quoted from Reference [1]

The expression between parenthesis in equation (3.22) is the boundary layer function. The first term in the expression is the downstream boundary layer component and the second term is the vortex core loss component. The author emphasized that this tentative expression needs experimental verification particularly for turbine cascades with high turning angles.

Came [40] introduced another correlation for secondary losses based on measurements in a larger turbine cascade with a maximum turning of 85° where the inlet boundary layer thickness and inlet angle were varied. The author presented loss contour maps and spanwise variations of loss as a function of the inlet conditions. The correlation introduced by Came for Y_s can be written as

$$Y_s = \left(\frac{C_L}{S/C}\right)^2 \frac{\cos^2\alpha_2}{\cos^3\alpha_m} \frac{\cos\alpha_2}{\cos\beta_1} \left(0.25\, Y_1^* + 0.009\, \frac{C}{H}\right) \qquad (3.23)$$

where Y_1^* defines the inlet boundary layer losses. It was also shown that Dunham's correlation agreed well with Came's results.

Dunham and Came [41] introduced a improvement to the correlation of Ainley and Mathieson which is still widely used. The authors suggest the expression

$$Y_s = 0.0334\, \frac{C}{H}\, \frac{\cos\alpha_2}{\cos\beta_1}\, Z \qquad (3.24)$$

instead of Ainley's expression

$$Y_s = \lambda\, Z \qquad (3.25)$$

where λ is an empirical function (see Reference [38], Figure 8) and Z is the Ainely Loading Parameter defined as

$$Z = \left(\frac{C_L}{S/C}\right)^2 \frac{\cos^2 \alpha_2}{\cos^3 \alpha_m} \tag{3.26}$$

Bown [42] conducted tests on models of rotor blades of high deflection (132°) impulse turbine blades in a rectlinear cascade. The results showed that the predicted secondary loss (using various correlations) were as high as ten times the measured values. Woods [43] conducted similar tests for blade aspect ratios ranging from 1.480 to 0.592 and found that the secondary losses increased with decreasing aspect ratio. The author also pointed out the discrepancies between the measured and the predicted values.

Recently, Langston et al. [44] conducted detailed measurements of subsonic flow in a large scale plane turbine cascade with an aspect ratio of 1.0 with a collateral inlet boundary layer and a turning angle of 110°. Velocity and pressure measurements were taken at eight axial planes from the inlet to the outlet. The measurements indicated that a large part of the endwall boundary layer was very thin when compared with the cascade inlet boundary layer. The three-dimensional separation was traced on the endwall and the suction surface of the blade.

3.3.3 Flow Visualization

In a series of excellent flow visualization studies published by NACA (References [45] through [50]) a better understanding of the physical nature of secondary flow in cascades was achieved. Rohlik et al. [46] studied the secondary flow patterns originating in three sets of turbine nozzle blade passages by means of flow visualization and detailed flow measurements. The tests revealed that the low energy flow originating at the outer wall boundary layer was swept all the way down the trailing edge and discharged near the inner wall. In such a flow situation it is difficult to assess the profile losses.

Sjolander [22] performed extensive surface flow visualization, using the oil dot and oil film techniques, on both the blade surfaces and endwalls in an annular cascade of turbine nozzle guide vanes. The experimental measurements showed that even in a situation where the overall pressure gradients are strongly favourable, local areas of adverse pressure gradients can result in boundary layer separation which have a significant influence on the rest of the flow.

3.4 Conclusions

1) The secondary flow theory can predict, with reasonable accuracy, the secondary vorticity and outlet angle changes for cascades of moderate turning and non-steep inlet velocity profiles.

2) The losses associated with the endwall boundary layer and its interaction with the blade boundary layers cannot be predicted by the available calculation schemes.

3) The prediction of secondary flow losses in annular cascades with high turning angles calls for more cascade data extracted from realistic test models.

4) The effect of the inlet boundary layer characteristics on the secondary losses needs further investigation.

CHAPTER 4

THE ANNULAR TEST RIG

4.1 General

The experimental investigation of the secondary flow phenomenon in annular cascades requires accurate measurements of both the free stream and the secondary flow. Many of the high work (output per stage) turbines, considering the individual blade passage, are of such a small scale as to prohibit detailed analysis of the three dimensional effects using even the most advanced measurement techniques. In order to minimize the probe size influence on the flow, and thus to improve the accuracy of measurements, large scale models are called for. Annular cascades of large size, however, usually pass such a mass flow as to prohibit - from an economical viewpoint - the use of a complete annulus as a test section. To circumvent these difficulties and to provide the maximum conditions of similarity of the effects taking place in twisted blade passages, a special annular test rig was designed [51] and constructed. The design facilitates the control of the inlet flow parameters in the radial and circumferential directions. It also provides a means for controlling the inlet flow boundary layer on the hub and casing.

The test facility is an open circuit wind tunnel consisting of three main parts:

1. A large scale sector of an annular turbine blade cascade.
2. An inlet section.
3. An outlet section.

An overall view of the apparatus is shown in Figures 4.1 and a cross-sectional view is shown in Figure 4.2. In order to provide uniform inlet and exit flow angles, the inlet and outlet ducts (part number 2,9) have walls of a hyperboloidal configuration as illustrated in Figures 4.3 and 4.4. A sector of two concentric hyperboloids of one sheet (extending to the axis of symmetry of the hyperbola) forms the annular boundary walls of each duct. The straight line generatrixes of the surface are inclined to the corresponding blade angle.

4.2 The Inlet Section

The inlet section consists of a bellmouth entrance, two supplementary cascades (a curved cascade and a plane cascade) and the hyperboloidal inlet duct. Two suction chambers for boundary layer control are located near the exit from the inlet duct upstream of the blades. Also a circular arc segment providing for a sliding traverse is situated at the hub side of the inlet as shown in Figure 4.2.

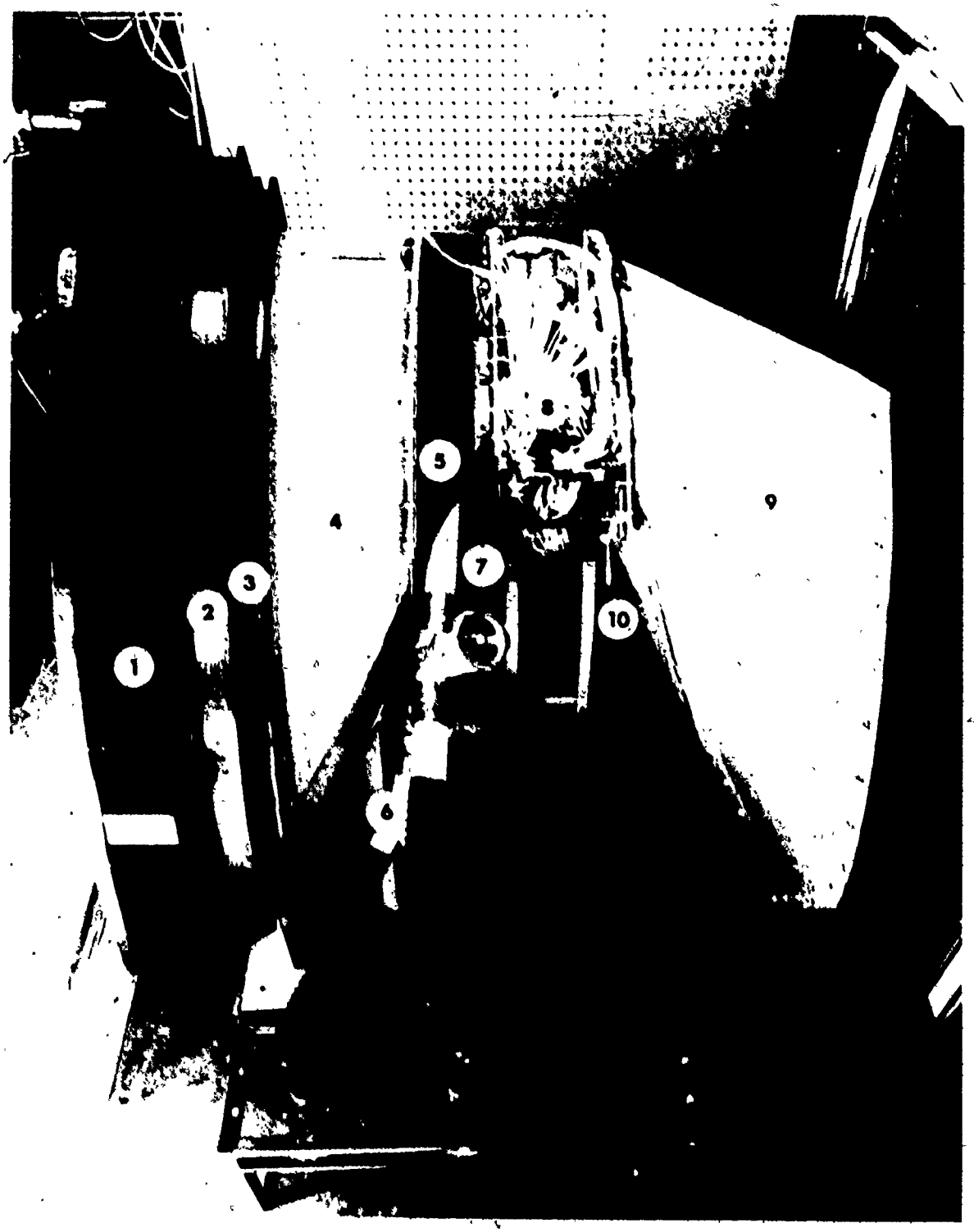

Figure 4.1 The Annular Cascade Rig (Overall View).

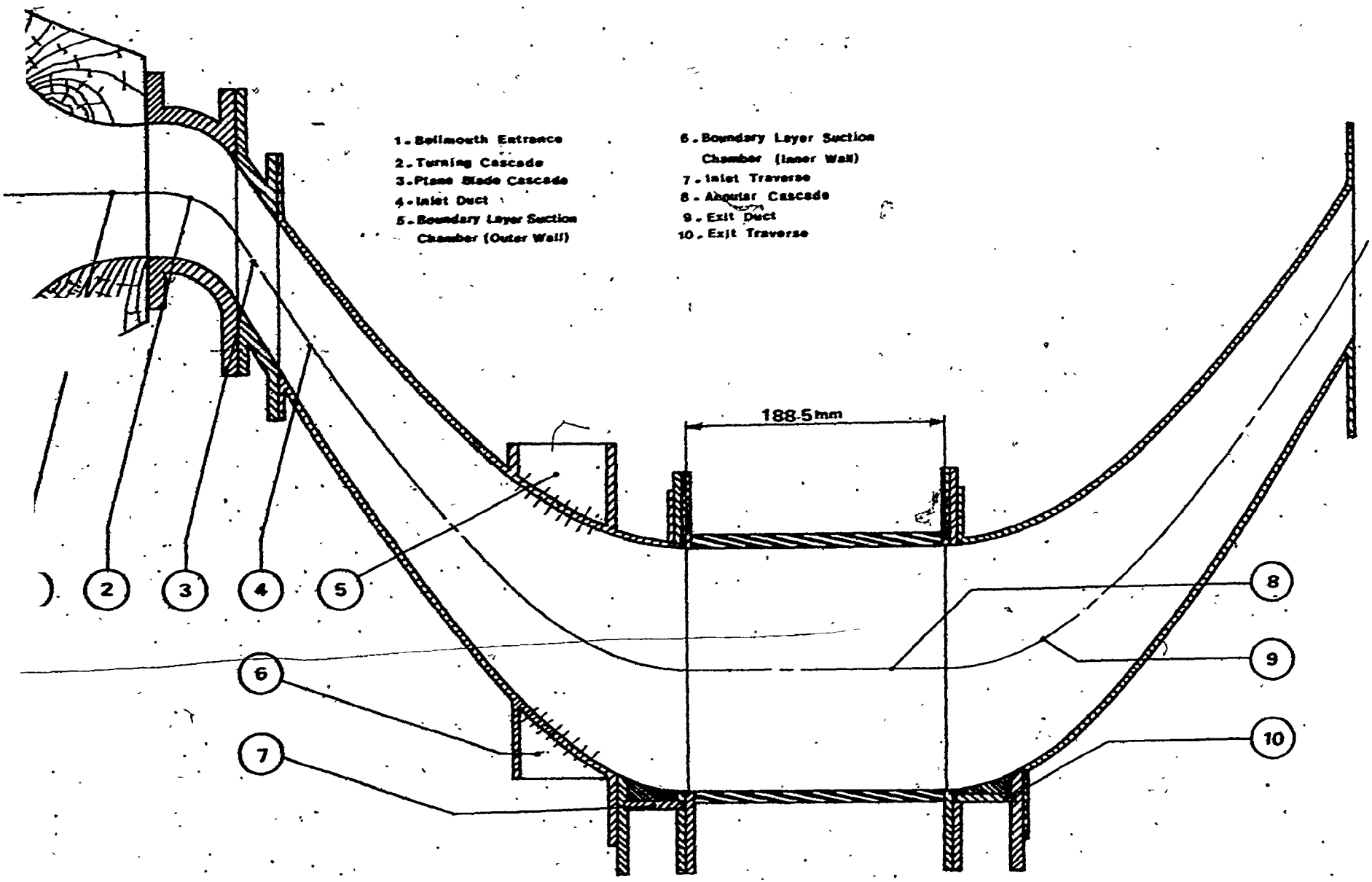

Figure 4.2 The Annular Cascade Rig Cross Sectional View.

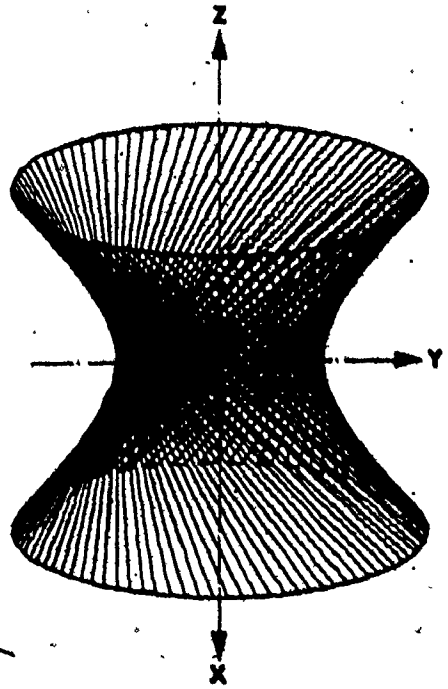

Figure 4.3 Configuration of the Hyperboloid of One Sheet.

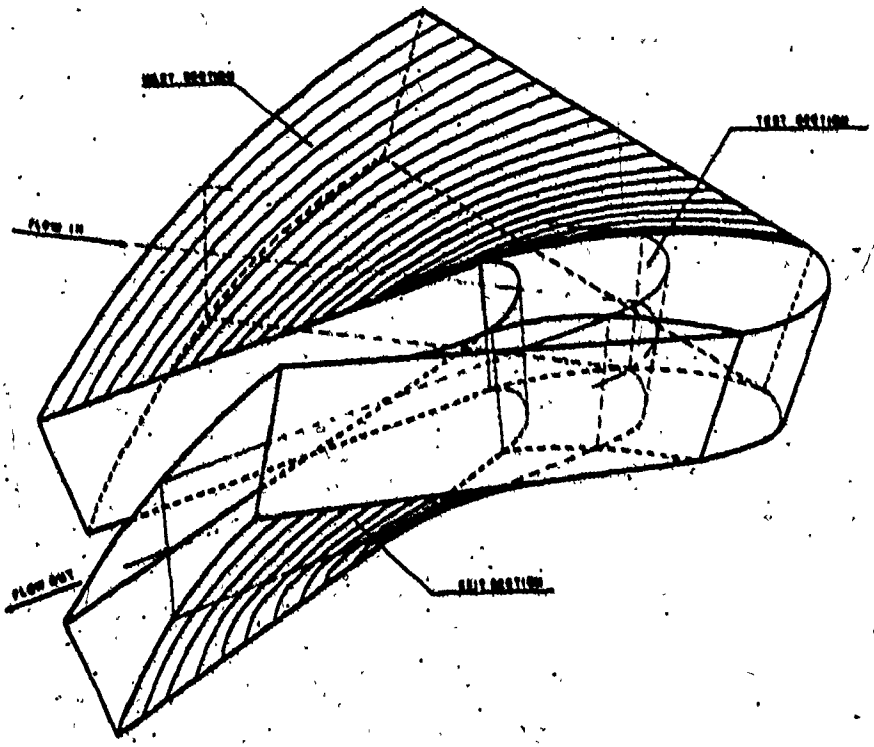

Figure 4.4 The Annular Cascade Rig Main Components.

4.2.1 The Bellmouth Entrance

The bellmouth entrance faces the axial direction. The purpose of using the bellmouth is to avoid the effects of sharp edges at the entrance to the rig. It has a lip radius of 100 mm followed by a short (10 mm) straight portion as shown in Figures 4.2 and 4.5. The bellmouth was manufactured from wood and fitted to the turning blade cascade. The thick wooden structure of the bellmouth made it possible to use it as a point of support for the rig.

4.2.2 The Turning Cascade

The bellmouth is followed by a curved blade cascade to turn the flow from the axial direction through a 64° angle which corresponds to the inlet blade angle. The cascade consists of 21 blades (Figure 4.6) equally spaced on a circular arc of 53°. The side walls of the cascade (of approximately circular arc contours) are manufactured from wood with grooves carved at both ends to position the blades.

4.2.3 The Plane Blade Cascade

In order to provide further guidance to the flow in the direction of the blade inlet angle, a straight blade cascade shown schematically in Figure 4.7 is located adjacent to the turning blade cascade. The side walls of the cascade are also made from wood with straight grooves

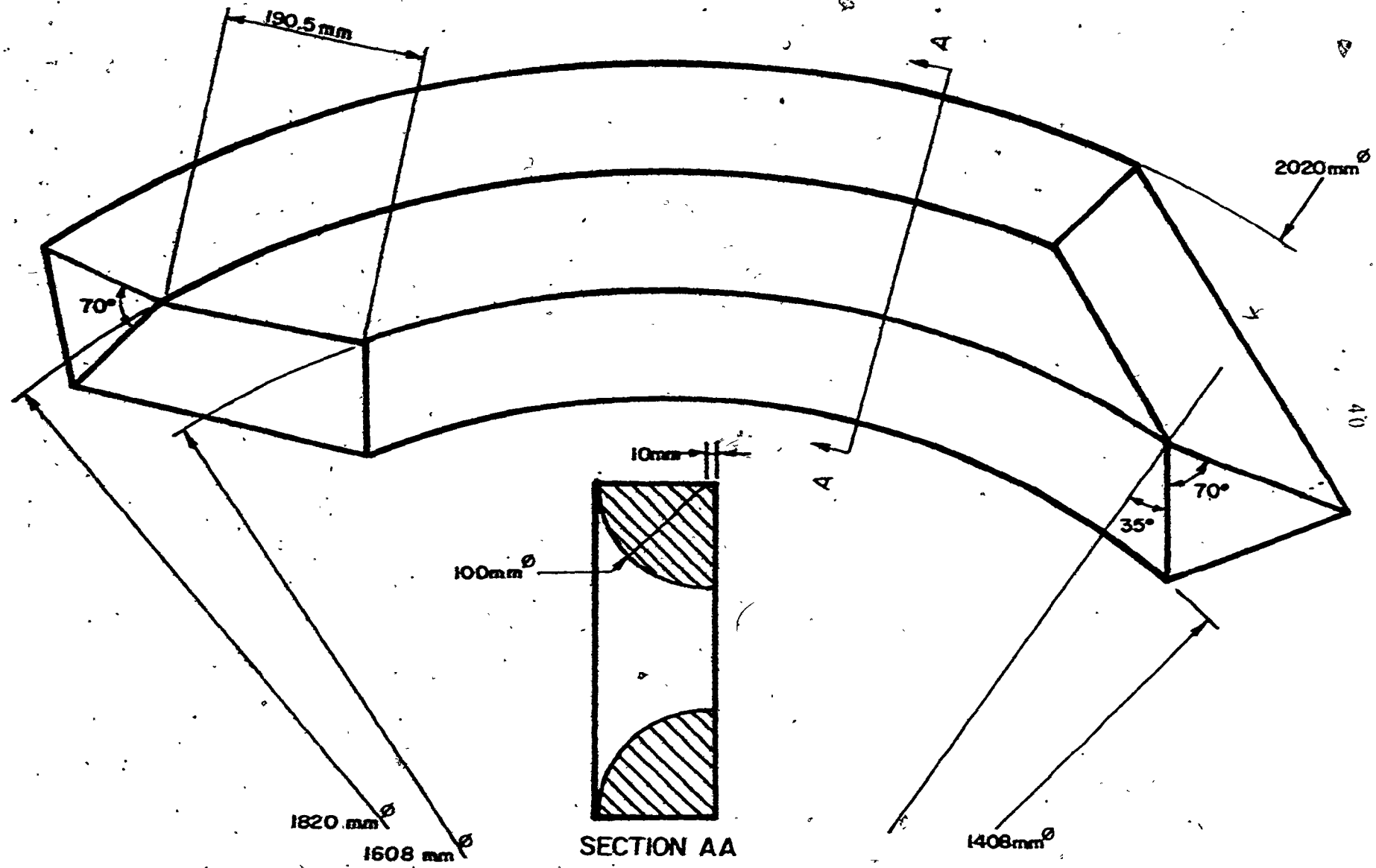

Figure 4.5 The Bellmouth Entrance.

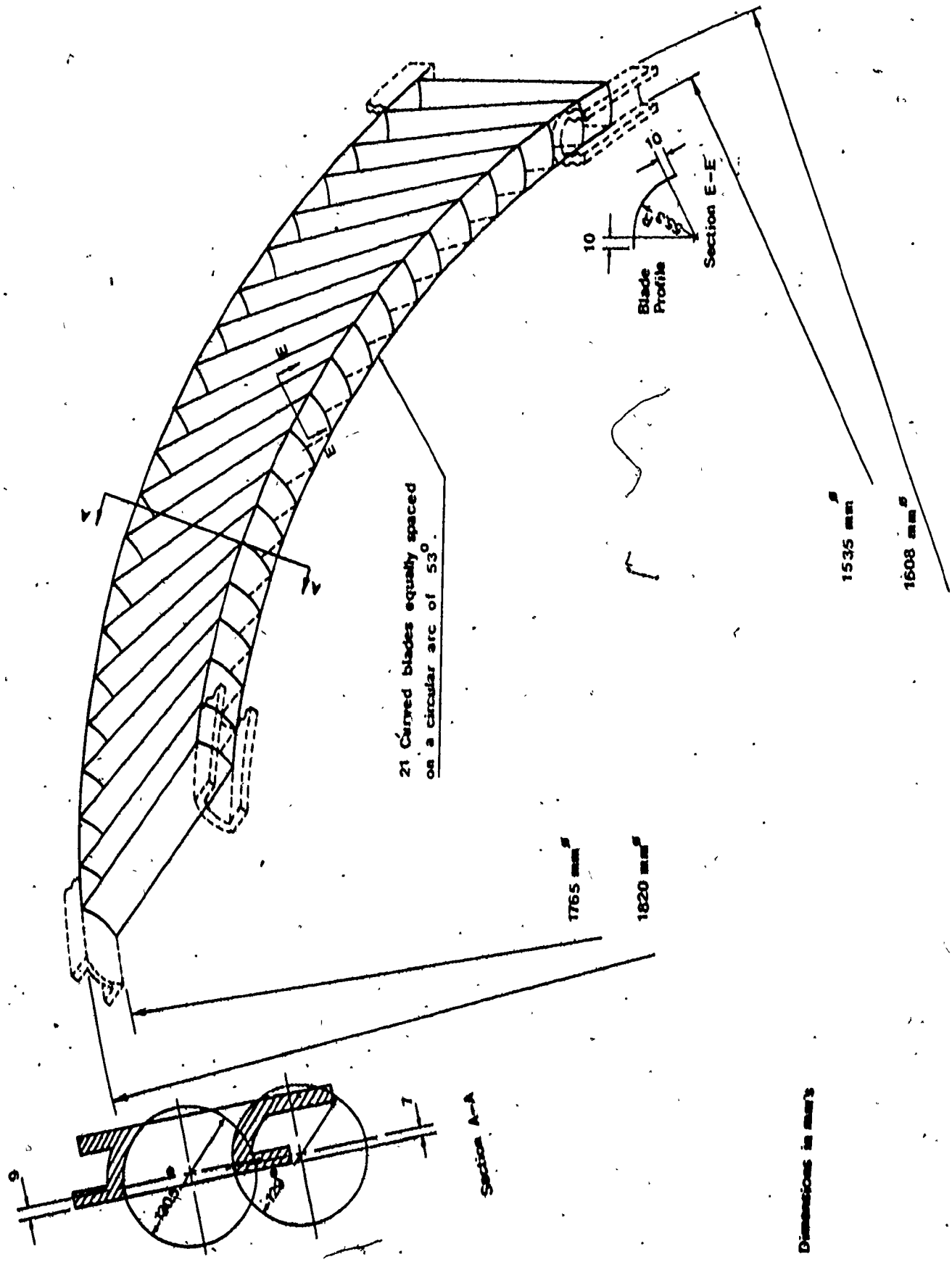

Figure 4.6 The Turning Cascade.

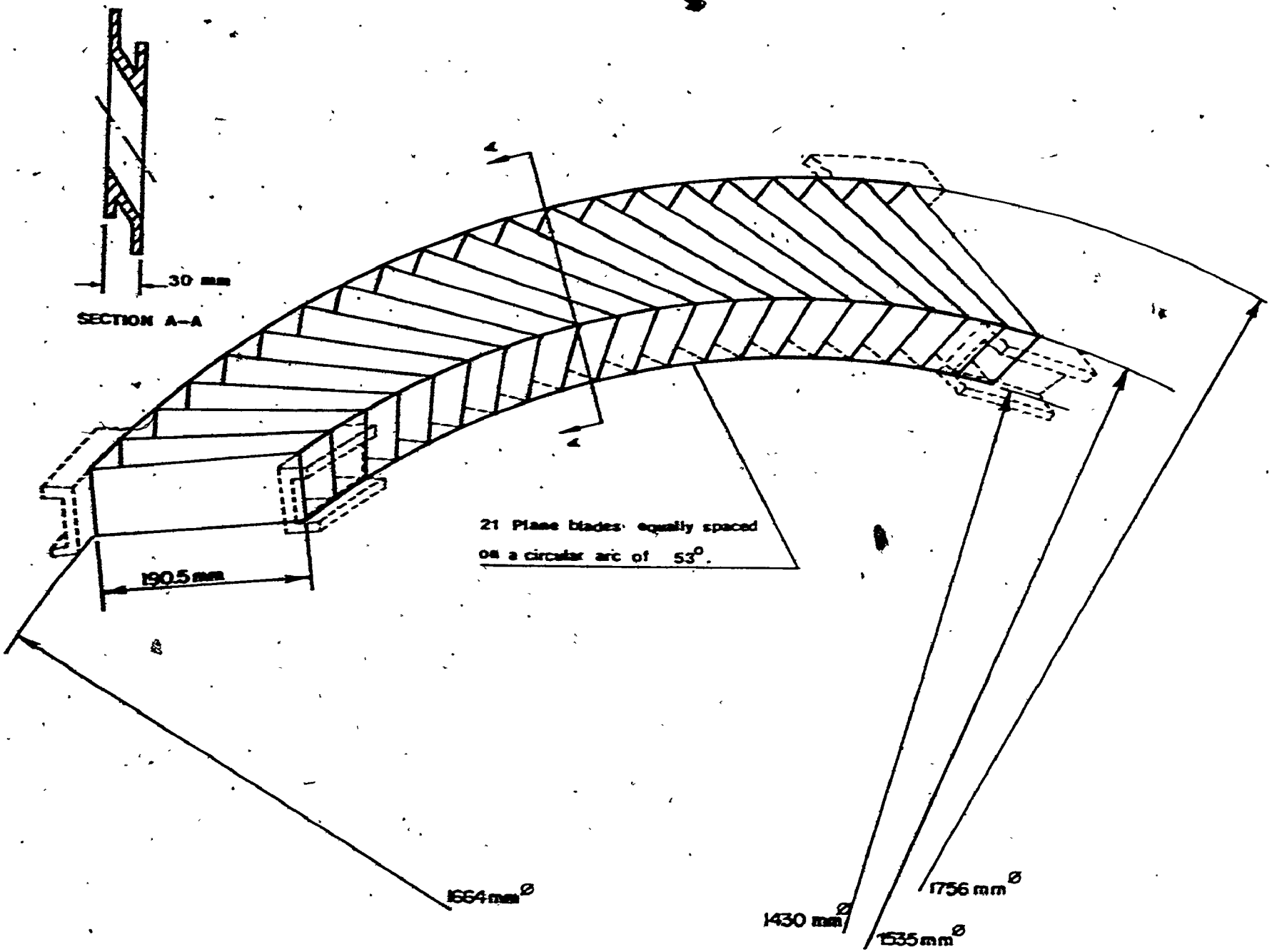

Figure 4.7 The Plane Blade Cascade.

for the blade mounting. For flow continuity and passage rigidity both the curved and straight blades were formed in one piece as shown in Figure 4.8.

4.2.4 The Inlet Duct

The inlet duct is shown in Figure 4.9 with equidistant cross sections normal to the axial direction. The generating plane stream surfaces are oriented radially at the duct exits to match the orientation of the leading edges of the blades. The surfaces are inclined (64°) to the axial direction. The annular boundary walls are generated by rotating the stream plates through an angle of 53° which is 8° in excess of the circumferential pitch of the test cascade. The extra 8° are divided equally on the outer sides of the segment to provide for suction ports that can be used to adjust the flow circumferentially and also to reduce the effect of the side walls on the centre blade passage. The duct has a uniform cross-sectional area from inlet to exit converging circumferentially and diverging radially.

The inlet duct was manufactured in two steps:

1. A male mould was made from laminated wood. Circular arc segments were stacked in a ladder form (oversize) and then carved down to the required dimension by a pattern maker.

2. The matching walls were made from Fibre Reinforced Plastic of 5 mm thickness.

Figure 4.8 Supplomontary Cascados Blade.

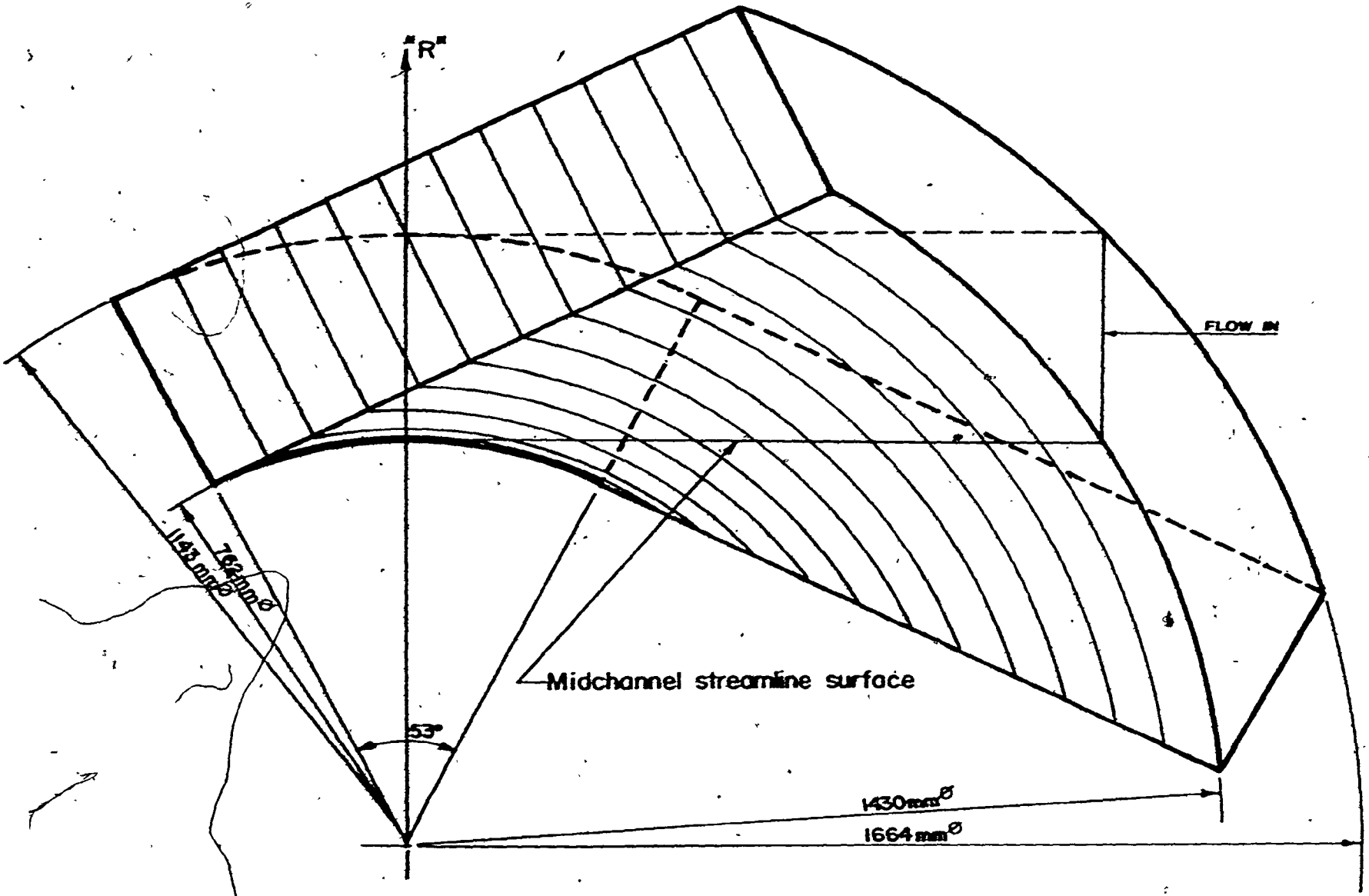

Figure 4.9 The Inlet Duct.

The walls were made in three parts: an inner and an outer part to allow the removal of the mould and surface finishing, and a 90° sliding segment at the inner wall for inlet flow traversing.

4.2.5 The Boundary Layer Suction Chambers

On the annular walls of the inlet duct at an axial distance of 67 mm from the leading edge of the test section, there are located two chambers ((5,6) on Figure 4.2) for boundary layer control. The boundary layer suction is applied through a set of 2 mm diameter holes distributed on the annular walls. The layout of the location of the holes on the inner and the outer walls are shown in Figure 4.10. The rows are inclined to the streamline directions to provide as uniform a suction as possible. The suction is applied using a set of three exhaustor type fans each driven by a 2.5 H.P. motor (1865 watts). The suction is regulated using a gate valve on the exit port from each chamber. The suction system is capable of developing -26" of water (-66.04 cm) in the chamber at the hub side and -15" of water (-38.10 cm) at the casing side.

4.3 The Annular Cascade Section

The annular cascade shown in Figure 4.11, has an inner radius of 381.5 mm and an axial length of 193.5 mm and extends over 45° circumferential pitch. The cascade

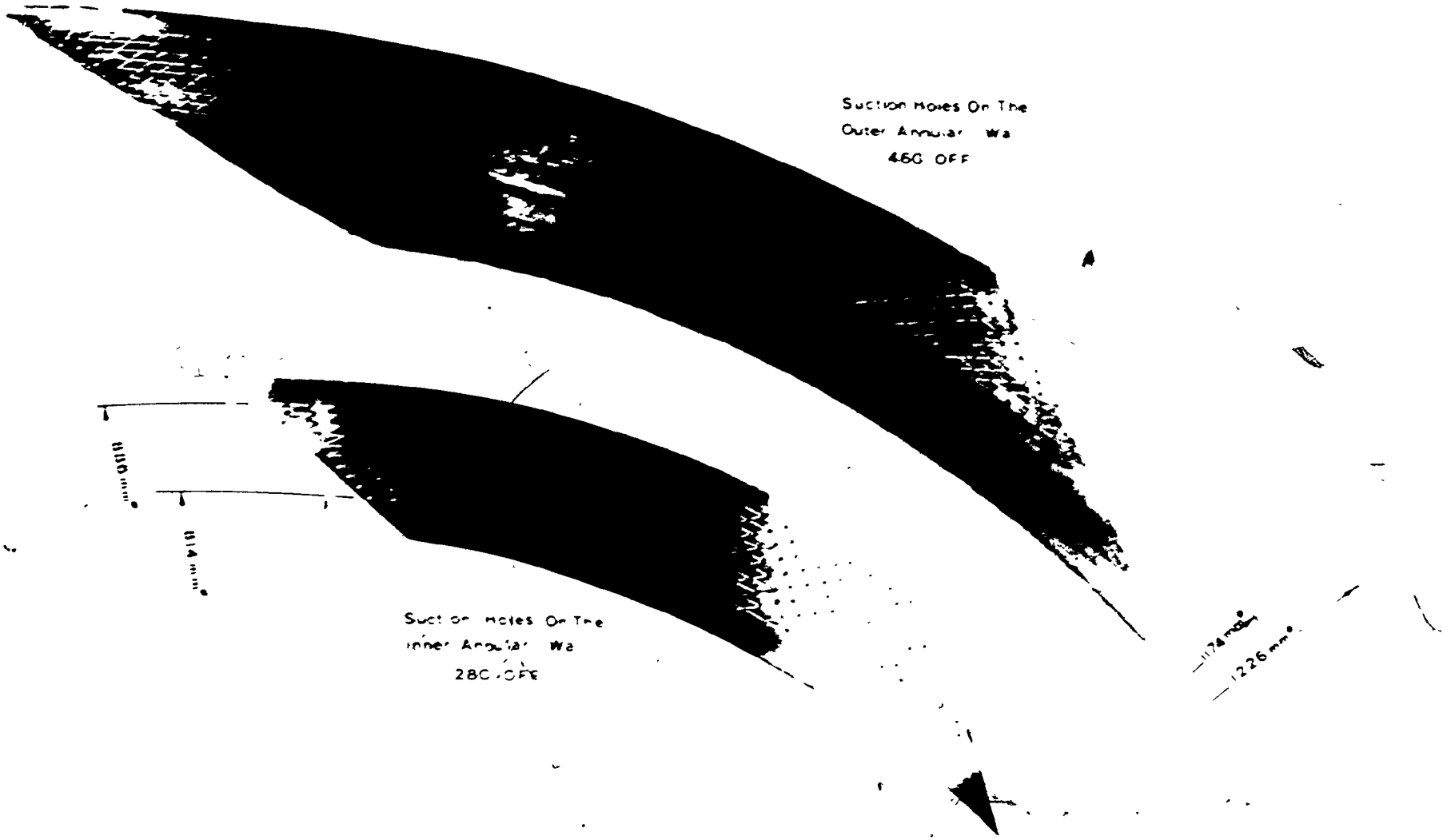
Suction Holes On The
Outer Annular Wa
460 OFF
Suct on Holes On The
inner Annular Wa
280 OFF
1226 mm

Figure 4.11 The Annular Cascade Section.

consists of four identical blades (three flow passages of 15° each). The two centre blades, made of clear acrylic plastic, were instrumented (Chapter 5) for static pressure measurements. The outer two blades, manufactured of aluminium, were used as side walls. The cascade geometric parameters are given in Table 4.1. Figures 4.12 and 4.13 show the orientation of the blades in the annular section. The radial line marked "R" was used as a reference for the circumferential locations.

The test blades (Figures 4.14 and 4.15) are cylindrical and of the flat back type. The blade profile was designed by Malhotra [52] and tested by Stannard [53] in a blow down wind tunnel at high pressure ratios. The blades were manufactured by the division of Mechanical Engineering, National Research Council in Ottawa.

The annular walls were made of 12 mm clear acrylic plastic to facilitate flow visualization. The blades were installed with the leading edges in the radial direction. The trailing edges of the blades are inclined 6.5° from the radial direction. The corresponding span at the trailing edge is 196.5 mm compared with 190.5 mm at the leading edge.

4.4 The Exit Duct

Similar to the inlet duct, the exit duct (Figure 4.16) was designed to provide uniform exit angle. The annular

Text continues on page 66.

Table 4.1

Cascade Geometric Parameters

Blade Chord	214 mm
Blade Axial Chord	188.5 mm
Blade Height at the Inlet	190.5 mm
Blade Height at the Exit	196.5 mm
Blade Turning Angle	128.5^{o}
Blade Inlet Angle	64^{o}
Blade Exit Angle	64.5^{o}
Blade Aspect Ratio	0.904
Cascade Aspect Ratio (Height/Axial Chord)	1.0
Pitch to Axial Chord Ratio at Middle Diameter	0.66
Middle Diameter to Blade Height Ratio	5.0

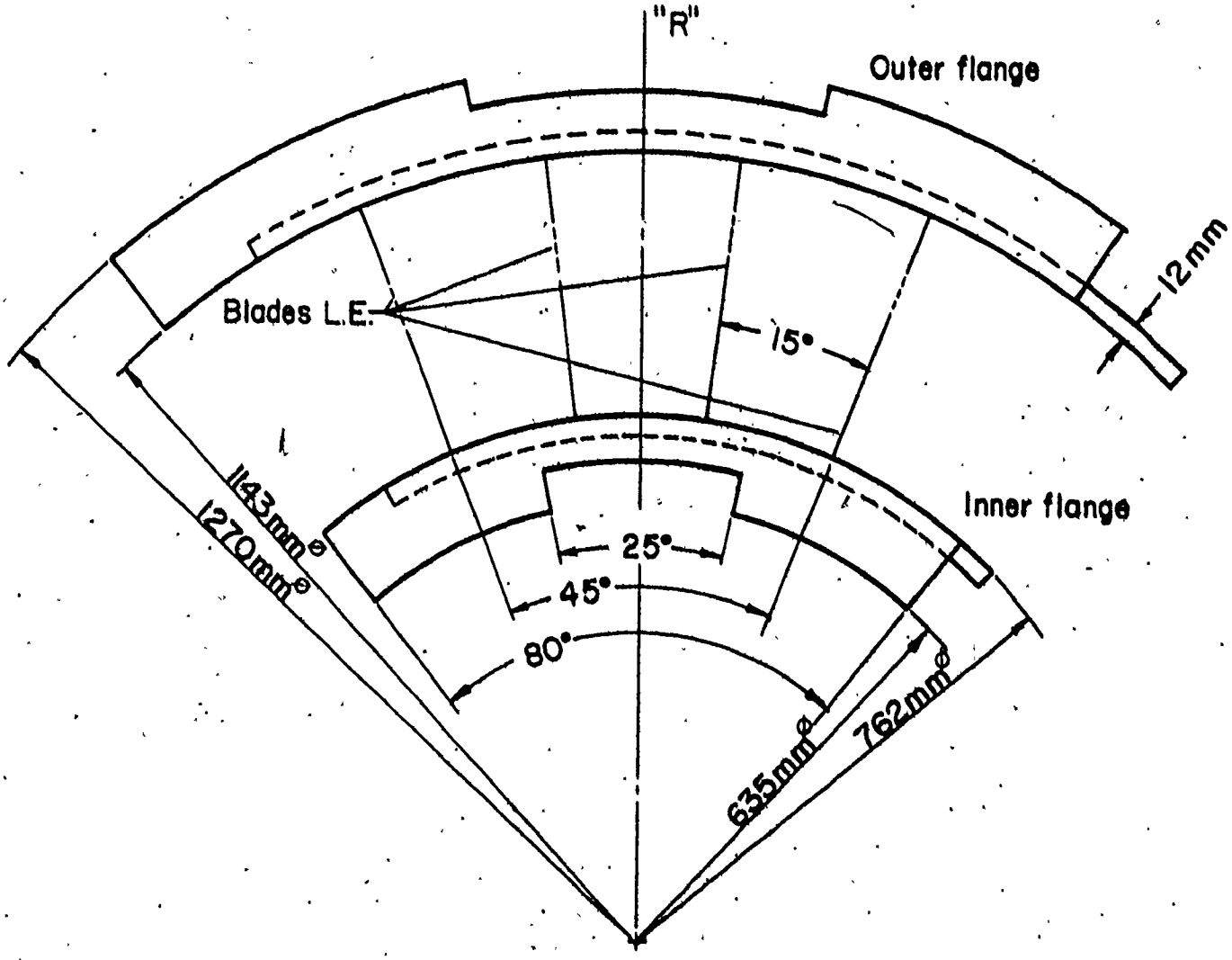

Figure 4.12 Orientation of the Leading Edges in the Test Section.

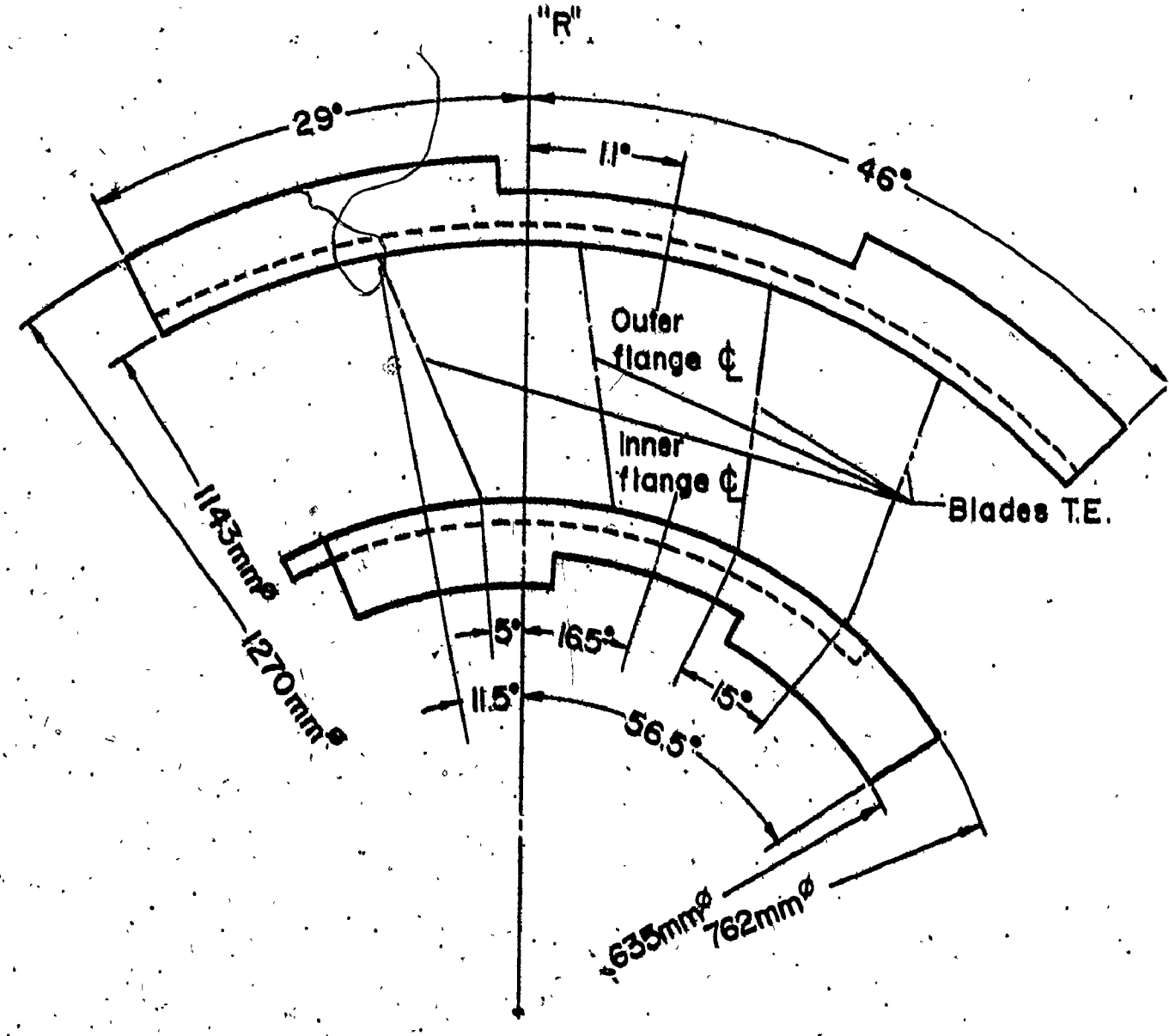

Figure 4.13 Orientation of the Trailing Edges in the Test Section.

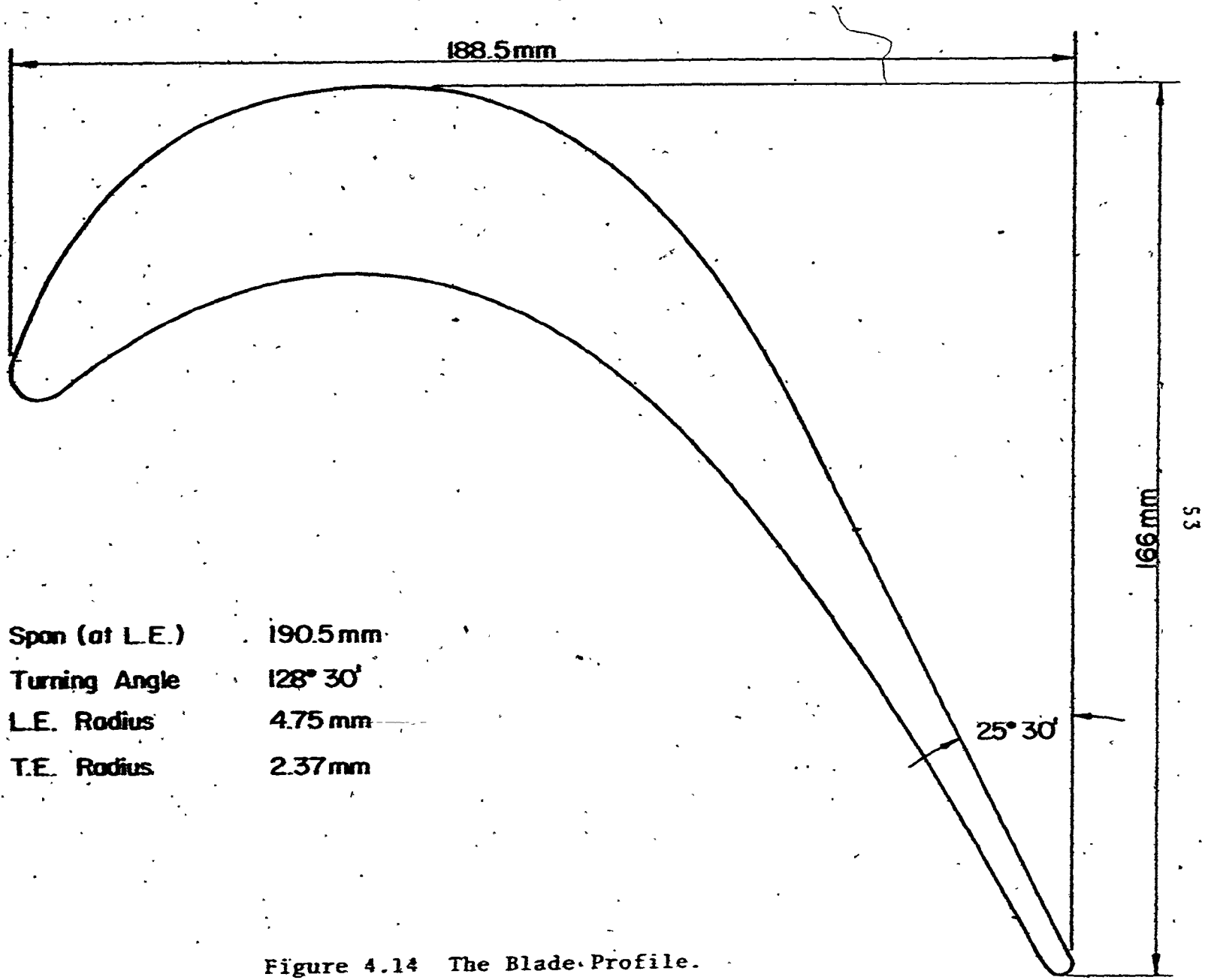

Span (at L.E.)	190.5 mm
Turning Angle	128° 30'
L.E. Radius	4.75 mm
T.E. Radius	2.37 mm

Figure 4.14 The Blade Profile.

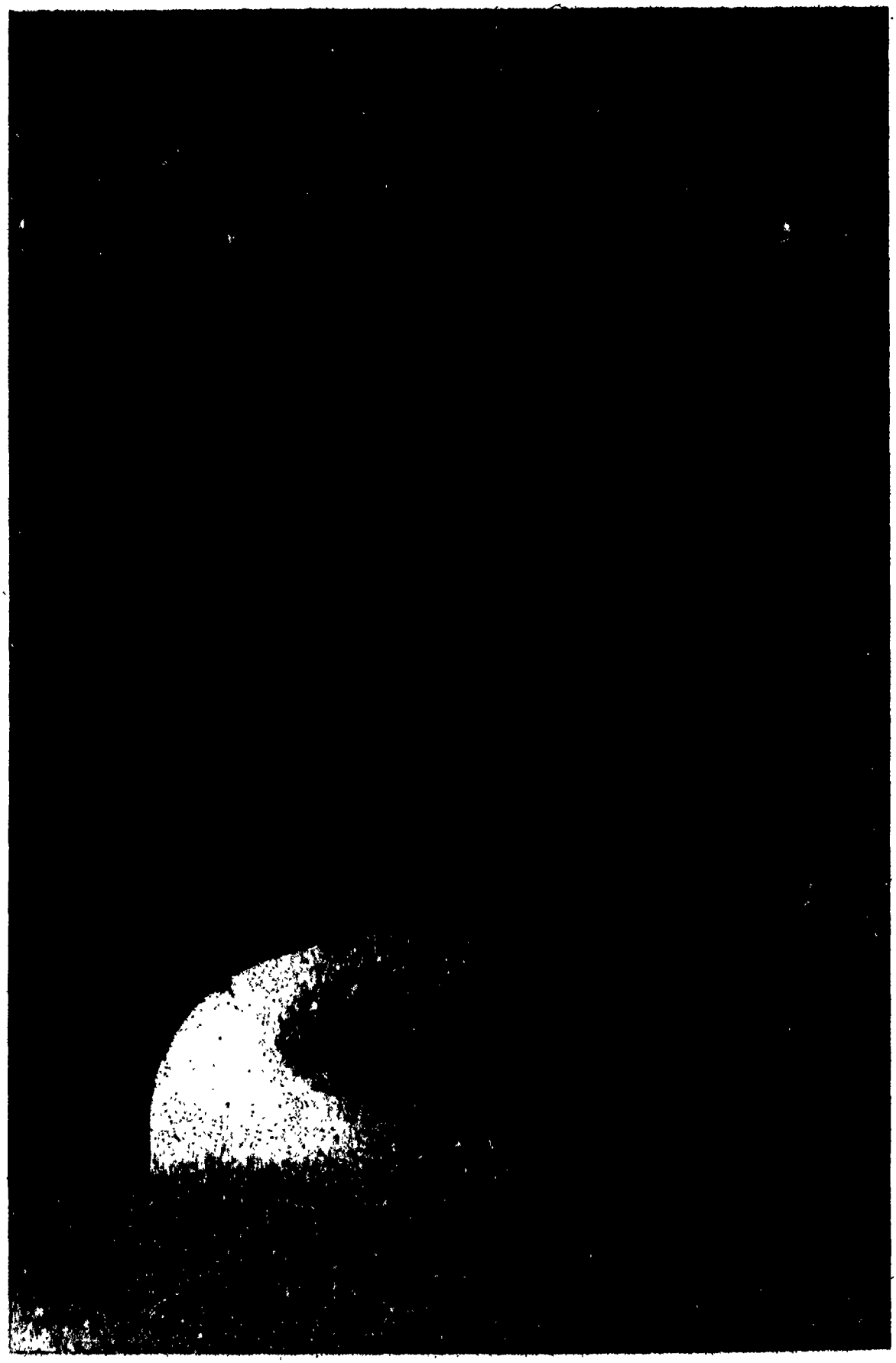

Figure 4.15 Blade Configuration.

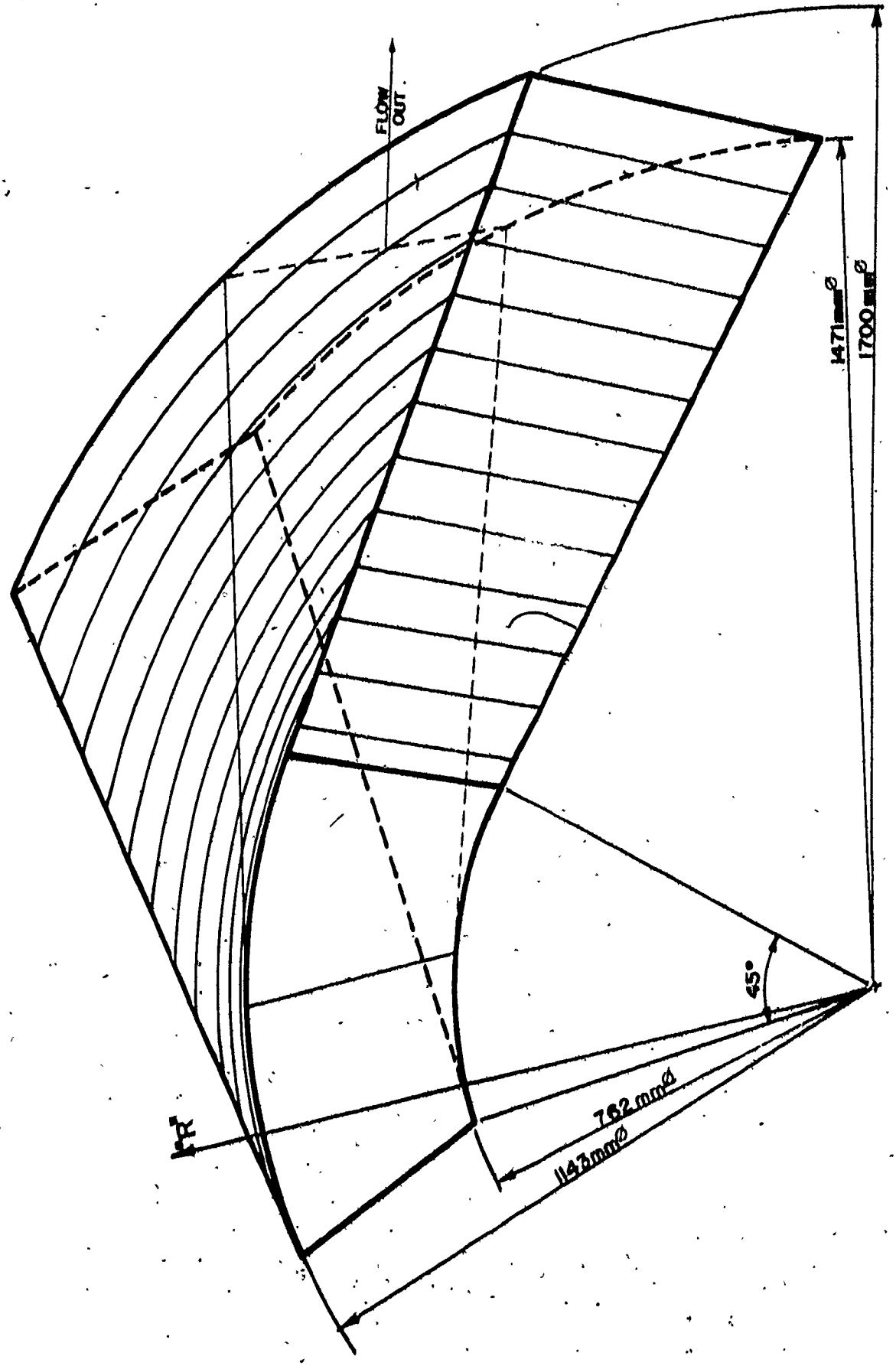

Figure 4.16 The Exit Duct.

boundary surfaces are generated by the rotation of straight lines extending from the blade trailing edge, and inclined at 61.5° to the axial direction. The two generating lines, being non coplanar give rise to a small twist in the blade walls. The mould for the exit duct was manufactured from high density foam using a numerically controlled machine.

4.5 The Test Rig Air Supply

The general layout of the apparatus and measuring instrumentation is shown in Figures 4.1 and 4.18. The air flow is induced using a Sheldon Type XB 19 exhaust fan. The fan is capable of delivering a discharge of 19000 ft³/min. (538.6 m³/min.) against a six inch static head of water (15.4 mm) at 1738 revs/min, and 18.6 Brake Horse Power (13.9 kw). For preliminary testing the fan was driven by a 30 Horse Power (11.2 kw) Greenwood and Batley steam turbine. The fan speed was controlled by means of a Heenan and Froude water brake dynamometer on the turbine shaft. The fan was connected to a plenum chamber through a 90° bend, and fitted with a straightener section and a by-pass control on the fan inlet. The use of the steam turbine as a prime mover was thought to have the advantage of constant fan speeds over extended periods of time. However, intermittent failure of the condenser pump was detected which led to some fluctuations in the fan speed. It was therefore decided to mount a D.C. motor with a pulley belt

Figure 1.6 Overall View of Test Rig and Instrumentation.

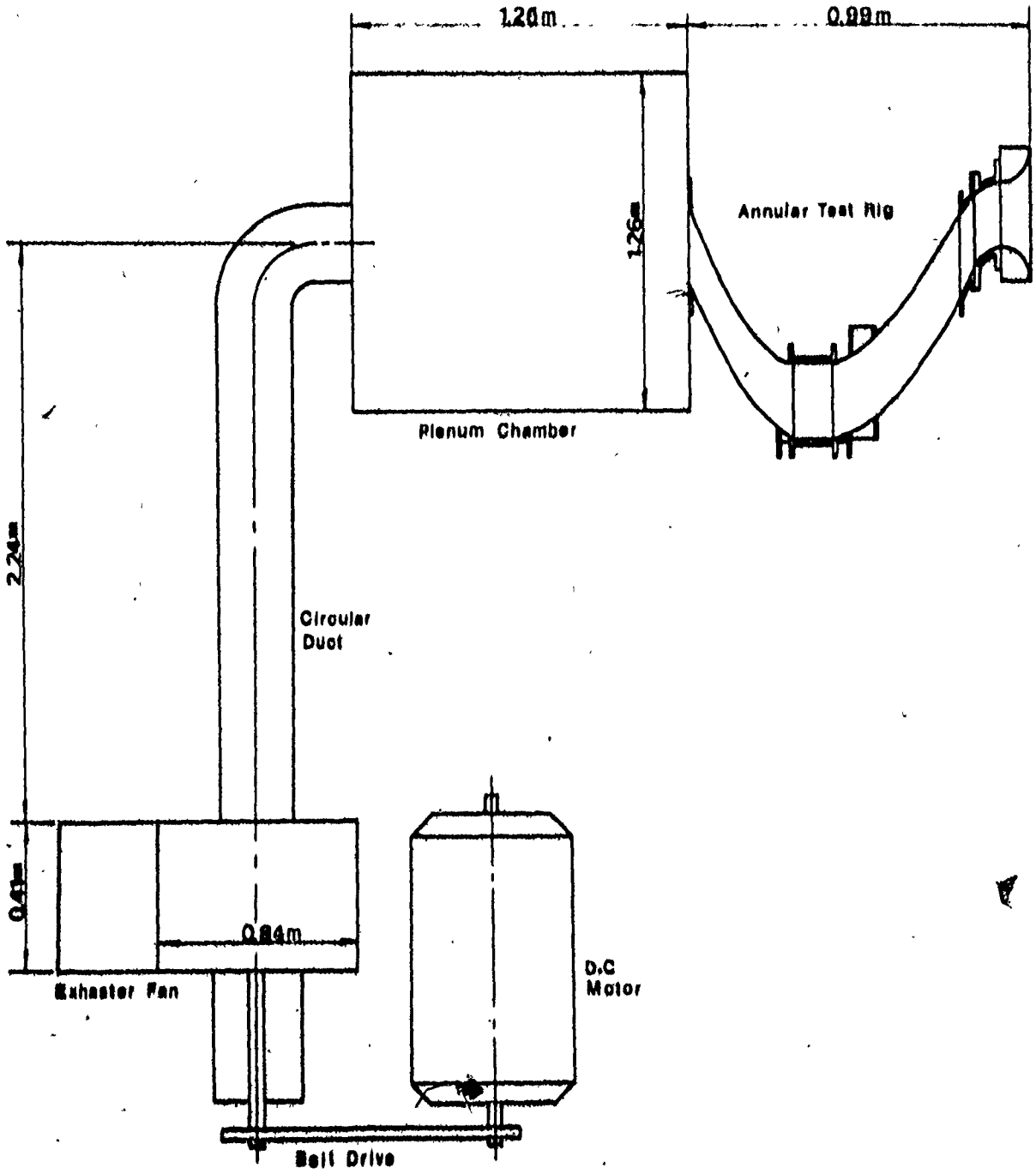

Figure 4.18 Test Facility General Layout.

arrangement to drive the fan. The motor has a maximum power output of 24 Brake Horse Power (18 Kw) at 3000 revs/min. The motor speed can be accurately regulated by a power-stat (up to 0.2% of the operating test speed).

CHAPTER 5

INSTRUMENTATION

The study of the cascade performance required the measurement of the flow parameters at the inlet and the exit from the cascade as well as the measurement of the static pressure on the walls of the centre blade passage. The assessment of the qualitative behaviour of the flow was obtained through the use of flow visualization techniques.

The basic instrumentation for the annular rig can be classified as follows:

1) Instrumentation for the main flow upstream and downstream of the cascade.

2) Instrumentation for boundary layer measurements upstream and downstream of the cascade.

3) Instrumentation of the blade passage.

4) Instrumentation for flow visualization.

5.1 Main Flow Instrumentation

The main flow traverses were conducted at two measuring stations located at an axial distance of 27.5 mm upstream and downstream of the cascade test section. At each measuring station provisions were made for both radial and circumferential scanning. Due to the specific geometry of

the inlet and exit ducts, the effect of the duct shape was further studied.

5.1.1 Geometric Considerations

Figure 5.1 shows schematically the projection of the leading and trailing edges of the blades on the measuring stations for a certain circumferential cross-section. An isometric representation of the general configuration at the leading edge is shown in Figure 5.2. The stream surface $a_1b_1b_2a_2$ projecting from the leading edge intersects with any plane (B-B) normal to the axial direction at a straight line b_1b_2 parallel to the leading edge a_1a_2. The line of intersection b_1b_2 deviates from the radial direction O_1b_1 or O_1b_2 as the distance O_1O increases. The inlet measuring station is located at an axial distance O_1O of 27.5 mm upstream of the leading edge and the projection of the leading edge at this location b_1b_2 subtends an angle δ_1 of 2.81^0. An axial projection of the configuration is given in Figure 5.3. Since the probe traverses radial positions at an angle δ to b_1b_2 the indicated yaw angle y_1 and pitch angle p_1 would be different from the actual values at the leading edge namely y and zero pitch.

Referring to Figure 5.4,

$$\tan y = \tan y_1 \cos \delta \qquad (5.1)$$

$$\tan p_1 = \tan \delta \cos y_1 \qquad (5.2)$$

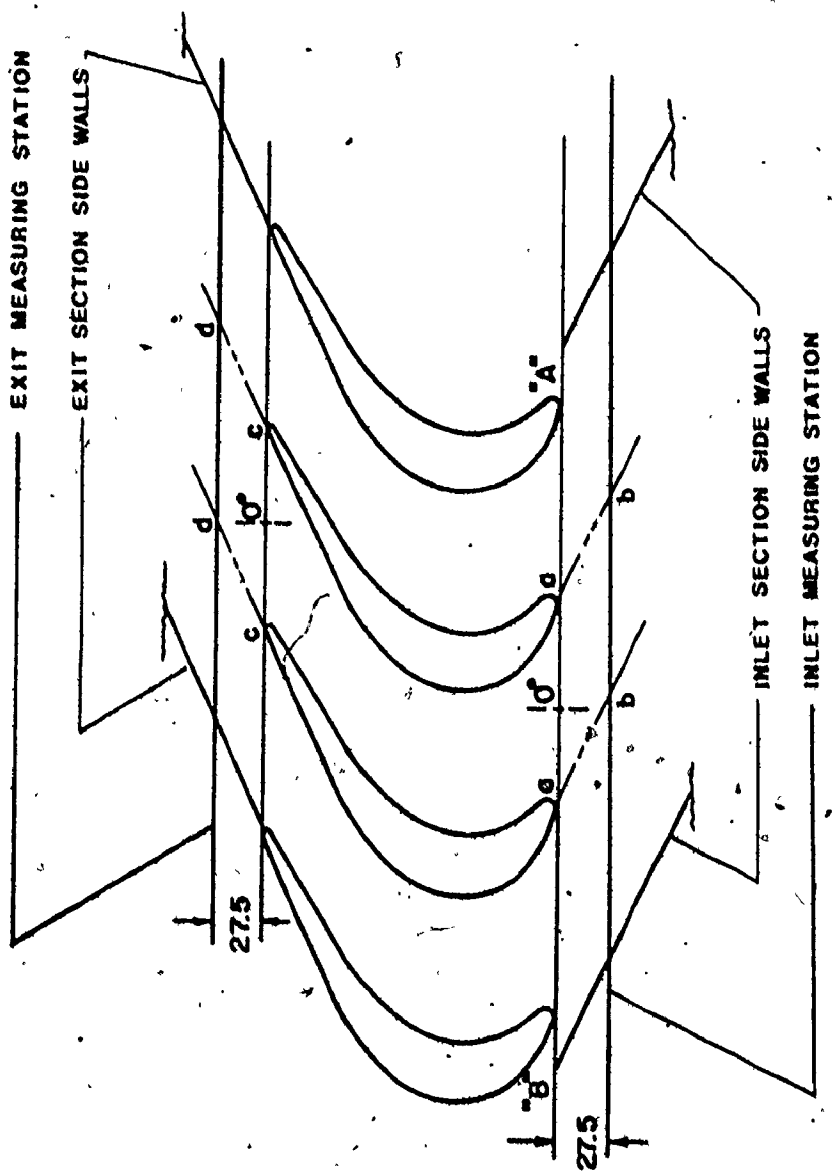

Figure 5.1 Inlet and Exit Measuring Stations.

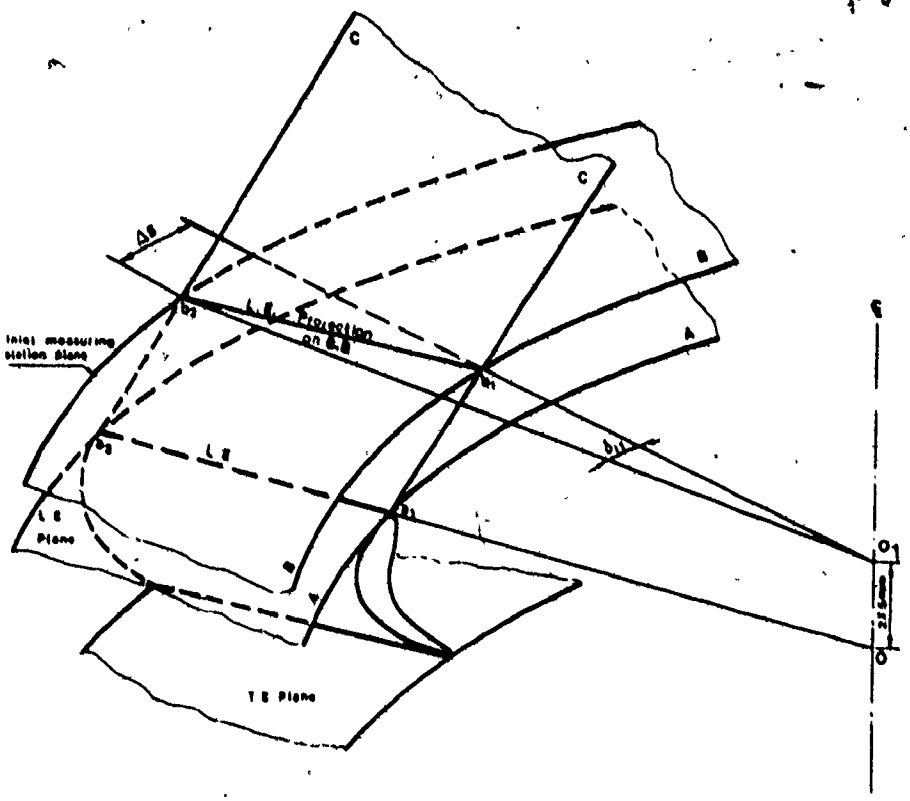

Figure 5.2 Inlet Measuring Station (Isometric View).

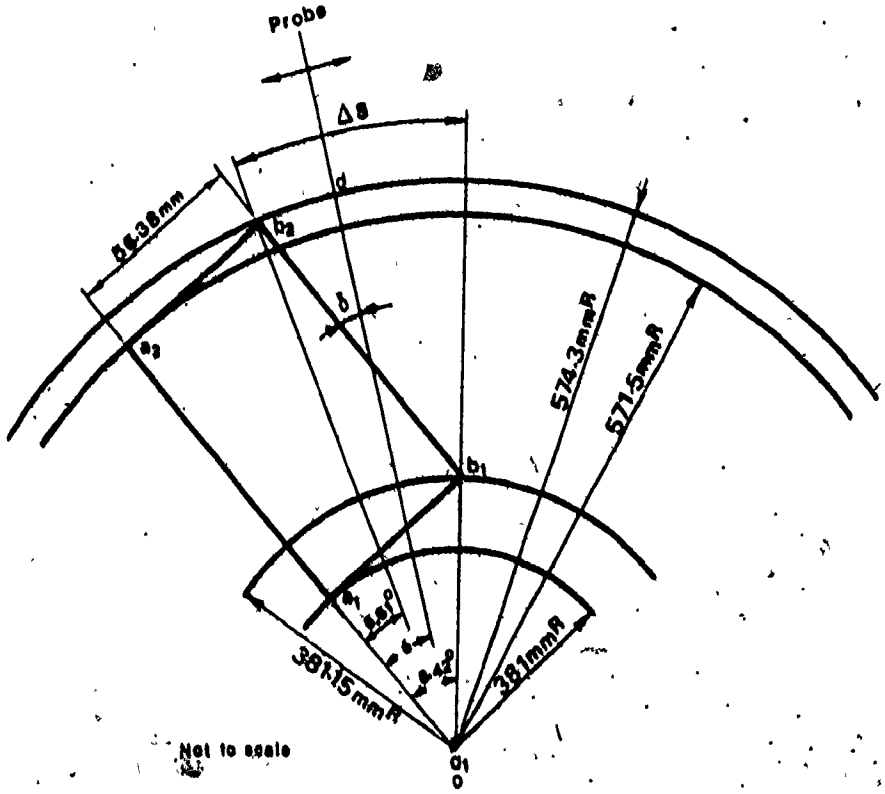

Figure 5.3 Inlet Measuring Station (Axial Projection).

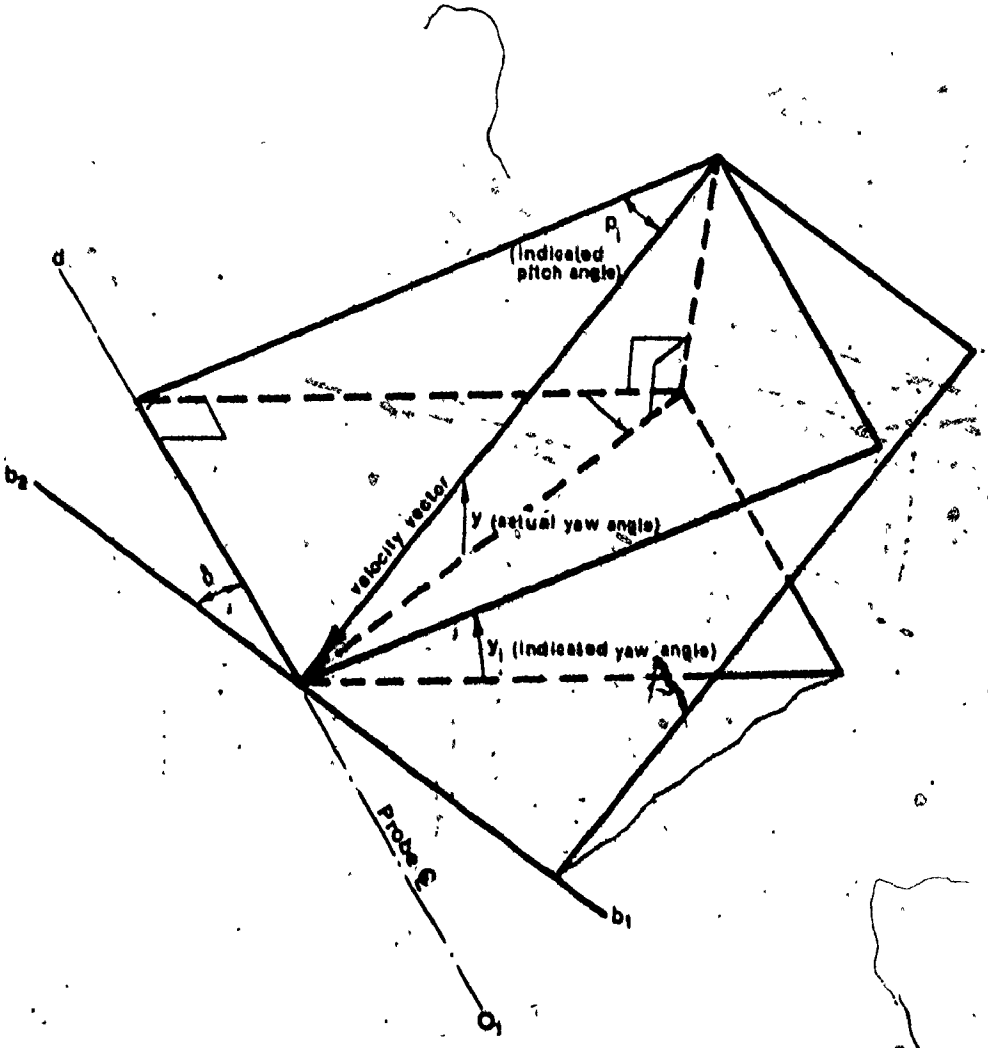

Figure 5.4 Actual and Indicated Pitch and Yaw Angles.

It is estimated that the probe would indicate a pitch angle of 7.56° (with reference to the axial direction) at the hub and 5.06° at the casing as compared to zero pitch at the leading edge plane. The indicated yaw angle is 63.75° at the hub and 63.89° at the casing as compared to blade inlet angle 64° at the leading edge plane.

Similar calculations were carried out at the exit measuring station (see Figure 5.5 and Figure 5.6). The indicated pitch angle was -7.4° at the hub and -4.82° at the casing. The indicated yaw angle was 64.27° at the hub and 64.4° at the casing, compared to 64.5° at the trailing edge plane. It should be noted that the centre of the passage at the inlet measuring station, faced an angle of 8.41° at the hub and an angle of 5.61° at the casing measured from the centre of the passage (the reference direction "R" as shown in Figure 4.12) at the leading edge plane.

5.1.2 The Traversing Gear

The traversing gear consists of two main parts:

1) A sliding annular segment for circumferential traversing (see Appendix 1).

2) A linear component for radial traversing (see Figure 5.7).

The sliding annular segment had a pointer that traces a graduated scale on the frame of the test section

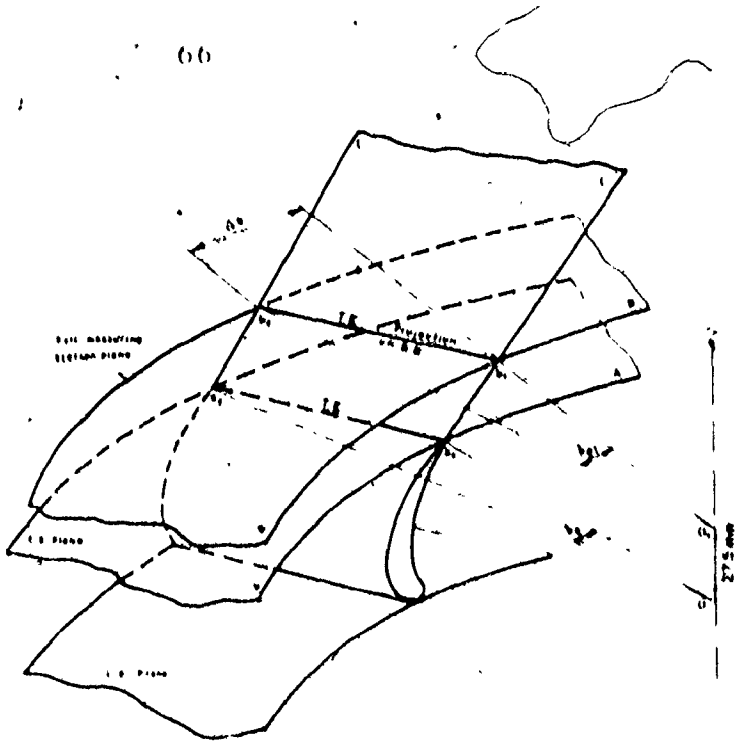

Figure 5.5 Exit Measuring Station (Isometric View).

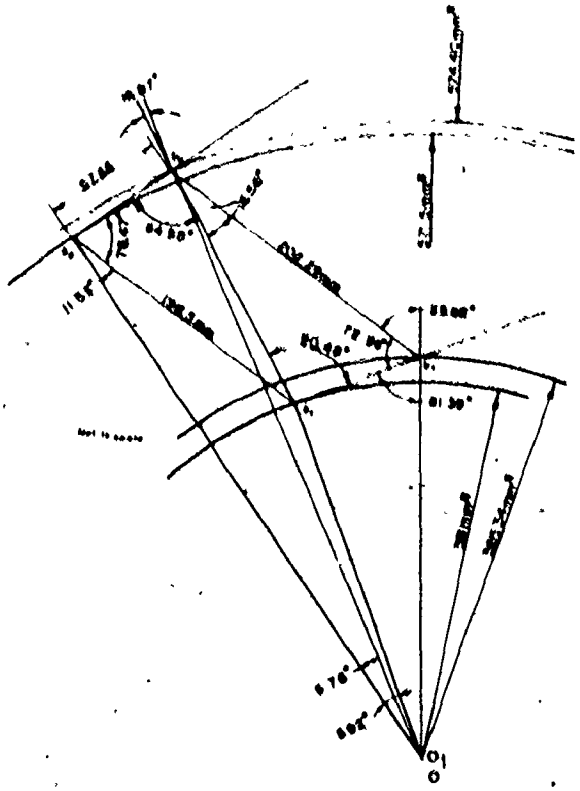

Figure 5.6 Exit Measuring Station (Axial Projection).

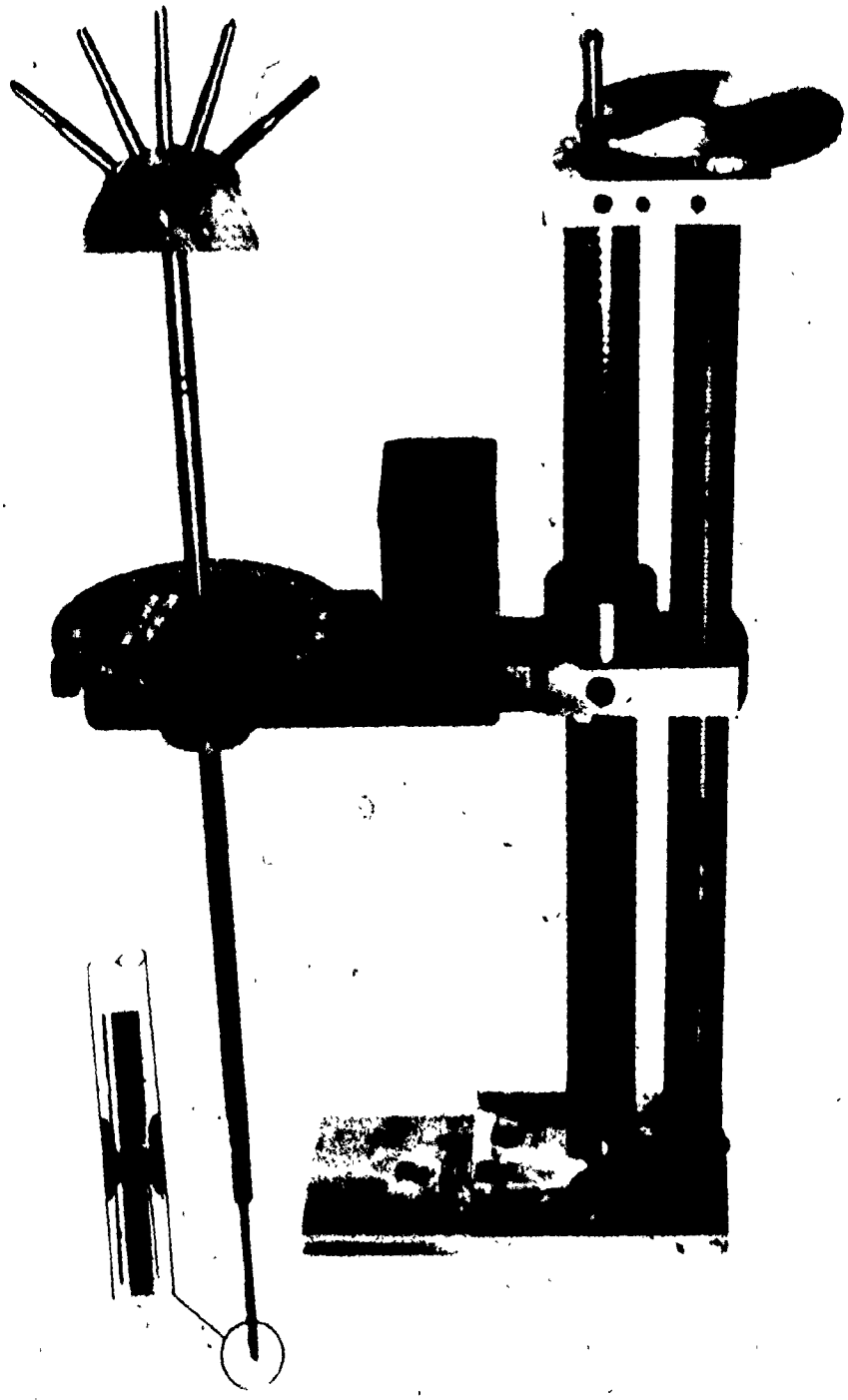

Figure 5.7 The Traversing Gear (Linear Component) and the Three Dimensional 5 Hole Probe.

and can locate circumferential positions to an accuracy of 0.5^{o}. The linear component, Figure 5.7, is mounted on the sliding segment. It has a linear range of 250 mm with a thread advance of 0.05 inch (1.27 mm) per revolution of the driving wheel. The wheel is further graduated into 50 divisions thus allowing for fine positioning to 0.001 inch (0.0254 mm).

A turntable with a 360^{o} protractor is mounted on the traverse for yaw angle measurements. The protractor is provided with a vernier scale which enables angle measurement to within $\pm$ 0.2^{o} accuracy. A potentiometer was mounted on the spindle of the protractor with the cup fixed to the traverse to facilitate another means of measuring the yaw angle. The calibration curve for the potentiometer is given in Figure 5.8.

5.1.3 Three-Dimensional Probe, Pressure and Flow Angle Measurements

Measurements in the mainstream - at inlet and exit from the cascade - were made using a United Sensor three-dimensional probe of the type DA-125-12P-10-CD. The probe has a sensing head diameter of 0.125 inches (3.175 mm) and a reinforcement tubing of 0.250 inches (6.35 mm) diameter. The probe has five sensing ports connected to five pressure take off taps marked 1 through 5. The centre tap, 1, is for total pressure measurements. The lateral taps 2 and 3 are for nulling and static pressure measurements.

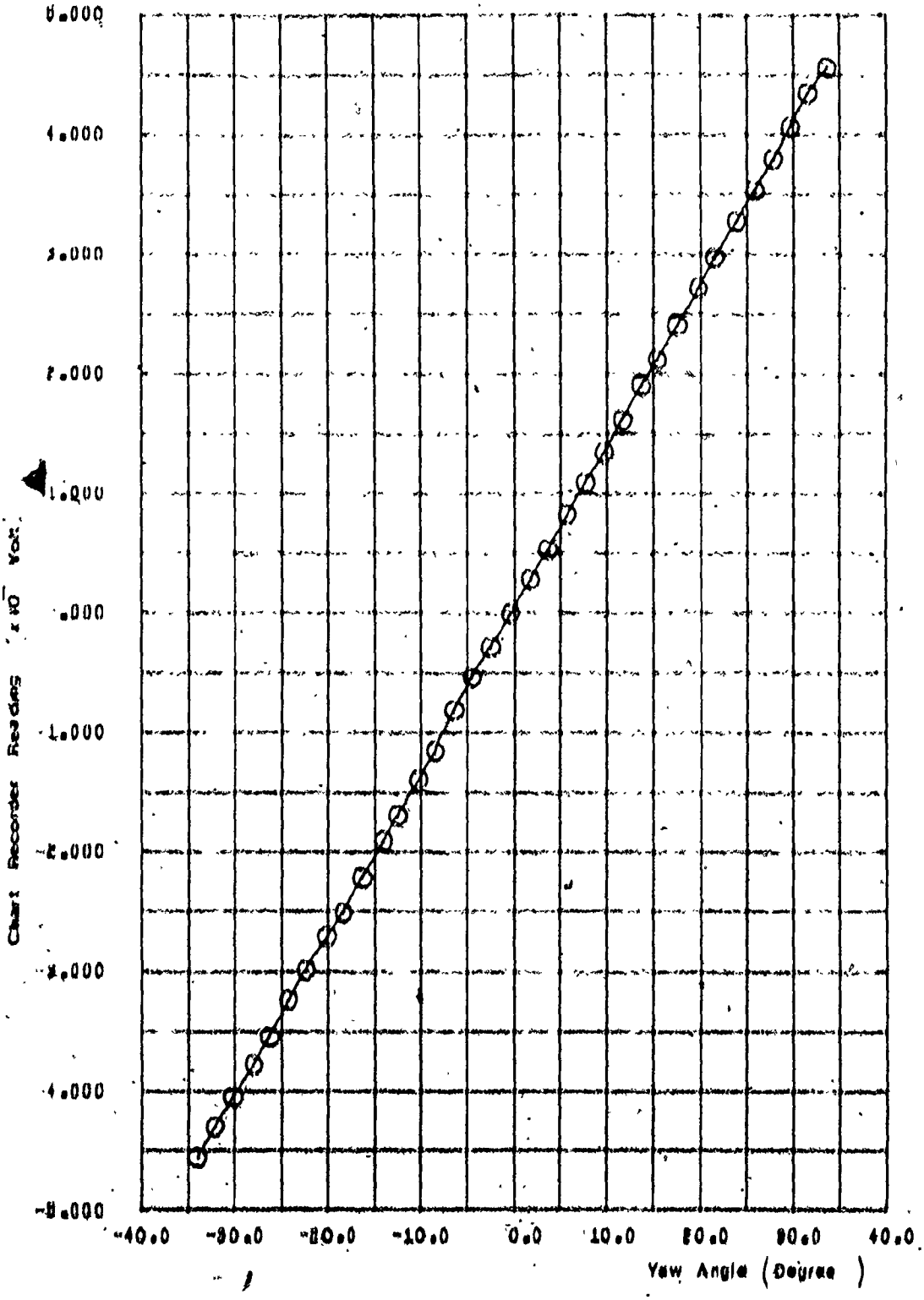

Figure 5.8 Potentiometer Calibration Data.

The top and bottom taps (4 and 5) are for pitch angle measurements. The probe geometry is shown in Figure 5.7 Calibration curves supplied by the manufacturer for the three dimensional probe are given in Appendix (2). Total pressure measurements were accurate to within 0.5% over an angular range of $\pm$ 10°. Measurements were taken by rotating the probe until the pressures indicated by the lateral taps 2, 3 were equal. The pressure indicated by the five taps and the yaw angle were then recorded. The calibration curves fitted with polynomials were used to calibrate the static pressure, total pressure, pitch and yaw angles.

The pressures were measured using a Setra Transducer, model no. 237 serial no. 18158. The transducer was a bi-directional differential type with a range of $\pm$ 0.5 lbf/in^2 (35 cm water). Specifications of the transducer are given in Appendix (2). The transducer was calibrated using a Betz manometer with an accuracy of 0.1 mm water. Calibration data is given in Figure 5.9. The output from the transducer was recorded on a Rikadenki chart recorder model B-281L serial no. 59682. The output was checked repeatedly for zero drift on a Hewlett Packard multi-meter type 34702A. Calibration was repeated frequently and excellent repeatability was obtained throughout the calibration tests.

The pressure leads from the probes were connected to a Scanivalve model 48D3 S/N 453 capable of handling 48

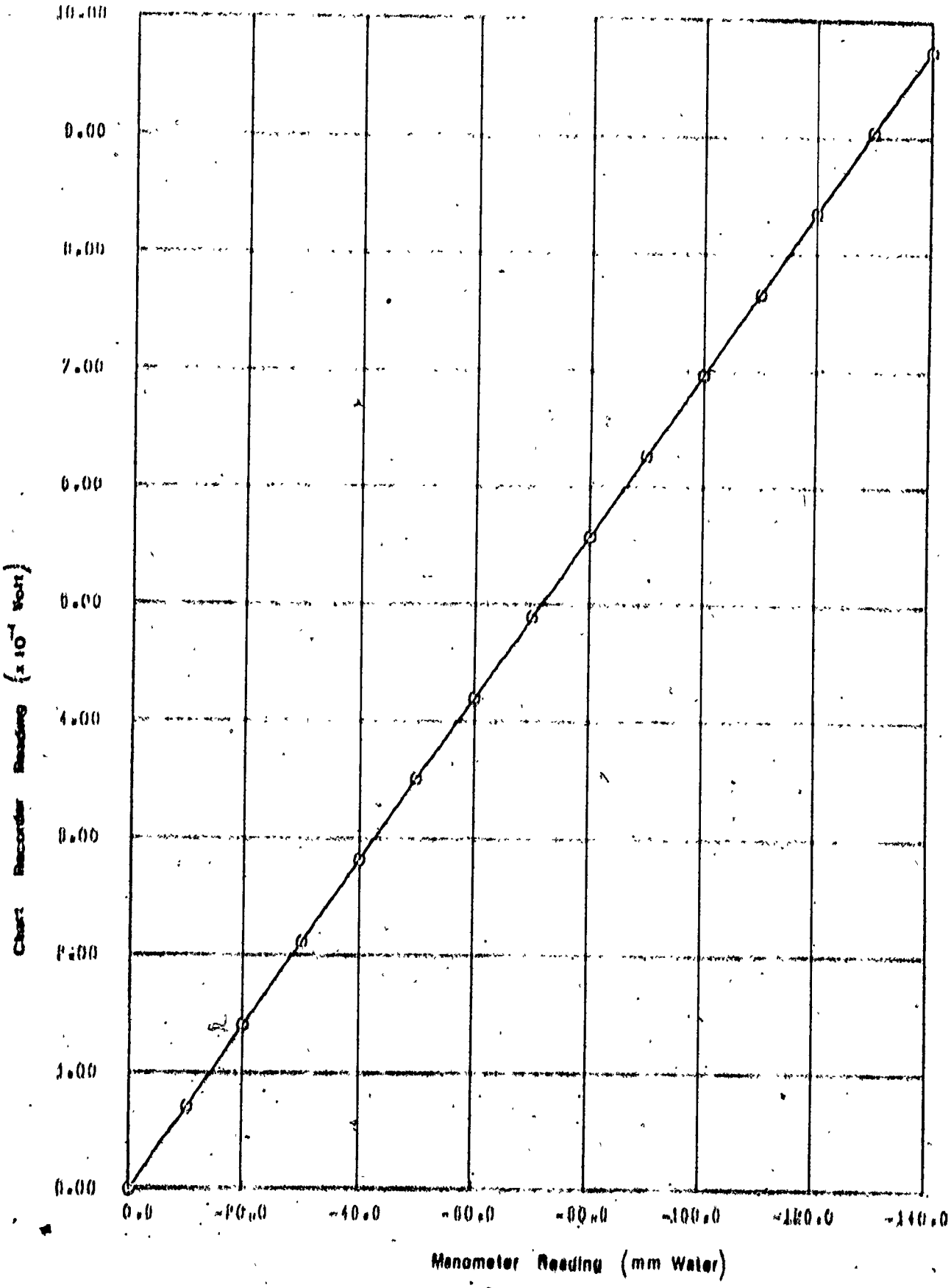

Figure 5.9 Transducer Calibration Data.

separate inputs. The main access to the Scanivalve was through an intermediate connector panel which facilitated connection to both the instrumentation and the model.

The chart recorded data was digitized using a Ruscum Logics Graph Digitizer (model -11). The digitized data was recorded on paper tapes and used with the data reduction program given in Appendix (3).

5.2 Boundary Layer Instrumentation

Two probes were manufactured from stainless steel tubing for boundary layer measurements at the hub and the casing. The pitot probes shown in Figure 5.10 were designed to minimize as much as possible the stem effect and were provided with a flattened tip which allowed measurements to be made close to the walls. Static pressure taps were drilled in the annular wall in the plane of the probe tip. Static taps on the inlet section, on the hub and casing were located at circumferential positions 4^{0} to 10^{0} at 1^{0} intervals. Total pressure measurements were made using the pressure transducer in conjunction with an air damper to minimize the fluctuations in the output signal. At each reading time was allowed for the signal to stabilize. The average damped signal was compared with the averaged undamped signal several times and good agreement was obtained throughout. Static pressures for the boundary layer measurements were recorded using the transducer output.

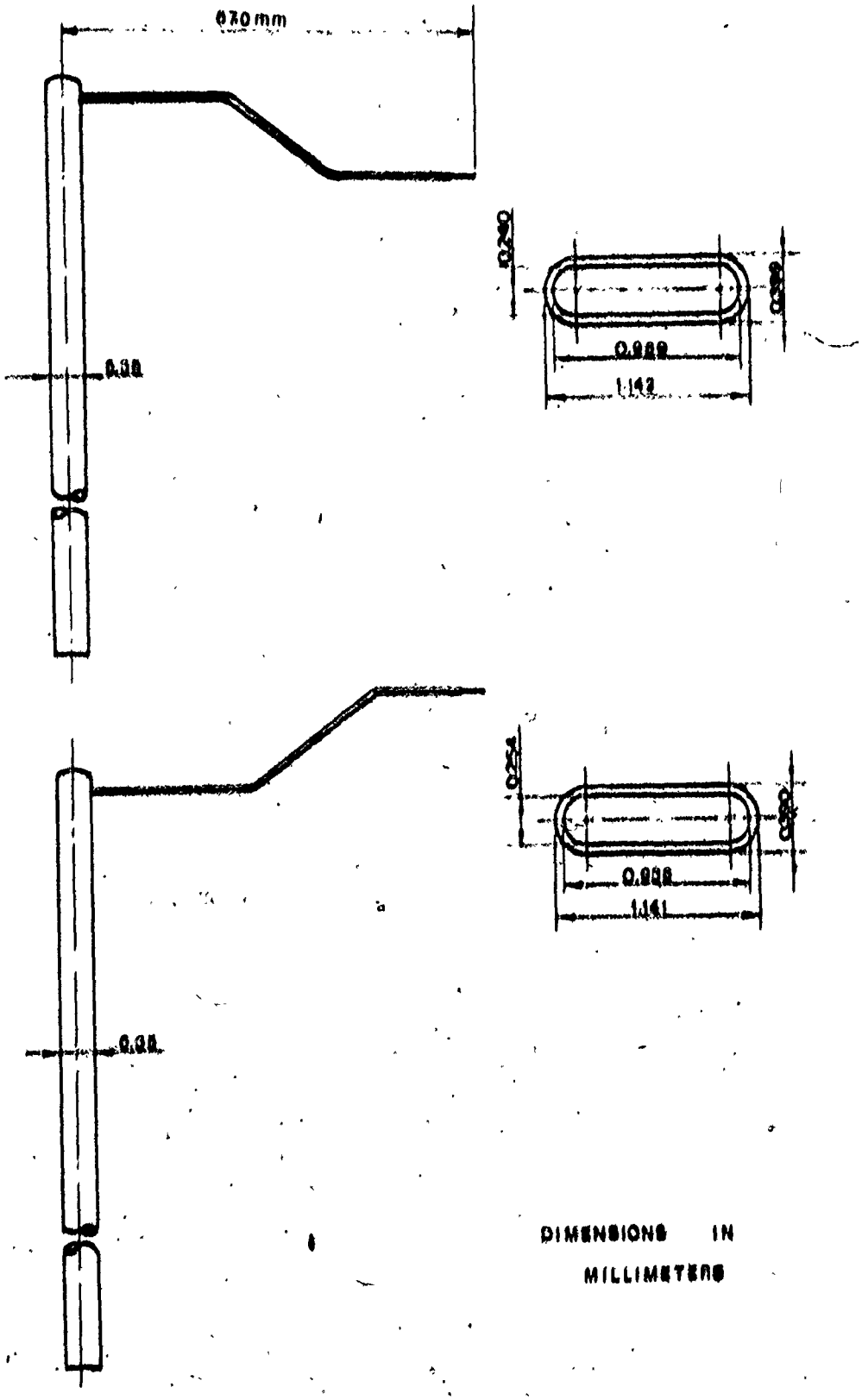

Figure 5.10 Boundary Layer Probes.

5.3 Centre Passage Instrumentation

Provisions were made for static pressure measurements on the walls of the centre blade passage. A total of 130 static taps were drilled at seven axial stations in the test section as shown in Figure 5.11.

5.3.1 Blade Static Taps

The axial and radial coordinates of the static taps on the blades are shown in Figure 5.12 and Figure 5.13 At each station five static taps of 1 mm diameter each are located at different radial positions. Station 1 is located at the blade leading edge. The taps in the first five stations are connected to stainless steel tubes at the blade ends through larger holes (3.7 mm diameter) drilled in the spanwise direction. The stainless steel tubes were inserted into the holes and epoxied to prevent leakage. At station number 6 small grooves were cut into the blade wall opposite from the centre passage. The static taps at this location were connected with stainless steel hypodermic tubing that were extended out of the end of the blades. These tubes were cemented into the grooves and the blade surfaces were refinished to the original blade shape.

5.3.2 Annular Wall Static Taps

The circumferential locations of the static taps

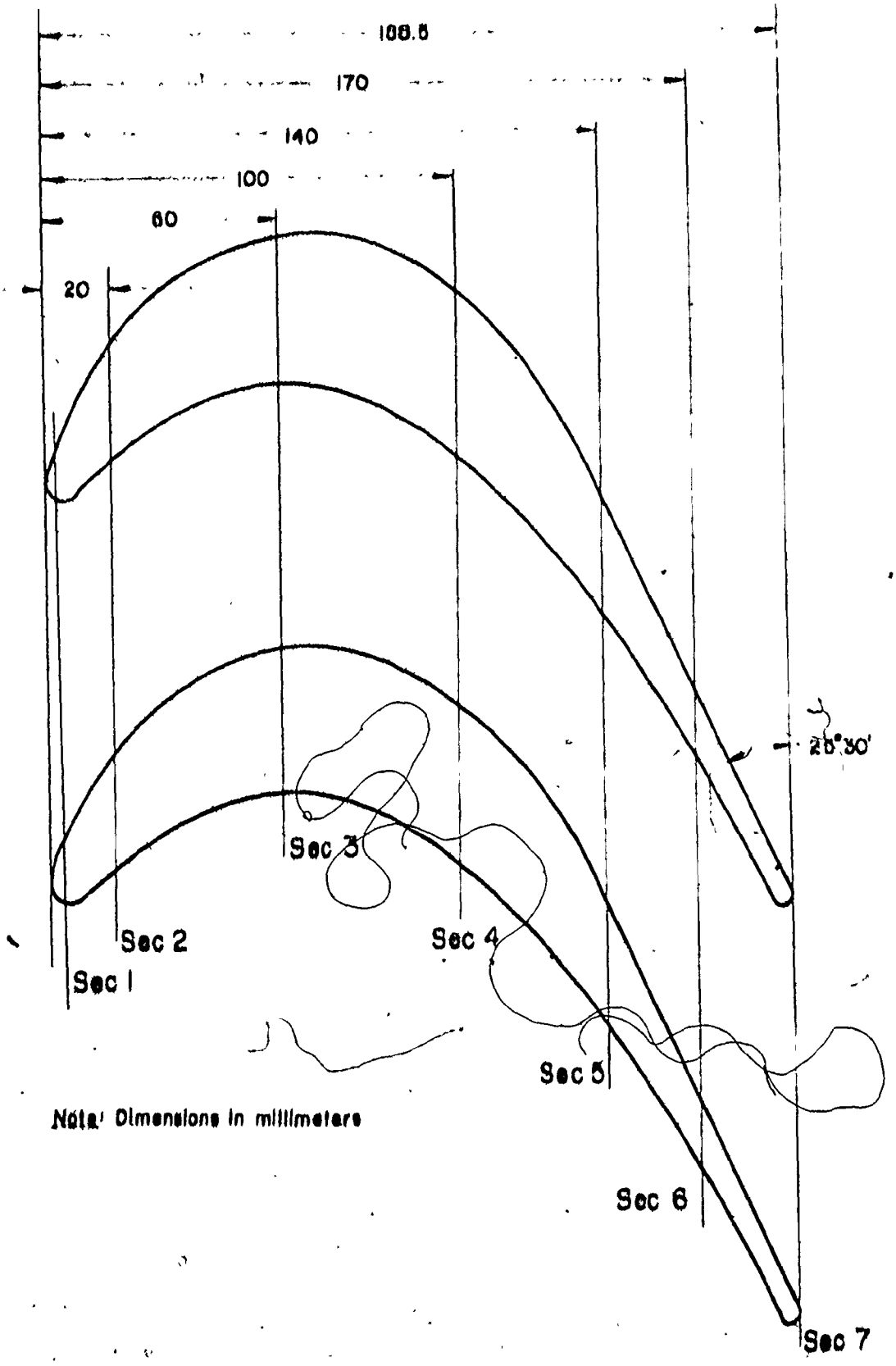

Figure 5.11 Axial Locations of the Static Taps in the Test Section.

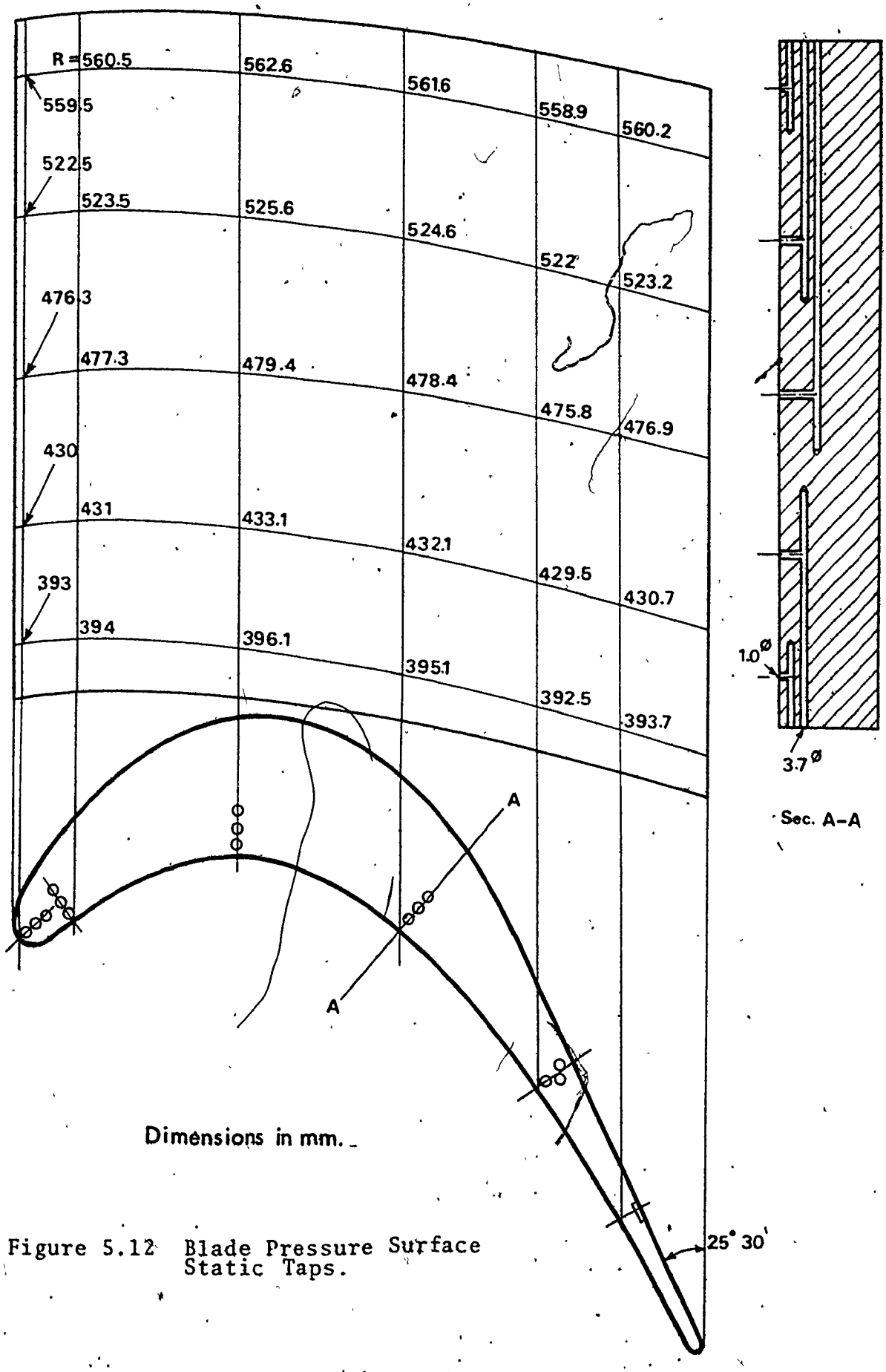

Figure 5.12 Blade Pressure Surface Static Taps.

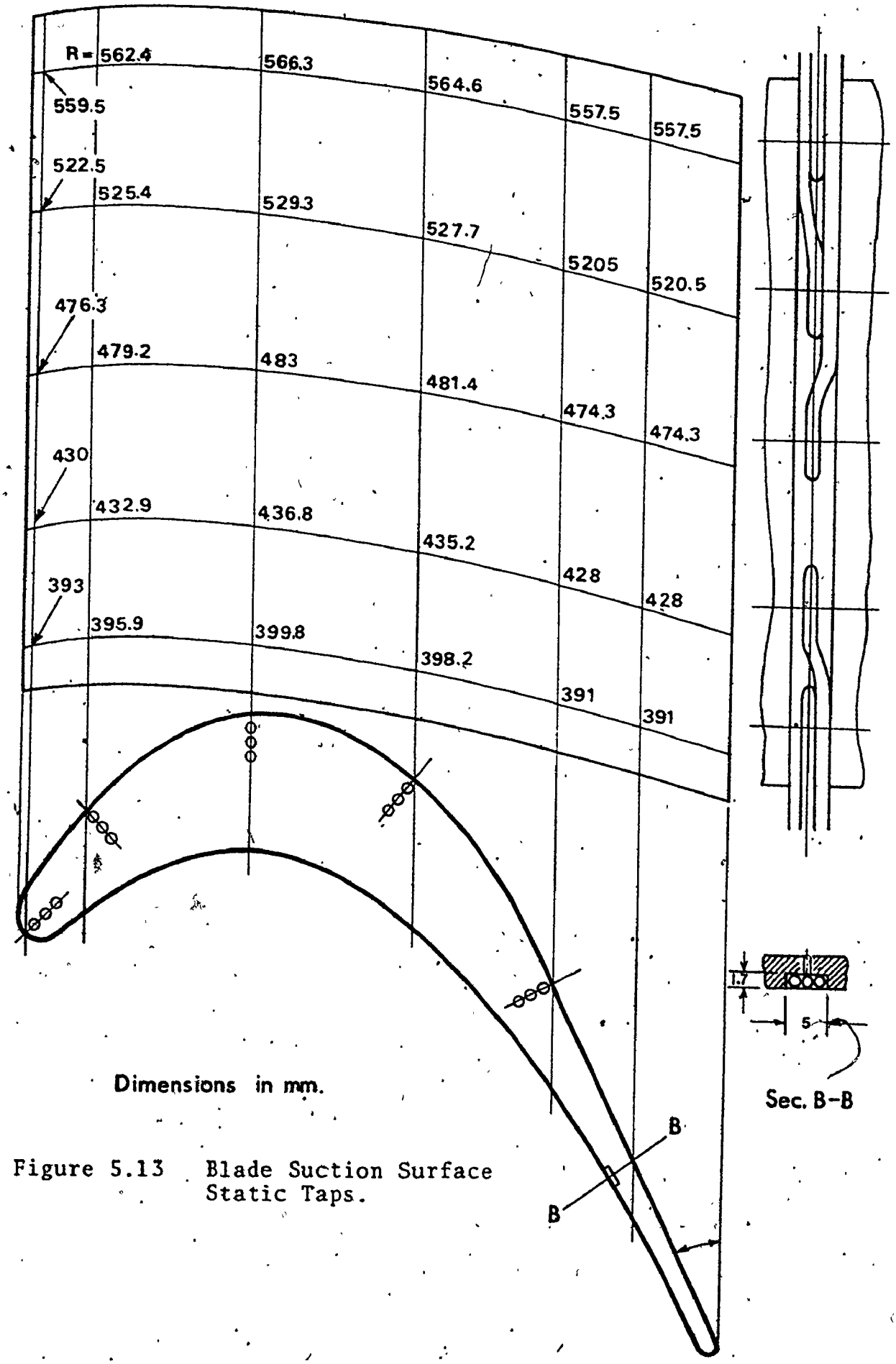

Figure 5.13 Blade Suction Surface Static Taps.

on the annular walls at various axial locations are given in Figure 4.12 and Table 5.1. The centre of the blade passage is the reference direction from which all circumferential locations are measured. The taps were chamfered to minimize the error in the measurements.

The stainless steel tubes at the ends of the blades were connected to two panels that provided permanent sealing of the static taps (unless measurements were being taken) to prevent air flow from the outside into the test section. Each panel is made up of two plastic plates with a soft rubber packing sandwiched in between.

5.4 Flow Visualization Instrumentation

A smoke probe* was used for the flow visualization study, Figure 5.14. The probe uses a mixture of two gases (anhydrous ammonia and sulphur dioxide) that form a dense white cloud of ammonia sulphite downstream of the probe tips. Because of the large mixing zone, rapid diffusion of the smoke does not allow fine tracing of the stream filaments.

---

* Designed by the National Aerodynamic Laboratory at the National Aeronautical Establishment in Ottawa, Low Speed Aerodynamic Laboratory.

Table 5.1

Circumferential Locations of Static Taps on the Annular Walls at Different Axial Positions (Measurements are Referred to the Direction "R" in Figure 4.12)

Section Number		Station Number 1	2	3	4	5
1	Inner Wall	-6.00°	-3.00°	0.00°	3.00°	6.00°
	Outer Wall	-6.00°	-3.00°	0.00°	3.00°	6.00°
2	Inner Wall	-7.25°	-5.15°	-3.05°	-0.95°	6.15°
	Outer Wall	-7.00°	-4.60°	-2.20°	-0.20°	2.60°
3	Inner Wall	-9.75°	-7.75°	-5.75°	-3.75°	-1.75°
	Outer Wall	-8.33°	-6.03°	-3.73°	-1.43°	0.87°
4	Inner Wall	-7.83°	-5.93°	-4.03°	-2.13°	-0.23
	Outer Wall	-7.10°	-4.87°	-7.64°	-0.41°	1.82
5	Inner Wall	-1.00°	1.20°	3.40°	-5.60°	7.80°
	Outer Wall	-2.75°	-3.20°	2.12°	-4.55°	6.88°
6	Inner Wall	6.25°	8.05°	11.45°	14.05°	16.65°
	Outer Wall	2.08°	4.81°	7.55°	10.28°	13.01°
7	Inner Wall	10.50°	13.5°	16.50°	18.50°	22.50°
	Outer Wall	5.00°	8.00°	11.00°	14.00°	17.00°

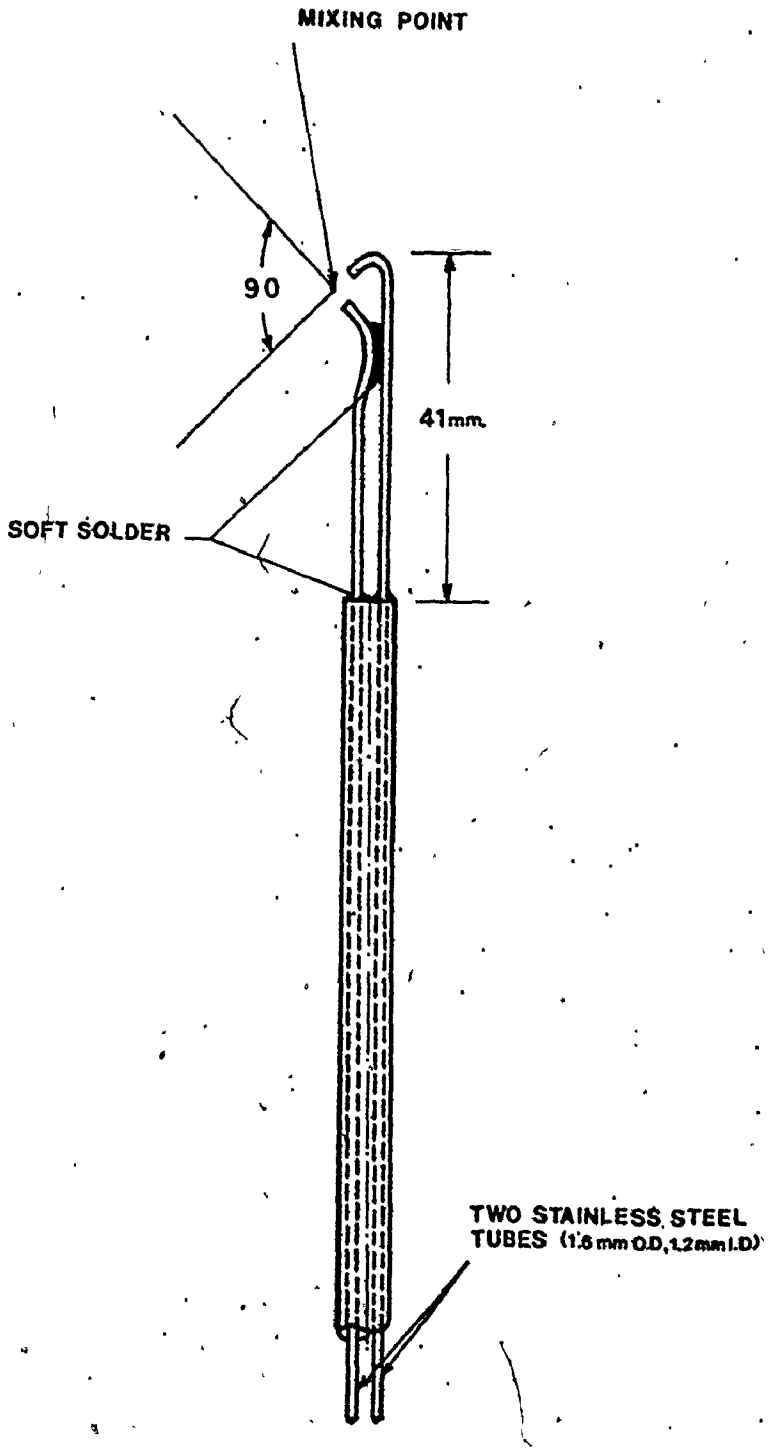

Figure 5.14 Smoke Probe Geometry.

CHAPTER 6

SCOPE OF INVESTIGATION

The literature review presented in Chapter 3 has indicated that the dependence of the turbine cascade performance upon the characteristics of inlet flow boundary layer is a problem of fundamental interest. In this study a series of tests were conducted through which the boundary layer displacement thickness was varied on the inner and outer walls of the cascade and the corresponding flow parameters at the exit plane of the cascade were measured. The operating speed at the cascade inlet was kept constant at 112 ft/sec (34.14 m/sec). This speed corresponds to a Reynolds number of 4.73×10^5 based on the blade chord. In most of the test data reported in the literature the Reynold's number falls in the range of 10^5 to 10^6. The series of tests can be summarized as follows:

1) The inlet main flow was traversed in the radial and circumferential directions. The mid span periodicity was observed and adjusted where necessary. The boundary layer displacement thickness was varied at the inner and outer walls. The main flow was checked in the radial direction under maximum suction conditions at each wall. A control parameter was established to correlate the boundary layer displacement thickness to the pressures in the

corresponding suction chamber. The procedure and results of these series of tests are given in Chapter 7.

2) The pressure distribution on the walls of the centre passage was measured for specific inlet conditions. The results are presented in Chapter 8.

3) Six inlet flow conditions were selected for further measurements at the exit from the cascade. The downstream traverses, corresponding to each inlet boundary layer condition, included the measurement of the total pressure, flow velocity and direction. The exit endwall boundary layers were also measured. The local values of the total pressure loss coefficient and the static pressure coefficient were plotted in the form of contour maps. The secondary flow velocities in the exit plane were calculated and presented in a vector form. The pitchwise averaged values of the total pressure coefficient, the axial flow velocity and the deviation in the exit flow angle were also presented. The secondary loss coefficient was estimated and compared with some of the correlations reported in the literature. The results of the exit flow study is given in Chapter 9.

CHAPTER 7

INLET FLOW PARAMETERS

In this chapter the results of extensive flow measurements and control at the inlet to the cascade are presented. The measurements were taken in the main flow and in the endwall boundary layer.

7.1 Main Flow Measurements

7.1.1 Circumferential Distribution of Velocity

The main flow was traversed in the circumferential direction at three spanwise locations corresponding to Z/H values of 0.25, 0.5 and 0.75. Readings were taken with the three-dimensional probe at circumferential increments of 1^{o} covering a total angle of 40^{o}. The reference direction for the circumferential locations was radial line "R" (as shown in Figure 4.12) which was the centre of the test passage at the leading edge plane. The distribution of the velocity and incidence for Z/H values of 0.25, 0.5 and 0.75 are given in Figures 7.1, 7.2 and 7.3 respectively. The velocity has been expressed as a ratio of the local values to the mean velocity across the test passage at midspan (V_1 = 112 Ft/sec (34.14 m/sec)). It can be seen from Figure 7.2 that the circumferential variation of the velocity at midspan lies within 10% of the mean value. The maximum

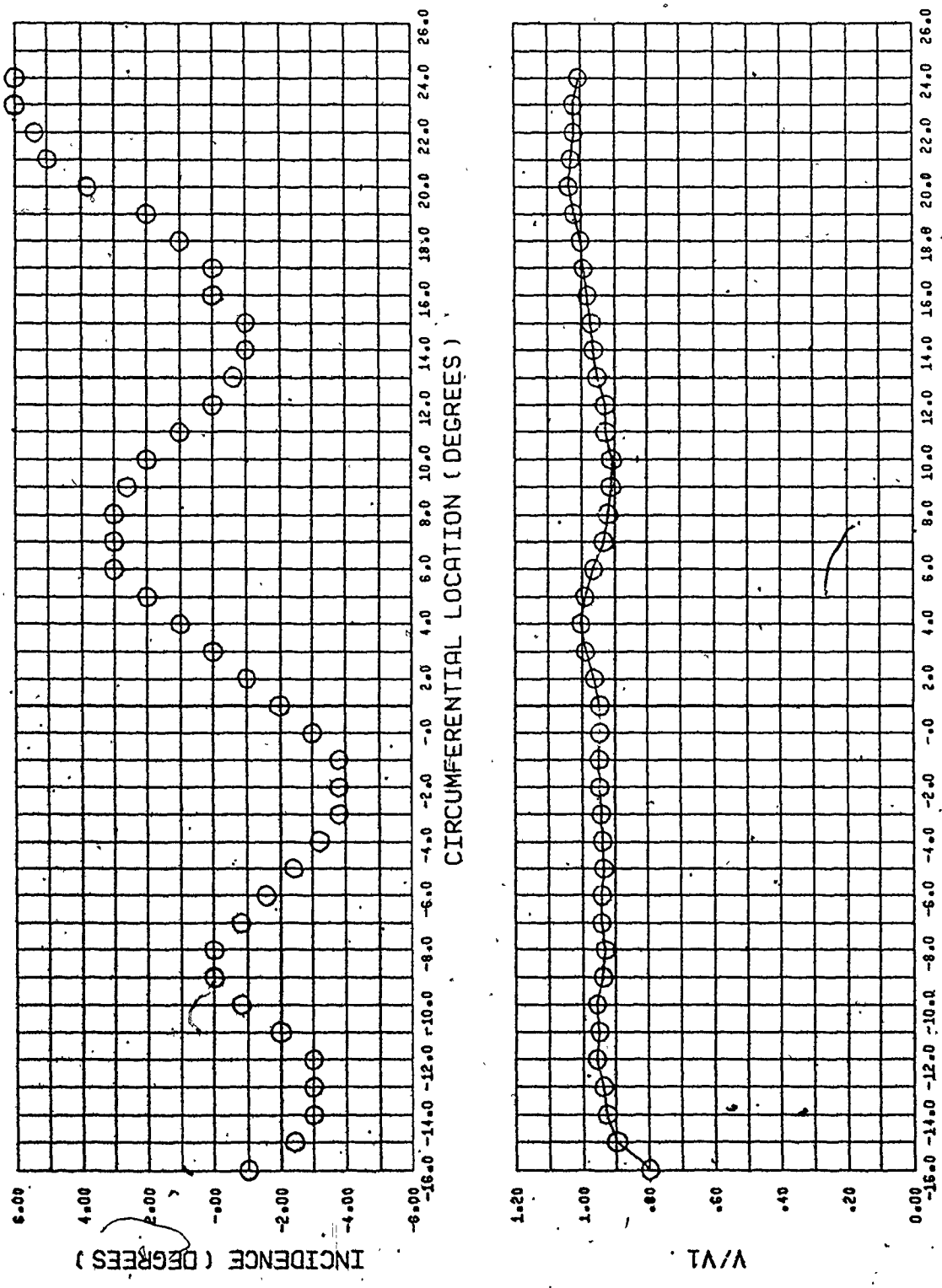

Figure 7.1 Circumferential Distribution of Velocity and Incidence at 25% Span.

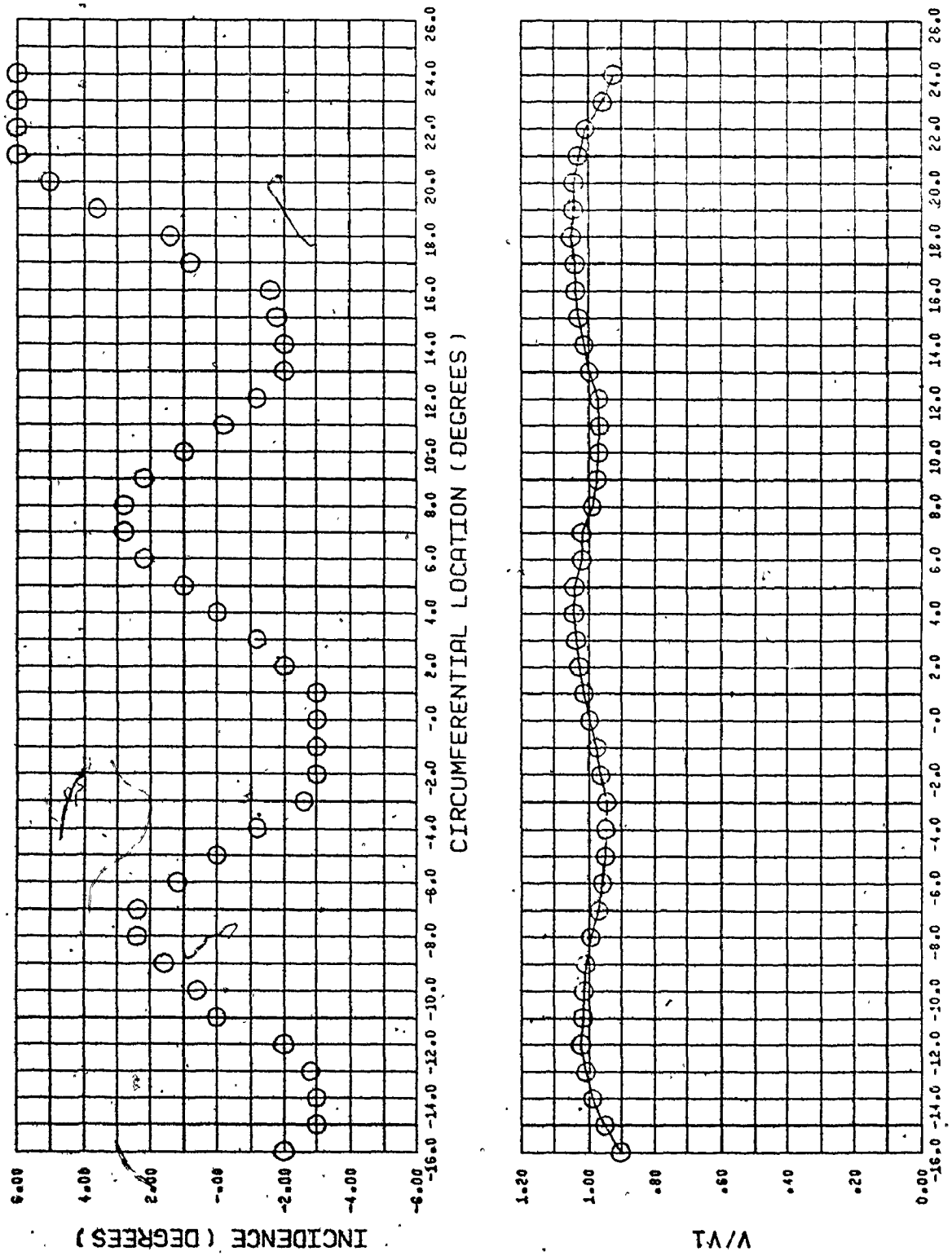

Figure 7.2 Circumferential Distribution of Velocity and Incidence at 50% Span.

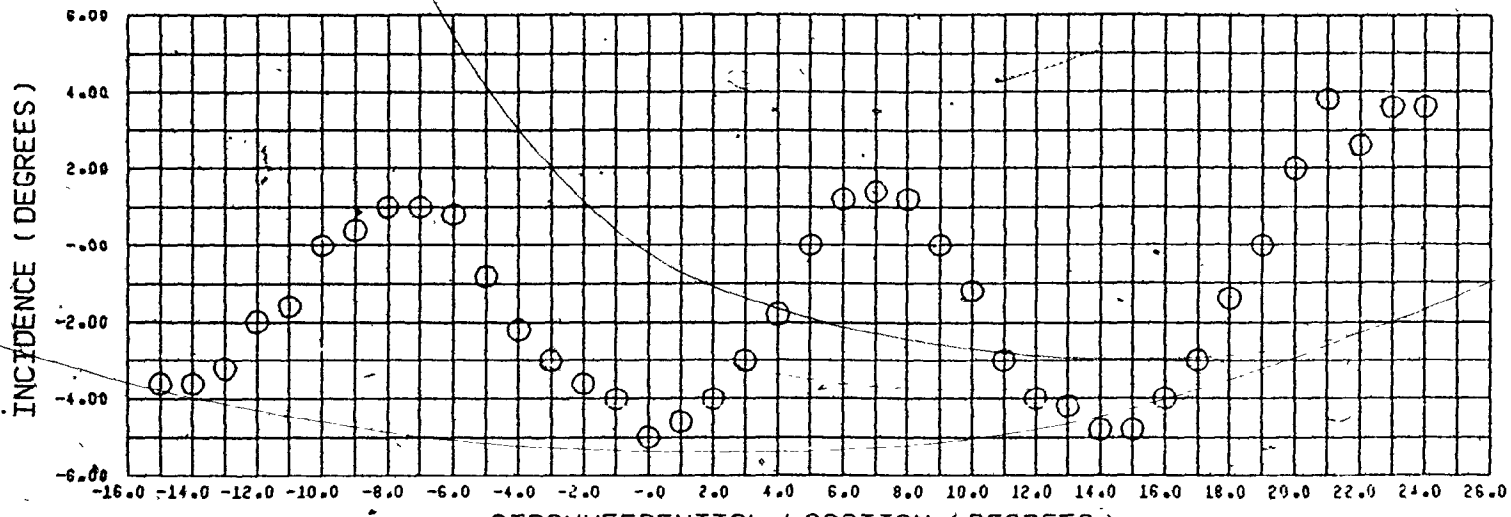

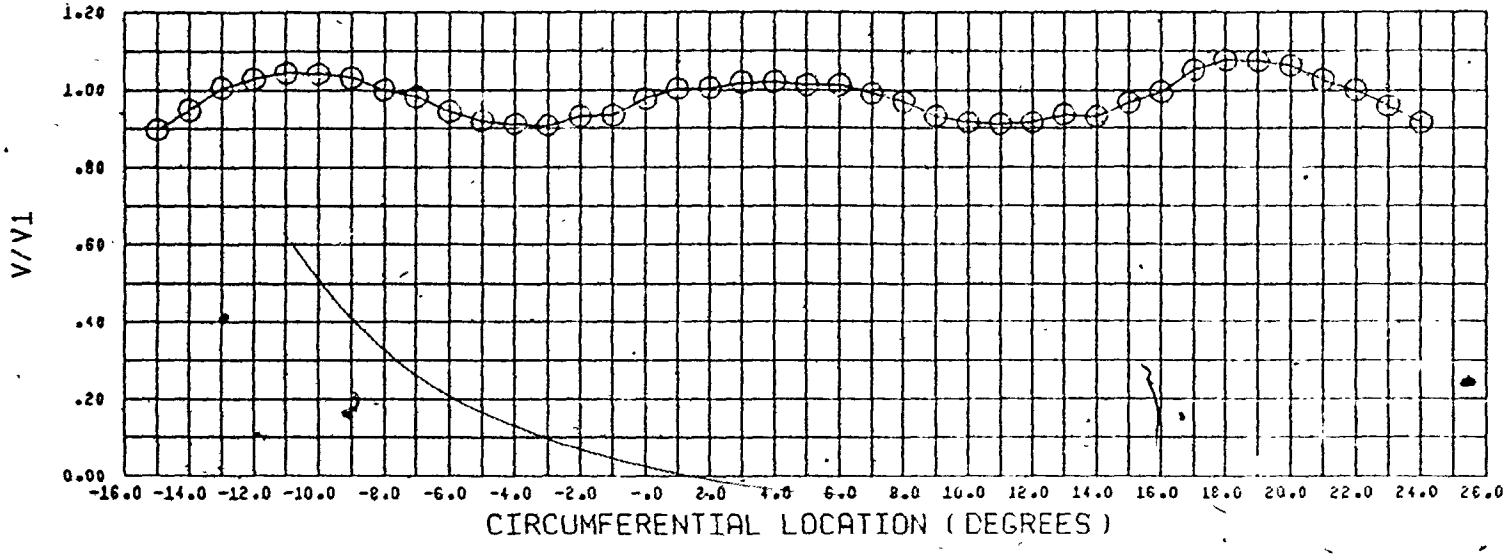

Figure 7.3 Circumferential Distribution of Velocity and Incidence at 75% Span.

velocity at the three spanwise locations occurs at an angle of 4^{o}. It will be recalled that the geometric centre of the passage (as discussed in Chapter 5) faces an angle of 8.42^{o} at the inner wall (Z/H = 0) and an angle of 5.61^{o} at the outer wall (Z/H = 1) both calculated at the upstream measuring station.

A review of the experimental results shown in Figures 7.1, 7.2 and 7.3 reveals that reasonable periodicity was established at the inlet measuring station. Periodicity here is defined to be the cyclic variation of the velocity and incidence of the flow as a function of the blade pitch. At the midspan location the periodicity is fairly satisfied over a circumferential distance extending between the adjacent passages to the centre of each. The incidence variation is noticed to be between $\pm 3^{o}$ over the same distance. The periodicity closer to the inner wall (Z/H = 0.25) is satisfied to a lesser extent while near the outer wall (Z/H = 0.75) the periodicity is satisfactory.

7.1.2 Radial Distribution of Velocity

In order to establish a clear picture of the flow at the inlet to the cascade, several radial traverses were taken using the three dimensional probe. The survey covered the area between the location where the maximum velocity occurred and the locations corresponding to the geometric centre of the passage at the inlet measuring

station. These locations were selected at circumferential positions of 4^{o}, 5^{o}, 6^{o}, 7^{o}, 8^{o}, and 10^{o}. The results of these series of tests are given in Figures 7.4 through 7.9. Due to the fact that the use of the three dimensional, probe does not yield accurate data (particularly the pitch angle) in the vicinity of the walls, the results given cover only a spanwise distance Z/H, ranging from 10% to 90%. It was decided to use the boundary layer probes in conjunction with the three dimensional probe to obtain the full range of the velocity distribution in the radial direction. The measurements taken using each probe were extending beyond the range of the probe and the data obtained in the overlapping zone were averaged around the junction to produce a faired curve (complete traverses are discussed in Chapter 9).

At the circumferential location of $\theta = 4^{o}$, the maximum velocity occurs at the mid span with only a slight variation in the range of Z/H from 20% to 85%. It is apparent that the gradient of the velocity near the inner wall starts at a larger distance than that at the outer wall. The presence of the gradient in the main flow results in some difficulties in defining the edge of the boundary layer, this problem however, will be discussed in a following section.

It can be seen that the point of maximum velocity moves closer to the inner wall as θ increases. For any of

Text continued on page 95

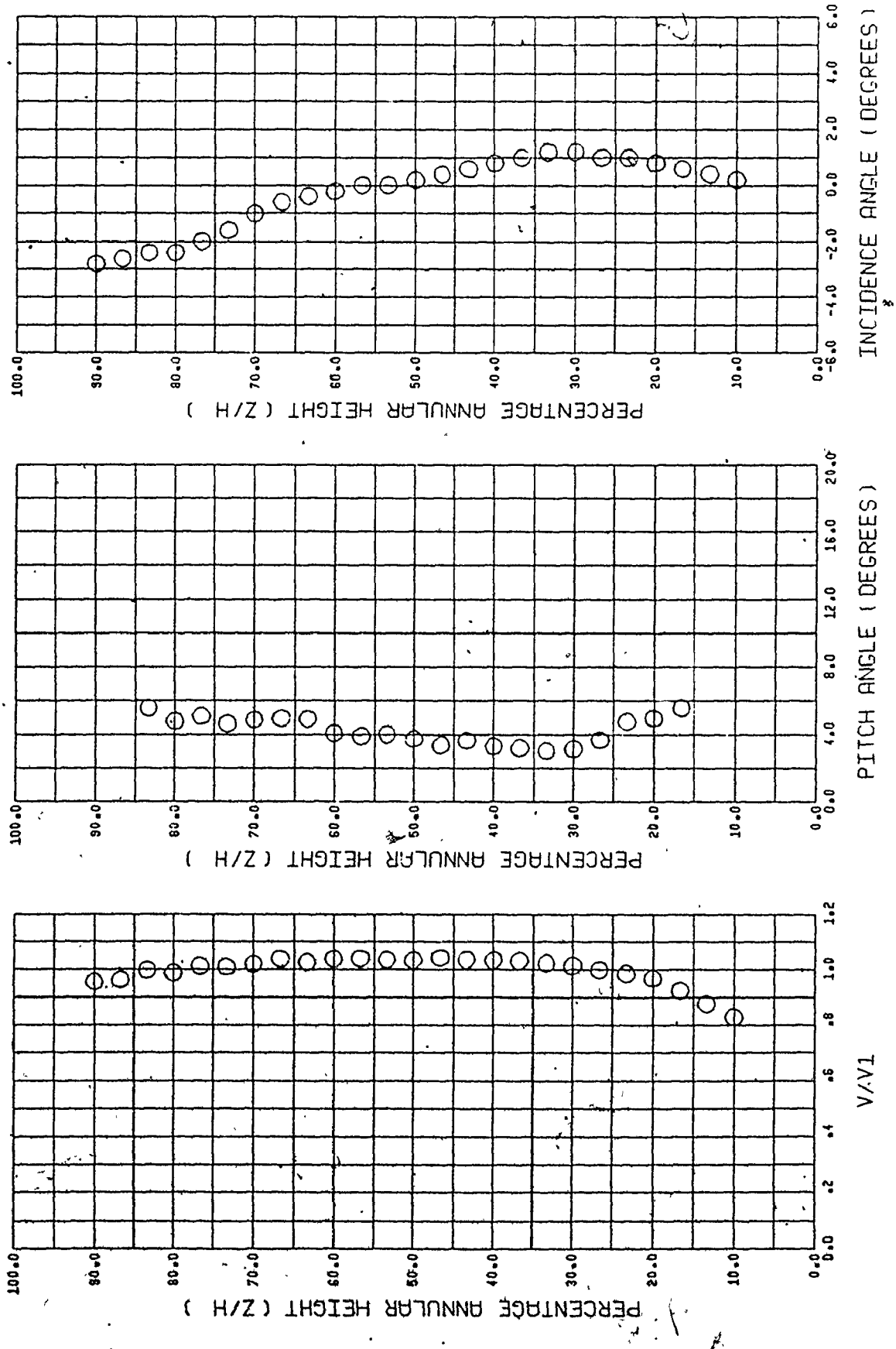

Figure 7.4 Radial Traverse at $\theta = 4^{o}$.

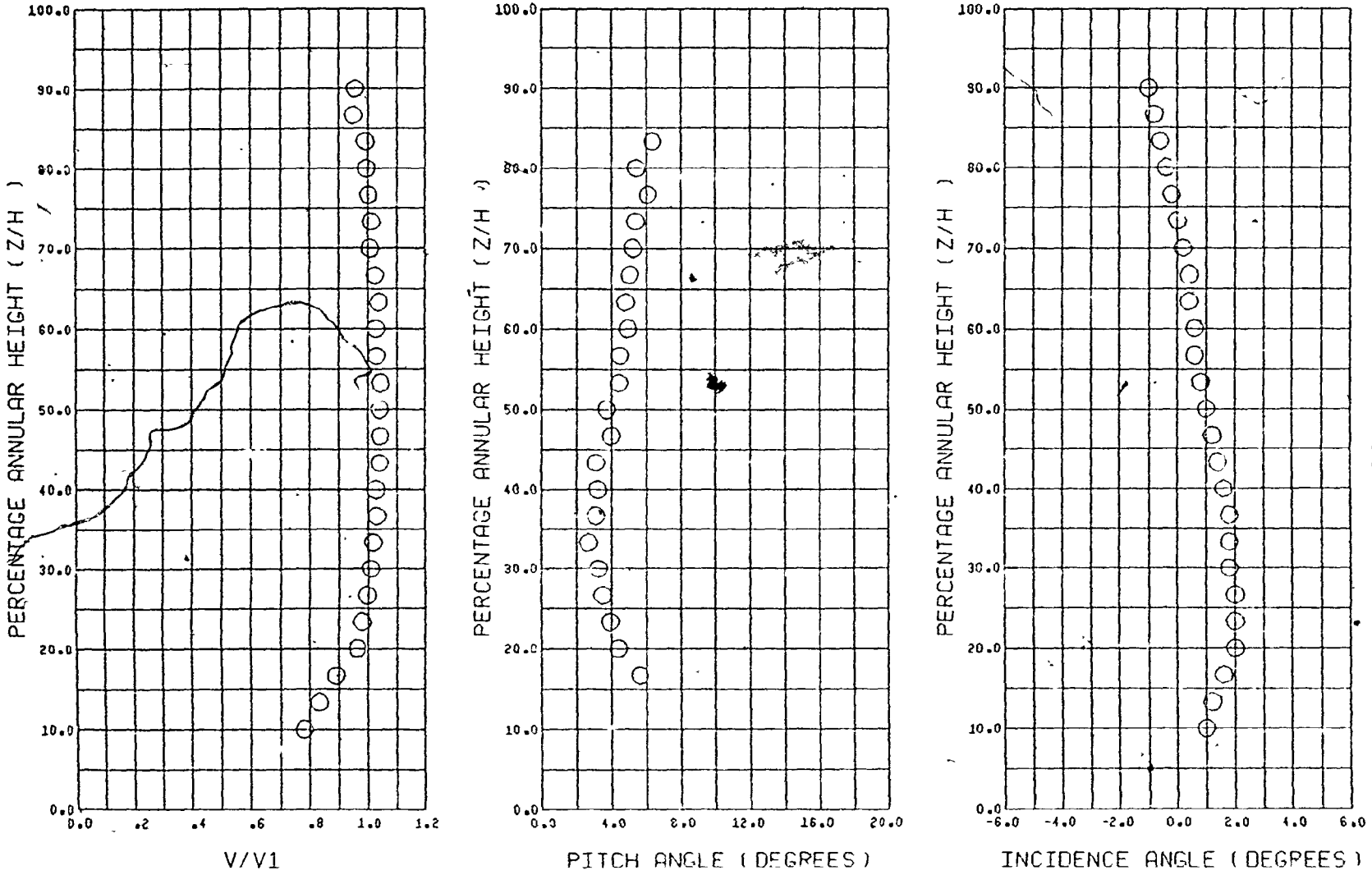

Figure 7.5 Radial Traverse at $\theta = 5^{o}$.

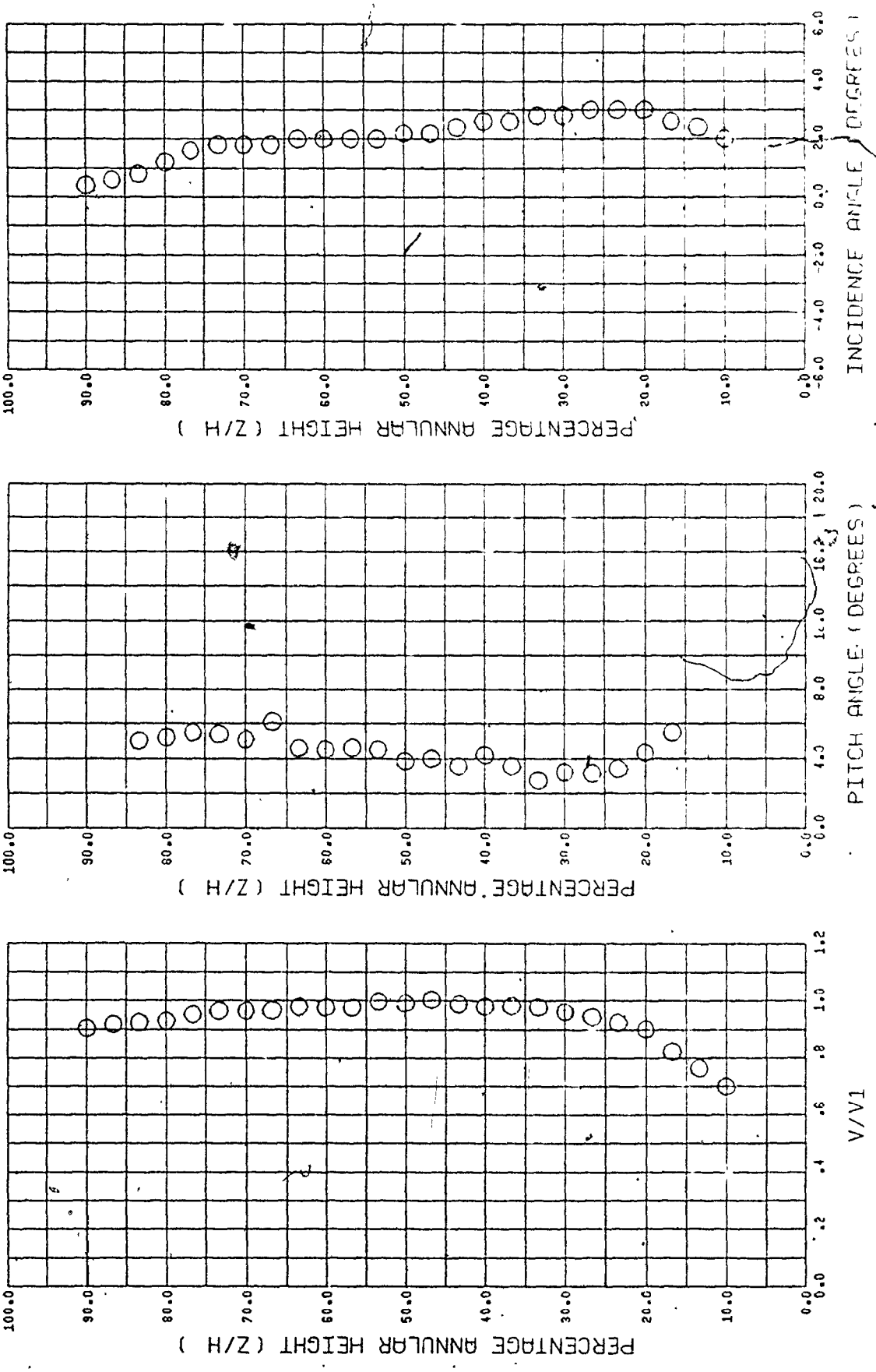

Figure 7.6 Radial Traverse at $\theta = 6^{o}$.

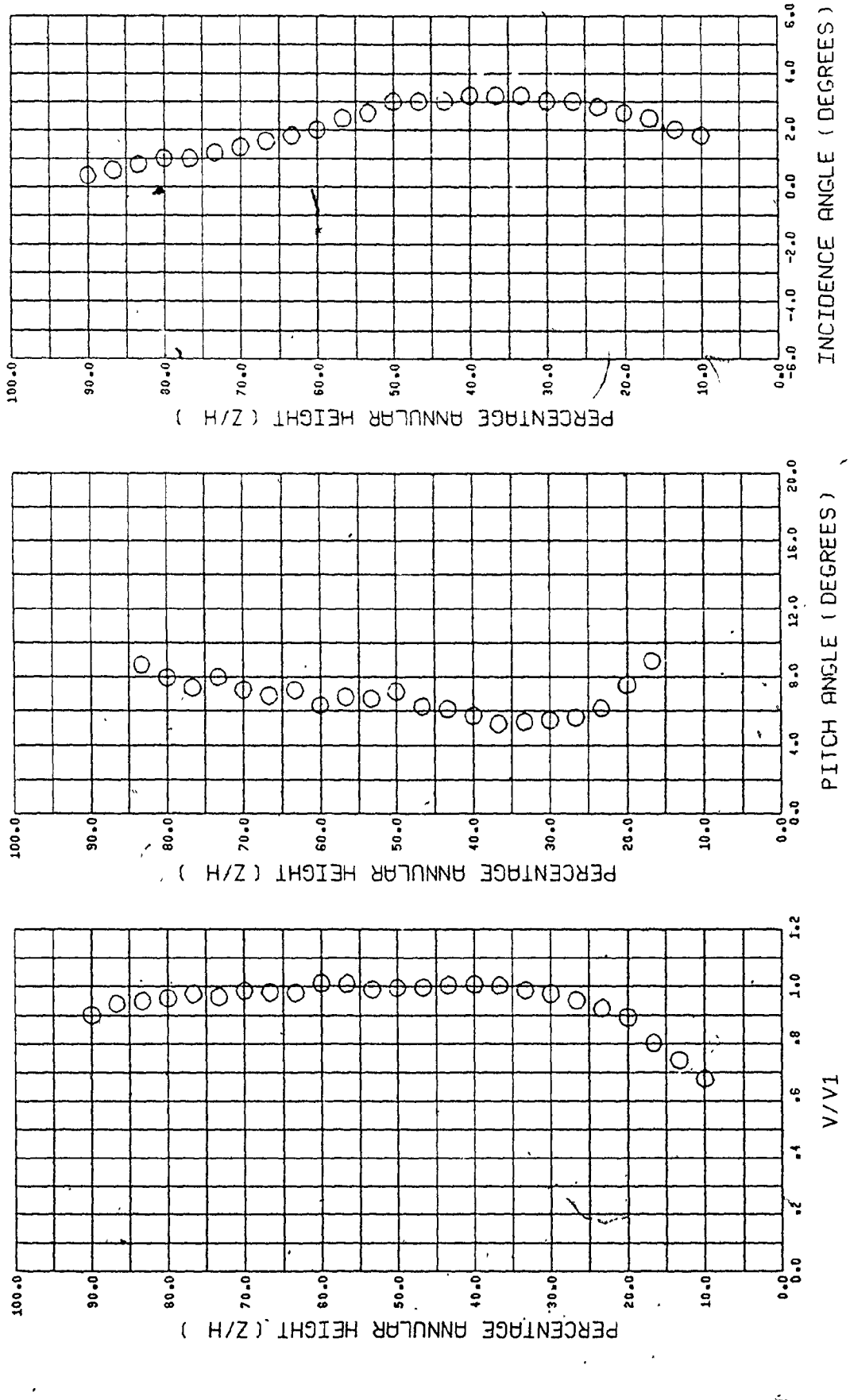

Figure 7.7 Radial Traverse at $\theta = 7^{o}$.

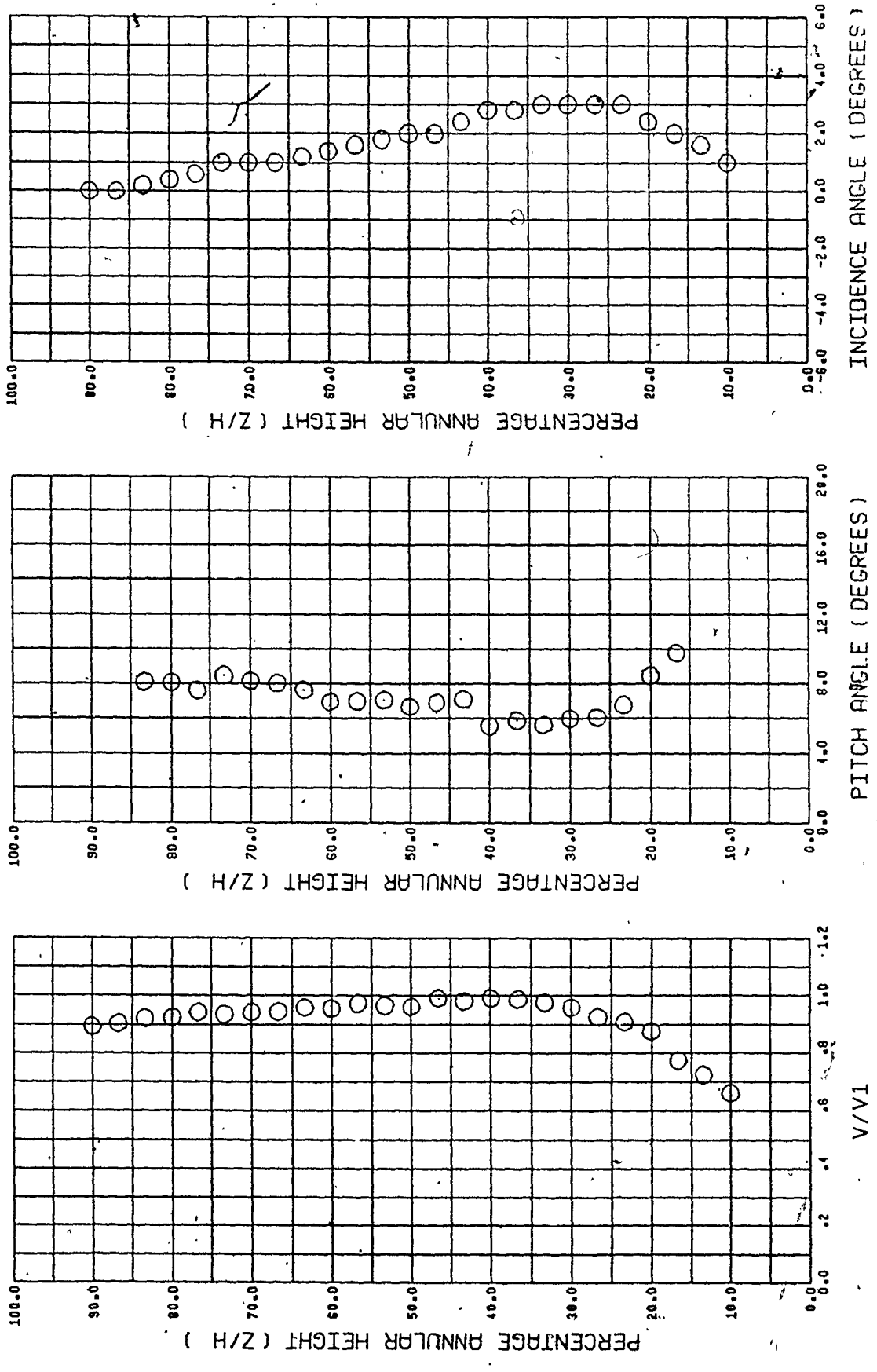

Figure 7.8 Radial Traverse at $\theta = 8^{o}$.

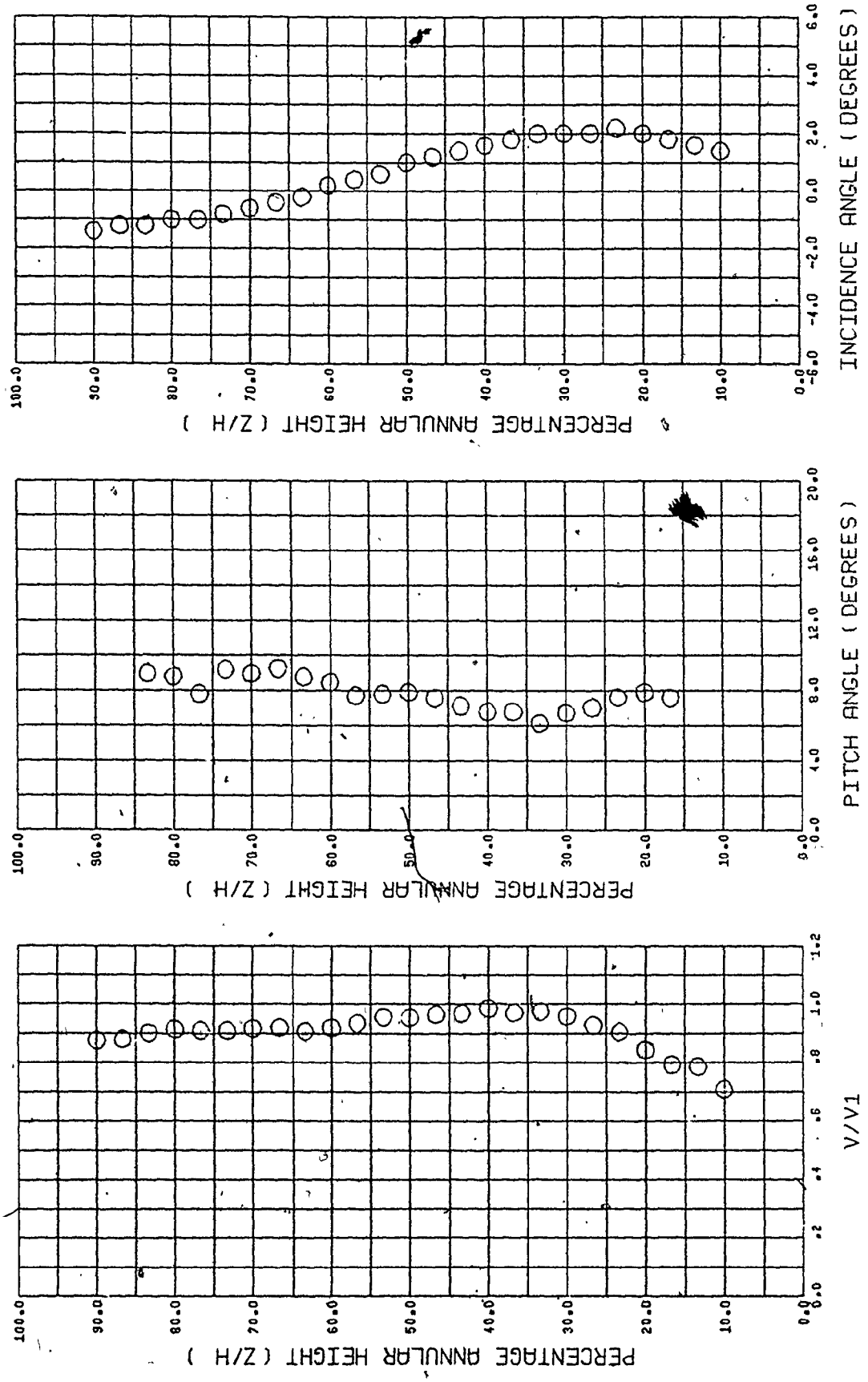

Figure 7.9 Radial Traverse at $\theta = 10^{o}$.

the radial traverses shown, the change in velocity, however, over a spanwise range from 0.15 to 0.85 is no more than 10% of the average value at mid span.

The change of the incidence angle is attributed to the upstream effect of the blade leading edges. The incidence variation for any of the radial locations traversed has similar patterns. The incidence increases from the outer wall to the inner wall. This is expected from the geometric set up of the blades and the probe at the measuring stations. The incidence change in the radial direction is generally within 4^{o}. It should be noticed that the incidence at mid span, in the given range of θ (from 4^{o} to 10^{o}), is always positive.

The pitch angle variation in any radial traverse is within 5^{o} over a spanwise range of Z/H from 15% to 85%. It should be remembered (from Chapter 5) that it was expected to have an indicated pitch angle within the range of 4.82^{o} to 7.4^{o} at the inlet measuring station.

7.2 Boundary Layer Measurements and Control

As shown from the results of the radial distribution of velocity it was clear that the boundary layer at the inner annular wall was relatively thicker than that at the outer wall. The definition of the edge of the boundary layer required the study of the main flow profile and the boundary layer profile. The presence of a gradient

(although small) in the main flow required a somewhat arbitrary criterion to identify the edge of the boundary layer. In the case of a simple two dimensional boundary layer and for general engineering applications it is common to use the height at which the velocity reaches 99.5 percent of the value far from the wall. In such cases the free stream value is well defined. In the case of an ill-defined main stream velocity another measure must be established. The following points were considered:

1) If the main stream has a distinct shape (e.g., constant velocity, or linear variation with distance from walls) that distinguishes it from the boundary layer, then it becomes possible to identify the boundary layer edge approximately by visual inspection.

2) Since the velocity gradient in the boundary layer is generally steeper than the gradient in the main stream, the displacement thickness will converge to a certain value. The rate of convergence will be faster in the boundary layer and, would then slow down or diverge in the main stream.

3) In internal flows, if a potential core exists in the flow, then the total pressure remains constant outside the boundary layer and varies within the boundary layer. The deficiency of the total pressure is thus a logical criterion to detect the extent of viscous effects.

4) Since the displacement thickness is of more importance to this study than the boundary layer thickness

the calculation of the displacement thickness for different boundary layers with an assumed fixed thickness still yields the required information.

From the above mentioned discussion it was decided to use the total pressure as criterion to judge the extent of the viscous effects near the walls.

Preliminary tests were conducted to estimate the effectiveness of the boundary layer suction system and to establish an accurate measurable control parameter for further tests. The suction system was found capable of providing enough suction to control the boundary layer over a reasonable range of the displacement thickness. With two exhauster fans in operation, below atmospheric pressures of up to 26 inches of water (66.04 cm) were obtainable in the inner wall suction chamber. In the outer wall suction chamber a similar arrangement generated up to 15 inches of water (38.10 cm) as compared to a value of 3 inches (7.62 cm) of water below atmospheric pressures under no suction conditions. The pressure in the control chambers was accurately regulated with the aid of the gate valves mounted on the suction ports. It was found that fine regulation of the chamber pressure was required for precise control of the boundary layer particularly near the initial pressure in the suction chamber. It was also found that the read-out instrumentation for the chamber pressure must be equally sensitive and accurate. In the preliminary

testing an ordinary U-tube water manometer was first used for the chamber pressure measurements at the inner wall. At the outer walls a U-tube manometer, with a vernier scale was used as well as a Betz standard manometer. Difficulties were encountered in setting the pressure in the chambers to selected values using these types of pressure instrumentation. Since it was essential to facilitate a precise setting technique for the pressure at selected values, particularly for further measurements of the exit flow parameters, it was decided to use the improved accuracy of the pressure transducer for this purpose. The signal from the transducer as displayed on the chart recorder enabled resetting of the pressure in the control chamber to an accuracy of up to 0.5 mm of water. The refined boundary layer data was thus obtained with a greater degree of accuracy.

In order to relate the boundary layer characteristics to the pressure in the suction chambers a control parameter was defined for the data presentation purposes as follows:

$$\delta_p = \frac{p_{atm} - p_{S.Ch.}}{p_{atm} - p_{S.Ch.1}} \qquad (7.1)$$

where

p_{atm} is the atmospheric pressure

$p_{S.Ch.}$ is the pressure in the suction chamber under current test conditions.

$p_{S.Ch.1}$ is the initial pressure in the suction

chamber without suction or injection.

Thus $\delta_p > 1$ indicates suction and $\delta_p < 1$ indicates injection.

As mentioned before in Section 7.1.1, the main flow circumferential traverses indicated that the maximum velocity occurred at a location different from the geometric centre of the passage. Based on these observations it was considered appropriate to obtain the boundary layer control data at two circumferential locations, one corresponding to the maximum velocity ($\theta = 4^o$ at the inner and outer wall) and the other near the centre of the passage ($\theta = 8^o$ at the inner wall and $\theta = 6^o$ at the outer wall).

7.2.1 Inner Wall Boundary Layer Control Data

In order to establish the general characteristics of the boundary layer, measurements were taken at four circumferential locations on the inner wall, namely at $\theta = 4^o$, 6^o, 8^o and 10^o. Surveys were first conducted without suction or injection. The results of these four tests are shown in Figure 7.10.

The measurements extended over a radial distance of 63.5 mm from the wall which corresponds to approximately 33% of the span. In order to estimate the location of the edge of the boundary, the total pressure deficiency criterion (as discussed before) was considered. It was estimated that

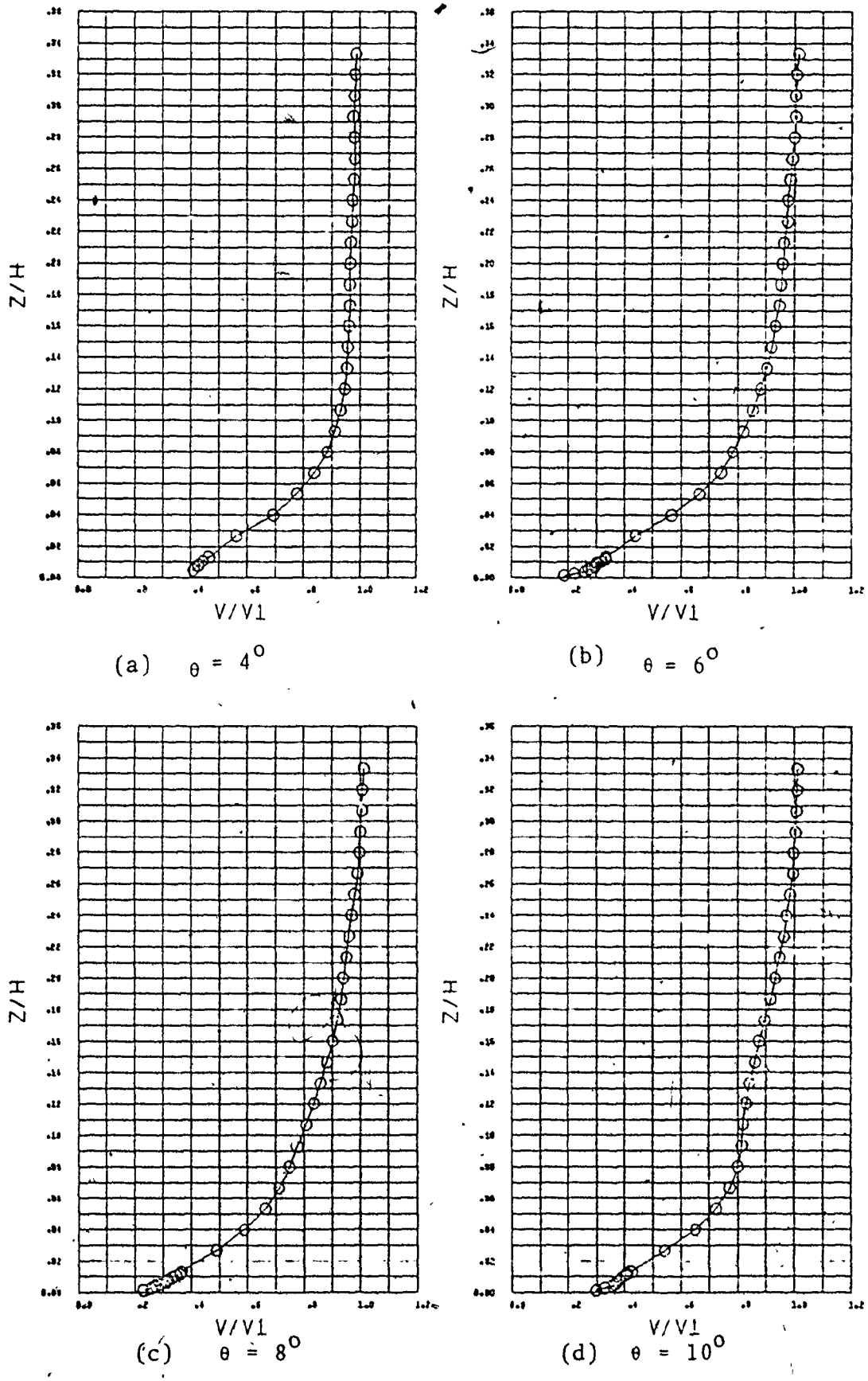

Figure 7.10 . Boundary Layer Profiles at Different
Cir

the boundary layer extended up to 36% of the span (63.5 mm) at the locations where $\theta = 6^{o}$, 8^{o} and 10^{o}. The experimental readings showed that at $\theta = 4^{o}$ the boundary layer was slightly more developed than at other locations. It was estimated that the height of the boundary layer thickness at this location was approximately 50 mm (about 26% span). At the estimated boundary layer edges it was noted that pressure transducer readings indicated a change of total pressure of less than 1% of the reference dynamic head at mid span. This variation was measured over steps of radial increments of 2.54 mm.

The control data of the boundary layer at the location $\theta = 4^{o}$ is given in Figures 7.11 and 7.12. The displacement thickness δ^*, the control parameter δ_p and the shape factor H_{12} corresponding to each test condition are also indicated on the diagrams. As mentioned previously, it was found that the boundary layer was very sensitive to the applied pressure in the suction chamber particularly near the value of $\delta_p = 1$. The reduction in δ^* for values of suction pressure below -25.4 cm of water were insignificant. It was apparent, therefore, that δ^* decreased assymptotically to a minimum value with increased suction. Accordingly it was decided not to exceed a suction pressure value of 24.5 cm of water when exit flow tests were conducted.

An examination of the boundary layer profiles obtained under reversed flow conditions in the suction

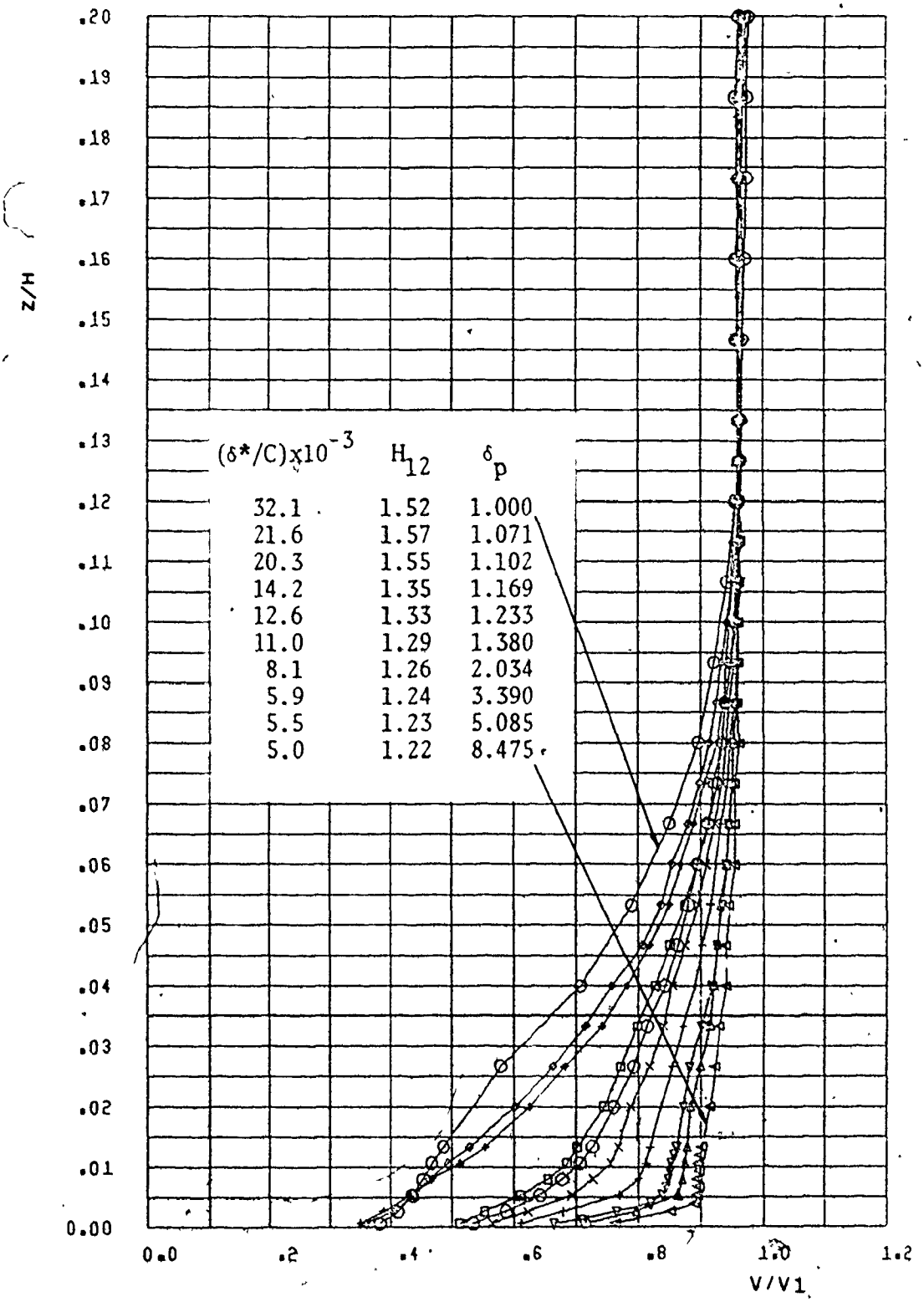

Figure 7.11 Boundary Layer Control Data at the Inner Wall at $\theta = 4^{o}$ (Effect of Suction).

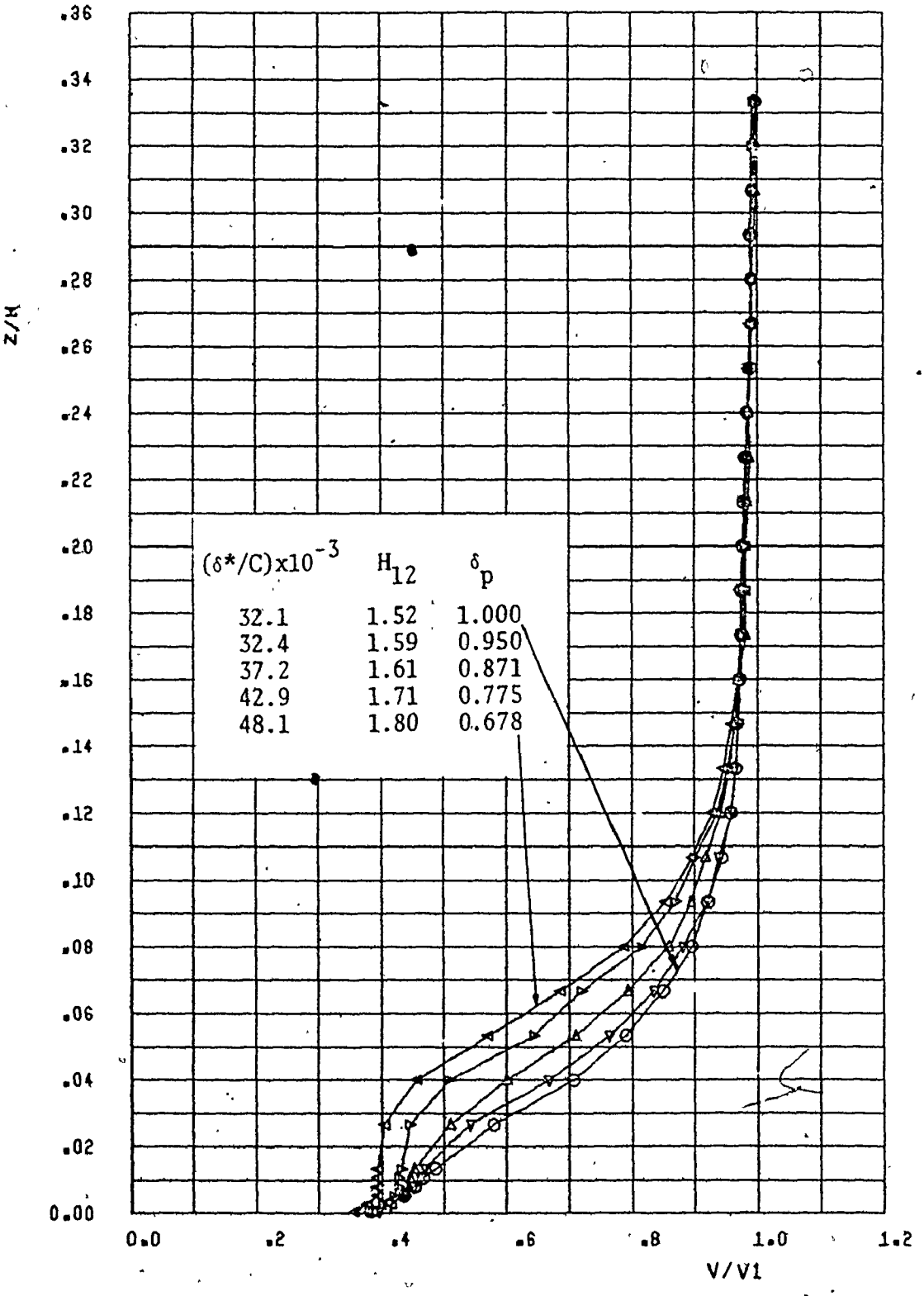

Figure 7.12 Boundary Layer Control Data at the Inner Wall at $\theta = 4^{\circ}$ (Effect of Transverse Injection).

chamber (i.e., injection) indicates that the flow may separate at the inner wall. The corresponding shape factor for these conditions exceeded the value of 1.8, a criterion for flow separation for two-dimensional boundary layers [54]. None of the profiles obtained under injection conditions was used in the further examination in the flow in the exit plane of the cascade.

The data obtained at the circumferential location $\theta = 8$ is given in Figures 7.13 and 7.14. Surveys were conducted under the same boundary layer control conditions as for $\theta = 4^{o}$.

7.2.2 Outer Wall Boundary Layer Control Data

The boundary layer on the outer wall was surveyed under different control conditions in a manner similar to that on the inner wall. Because of the experience gained from the preliminary testing on the inner wall fewer tests were required to establish the required control conditions on the outer wall. At the two chosen locations of $\theta = 4^{o}$ and $\theta = 6^{o}$ different suction and injection values were applied. The results of this series of tests are given in Figures 7.15 through 7.18. It can be seen that the boundary layer thickness was of the order of 15 mm (8% span) for the two circumferential locations. The suction required for bringing the displacement thickness to a minimum value was of the order of -10 cm of water.

Text continued on page 111

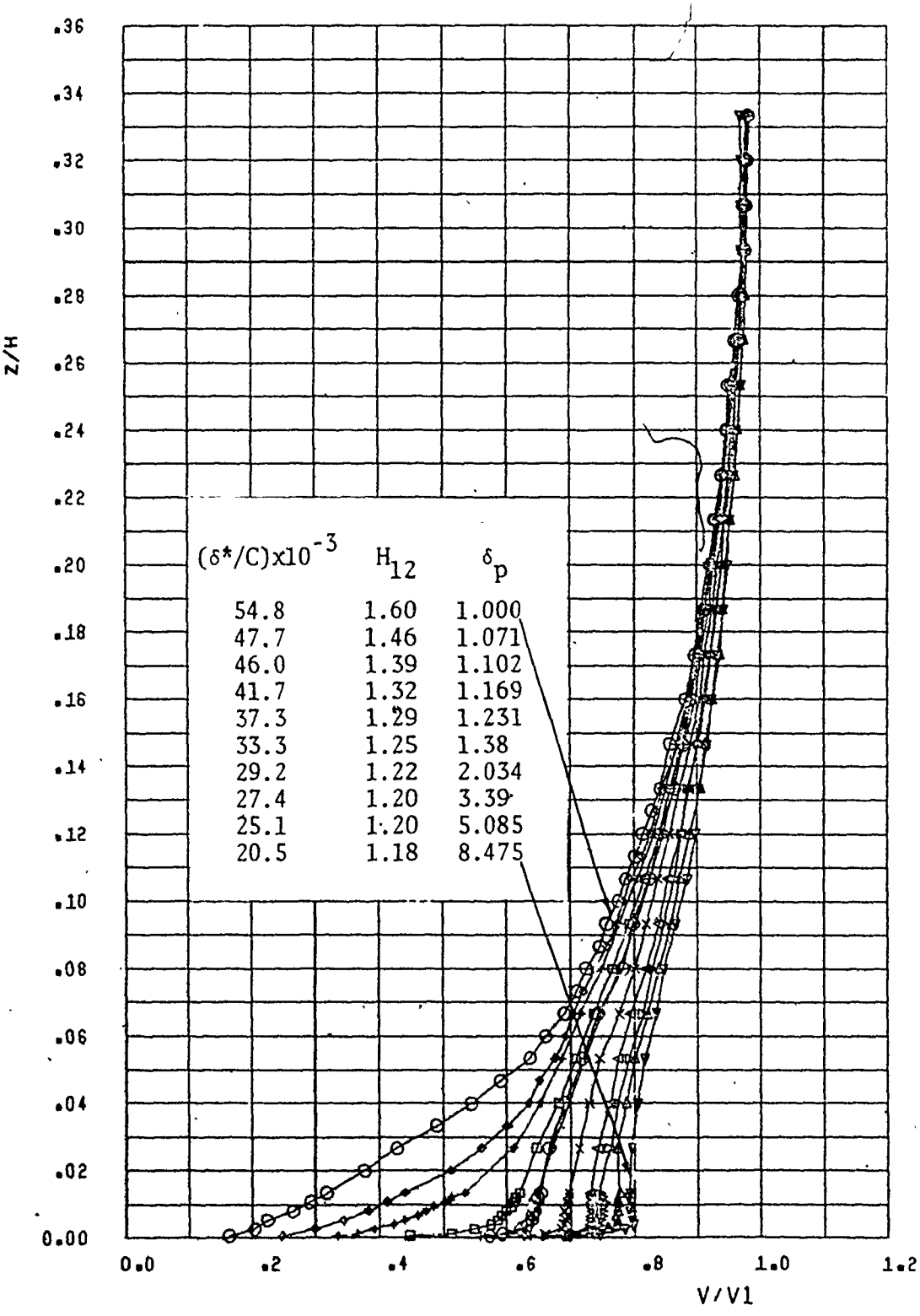

Figure 7.13 Boundary Layer Control Data at the Inner Wall at $\theta = 8^{o}$ (Effect of Suction).

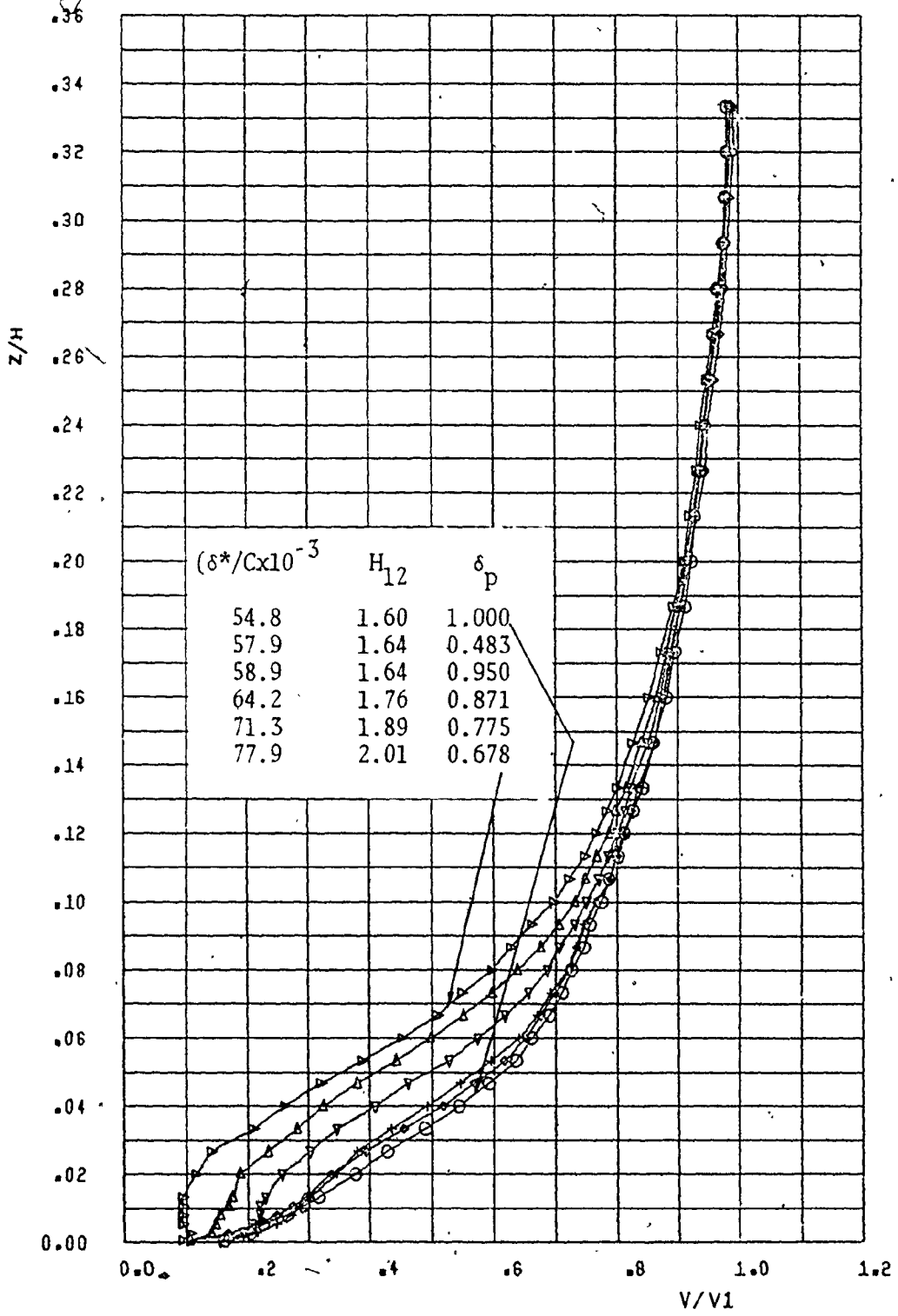

Figure 7.14 Boundary Layer Control Data at the Inner Wall $\theta = 8^{o}$ (Effect of Transverse Injection).

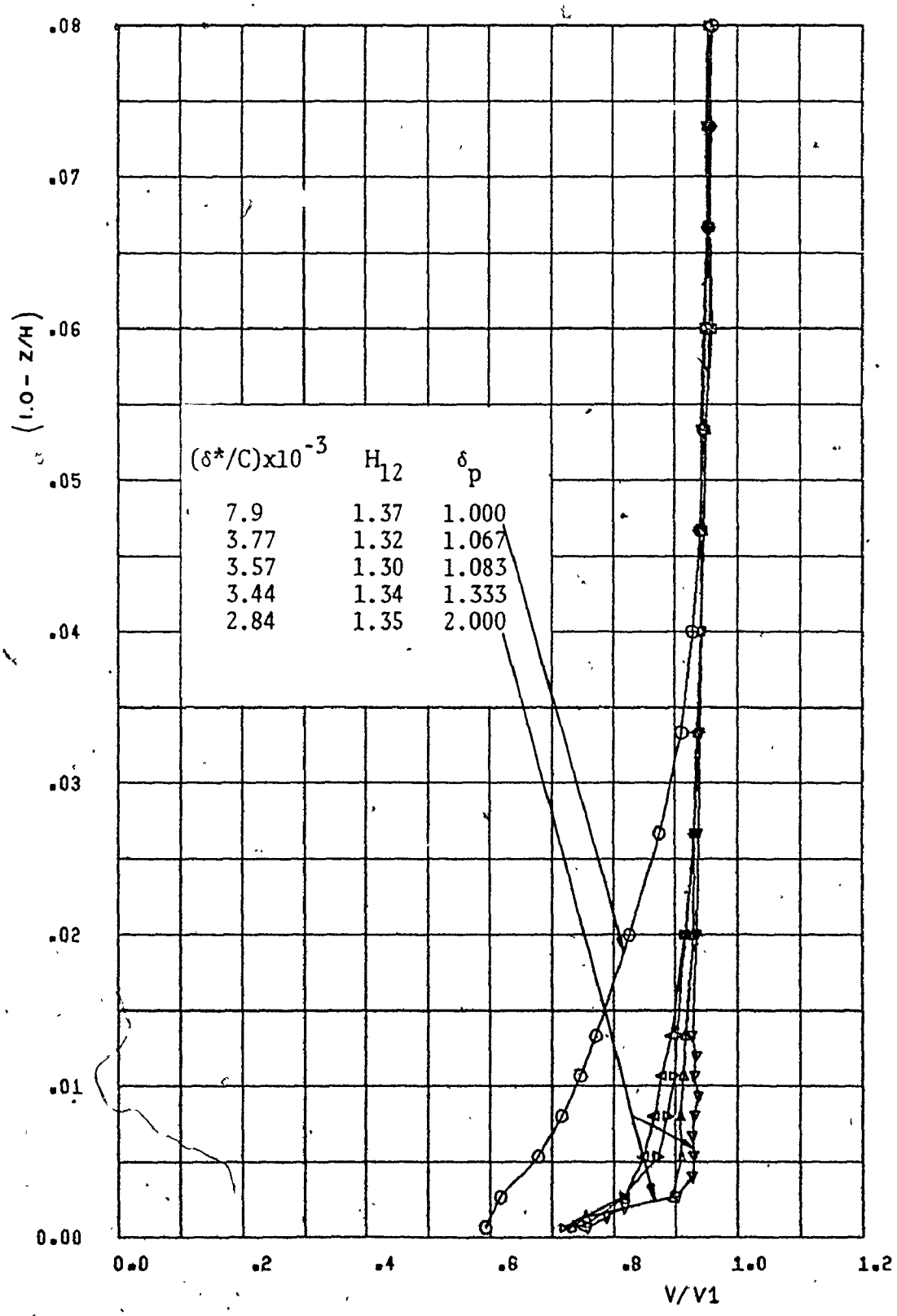

Figure 7.15 Boundary Layer Control Data at the Outer Wall $\theta = 4^{o}$ (Effect of Suction).

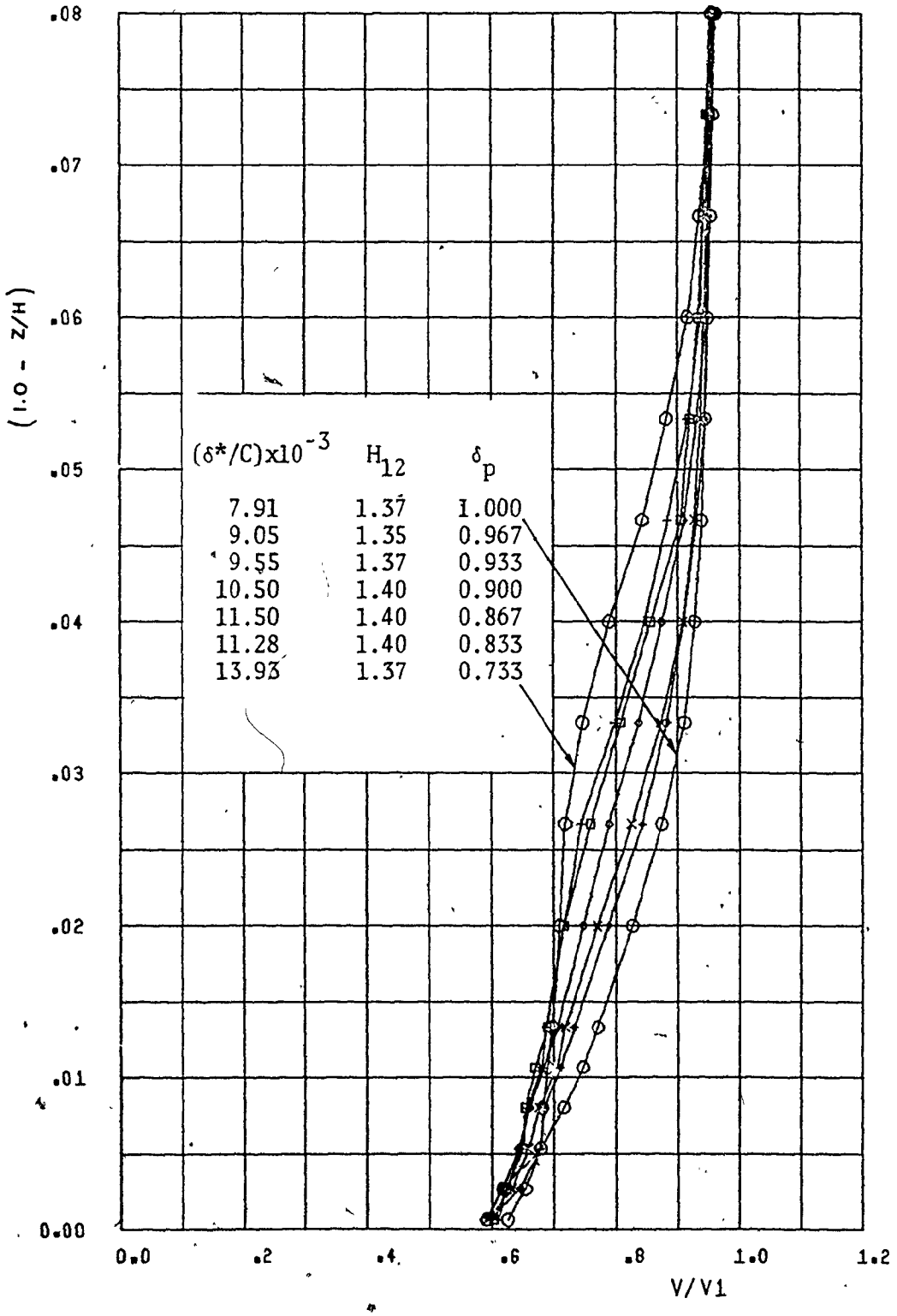

Figure 7.16 Boundary Layer Control Data at the Outer Wall $\theta = 4^{o}$ (Effect of Transverse Injection).

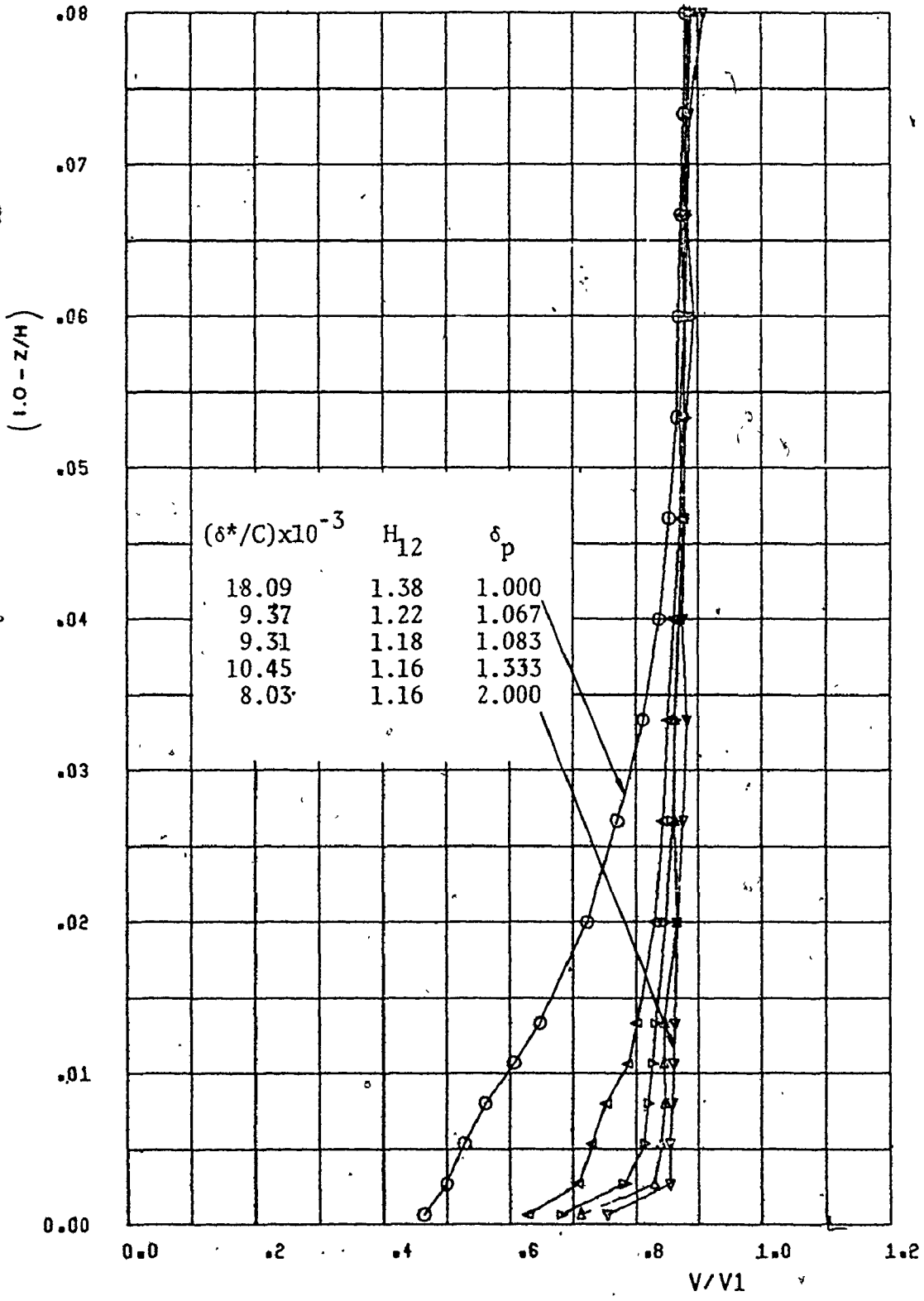

Figure 7.17 Boundary Layer Control Data at the Outer Wall at $\theta = 6^{o}$ (Effect of Suction).

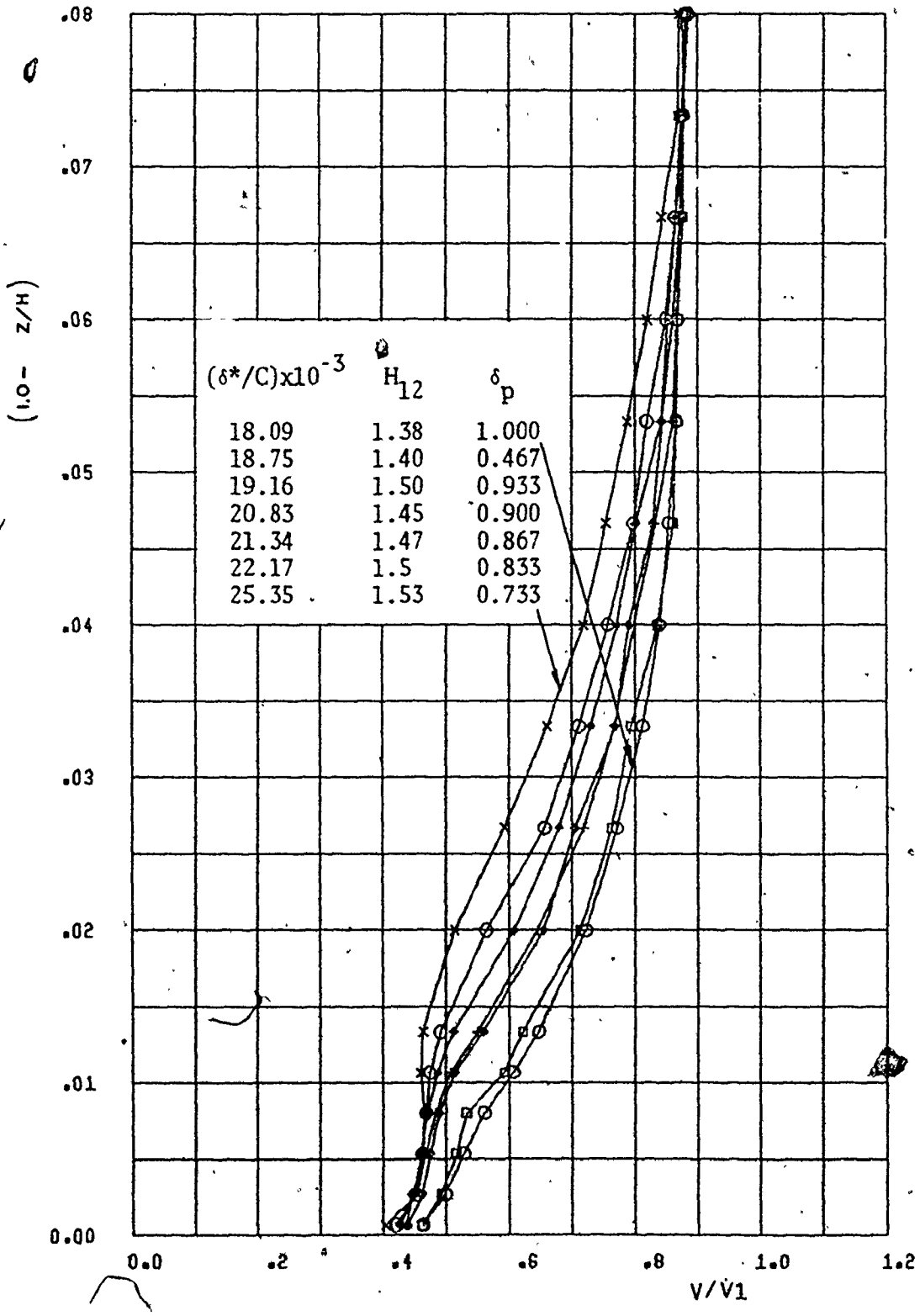

Figure 7.18 Boundary Layer Control Data at the Outer Wall at $\theta = 6^{o}$ (Effect of Transverse Injection).

7.3 Radial Traverses Under Boundary Layer Suction Conditions

In order to ensure that the effect of boundary layer suction was limited to the boundary layer region, two radial traverses were made at $\theta = 7^{o}$ with maximum suction applied at both the inner and outer walls as shown in Figures 7.19 and 7.20. A comparison of these experimental results with those obtained under the conditions of no suction (Figure 7.7) indicated that there was no significant change in the main flow parameters with the application of suction.

7.4 Turbulence Intensity

The turbulence intensity was measured at three radial locations at $\theta = 5^{o}$ at the initial condition (without suction) using a miniature Disa hot wire probe (Model # 55P14). The probe was calibrated in the potential core of a calibration nozzle (part number 2 in Figure 7.21) over a speed range of up to 50 m/s. Calibration data for the probe is shown in Figure 7.22. At each radial location the r.m.s. turbulence level was measured over a speed range of (20-50 m/s) (See Figure 7.23).

The percentage turbulence is defined as,

$$\% \text{ turbulence} = \frac{u}{V} \times 100$$

$$= \frac{e_{r.m.s.} \times 100}{V \frac{dE}{dV}} \qquad (7.2)$$

Text continued on page 117

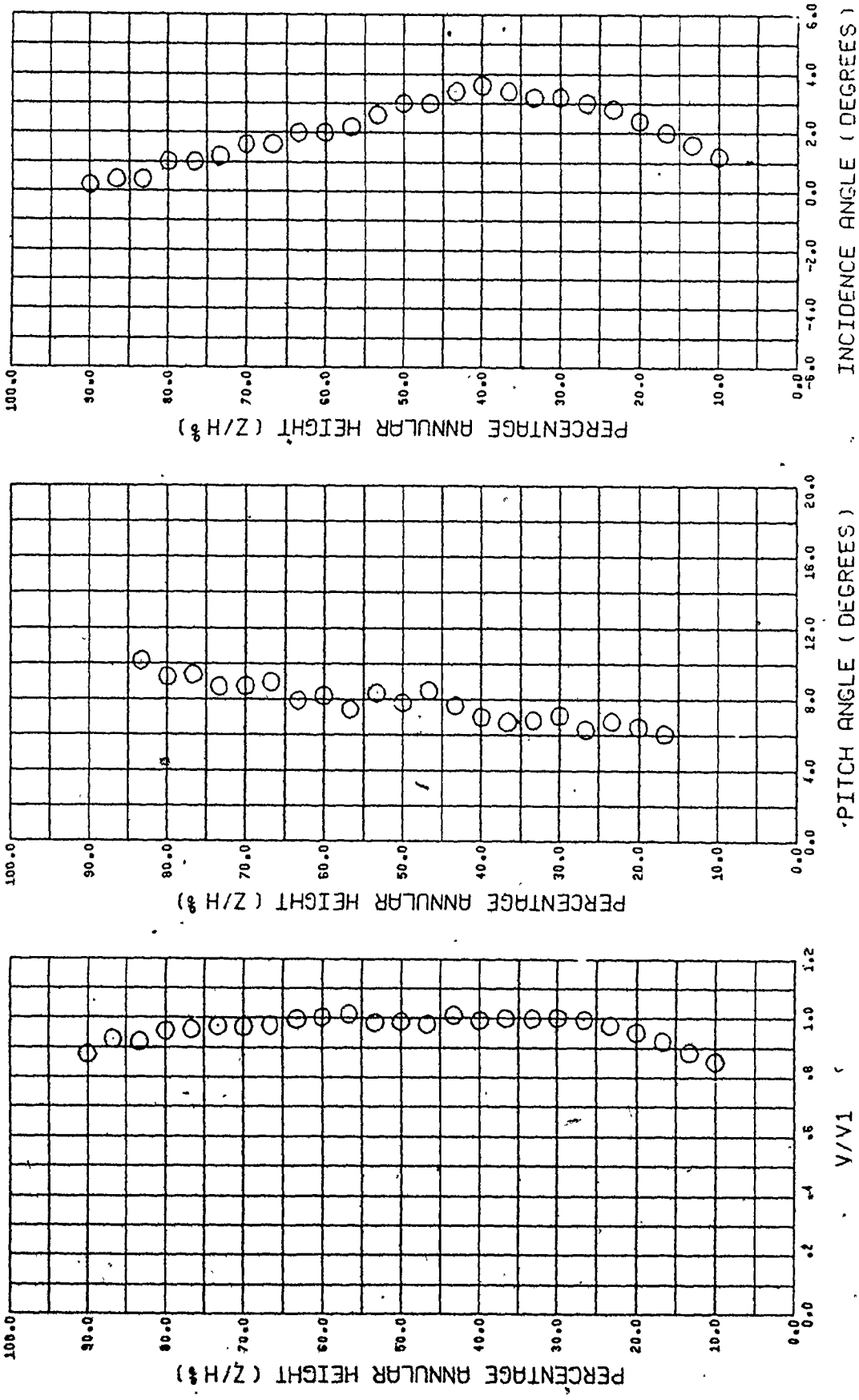

Figure 7.19 Radial Traverse at $\theta = 7^{o}$ Under Maximum Suction at the Inner Wall ($\delta p = 8.67$).

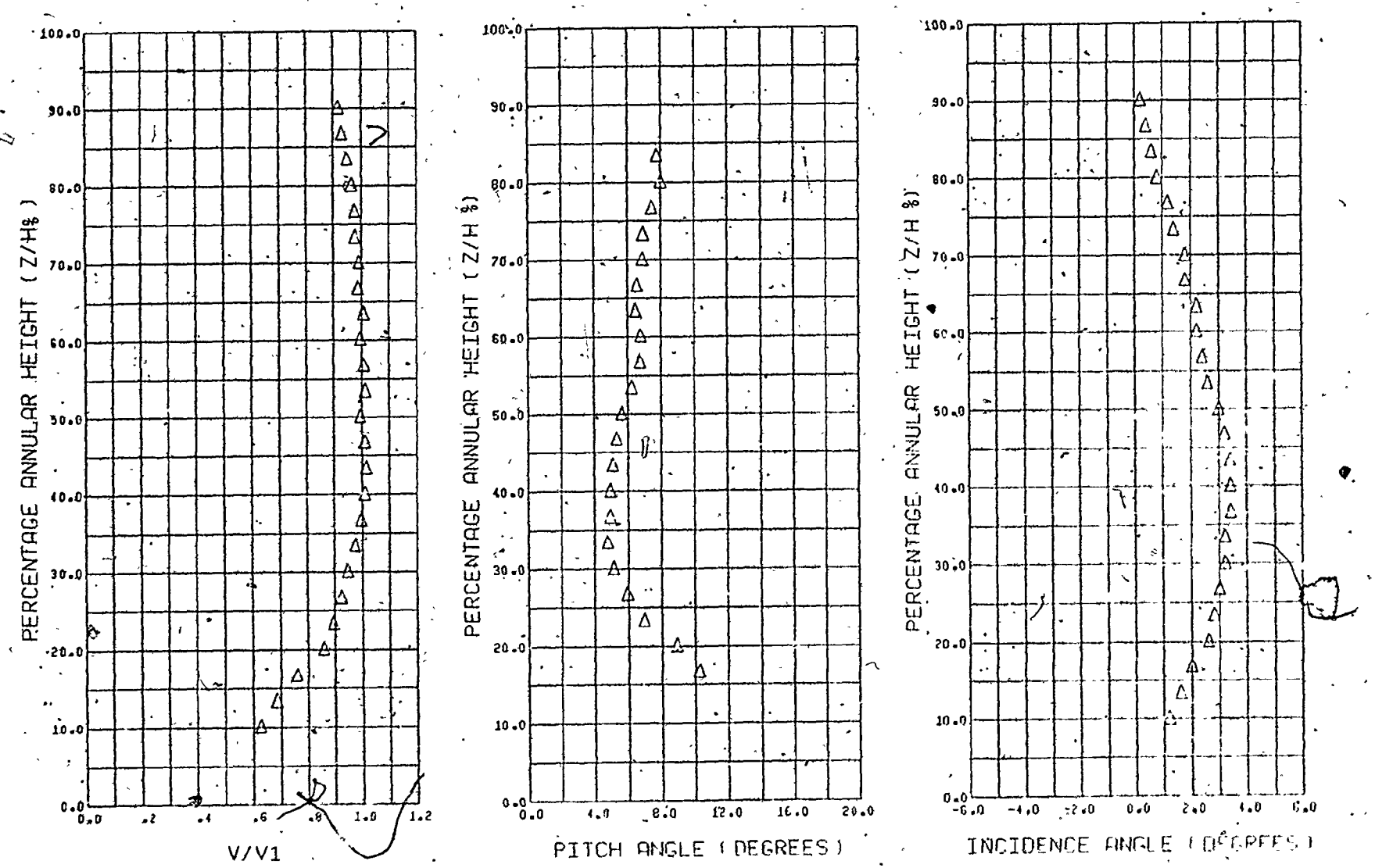

Figure 7.20 Radial Traverse at $\theta = 7^{\circ}$ Under Maximum Suction at the Outer Wall ($\delta p = 4.67$).

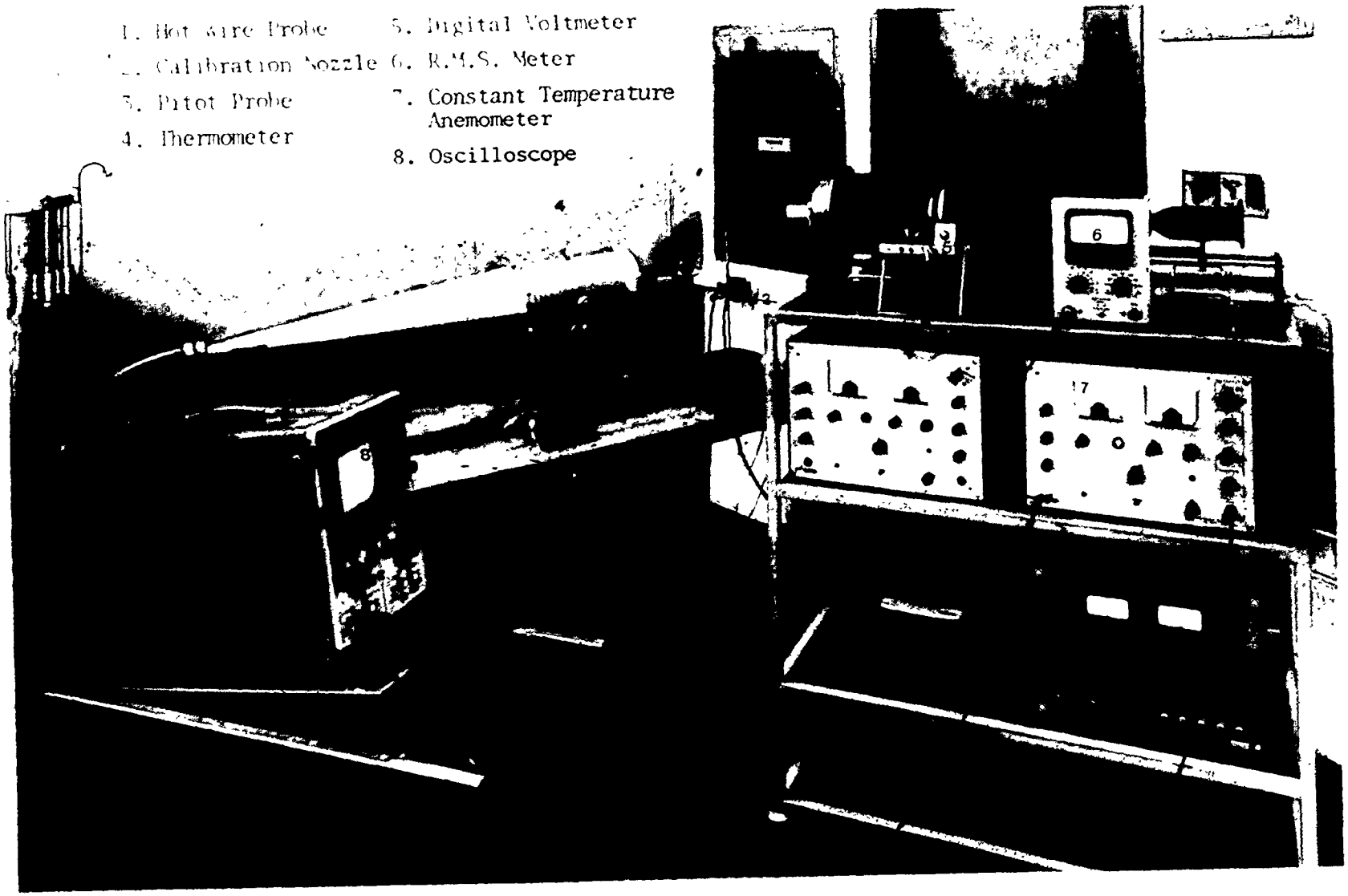

Figure 7.21 Hot Wire Probe Calibration and Instrumentation Set Up.

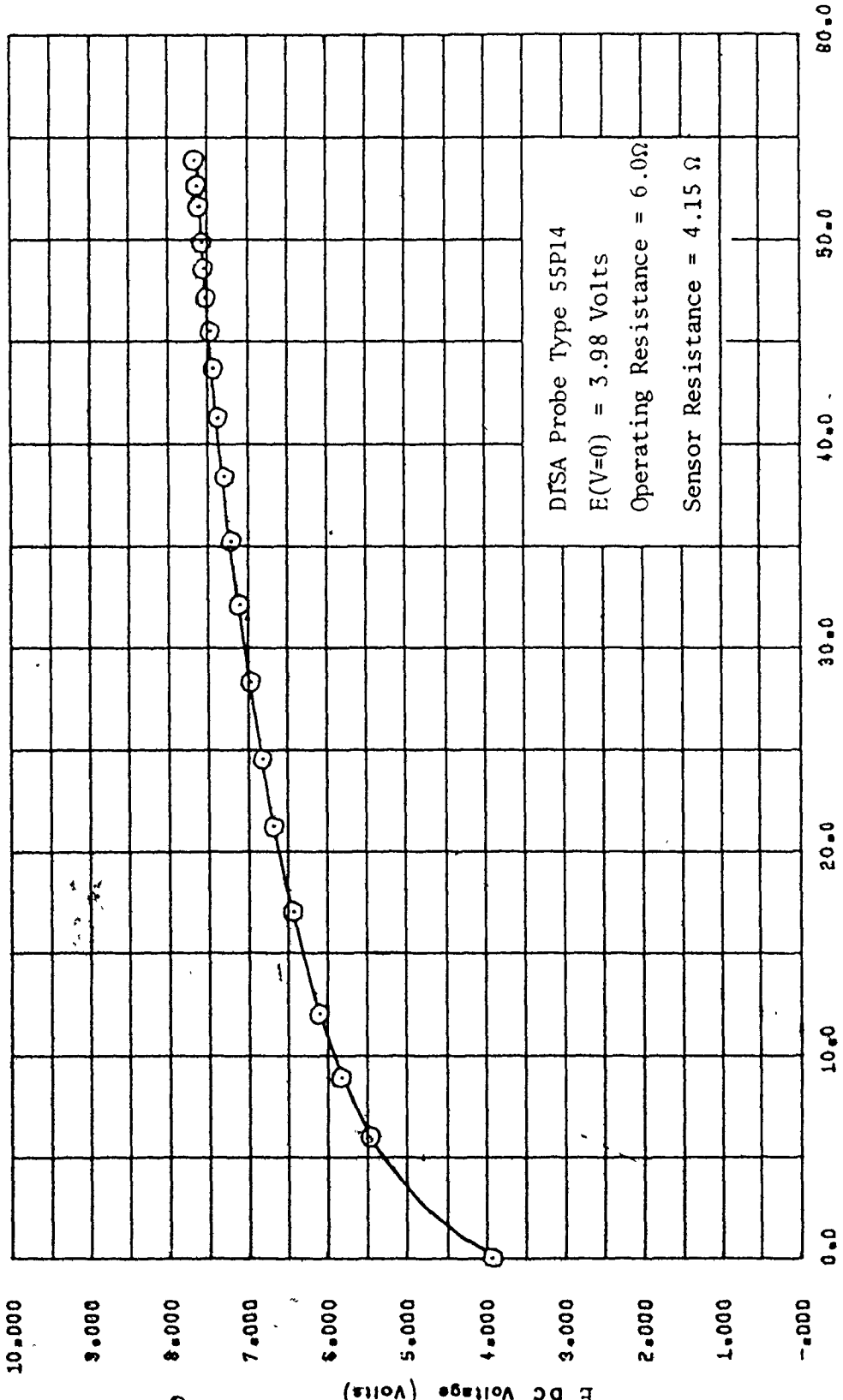

Figure 7.22 Hot Wire Probe Calibration Data.

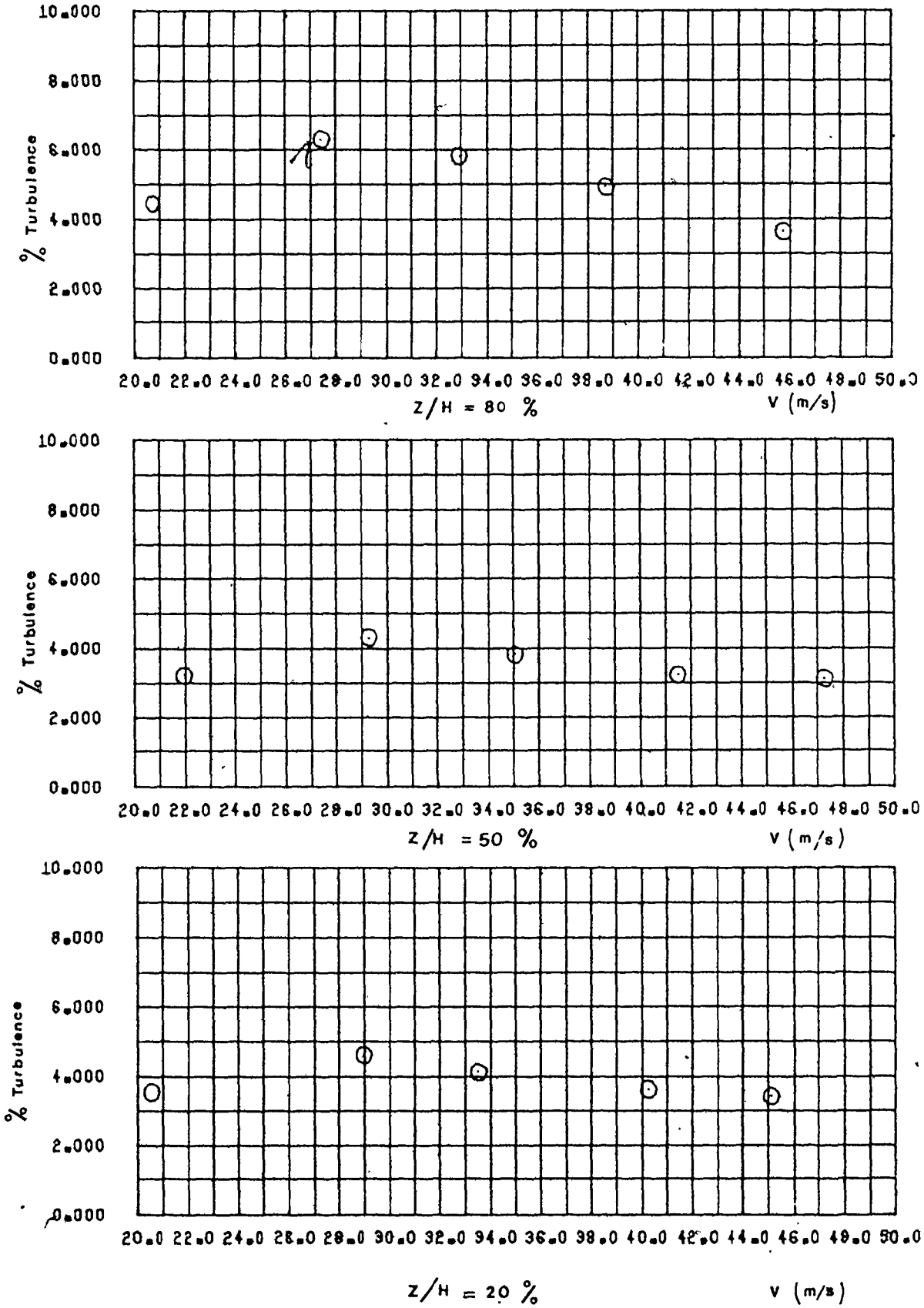

Figure 7.23 Turbulence Intensity at Different Radial Locations.

where

$e_{r.m.s}$ is the r.m.s. level measured

$\frac{dE}{dV}$ is the slope of the calibration curve at the speed V.

The percentage level as depicted for Figure 7.23 is within 3% to 6% a value that is comparable with several of the cascade tests reported in the literature.

CHAPTER 8

BLADE SURFACE AND ENDWALL PRESSURE DISTRIBUTION

The pressure on the surfaces of the centre blade passage was measured at a total of 130 points. The locations of the static taps on the blade surface and on the endwall is given in Chapter 5.3. An overall description of the coordinates of the measuring locations is given in Figure 8.1. The results given in this chapter are for the initial test conditions of no boundary layer suction. The pressure distribution expressed in terms of a standard static pressure coefficient C_{ps} defined in the following manner:

$$C_{ps} = \frac{P - P_1}{\frac{1}{2}\rho V_1^2} \qquad (8.1)$$

where

P_1 is a reference static pressure (free stream static pressure at the inlet measuring station).

$\frac{1}{2}\rho V_1^2$ the corresponding dynamic head at the inlet to the cascade using the mean values of the velocity obtained at mid span.

P the local static pressure on the passage surface.

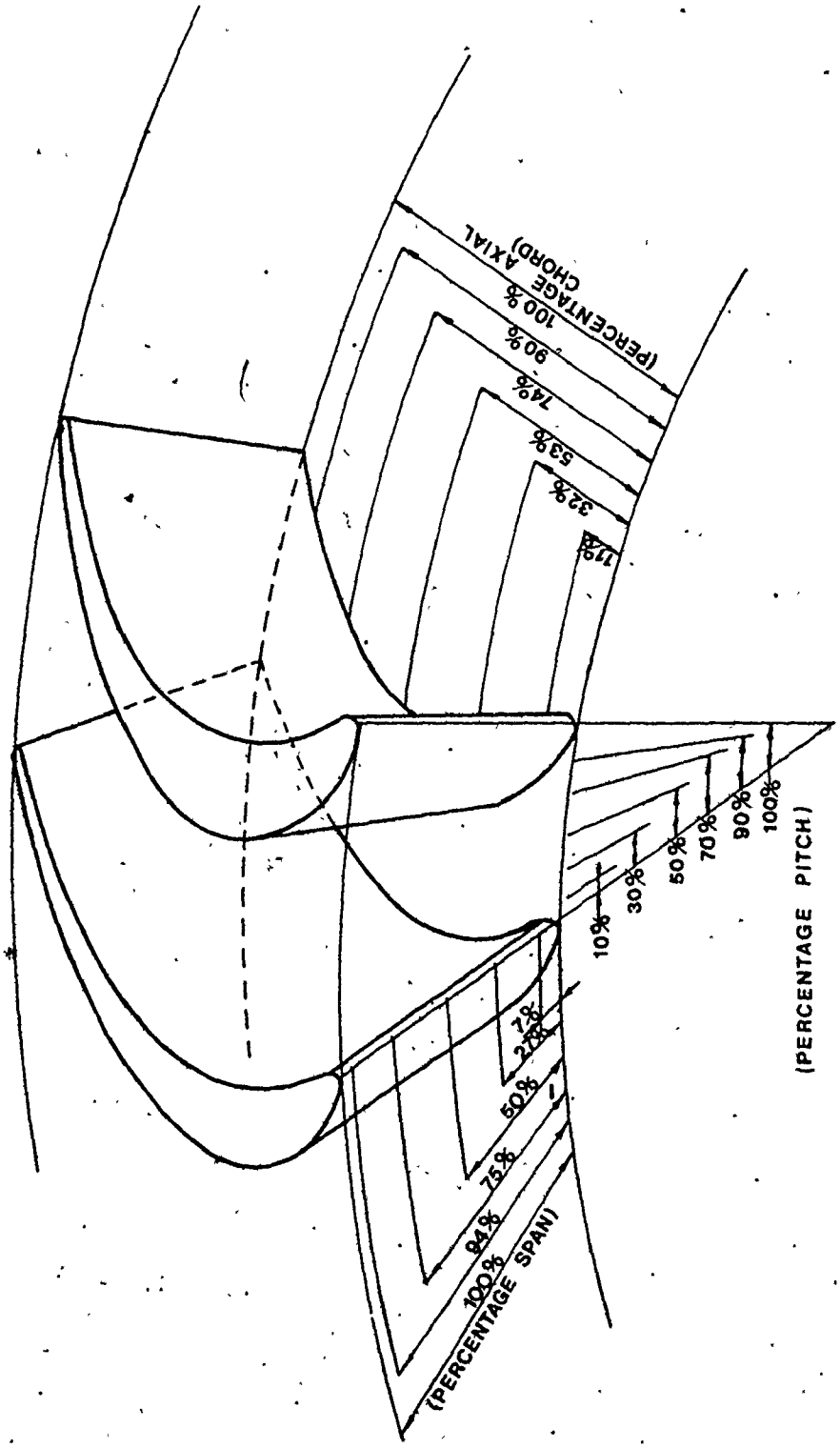

Figure 8.1 Locations of Static Taps on the Blade Passage Surfaces.

8.1 Blade-Surface Pressure Distribution

Contour maps of the isobars on the blade pressure side and suction side are given in Figures 8.2 and 8.3 respectively. On the pressure surface of the blade (Figure 8.2) the pressure varies little over the first 50% of the chord. Within this region the upper portion has more uniform pressure distribution than the lower portion of the blade. Radial gradients of pressure are more noticeable in the lower region near the leading edge. In the region between 50% axial chord and the trailing edge, the pressure falls rapidly and the pressure gradient is nearly axial with slight distortions near the inner wall. The asymmetry of the pressure distribution pattern about the mid span location can be attributed to the increase in pitch/chord ratio from the hub to the tip.

On the suction side of the blade (Figure 8.3) two low pressure regions were observed. The first region is located at about 12% axial chord and the second region is at about 60% axial chord. The axial pressure gradient is steepest near the leading edge. The radial pressure gradient is more apparent over the region extending from 30% chord to the trailing edge of the blade. It is evident that the flow on the suction surface will have significant radial components which can be associated with secondary flow pattern in the passage.

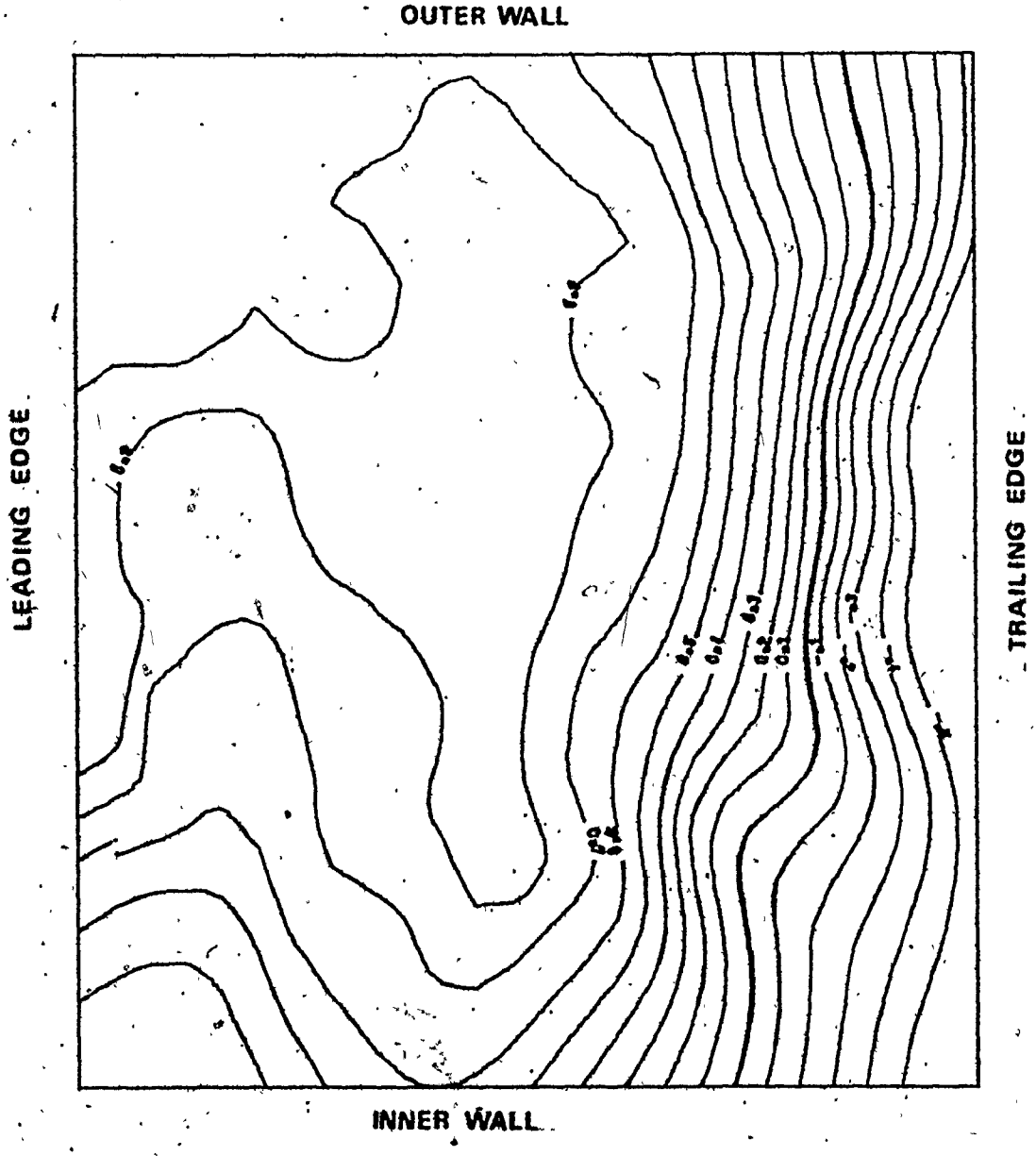

Figure 8.2 Static Pressure Coefficient Contours on the Pressure Side of the Blade.

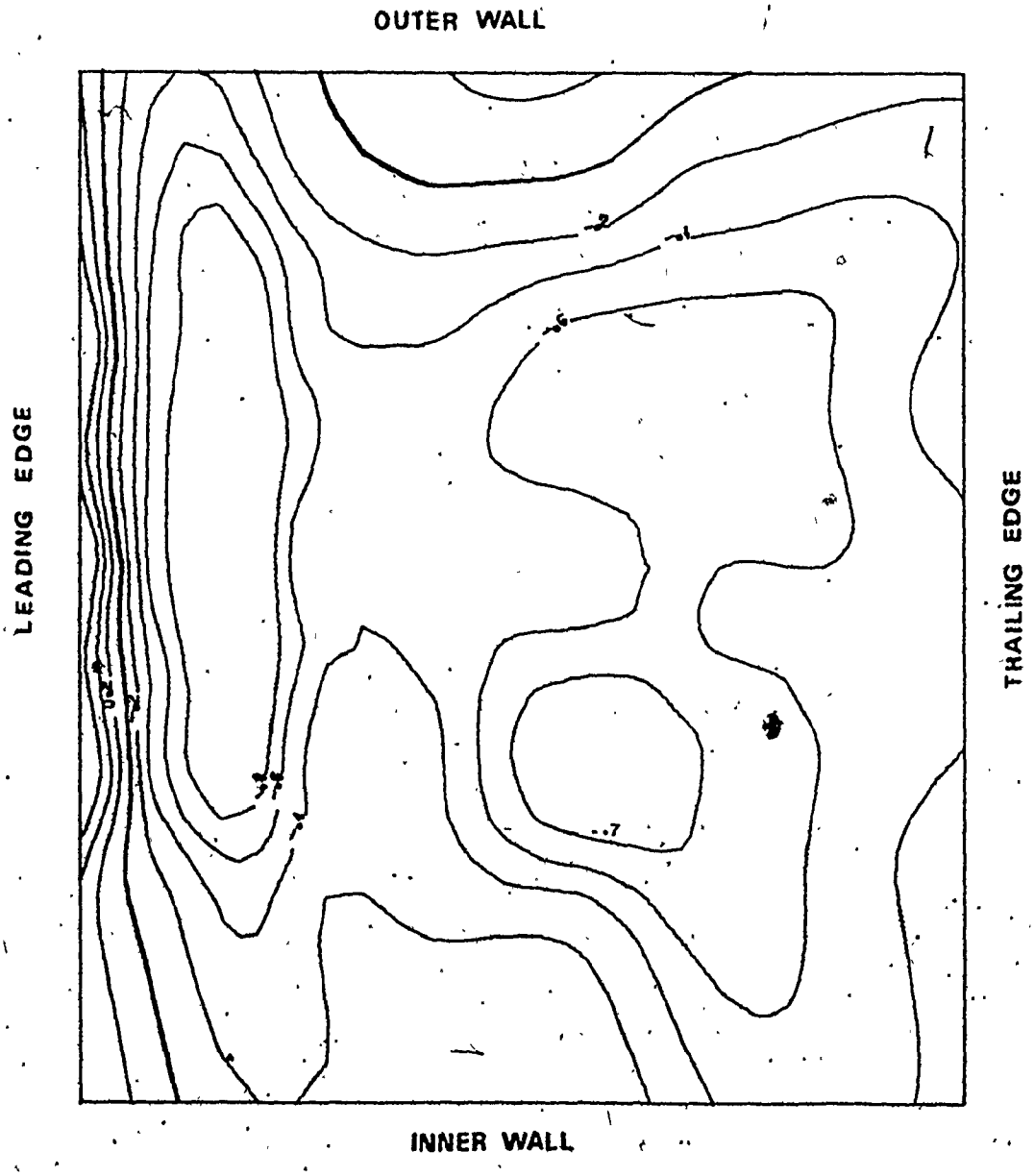

Figure 8.3 Static Pressure Coefficient Contours on the Suction Side of the Blade.

The blade loading is shown in Figure 8.4 which describes the condition of the static pressure on the blade suction side and pressure side as a function of axial chordwise distance at five spanwise locations (Z/H = 7%, 27%, 75% and 94%). The blade loading is seen to be smaller near the end walls (Figure 8.4 (a & e)) and larger close to 75% span (Figure 8.4 (d)). On the pressure surface of the blade the pressure changes slowly within the first 30% of the axial chord and then drops more rapidly indicating that the acceleration on the pressure side was mostly gained beyond 50% axial chord. The increase in pressure near the inner wall and close to the leading edge is associated with the presence of a radial component of the gradient as mentioned before.

On the suction side, rapid acceleration is noticed up to 12.5% axial chord. The pressure then rises due to local separation up to approximately 30% chord. The pressure then drops towards the throat region (75% chord) and starts to rise past the throat till the trailing edge. The rise in pressure beyond the throat is due to transverse area changes resulting in flow deceleration.

It is apparent from Figures 8.2, 8.3 and 8.4 that the spanwise location of maximum loading (75% span) corresponds to the lowest radial pressure gradient. At this location the pressure distribution is compared with a theoretical two-dimensional potential flow model due to Stannard [53].

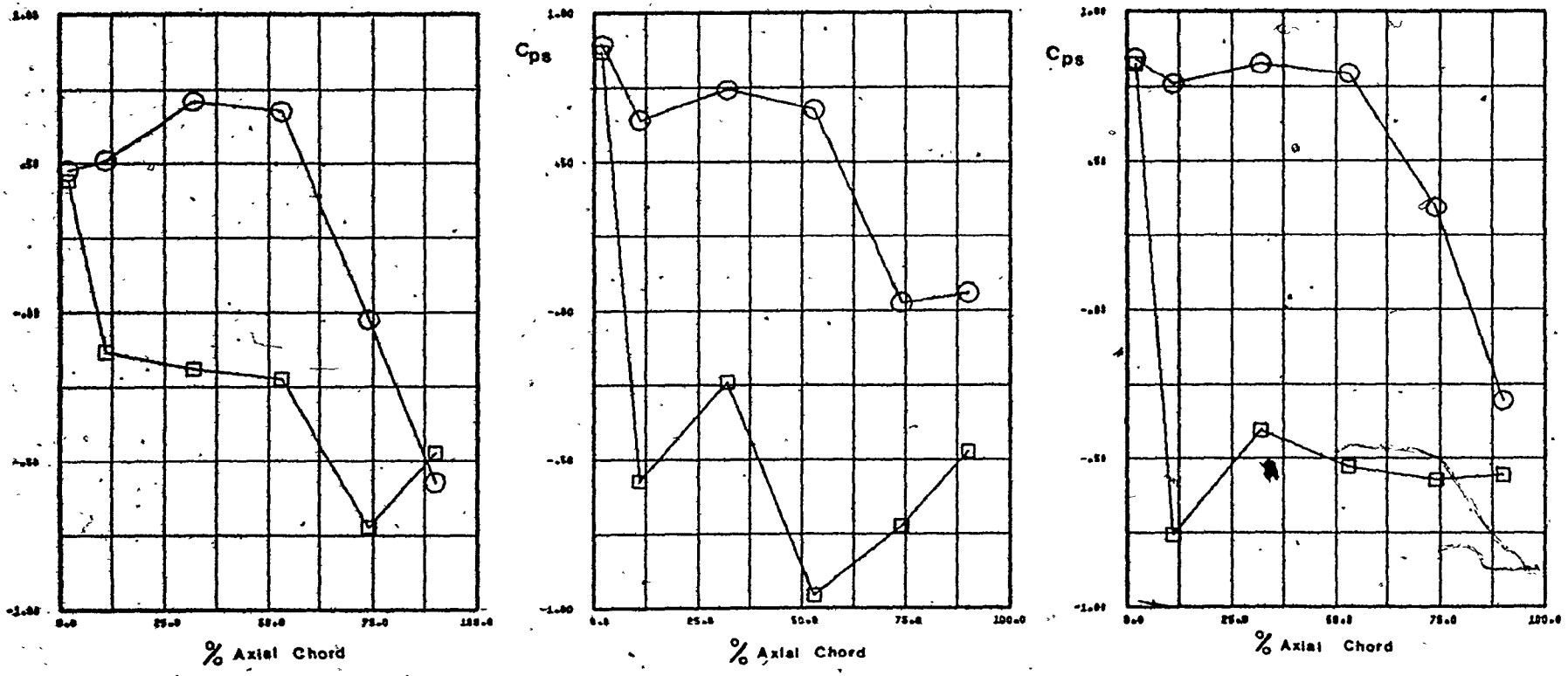

a) Z/H = 7%

b) Z/H = 27%

c) Z/H = 50%

Figure 8.4 Blade Surface Pressure Distribution (Continued on the next page).

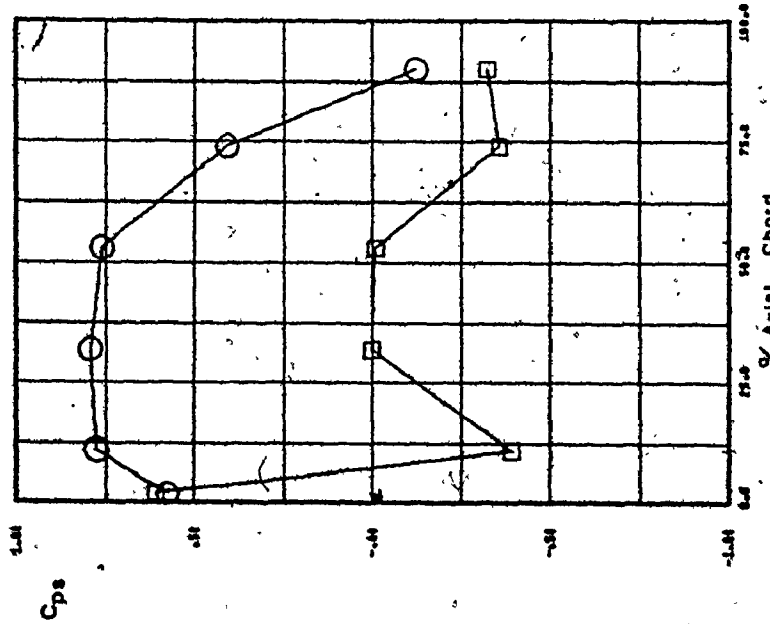

e) Z/H = 94 %

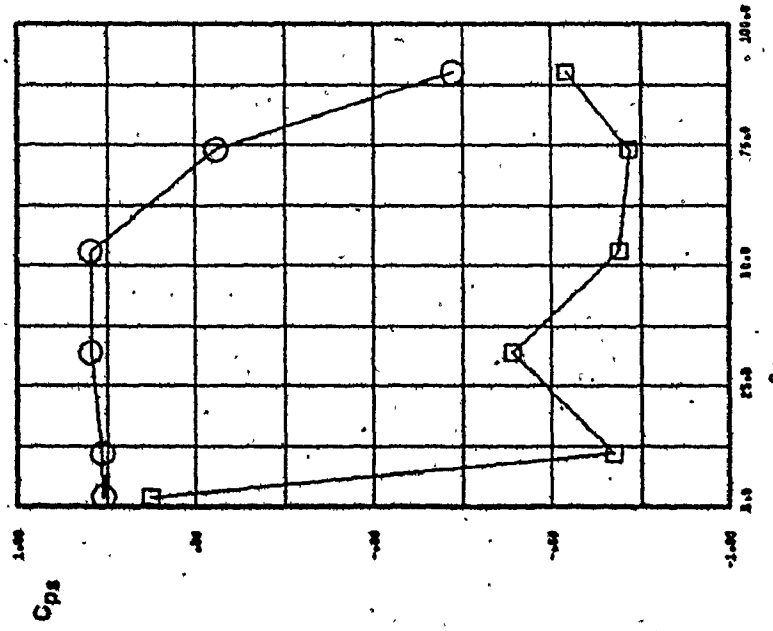

d) Z/H = 75 %

Figure 8.4 Blade Surface Pressure Distribution (Concluded).

As shown in Figure 8.5, good agreement is noticed on the pressure side except for the leading edge zone. On the suction side, however, some deviations are noticed but the trend of variation is reasonably similar. The deviations are associated with the three dimensional effects in the vicinity of the suction surface (i.e., the roll-up of the passage vortex from the inlet boundary layer flow) and the separation pattern on the blade surface. More deviation is observed at other spanwise locations for the same reasons.

8.2 Endwall Pressure Distribution

Isobar contour maps of the inner and outer annular walls are shown in Figure 8.6 and Figure 8.7 respectively. The cross channel gradient extends over a larger distance on the outer endwall than on the inner endwall. This is in agreement with the low blade loading near the inner endwall depicted in Figure 8.4. It is also noticed that the minimum pressure occurs at a point shifted away from the suction side of the blade. Langston et al. [44] observed a similar situation and associated it with the local separation occurring in the vicinity of the suction side upstream of the throat region. The authors noted considerable difference between the measured endwall pressure and the calculated potential flow pressure distribution. Sjolander [22] found that

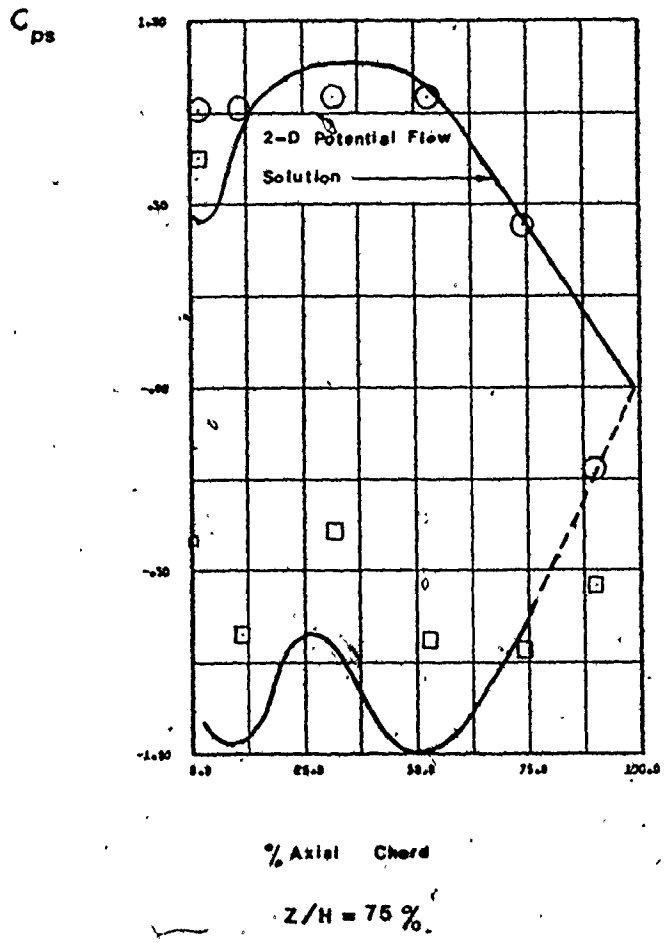

Figure 8.5 Blade Surface Pressure Distribution at Z/H = 75% in Comparison with 2-D Potential Flow Solution of Ref. [53].

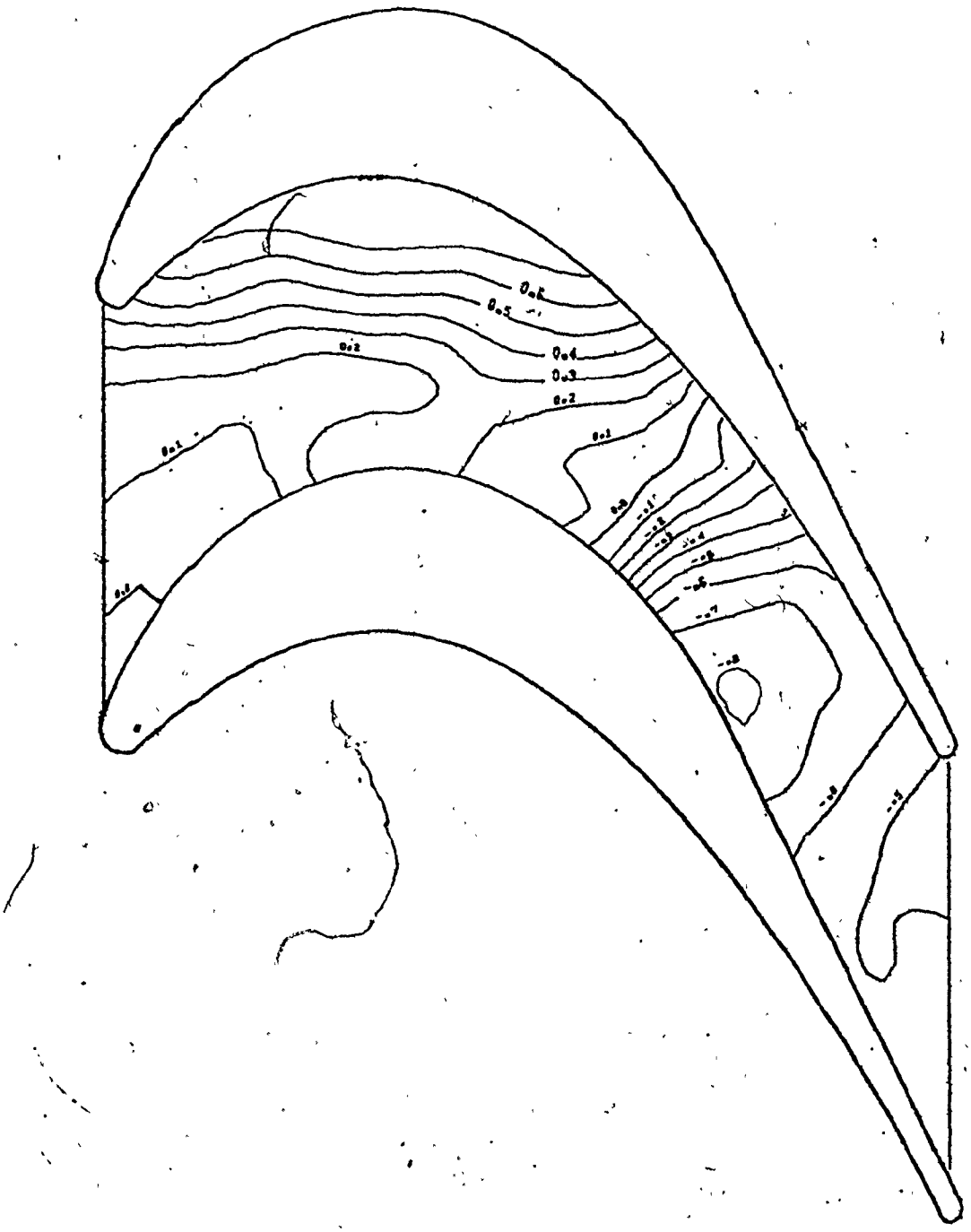

Figure 8.6 Isobars of Static Pressure Coefficient on the Inner Wall.

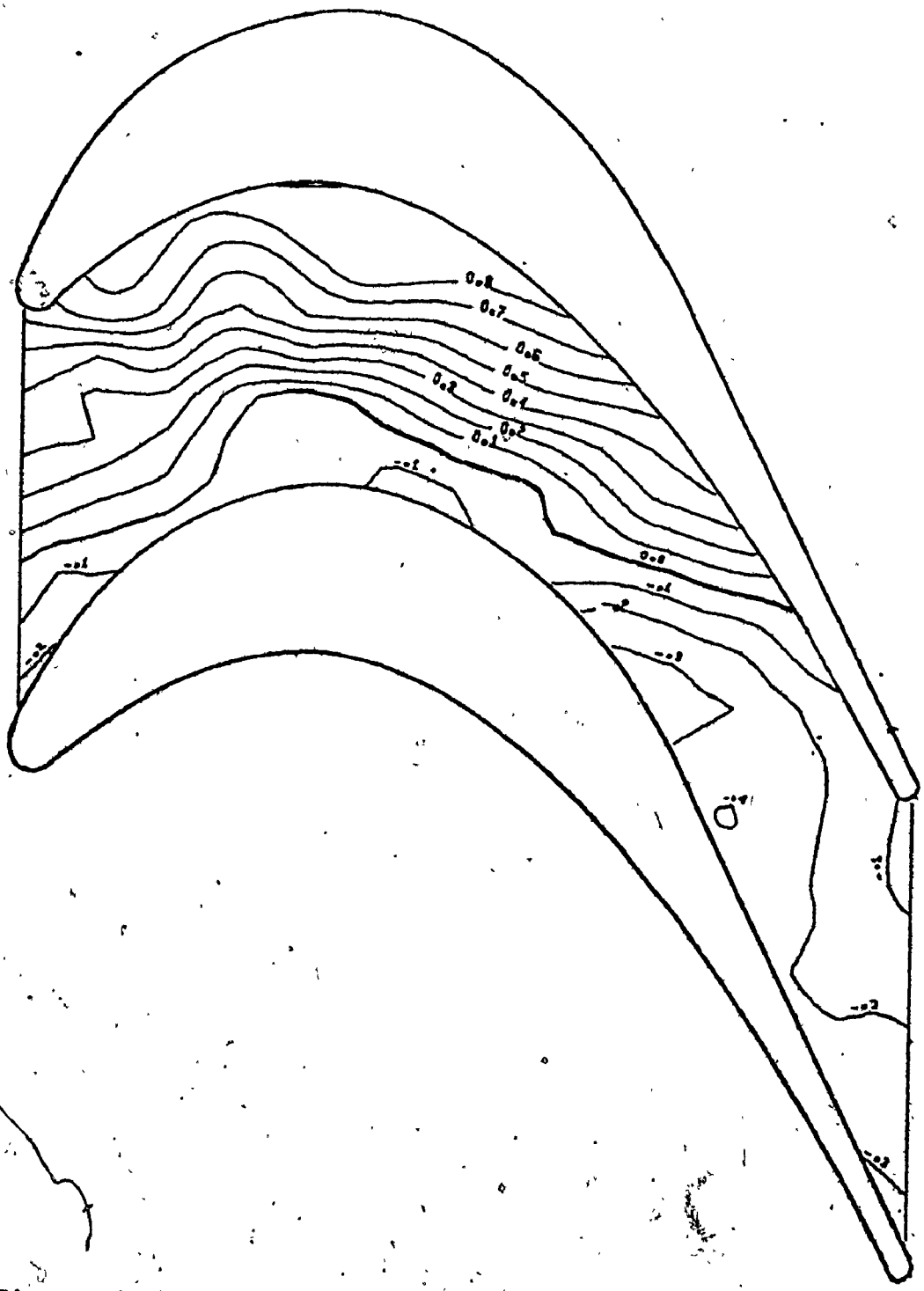

Figure 8.7 Isobars of Static Pressure Coefficient on the Outer Wall.

the shear stress trajectories in the endwall region were essentially parallel to the pressure gradient, indicating that the energy of the fluid is so small that inertia effects are unimportant. Thus the endwall pressure is dominant in determining the direction of the endwall shear stress and consequently the cross channel flow. Accordingly the cross flow on the outer endwall is expected to extend over most of the passage. On the inner endwall it is expected to find more cross flow within the first 60% of the chordwise distance in the passage than in the remainder of the passage. The pitchwise pressure distribution on the endwalls at the exit measuring station is shown in Figure 8.8.

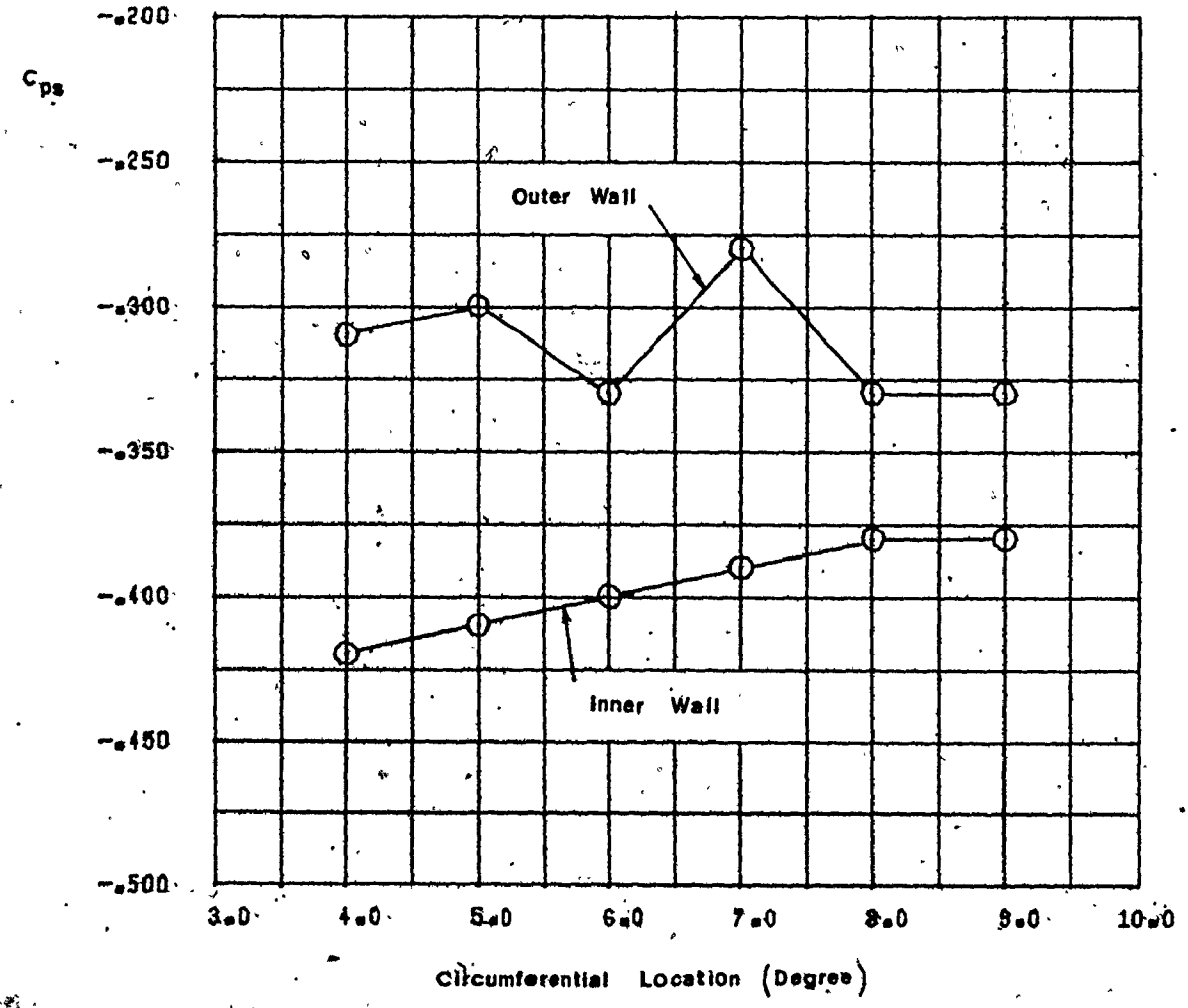

Figure 8.8 Static Pressure Distribution on the Endwalls at the Exit Measuring Plane.

CHAPTER 9

EXIT FLOW PARAMETERS

The flow at the exit measuring station was traversed for six inlet flow conditions with different combinations of boundary layer displacement thicknesses at the inner and the outer annular walls. The tests were conducted at an inlet mean velocity of 34.14 m/s (corresponding to a Reynolds number of 4.73×10^5 based on the blade chord). The measurements included the total and static pressure as well as the flow angles. A complete traverse, covering a circumferential distance of twice the blade pitch, was first performed to examine the periodicity of the flow at the exit from the cascade. During the test, readings were taken at 16 radial locations (over the annular height of 7.5 inches (190.5 mm) and 15 circumferential positions (at 2^o increments). The remaining tests covered the center passage of the cascade with an average of 120 points in the main flow and 20 points in each of the endwall boundary layers. Measurements in the main flow were taken using the three-dimensional five-hole probe. The exit blade angle was used as a reference for measuring the yaw angle, thus the yaw angle measured ($\Delta\alpha_2$) indicated the difference between the exit flow angle and the exit blade angle (underturning or overturning).

From the total and static pressure readings, the local total pressure loss coefficient C_{po}, and the local static pressure coefficient C_{ps} were calculated according to the following formulas,

$$C_{po} = \frac{P_{o1} - P_o}{\frac{1}{2} \rho V_1^2} \tag{9.1}$$

$$C_{ps} = \frac{P_1 - P}{\frac{1}{2} \rho V_1^2} \tag{9.2}$$

where

P_{o1} is the inlet free stream total pressure measured at mid span.

P_o is the local total pressure at the exit measuring plane.

P_1 is the inlet free stream static pressure corresponding to P_{o1}.

P is the local static pressure.

V_1 is the inlet reference velocity.

From the exit flow velocity, pitch and yaw angles the axial flow velocity as well as the secondary flow velocity (in-plane velocity of the exit measuring station) can be calculated.

A data reduction program was developed (Appendix 3) for calculating the local flow parameters, the pitchwise averaged values and the total pressure loss coefficients. The program facilitated data presentation in several forms including contour maps, vector presentation of the

secondary flow and a three-dimensional illustration of the local values. In the following sections, the inlet flow conditions selected for the exit plane testing are defined. Maps of the local parameters are presented and analysed. The pitchwise averaged values of the total pressure loss coefficient and the exit angle deviation ($\Delta\alpha_2$) are studied and compared with previous cascade data. The overall total pressure loss coefficient and the secondary loss coefficient are calculated and compared with existing correlations.

9.1 Selected Inlet Flow Conditions for Exit Flow Measurement

In order to examine the influence of the inlet boundary layer characteristics on the flow at the exit from the cascade, it was essential to select those inlet conditions that were expected to have a significant effect on the exit flow. In order to study the effect of each endwall boundary layer as well as their combined effect the following test conditions at the inlet were considered for further measurements at the exit:

1. Initial conditions with no suction at either endwall.
2. Suction applied at the inner endwall.
3. Suction applied at the outer endwall.
4. Suction applied at both endwalls (at the same values of suction established for tests 2 and 3).
5. Suction applied at both endwalls (at different

values from those for 2 and 3).

6. Transverse injection at the outer wall.

The difference in the values of the displacement thickness at the endwalls presented some difficulty in establishing a representative value of δ^* for the cascade that would be indicative of the boundary layer characteristics at both walls. Since it was required to find such a value, for the purpose of comparing the losses at the exit with existing correlations, an averaging procedure for δ_i^* and δ_o^* was introduced. Two alternatives were proposed.

1. To take the arithmetic average of δ_i^* and δ_o^*, i.e.,

$$\delta_m^* = (\delta_i^* + \delta_o^*)/2 \qquad (9.3)$$

2. To scale the values of δ_i^* and δ_o^* by the ratio of r_i and r_o namely,

$$\delta_{av}^* = \frac{\delta_i^* r_i + \delta_o^* r_o}{r_i + r_o} \qquad (9.4)$$

It should be noticed that the second alternative incorporated the relative area of flow in each boundary layer. Another possibility considered was to calculate the loss in the inlet flow by integrating the total pressure deficit over the span. This alternative will be considered in a following section.

The selected control conditions for further measurements at the exit were chosen such that noticeable differ-

ences in δ^*_{av} existed between different inlet conditions. The data for these inlet conditions are given in Table 9.1. The corresponding inlet velocity profiles at $\theta = 4^o$ are given in Figures 9.1.

9.2 Total Pressure Loss Contours

The contour maps of the local pressure loss coefficient (C_{po}) corresponding to the six selected inlet conditions are shown in Figures 9.2 to 9.7. An incremental value of ΔC_{po} equal to 0.1 was chosen to provide a reasonable number of contours in each map. The traverse shown in Figure 9.2 was for the initial inlet condition with no suction applied and covered the center blade passage extending to the center of each adjacent passage. The overall picture of the loss distribution depicted in Figure 9.2 gave evidence that reasonable periodicity prevailed at the exit measuring plane.

A study of the loss coefficient maps for the six inlet conditions revealed some common features:

1. The presence of a large high-loss core ($C_{po} = 0.6$) in the region between Z/H = 40% and Z/H = 80%.
2. The presence of a loss peak located at the junction of the blade trailing edges and the inner wall.
3. The presence of two low-loss zones, one close to the inner wall (extending up to a Z/H value of 30%) and the other near the outer wall (starting

Table 9.1

Averaged Inlet Boundary Layer Displacement Thickness

Test Number	$(\frac{\delta^*}{C})_i$	$(\frac{\delta^*}{C})_o$	$(\frac{\delta_1^*+\delta_o^*}{2})/C$	$(\frac{\delta_1^* r_i+\delta_o^* r_o}{r_i + r_o})/C$
1	32.0×10^{-3}	7.91×10^{-3}	20.0×10^{-3}	17.6×10^{-3}
2	5.9×10^{-3}	7.91×10^{-3}	6.9×10^{-3}	7.1×10^{-3}
3	32.0×10^{-3}	3.44×10^{-3}	17.8×10^{-3}	14.9×10^{-3}
4	5.9×10^{-3}	3.44×10^{-3}	4.67×10^{-3}	4.4×10^{-3}
5	14.2×10^{-3}	3.57×10^{-3}	8.89×10^{-3}	7.8×10^{-3}
6	32.0×10^{-3}	11.3×10^{-3}	21.7×10^{-3}	19.8×10^{-3}

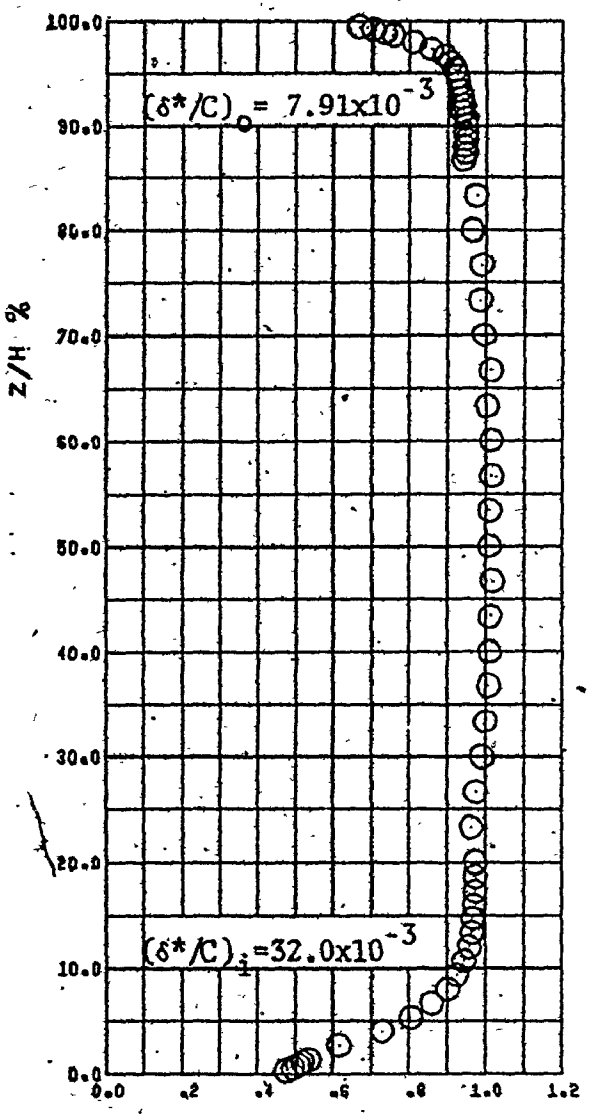

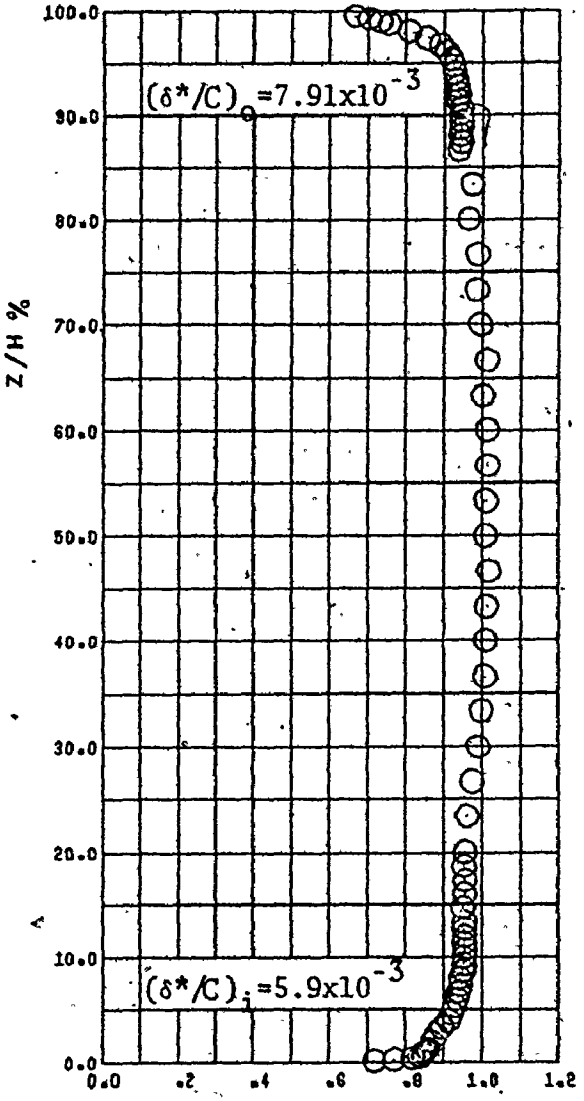

Figure 9.1 Inlet Velocity Profiles.

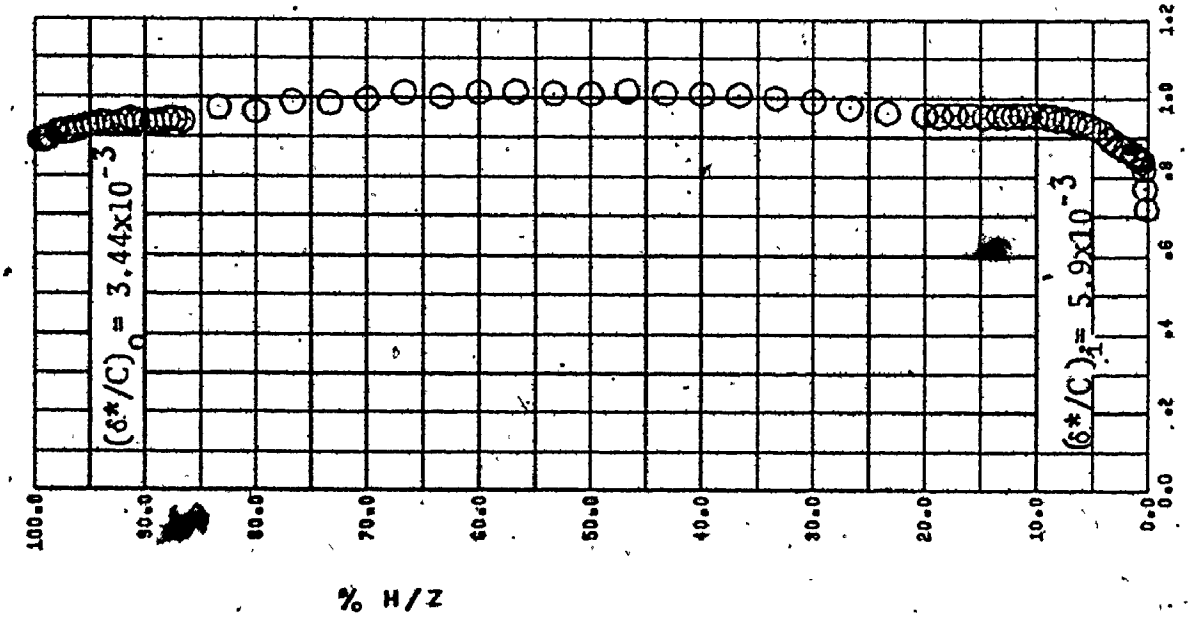

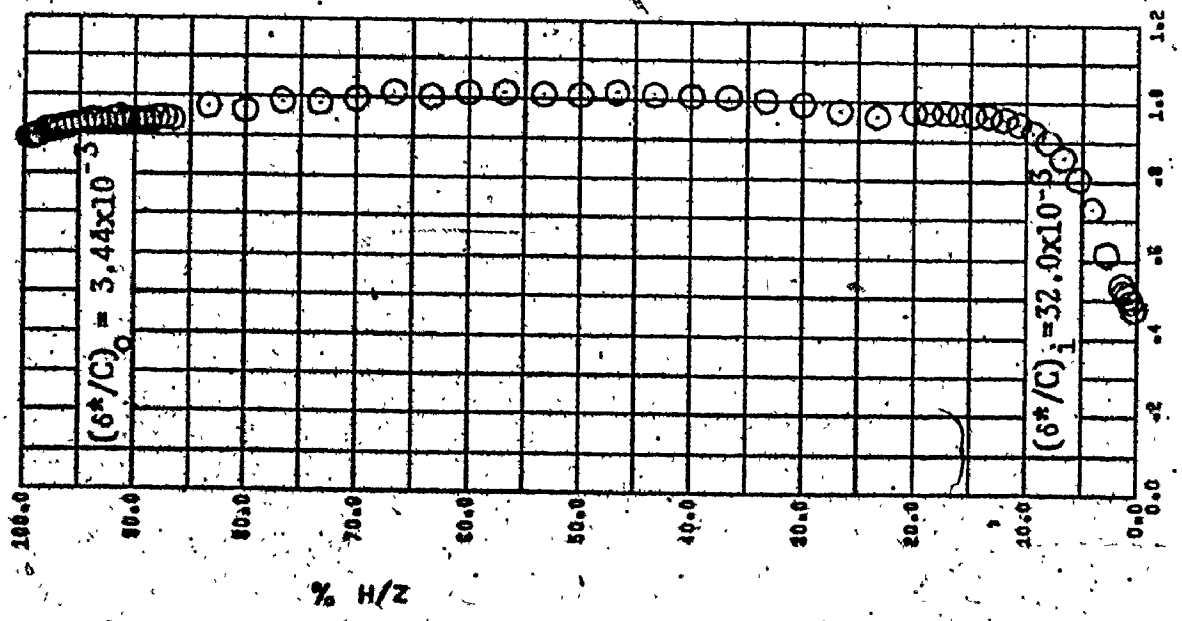

Figure 9.1 Inlet Velocity Profiles (Continued).

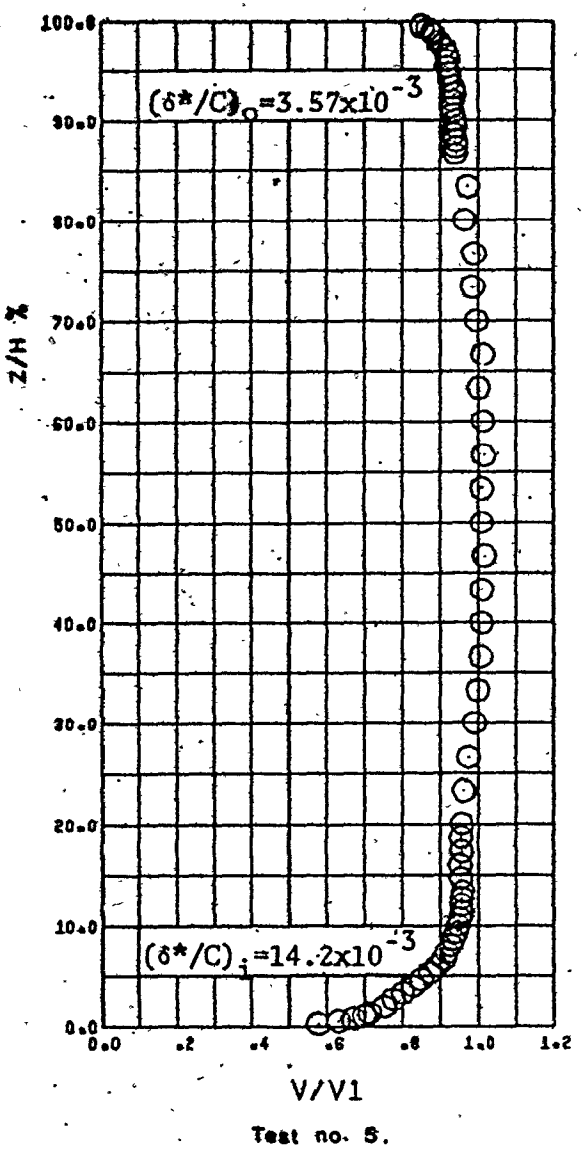

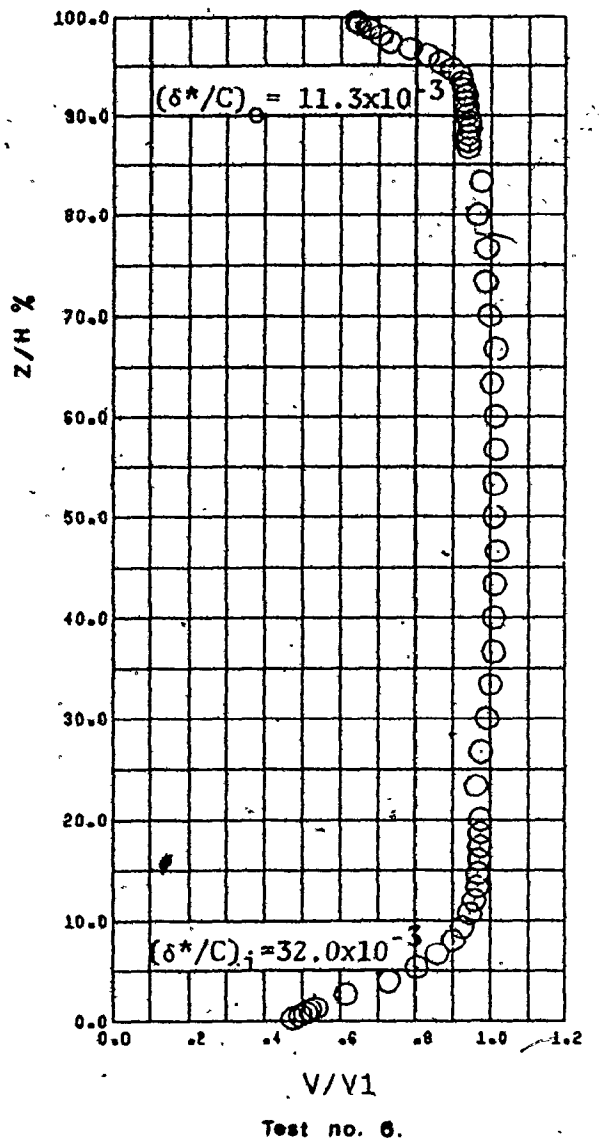

Figure 9.1 Inlet Velocity Profiles (Concluded).

from Z/H = 80%).

In Figure 9.2 the high-loss core C_{po} = 0.6 is seen to enclose two higher peak zones (C_{po} = 0.7) located at Z/H of approximately 50% and 65%. Figure 9.3 shows the exit traverse for the case where boundary layer suction was applied at the inner wall. The comparison of Figure 9.3 with Figure 9.2 reveals that the removal of some of the inner endwall boundary layer fluid resulted in a reduction of the high-loss core area (C_{po} = 0.6). It was also noticed that the inner peak of C_{po} = 0.7 completely disappeared. The outer peak zone (C_{po} = 0.7) was still observed with a slight reduction in size. It can also be seen that the low-loss zone (C_{po} = 0.1) located close to each endwall (shown in Figure 9.3) have increased in area with the applied suction.

Shown in Figure 9.4 are the results obtained when boundary layer suction was applied at the outer wall. A comparison of Figure 9.4 and Figure 9.2 shows that the inner and outer peaks of (C_{po} = 0.7) were eliminated with application of suction. Furthermore a noticeable reduction in the high-loss area of C_{po} = 0.6 can be observed. It can also be noticed that the loss zone of C_{po} = 0.3 was shifted outwards. The outer low-loss zone (C_{po} = 0.1) has grown even further and extended towards the inner wall.

When boundary layer suction was applied at both endwalls (Figure 9.5) a significant reduction in the high-loss

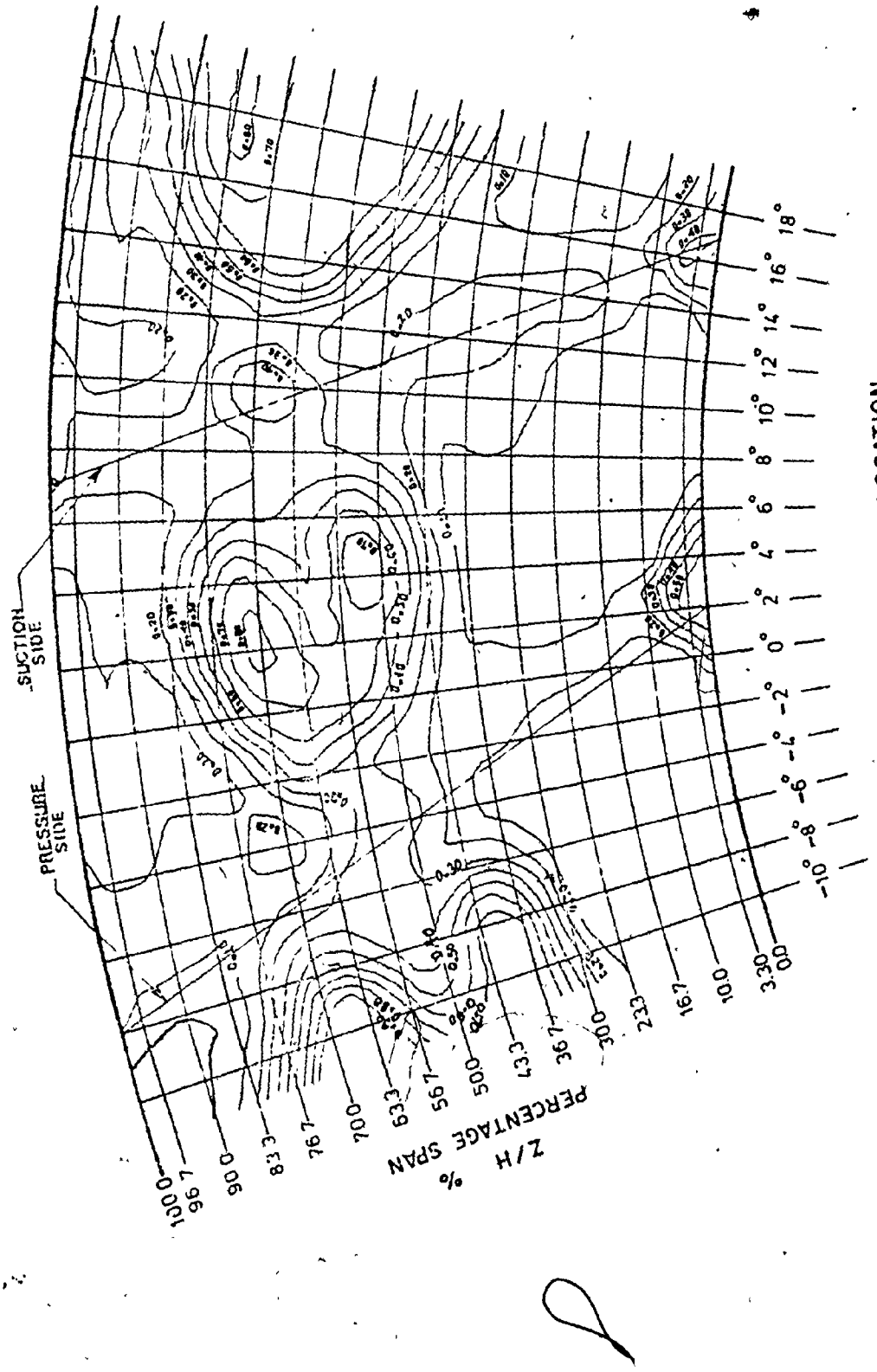

Figure 9.2 Total Pressure Loss Contours for Test #1 (No Suction).

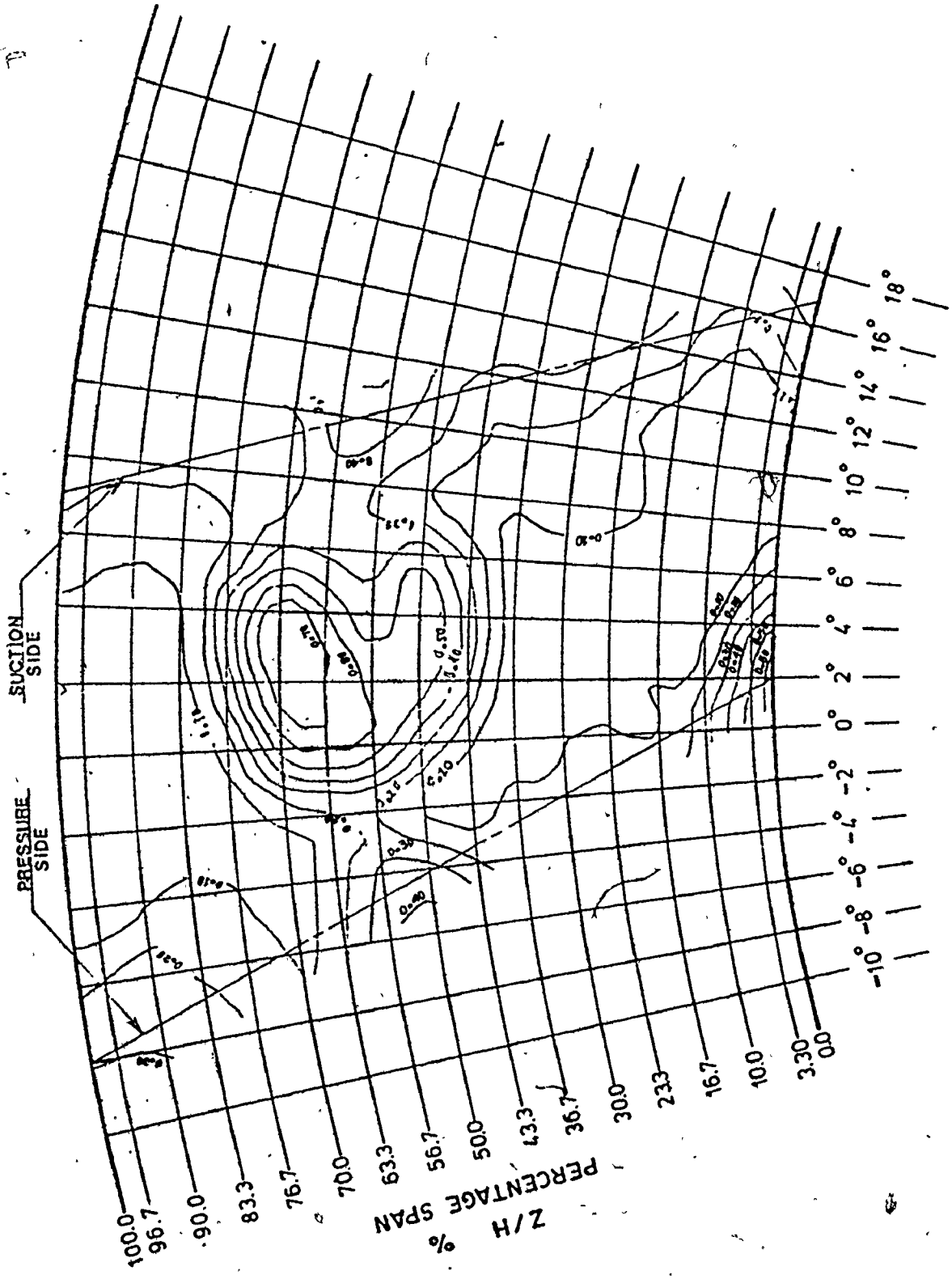

Figure 9.3 Total Pressure Loss Contours for Test #2 (Suction Applied at the Inner Wall).

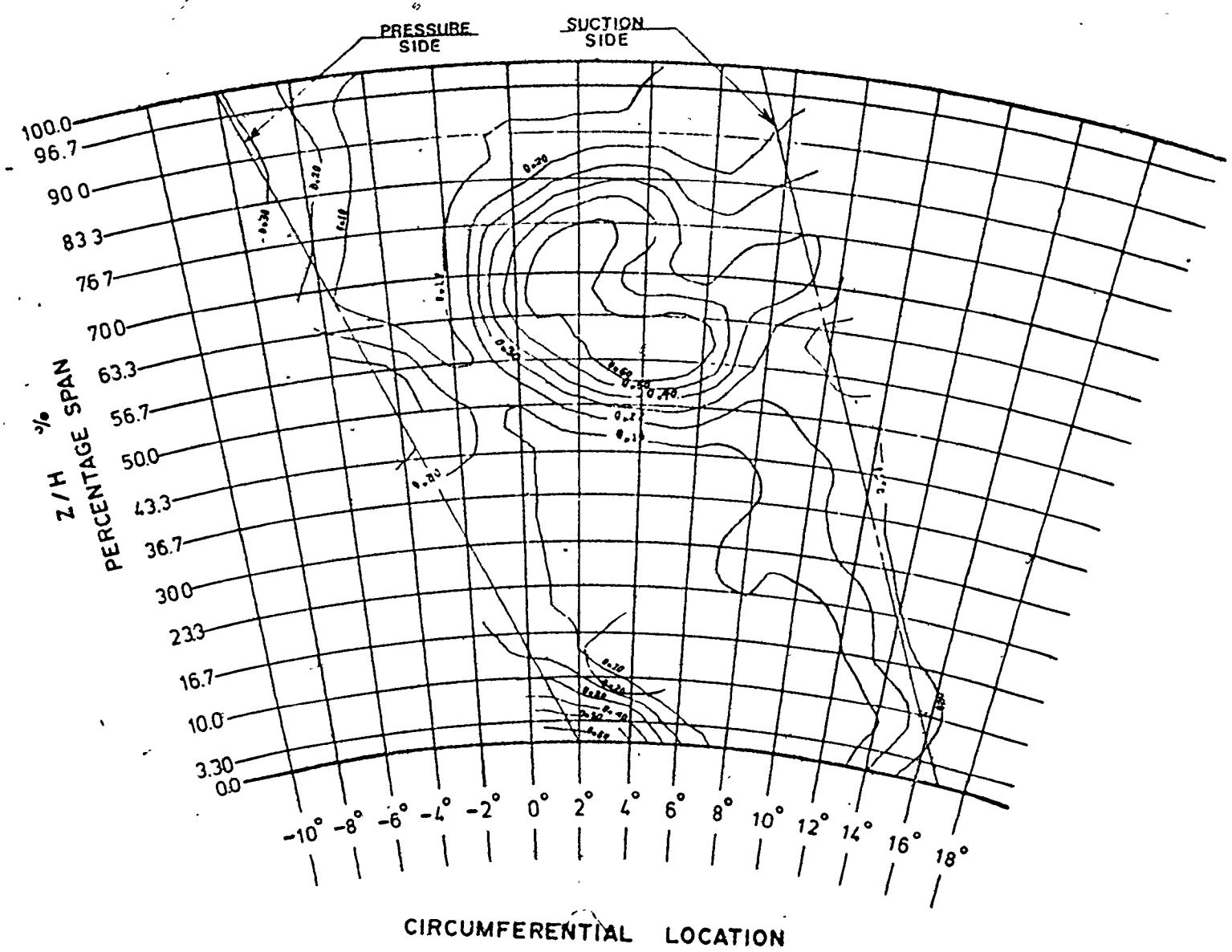

Figure 9.4 Total Pressure Loss Contours for Test #3 (Suction Applied at the Outer Wall).

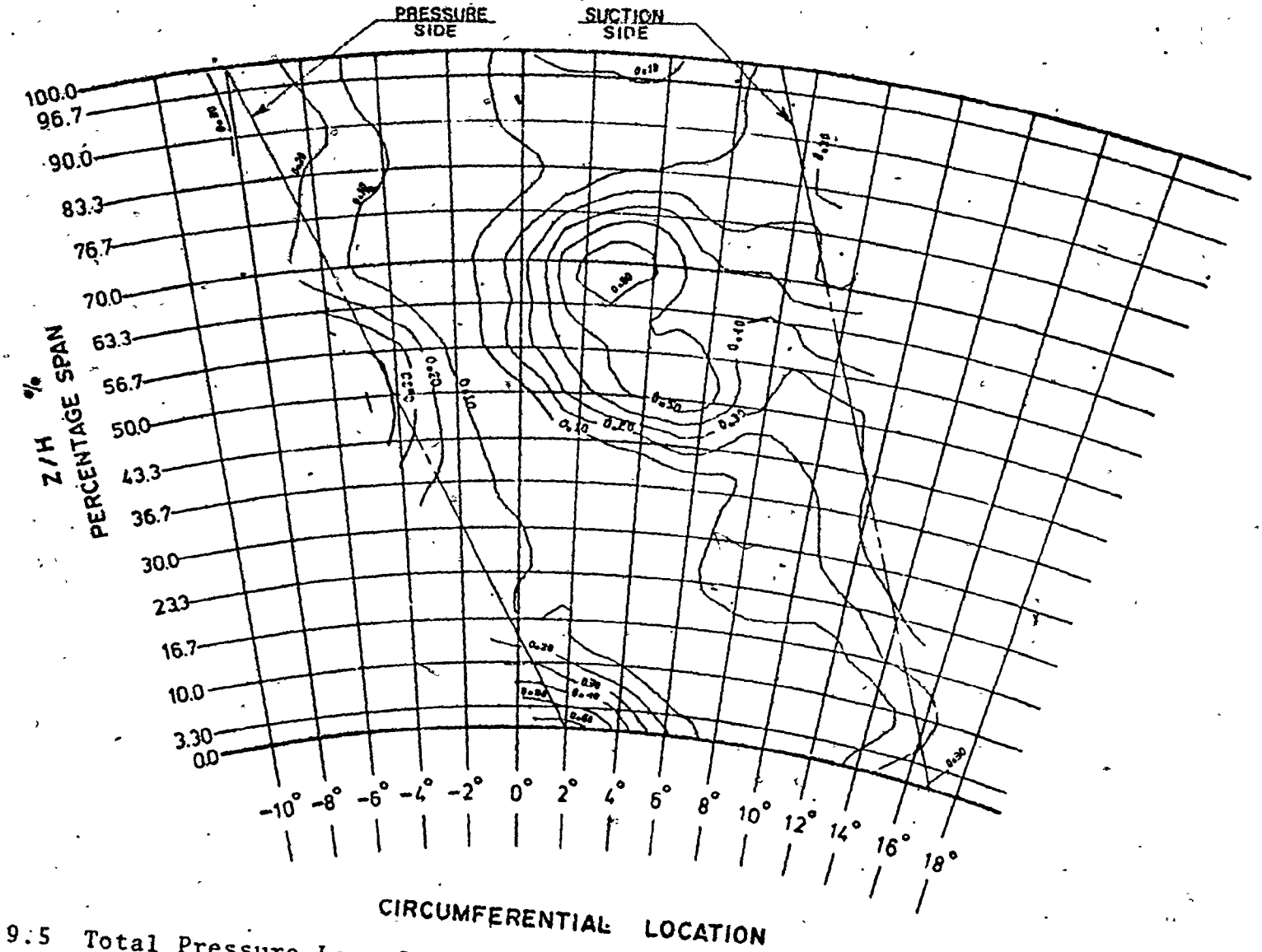

Figure 9.5 Total Pressure Loss Contours for Test #4 (Suction Applied at Both Endwalls Corresponding to Tests 2, 3).

core (C_{po} = 0.6) was observed. The reduction is further noticed in the circumferential direction in the area between Z/H = 40% and Z/H = 60%. The low-loss zones (C_{po} = 0.1) have extended in the spanwise direction and joined to form a single low-loss valley separating the high loss cores of adjacent passages. When the suction effect was reduced on both endwalls the loss area (C_{po} = 0.6) was observed to increase as shown in Figure 9:6.

In an attempt to examine the exit flow characteristics when low energy fluid is injected at the inlet endwalls, only one test was conducted with transverse injection at the outer wall. The test results indicated a definite growth of the loss zones (Figure 9.7). The appearance of even higher peaks within the zone of C_{po} = 0.6 is readily observed in Figure 9.7.

In comparing the present experimental results with previous data it would appear that the spanwise location of the high loss core is associated with flow turning, aspect ratio and radial pressure gradients in annular cascades. In tests reported in the literature on rectilinear cascades the secondary loss cores were normally located near the endwalls and the suction surface of the blades. Came [40] conducted tests on a plane cascade of a 70° turning angle varying the incidence and the inlet boundary layer displacement thickness. The author found that loss peaks increased in size with upstream boundary layer displacement thickness.

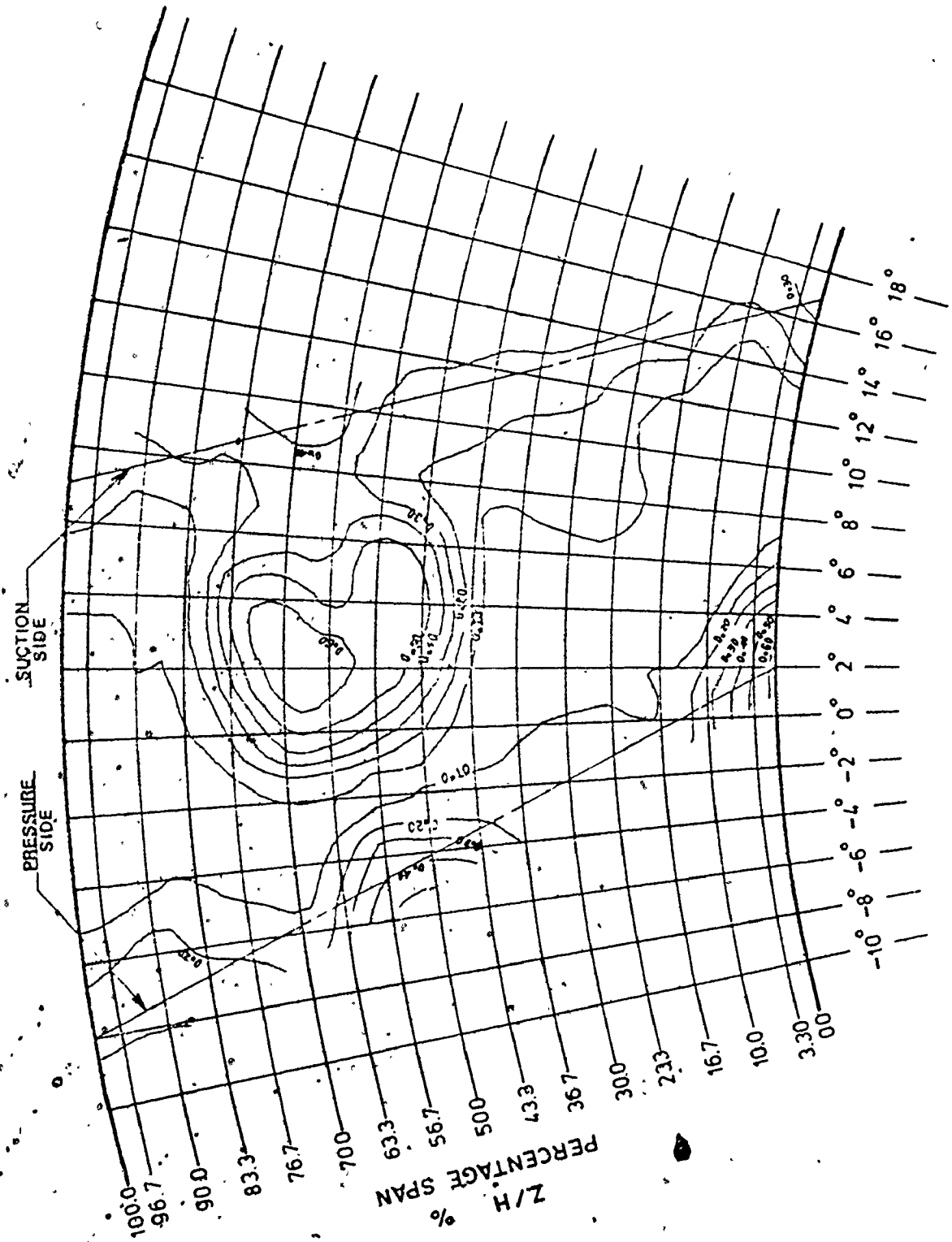

Figure 9.6 Total Pressure Loss Contours for Test #5 (Less Suction Applied at Both Endwalls Than Test #4).

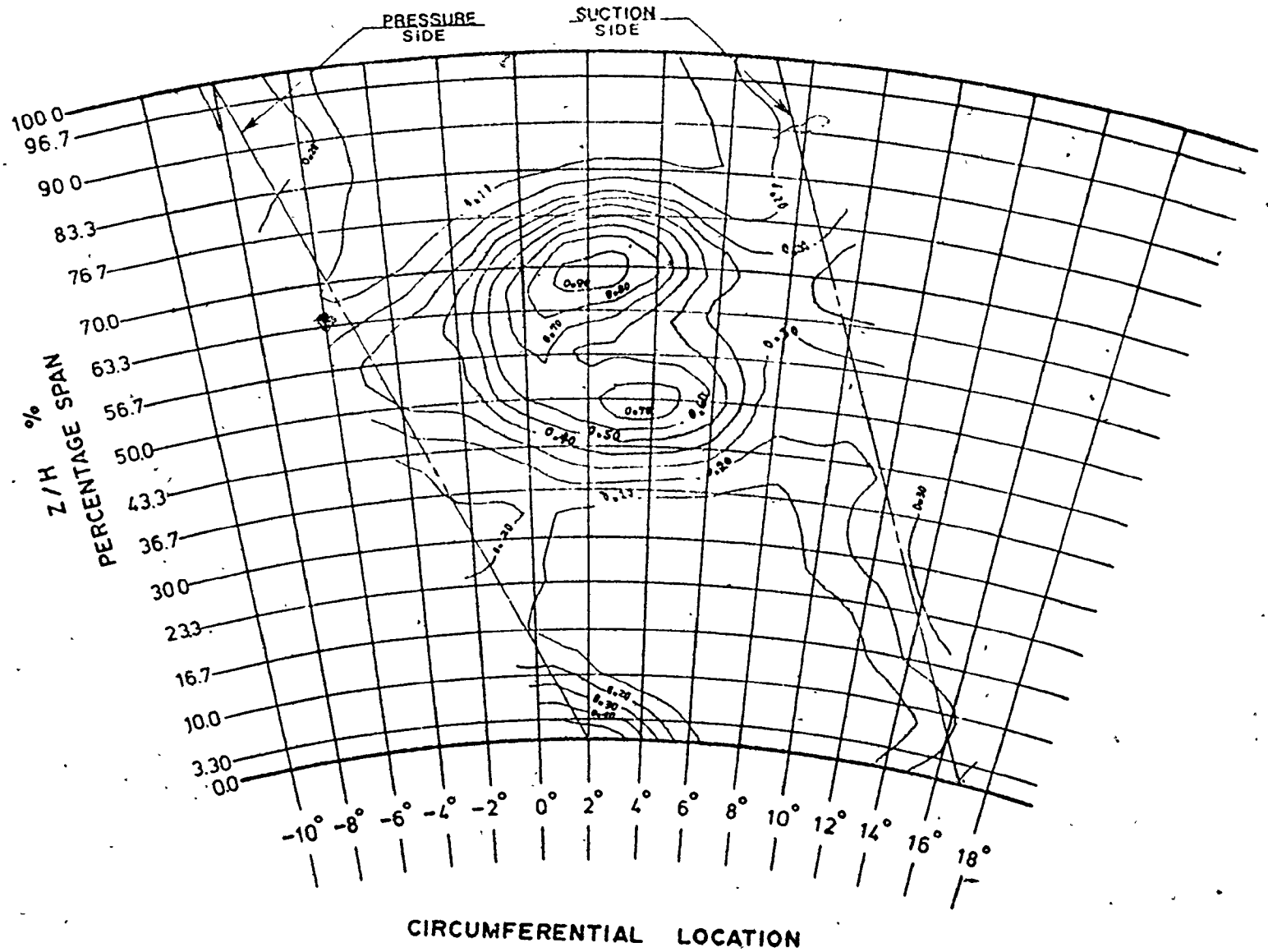

Figure 9.7 Total Pressure Loss Contours for Test #6 (Transverse Injection Applied at the Outer Wall).

The results also showed that the location of the loss cores shifted away from the blade suction surface and the endwall into the passage as flow turning was increased. Woods [43] carried out an experimental study on a 132° turning rectilinear cascade of an impulse type turbine rotor blade varying the blade aspect ratio. The test results indicated the presence of two definite loss peaks shifted away from the endwalls. A region of lower loss was also observed near the walls. As the blade height was reduced the relative position of the core of the low momentum fluid was moved further away from the endwall. The loss peak moved from a spanwise location between Z/H of approximately 15% to a location of Z/H = 24% as the aspect ratio was reduced from 1.036 to 0.592. The author concluded that the secondary flow influenced the flow in the blade passage as well as that on the blade suction surface boundary layer. It was pointed out that the three-dimensional flow had the effect of moving the loss peaks relatively closer to the mid-span location as the blade height was reduced and therefore that the size of the lower loss region near the endwall increased. Langston [44], in tests carried out on a rectilinear cascade of 110° deflection, took measurements within and outside the passage at different axial locations. The loss core was observed to climb up the suction surface of the blade growing in size as the turning increased along the cascade axis. The loss peak at the exit plane was located at Z/H of app[illegible] 25% and

loss zone extended up to 48% span from the endwall.

In annular cascades a more fundamental difficulty arises which is of importance to turbine blade rows. The spanwise pressure gradients move the low-energy air along the span. This effect will cause the loss cores to be shifted even further into the flow passage. Sjolander [22] carried out tests on an annular cascade of nozzle blades with 50^{o} deflection. The experimental results identified two loss peaks, each near the suction surface of the blade at a radial location of approximately 25% span from the endwall. Rohlik et al. [41] showed clearly how low-energy air originating in the outer wall boundary layer was swept not merely on the blade surface but all the way down the trailing edge towards the hub and was finally discharged near the inner wall. This effect was noticed to increase with the Mach number of the flow in the passage. In this case the tip secondary loss was observed to be very small and the hub secondary loss was correspondingly larger. The assessment of the secondary and profile loss becomes difficult and the extent to which the profile loss is affected is not known.

The analysis of the test results presented in [40] and [43] suggests that in the present tests the displacement of the loss cores into the middle of the passage is associated with the cascade geometry and flow turning since the cascade has a low aspect ratio (1.0), a high

turning angle (128.5°) and a low inner to outer diameter ratio (0.667). The variation of pitch/chord ratio along the span and the orientation of the blades in the annulus are also believed to affect the location of the loss cores. A typical three-dimensional illustration for the variation of C_{po} across the exit plane is shown in Figure 9.8.

9.3 The Secondary Flow at the Exit from the Cascade

The secondary flow velocities in the plane of the exit measuring station were obtained by calculating the component of velocity perpendicular to a reference direction inclined at the blade exit angle. The reference in this case was the same as that of the generatratrices of the exit duct (Chapter 4). The normal velocity component was projected along the reference direction onto the plane of the exit measuring station. The effect of the exit duct geometry on the pitch angle measurements (Chapter 5) was taken into account. The calculation procedure was summarized as follows:

$$V_r = V \sin \Delta\gamma \tag{9.5}$$

$$V_t = V \cos \Delta\gamma \sin \Delta\alpha_2 / \cos \alpha_2 \tag{9.6}$$

$$V_s = \sqrt{V_r^2 + V_t^2} \tag{9.7}$$

where

V_r = the radial component of the secondary flow velocity,

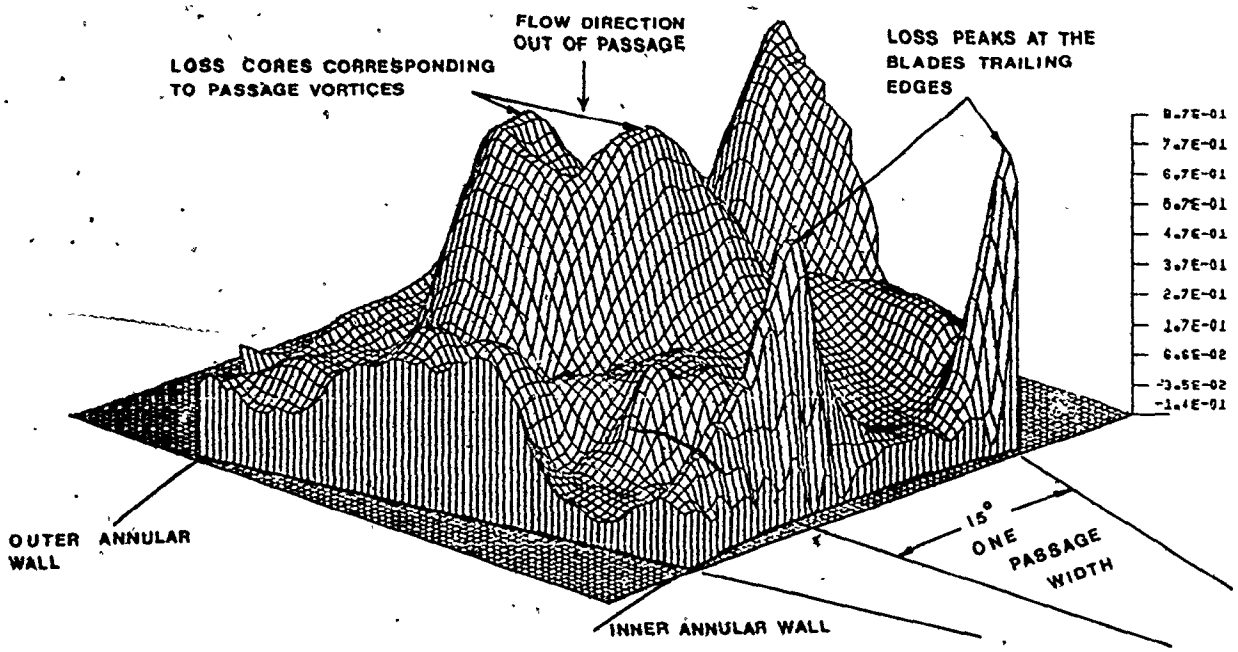

Figure 9.8 A Typical Three-Dimensional Illustration for the Variation of C_{po} Across the Exit Plane.

V_t = the tangential velocity component in the plane of the exit measuring station,

V_s = the resultant secondary flow velocity projected onto the plane of the exit measuring station,

$\Delta\gamma$ = the actual pitch angle measured from the reference direction,

$\Delta\alpha_2$ = the deviation in the exit angle (difference between the exit flow angle and the exit blade angle),

α_2 = the blade exit angle.

The calculation procedure outlined was incorporated in the data reduction sub-program "Dart" (Appendix 3). Vectors representing the secondary velocity were plotted at each location in the exit measuring plane with an arrow length proportional to the magnitude of the velocity. The vector maps corresponding to the six inlet test conditions (discussed in Section 9.2) are shown in Figures 9.9 through 9.14. In the secondary flow vector maps for the complete traverse (Figure 9.9) a repeated pattern is observed in the area surveyed for the three blade passages. The pattern indicates the same type of periodicity depicted in Figure 9.2, and is, in this respect, consistent with the total pressure loss pattern, where the areas of high loss coincide closely with the vortex cores.

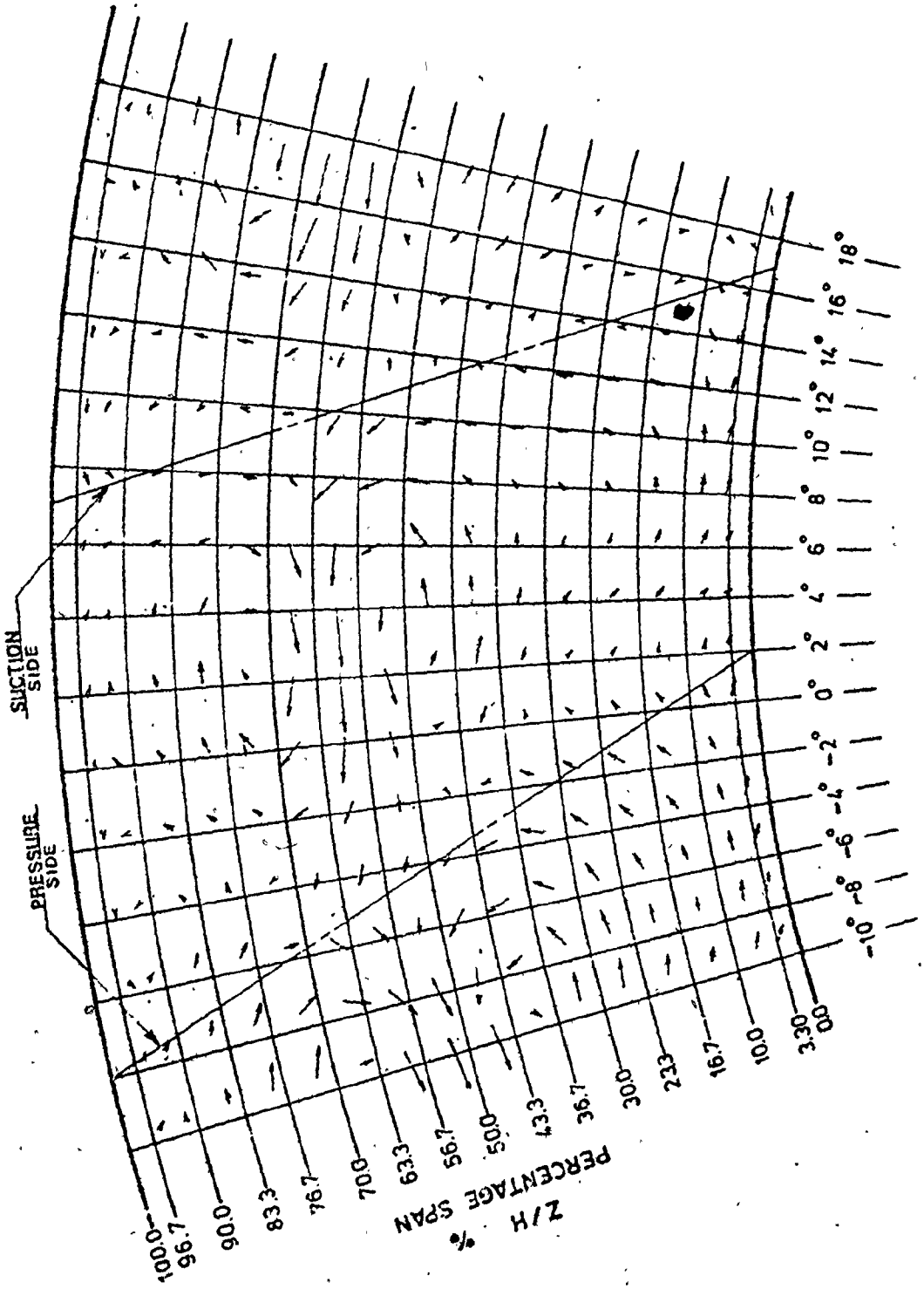

Figure 9.9 Secondary Flow Velocities for Test # 1 (No Suction).

The general features of the secondary flow at the cascade exit as can be seen from Figures 9.9 through 9.14 can be summarized as follows:

1. Two areas of overturning are observed, one near the inner wall and one near the outer wall.
2. The overturning increases with distance away from the endwalls (overturning of up to 12^{o} was measured).
3. The experimental results also indicate the presence of a band of high underturning located at a radial distance Z/H of approximately 60%.
4. It is also apparent that two vortex cores are present in the exit plane, one located at approximately 50% span and the other at approximately 75% span. The vector plots show clearly these vortices and their extent.

The merging of the boundaries of the two vortices at a spanwise location of approximately 60% is obviously the reason for the presence of the high underturning band (maximum values of up to 27^{o} underturning were measured at this radial location).

The comparison of six cases tested shows clearly the effect of the inlet boundary layer on the strength of the vortex and exit angle deviation in terms of overturning and underturning. The application of boundary layer suction at the inner wall alone results in a reduction of the strength of the inner vortex (Figure 9.10). The reduction

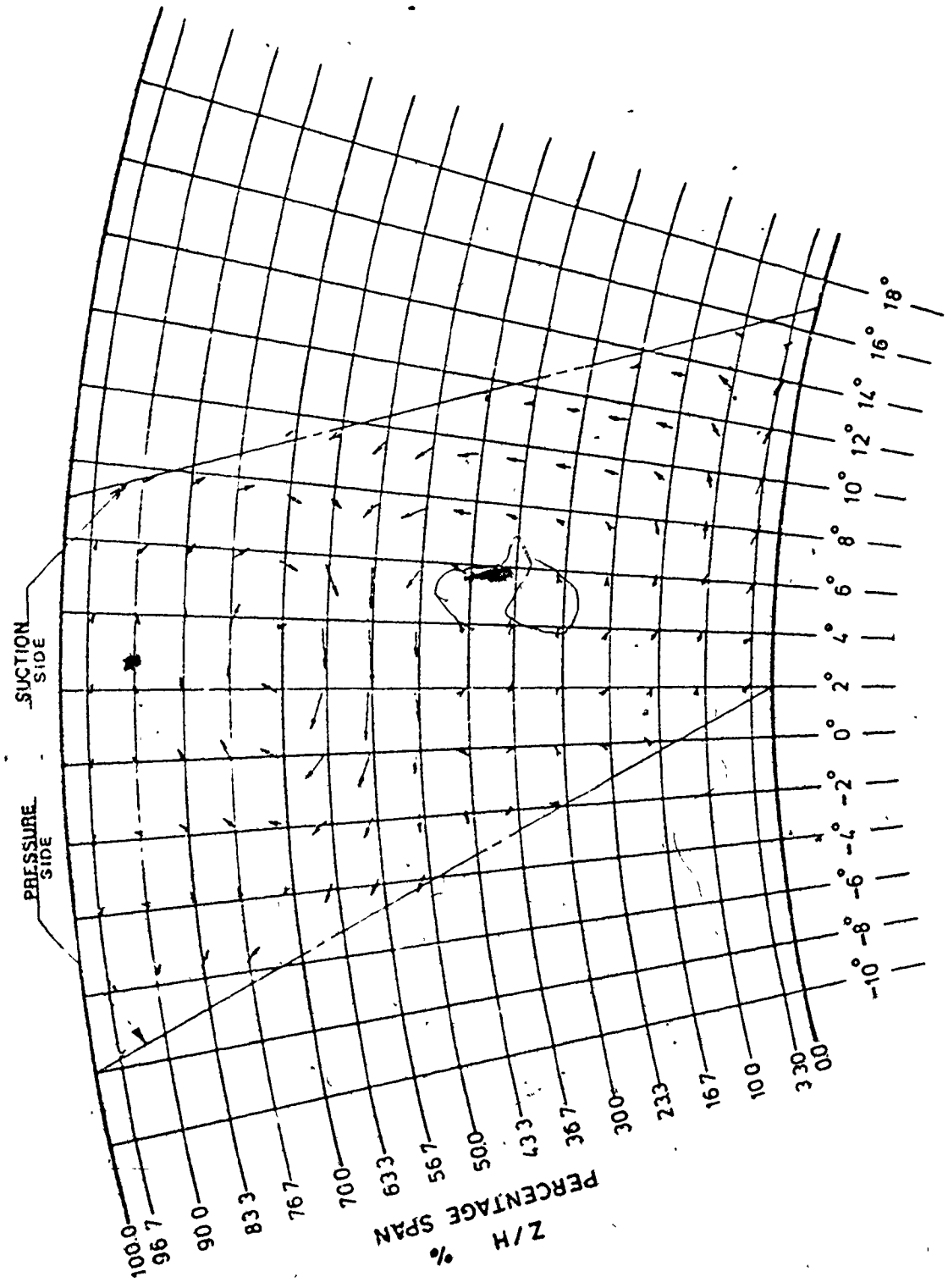

Figure 9.10 Secondary Flow Velocities for Test #2 (Suction Applied at the Inner Wall).

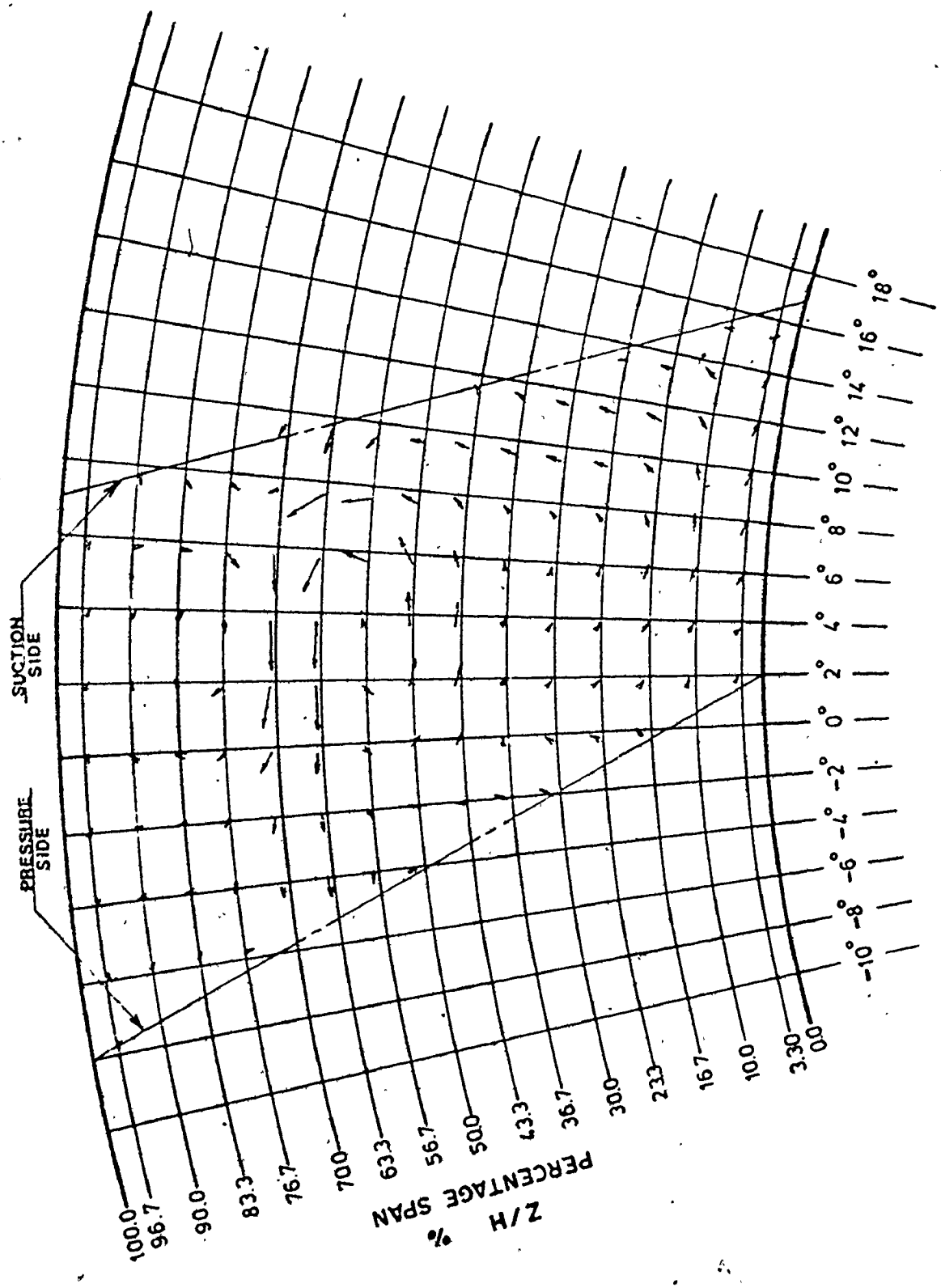

Figure 9.11 Secondary Flow Velocity For Test #3 (Suction Applied at the Outer Wall).

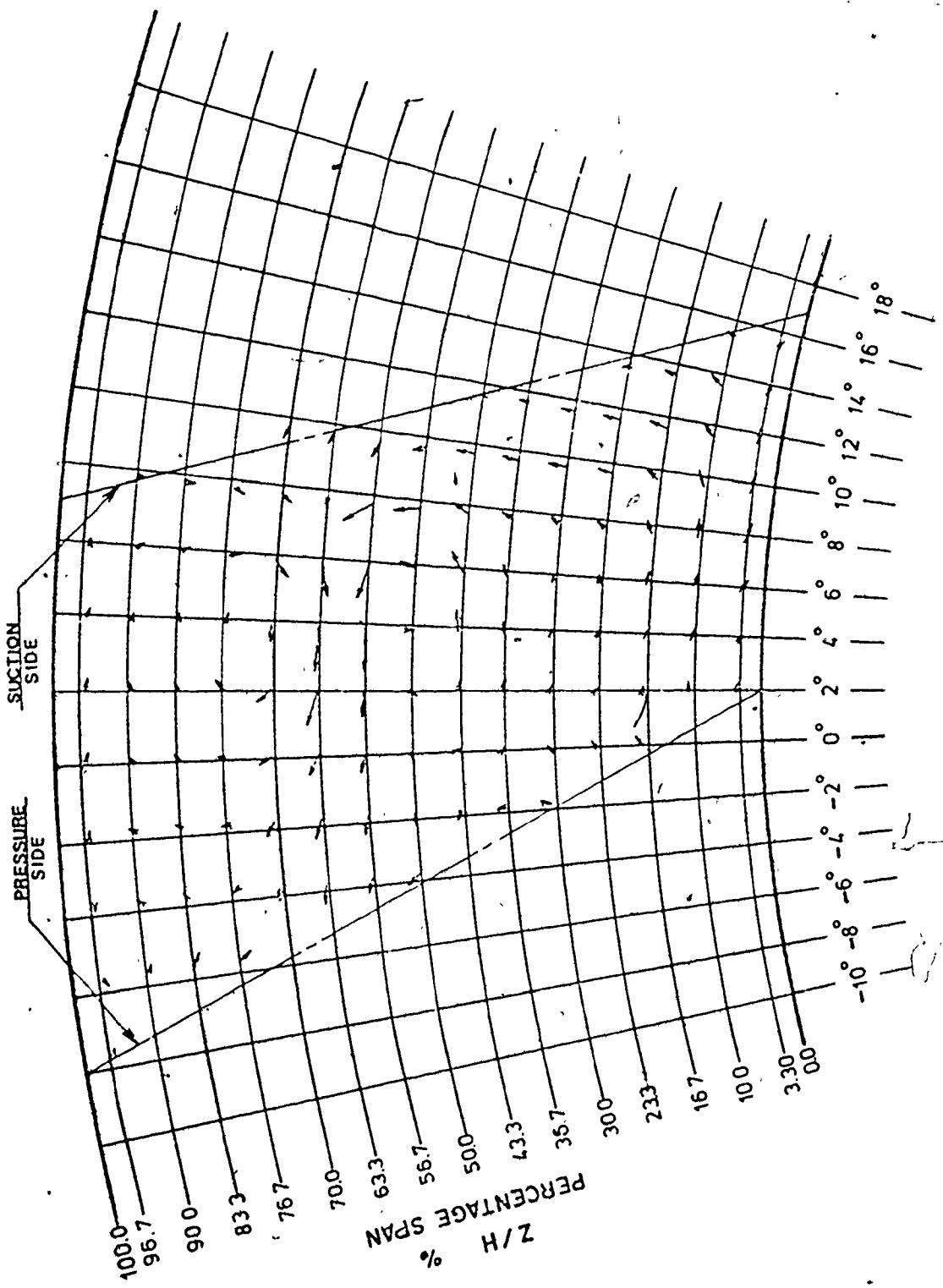

Figure 9.12 Secondary Flow Velocities for Test #4 (Combined Suction at Both Endwalls Corresponding to Test 2 and 3).

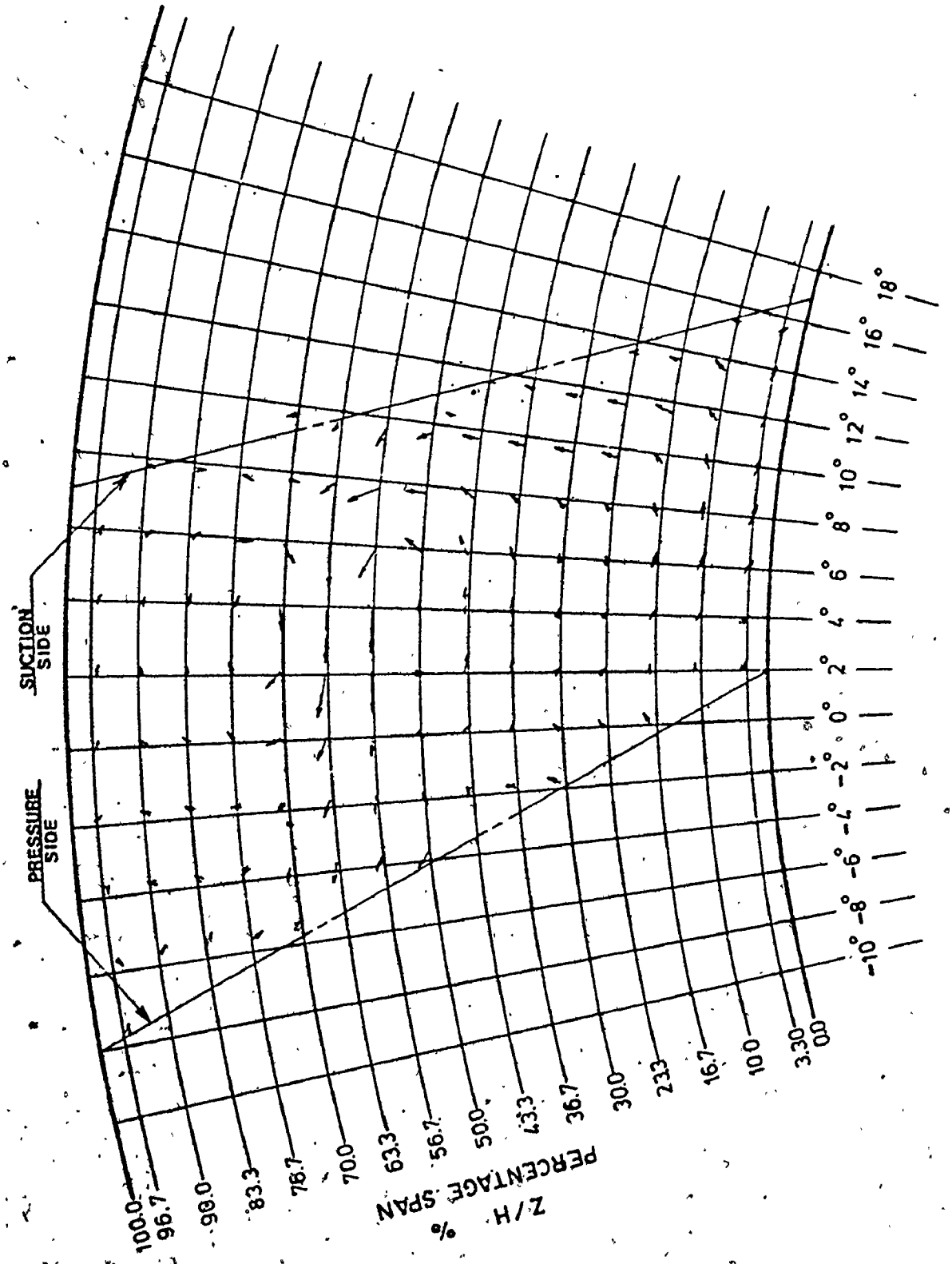

Figure 9.13 Secondary Flow Velocities for Test #5 (Less Suction Applied at Both Endwalls Than Test # 4).

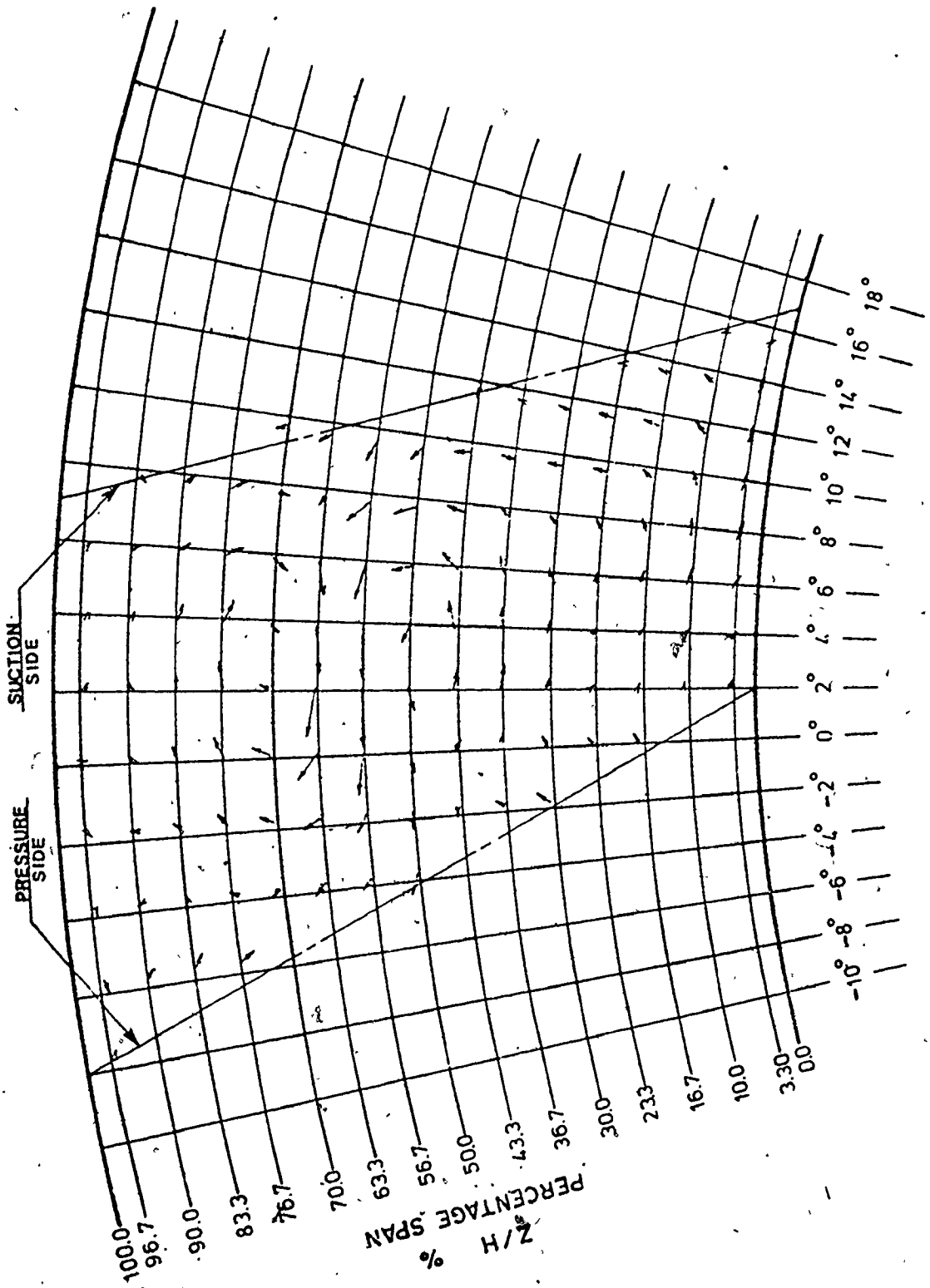

Figure 9.14 Secondary Flow Velocities for Test #6 (Transverse Injection Applied at the Outer Wall).

in the overturning associated with this vortex is more obvious than the reduction in underturning. A similar effect was noted on the outer vortex when suction was applied on the outer wall (Figure 9.11). Combined suction on both endwalls (Figures 9.12, 9.13) affected the two vortices in a simultaneous fashion. The reduction in underturning in this case is more pronounced. Flow injection at the outer wall, on the other hand, (Figure 9.14) resulted in a strengthening of the vortices and a widening of the area that they occupied.

It is evident, therefore, from the analysis of the total pressure loss maps and the secondary flow velocity vectors that the vortices are formed by the roll up of the inlet endwall boundary layers on the blade suction surface which is finally discharged at the center of the passage. The sequence of the boundary layer fluid migration across the passage is shown schematically in Figure 9.15.

9.4 Static Pressure Distribution

The static pressure coefficient contour maps for the six cases under investigation are shown in Figures 9.16 through 9.21. The static pressure distribution exhibits a similar behaviour to that of the total pressure and secondary flow velocity. The general characteristics of the static pressure distribution indicate that the center of vortical motion coincides closely with the center of minimum pressure. The slight shift in some cases can be attributed

Text continued on page 169

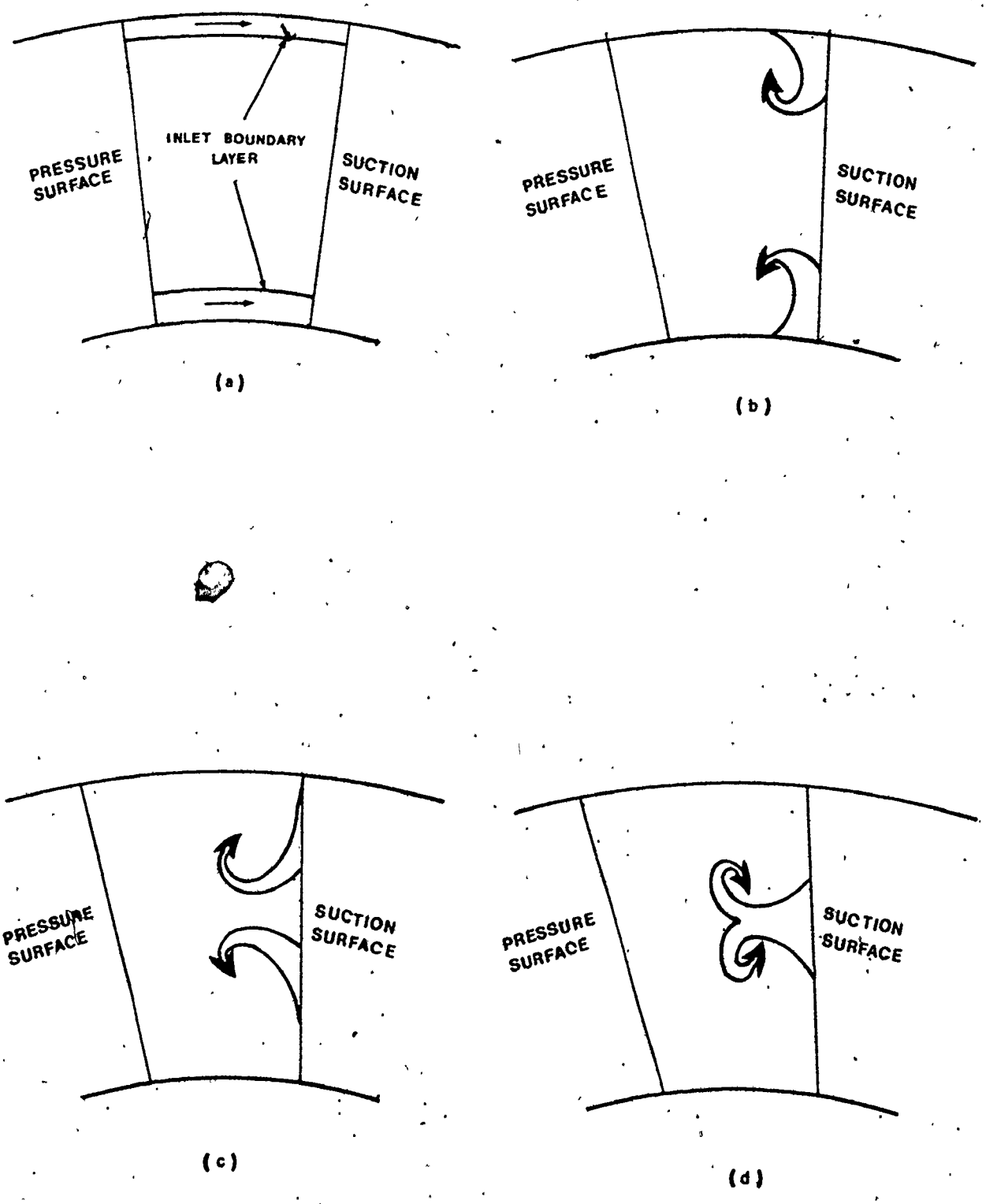

Figure 9.15 . Formation and Merging of the Two Passage Vortices.

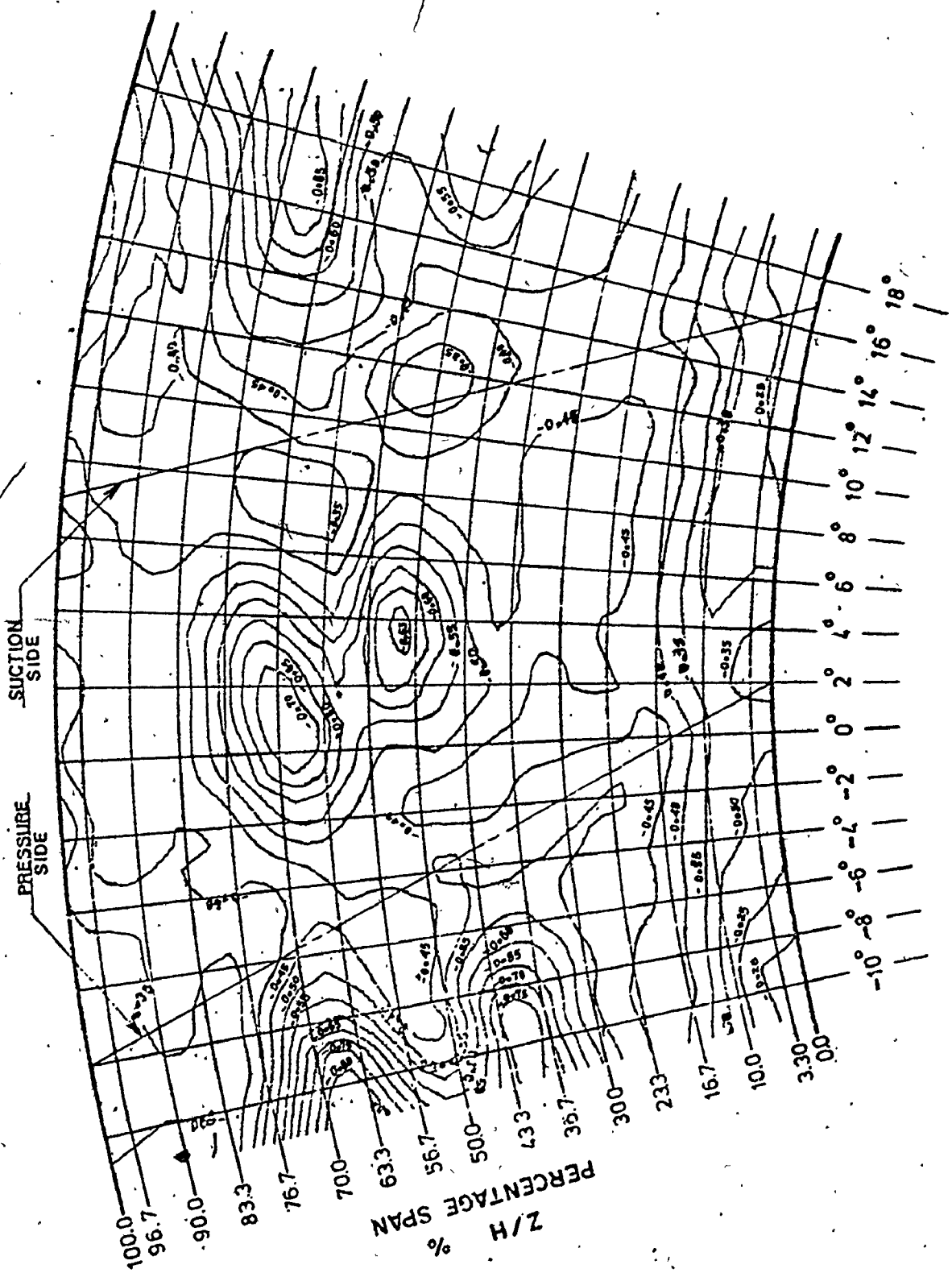

Figure 9.16 Static Press Coefficient Contour for Test #1 (No Suction).

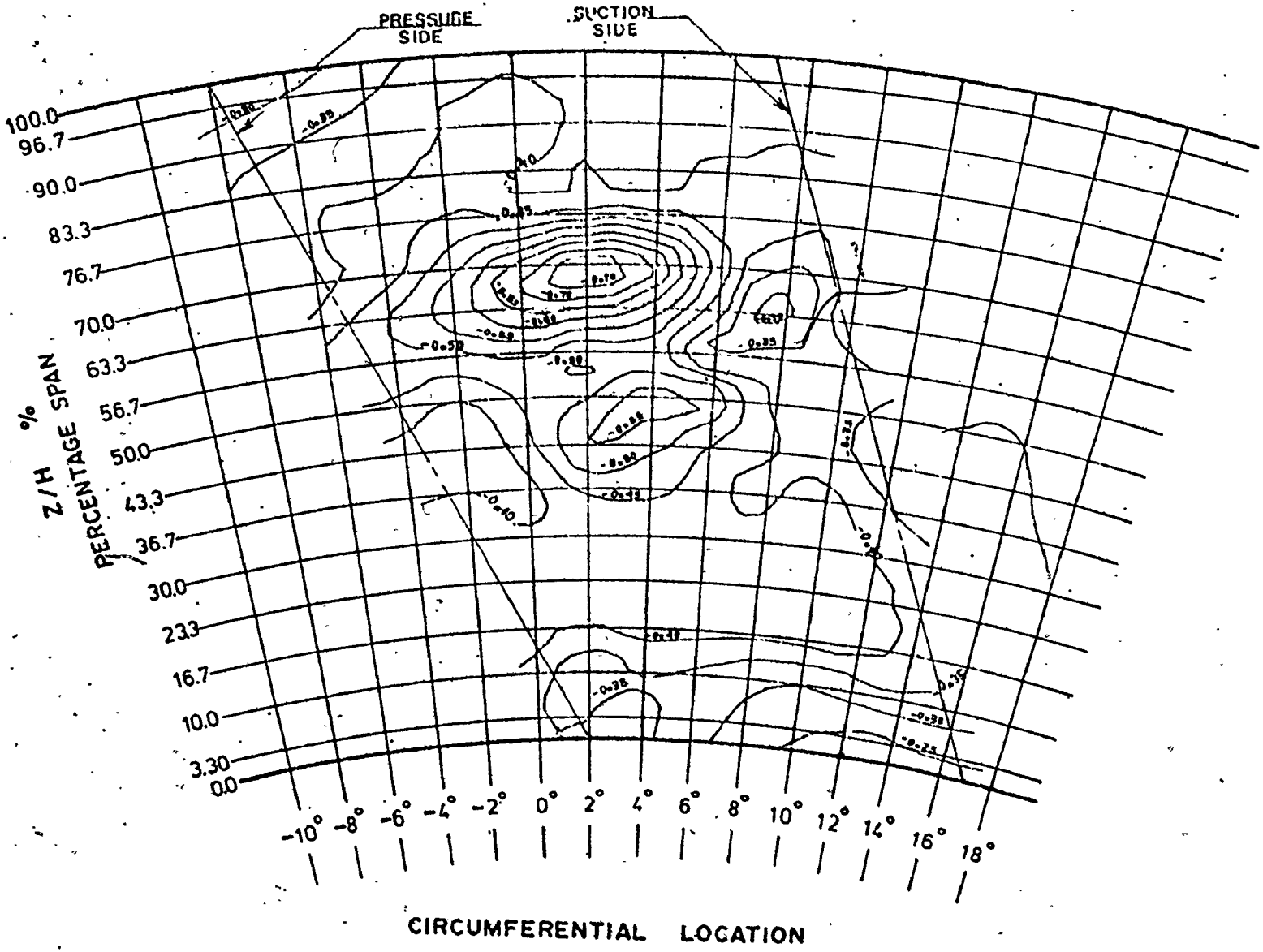

Figure 9.17 Static Press Coefficient Contour for Test # 2 (Suction Applied at the Inner Wall).

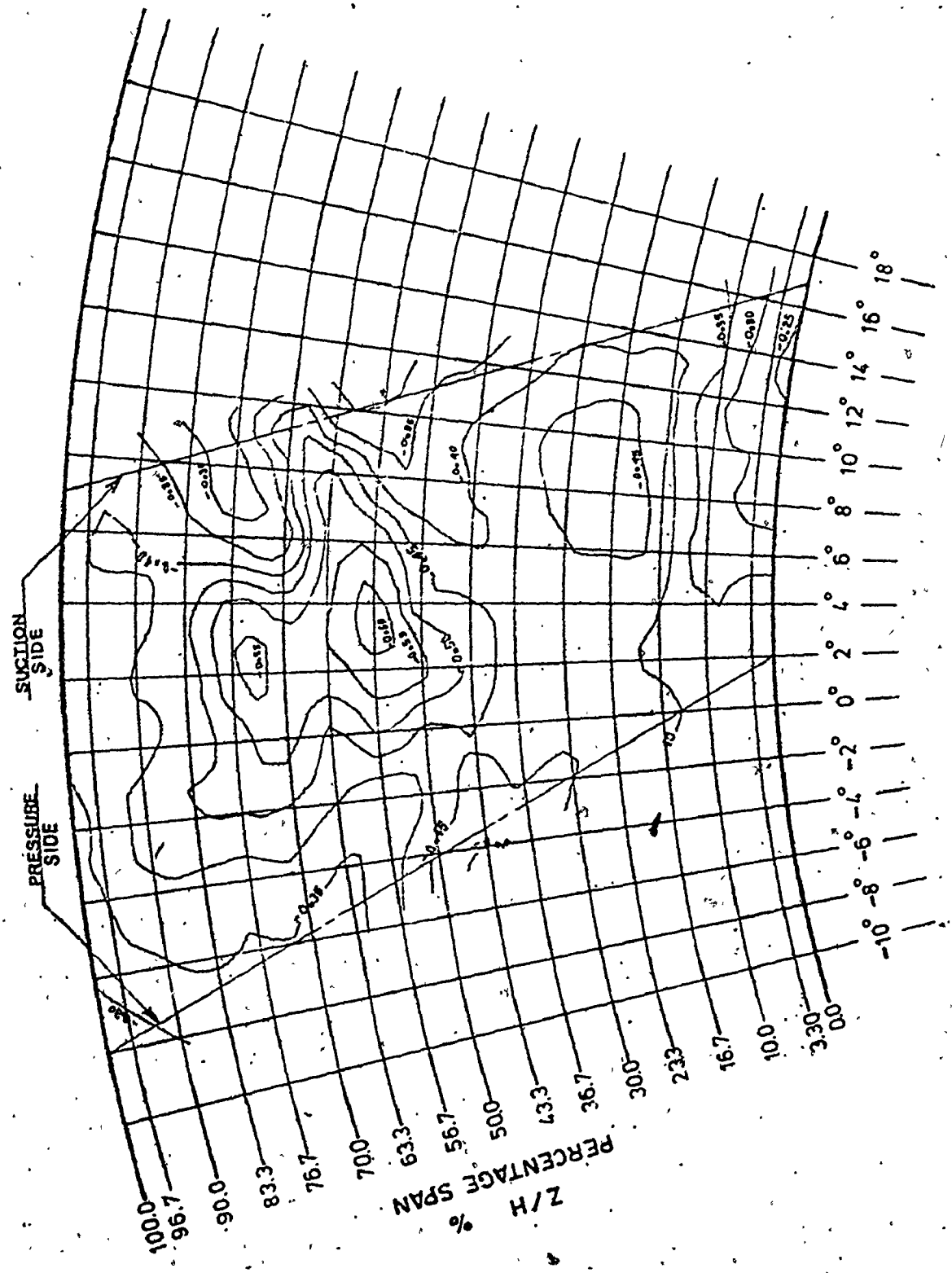

Figure 9.18 Static Press Coefficient Contour for Test # 3 (Suction Applied at the Outer Wall).

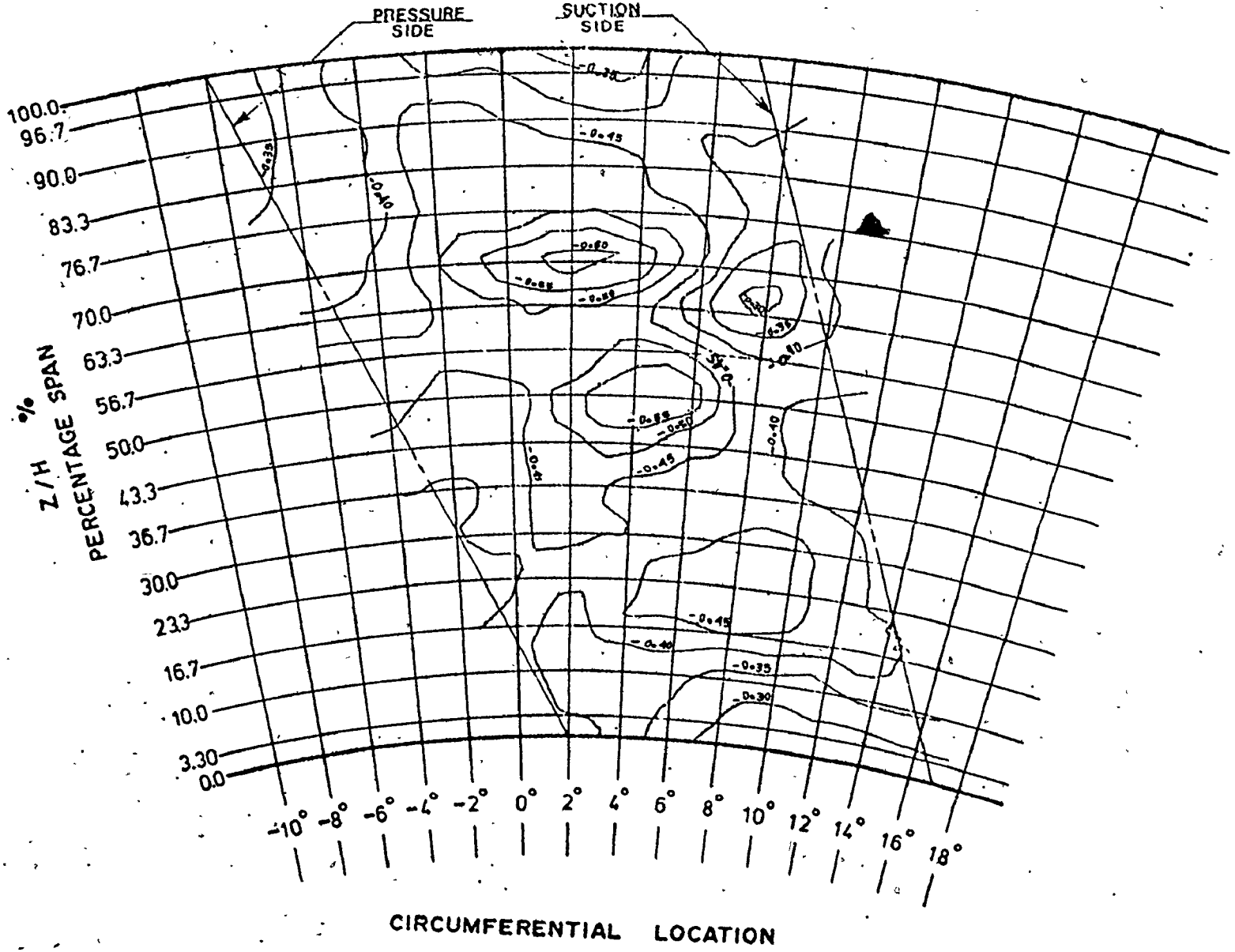

Figure 9.19 Static Press Coefficient Contour for Test # 4 (Combined Suction Applied at Both Endwalls Corresponding to Tests 2 and 3).

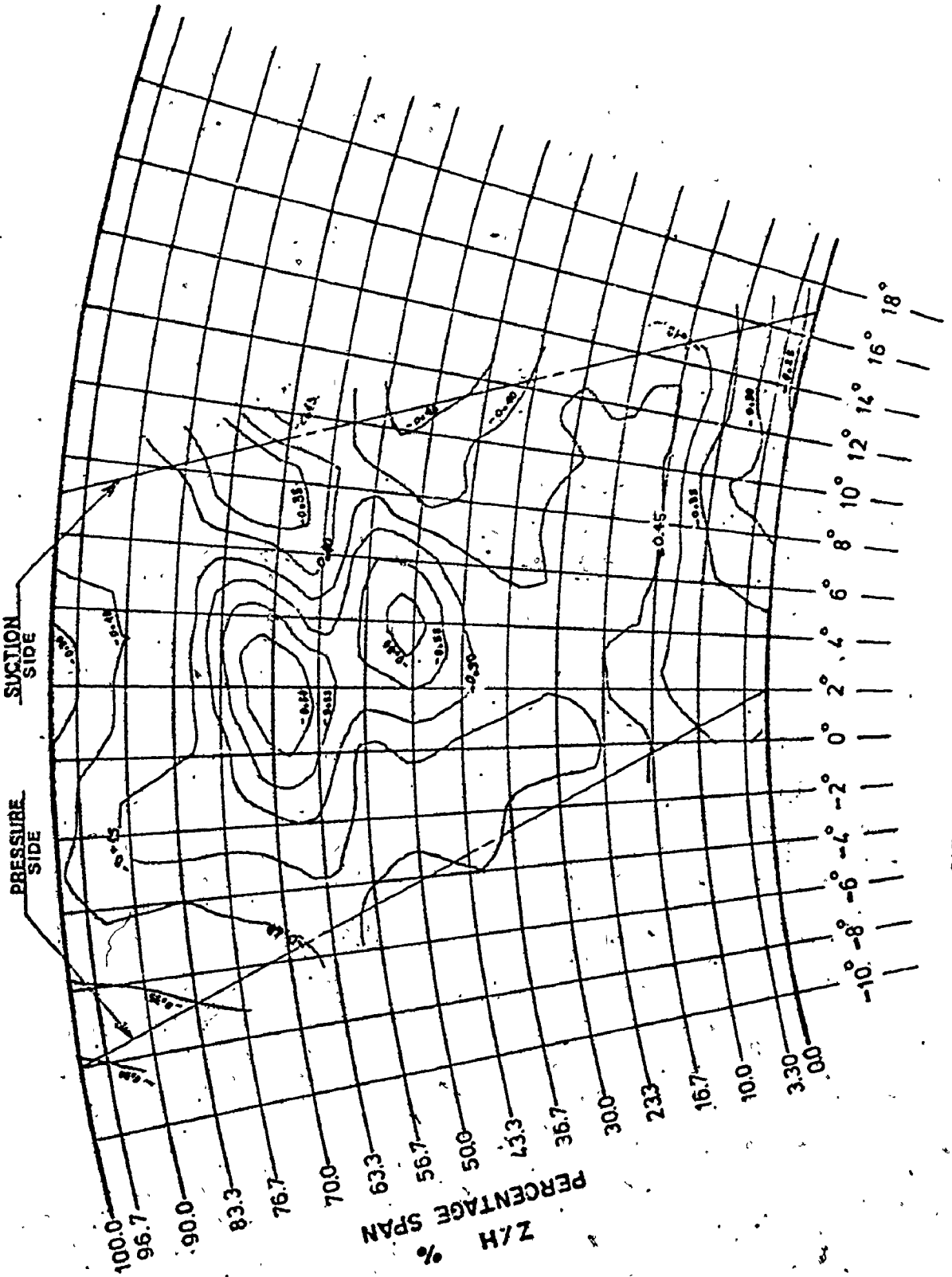

Figure 9.20 Static Press Coefficient Contour for Test # 5 (Less Suction Applied at Both Endwalls Than Test # 4).

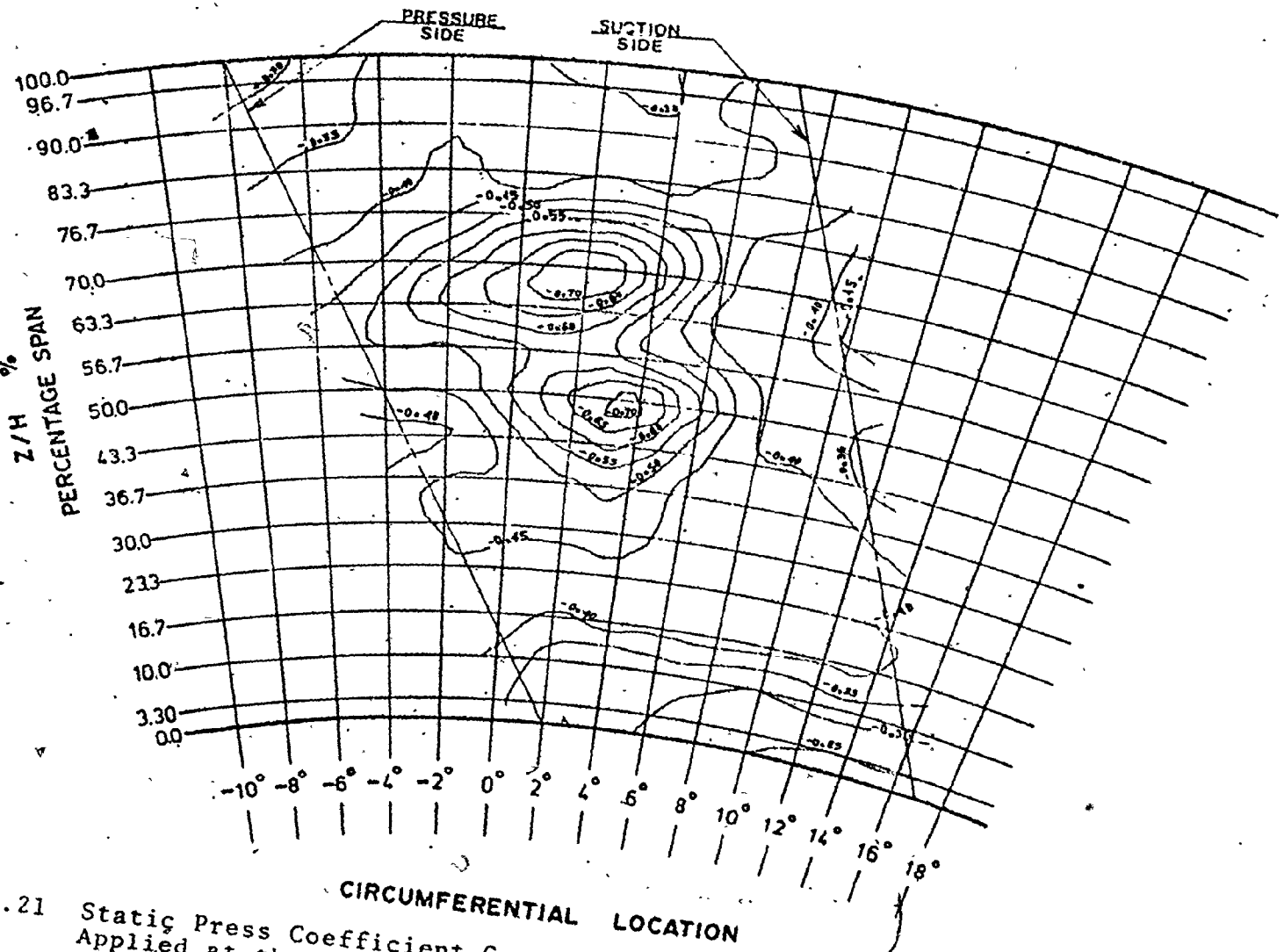

Figure 9.21 Static Press Coefficient Contour for Test #6 (Transverse Injection Applied at the Outer Wall).

to two factors:

1. The definition of the secondary flow used in obtaining the secondary velocity vectors.
2. The instability of the measurement of the flow angles (yaw) at or near the center of the vortices. (The characteristics of the 5-hole probe are undetermined in regions of high shear).

9.5 Spanwise Distribution of Pitchwise Averaged Flow Parameters

Further information about the patterns of the cascade losses and exit flow angles were obtained by plotting the averaged loss coefficient (Y_z), exit angle deviation ($\Delta\alpha_{2z}$) and axial velocity (V_{az}) for each pitchwise traverse against the distance along the span of the blade.

Since the local parameters C_{po}, $\Delta\alpha_2$ and V_a are a function of both radial and circumferential locations (r,θ), the mass averaged parameters can be defined as follows:

$$Y_z(r) = \frac{\int_S C_{po}(r,\theta)V_a(r,\theta)d\theta}{\int_S V_a(r,\theta)d\theta}$$

$$\approx \frac{\sum^{\theta} C_{po}(r,\theta)V_a(r,\theta)}{\sum^{\theta} V_a(r,\theta)} \qquad (9.8)$$

$$= \frac{\sum^{\theta} P_{o1}-P_{o2}(r,\theta)}{\sum^{\theta} V_a(r,\theta)} \Big/ (P_{o1}-P_1)$$

$$\Delta\alpha_{2z}(r) = \frac{\int_S \Delta\alpha_2(r,\theta)V_a(r,\theta)d\theta}{\int_S V_a(r,\theta)\,d\theta}$$

$$= \frac{\sum_\theta^\theta \Delta\alpha_2(r,\theta)V_a(r,\theta)}{\sum_\theta V_a(r,\theta)} \qquad (9.9)$$

$$V_{az} = \frac{\int_S V_a(r,\theta)\,d\theta}{\int_S d\theta} \qquad (9.10)$$

$$= \frac{\sum_\theta^\theta V_a(r,\theta)}{N_\theta}$$

where N_θ is the number of circumferential measurements at the same radius r.

The averaged parameters for the six tests are shown in Figures 9.22 through 9.27 respectively. The examination of the averaged parameters indicates that the two-dimensional (profile) losses are indistinguishable from the secondary losses. The general features of the local loss contour maps discussed before are manifested correspondingly in the averaged loss Y_z. The effect of the upstream boundary layer on the losses is evident. At this point however it should be emphasized that the loss coefficient Y_z includes the loss already present in the upstream boundary layer. The results presented also do not include measurements within the downstream boundary layers. The effect of the upstream and downstream boundary layer losses is discussed in

Text on 177

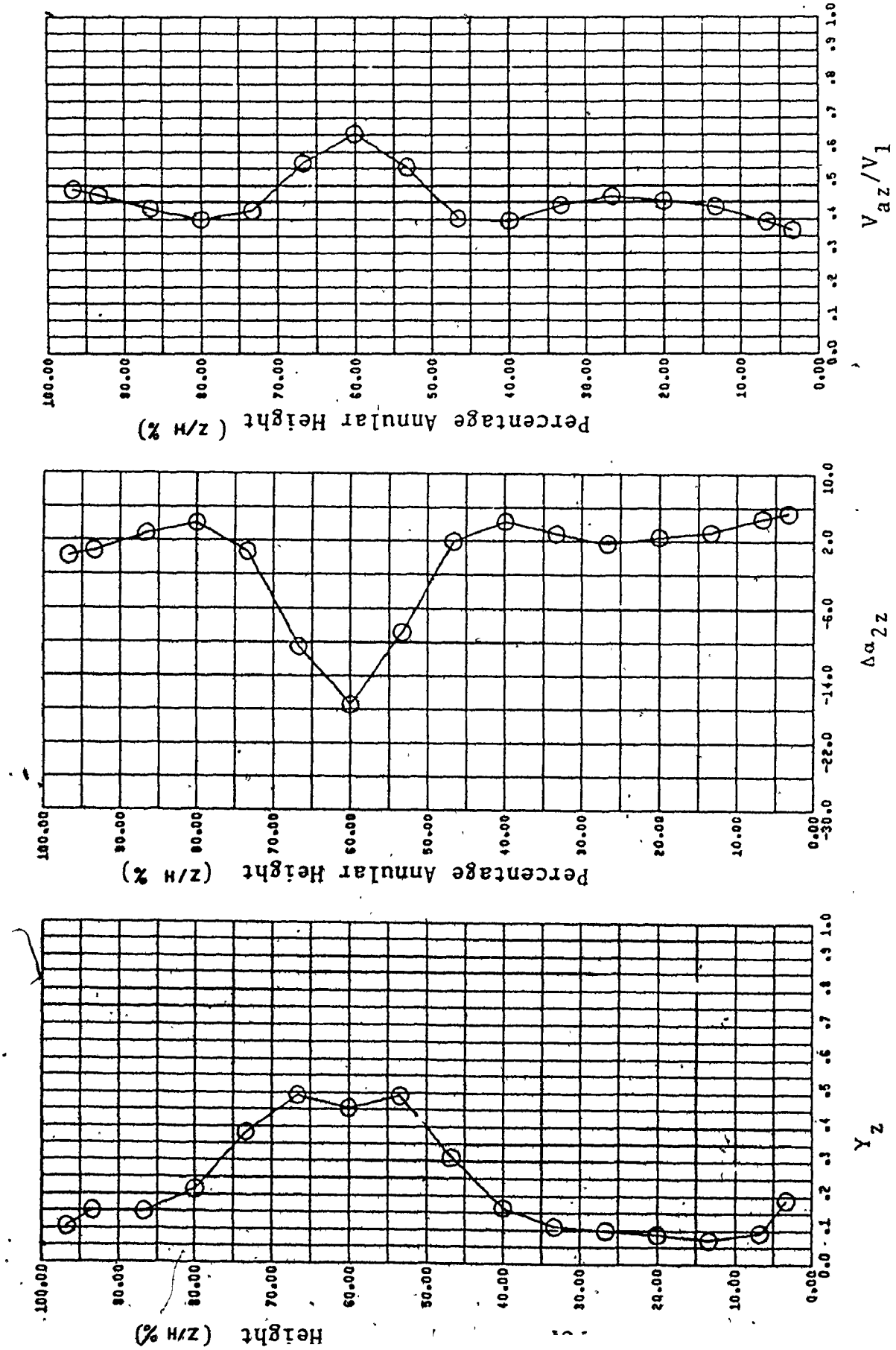

Figure 9.22 Pitchwise Averaged Flow Parameters for Test # 1.

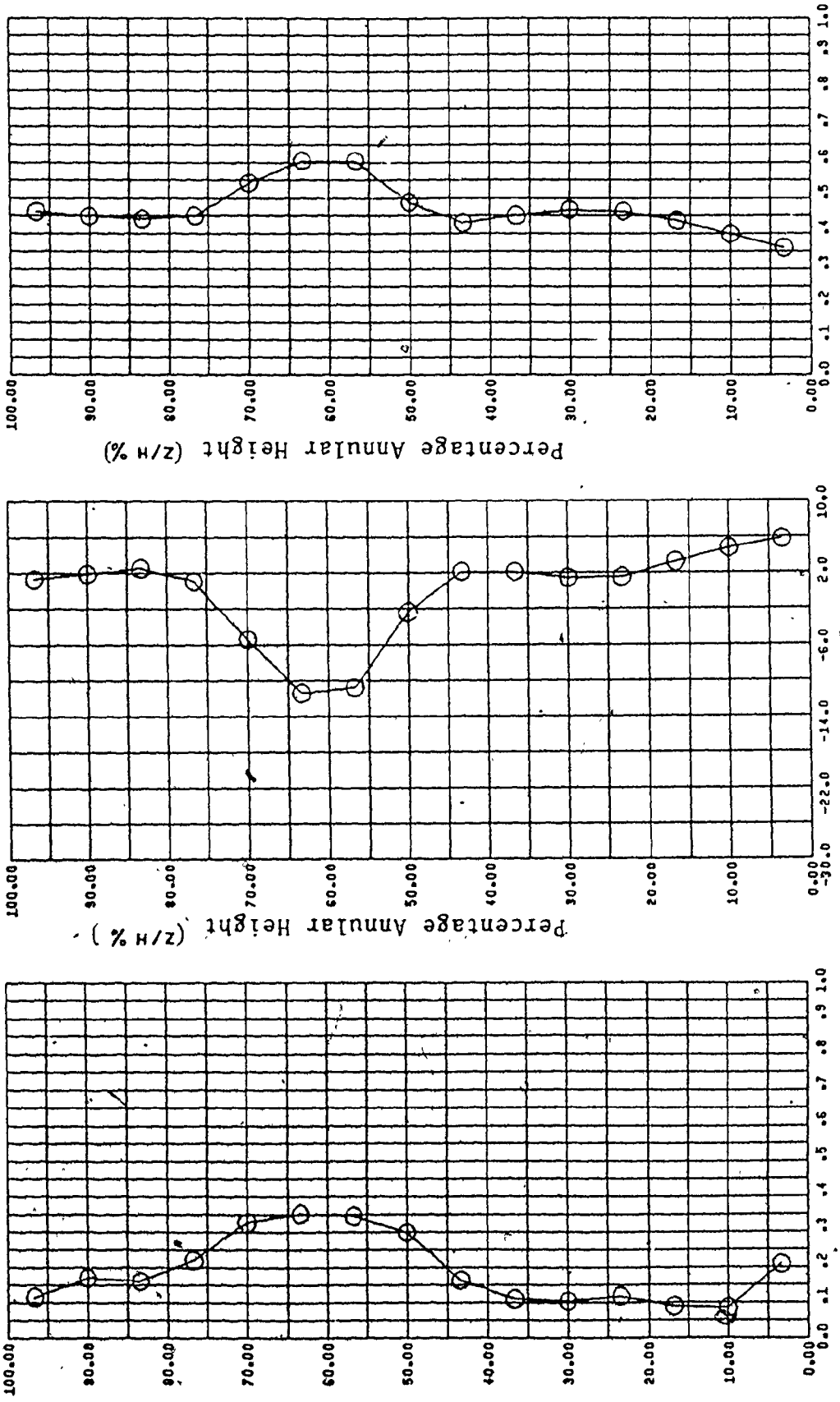

Figure 9.23 Pitchwise Averaged Flow Parameters for Test # 2.

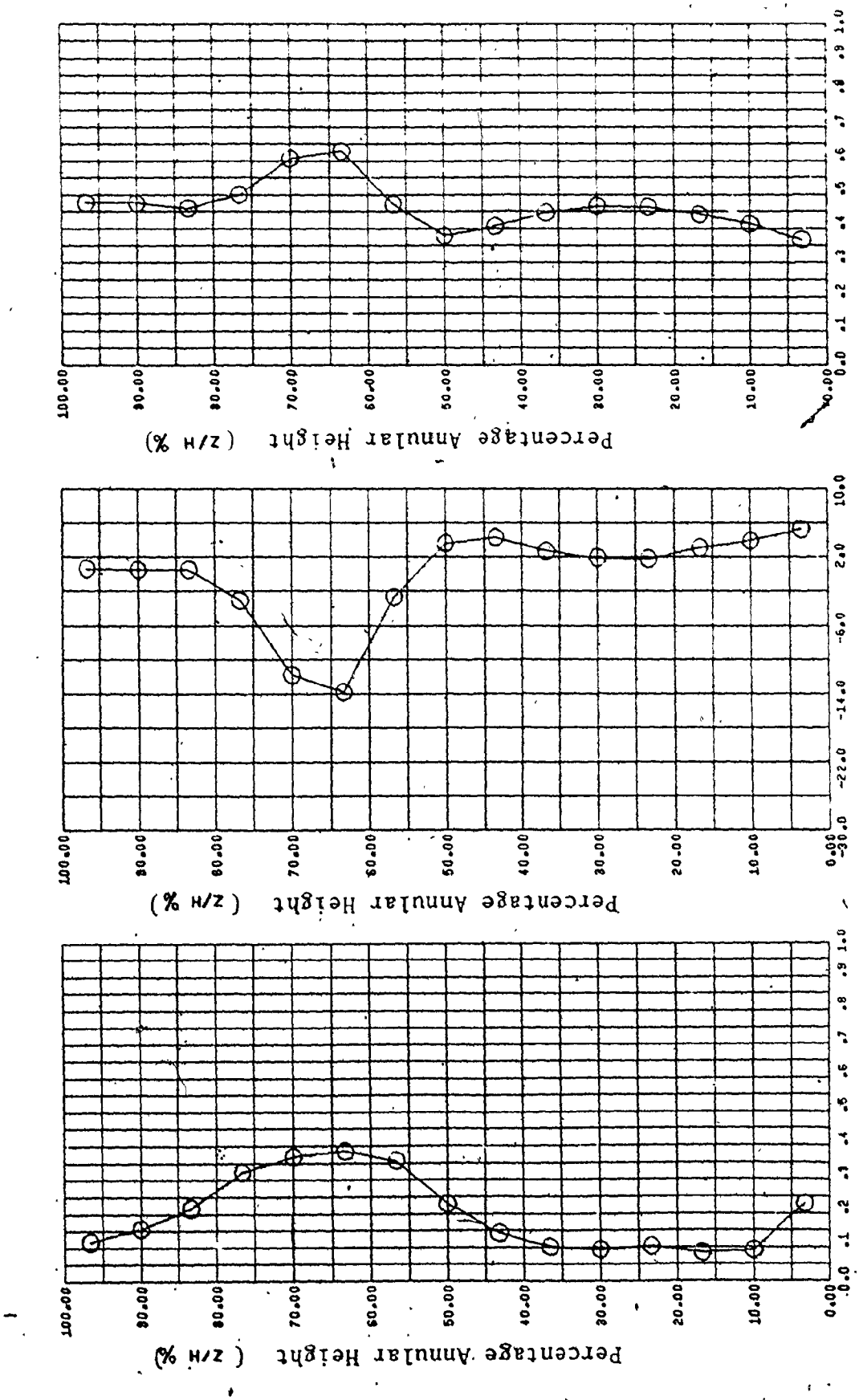

Figure 9.24 Pitchwise Averaged Flow Parameters for Test # 3.

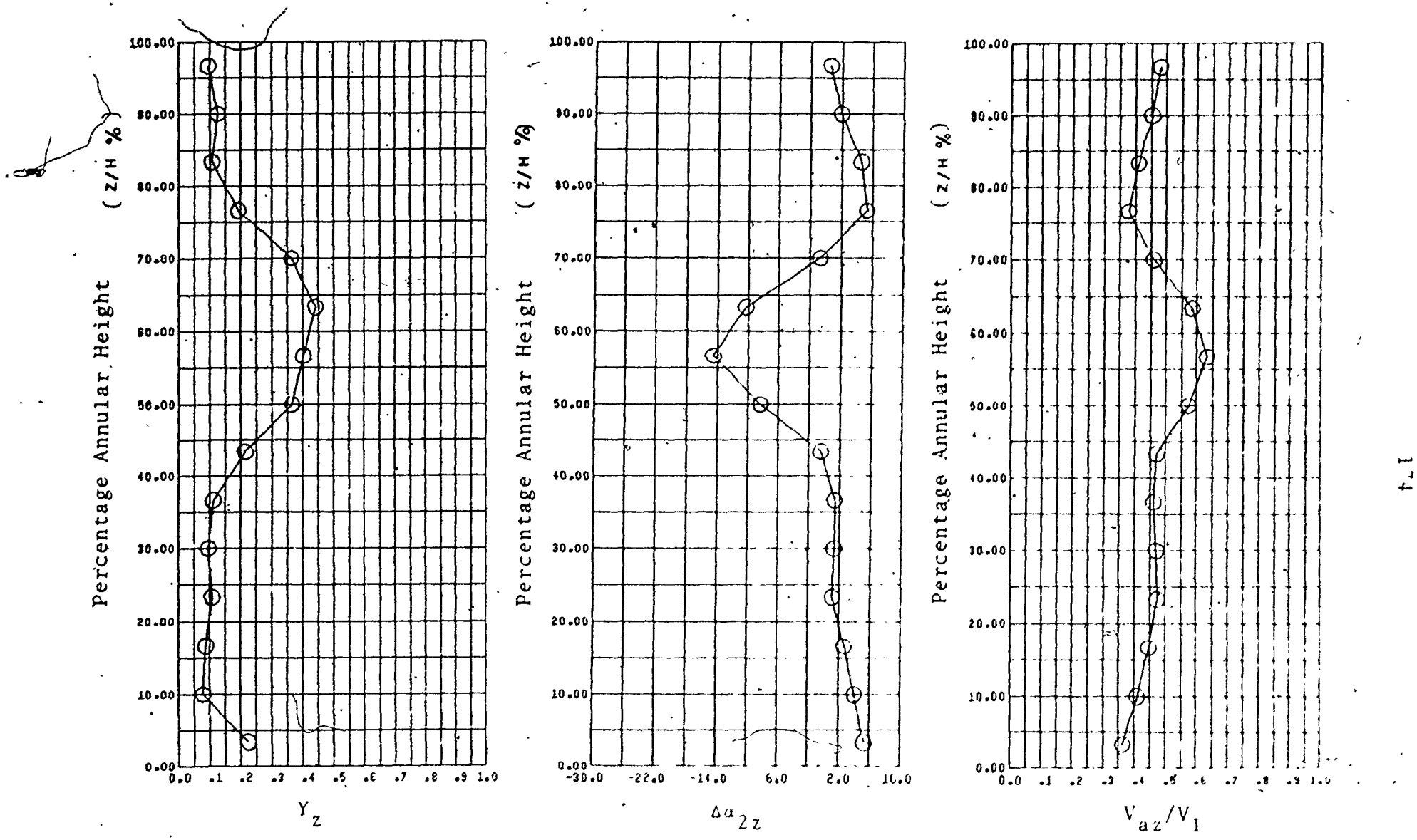

Figure 9.25 Pitchwise Averaged Flow Parameters for Test # 4.

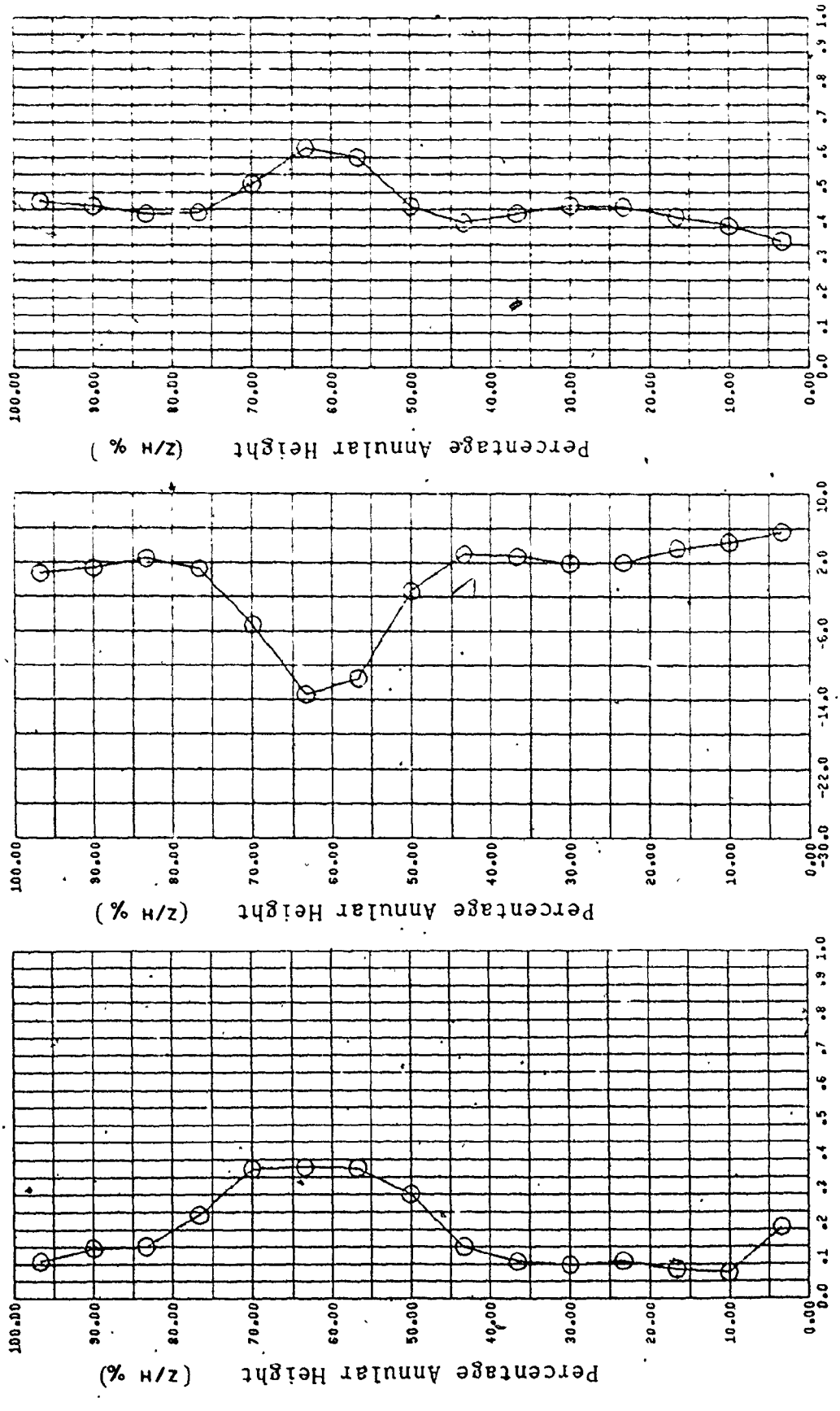

Figure 9.26 Pitchwise Averaged Flow Parameters for Test # 5.

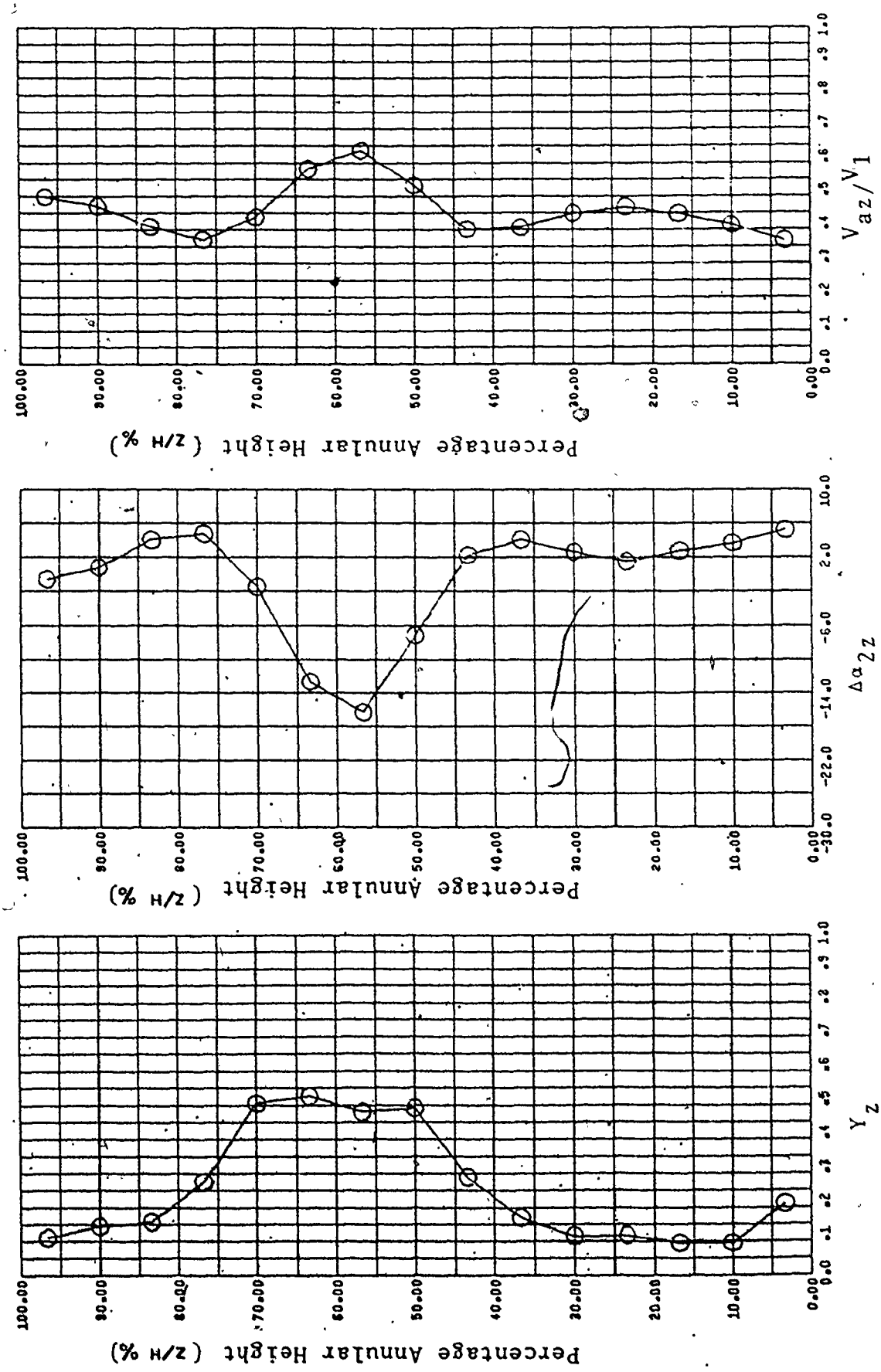

Figure 9.27 Pitchwise Averaged Flow Parameters for Test # 6.

subsequent sections of this chapter.

As mentioned before, the displacement of the high loss region into the passage is associated with low aspect ratio, high turning and low inner/outer diameter ratio of the cascade. In Ref. [43] pitchwise averaged spanwise distribution of the losses revealed that the region of constant loss near mid-span became smaller and finally vanished, for decreasing aspect ratios. The results also showed that the magnitude of the mid-span pitchwise averaged loss increased with decreasing blade heights.

In the test results presented by Came [40], the magnitude and the displacement (away from the endwall) of the loss core were found to increase with flow turning as well as the upstream boundary layer displacement thickness.

From the spanwise variation of the mass averaged $\Delta\alpha_2$, the overturning near the endwall, and the underturning near the center of the passage are quite apparent. The maximum averaged underturning was found to be of the order of 18°. The boundary layer suction had the effect of reducing the maximum underturning. Comparison of the exit angle with several test results reported in the literature indicate that in the present tests the regions of underturning are combined to form a single region. A comparison of the maximum underturning with previous results of calculated or measured values is given in Table 9.2.

Table 9.2

Reference	Blade Turning Angle	Maximum Under-turning
Lakshminarayana [11]	20°	1.8°
Moffatt [12]	20°	1.2°
	50°	4°
Rohlik et al. [41]	60°	0°
Dixon [17]	64.2°	4°
Hawthorne [19]	40°	8°
	100°	18°
Present tests	128.5°	18°

9.6 Exit Boundary Layer Measurement

At the initial inlet condition, the exit boundary layers on the inner and the outer walls were traversed at three circumferential locations (Figures 9.28, 9.29). At the geometric centers of the passage the boundary layers were measured for the six inlet conditions. The results are given in Figures 9.30 and 9.31. It is noticed that the boundary layer thickness at the passage exit is very small in comparison with the thickness of the inlet boundary layer. At the outer endwall the boundary layer is generally thinner than that on the inner endwall. Since the exit boundary layer is formed after the inlet boundary layer

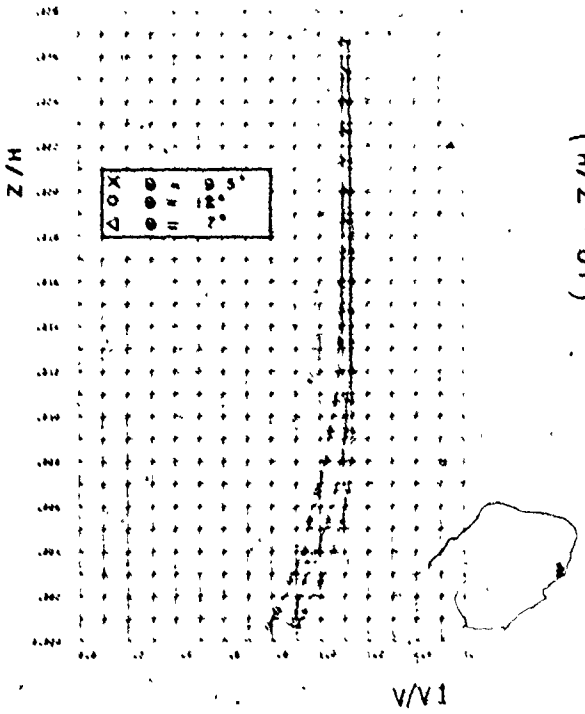

Figure 9.28 Inner Wall Boundary Layer at Different Locations.

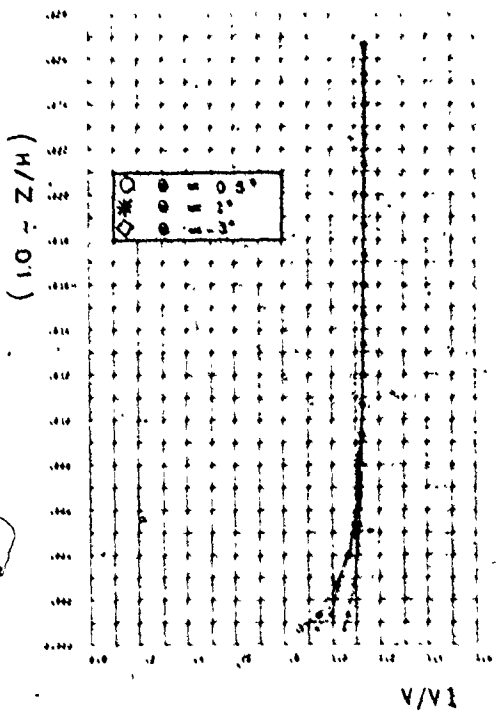

Figure 9.29 Outer Wall Boundary Layer at Different Locations.

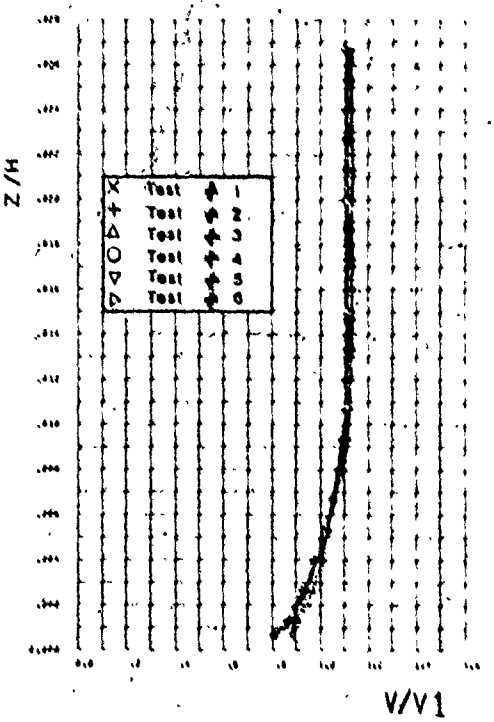

Figure 9.30 Inner Wall Boundary Layer (Effect of Suction)

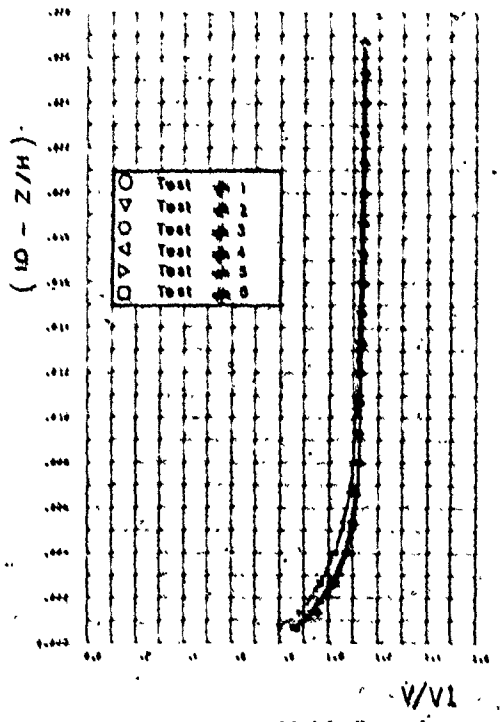

Figure 9.31 Outer Wall Boundary Layer (Effect of Suction).

separates, it is suggested that the inner wall boundary layer developed over a longer distance than that at the outer wall. This also indicates that the separation on the inner wall probably occurred at a shorter axial distance (from the leading edge) than on the outer wall.

As mentioned previously, the loss in the exit boundary layers was not included in the measurements of the local and pitchwise-averaged loss coefficients. Regarding the small thickness of the boundary layers in comparison with the spanwise resolution of the tests, its extent on the pitchwise-averaged loss plots is difficult to assess. The variation of the thickness across the blade pitch suggests that measurements should be averaged across the blade pitch. However, regarding the small magnitude of the loss associated with the exit boundary layer, it was decided to use the profiles obtained at the passage center for the estimation of the losses. The estimated losses thus obtained were found neglibly small in comparison with the other exit losses as well as the upstream boundary layer loss. The effect of the upstream boundary layer on the exit boundary layer is very small as shown in Figures 9.30 and 9.31.

Camo [40] found from his tests on a rectilinear cascade that variation of the exit boundary losses with that of the upstream boundary layer "is not great" (<20%).

9.7 Losses - Comparison with Correlations

The comparison of the cascade secondary losses with the existing data and correlations requires the calculation of the integrated overall loss coefficient and the secondary loss coefficient. The overall coefficient of the mass weighted average loss is defined as follows:

$$Y_T = \frac{\Delta P_T}{P_{o2m} - P_{2m}} \tag{9.11}$$

where,

$$\Delta P_T = \frac{\int_S \int_H [P_{o1} - P_o\ (r,\theta)]\ V_a\ (r,\theta)\ r dr d\theta}{\int_S \int_H V_a\ (r,\theta)\ r dr d\theta} \tag{9.12}$$

while $$P_{o2m} = P_{o1} - \Delta P_T \tag{9.13}$$

and $$P_{2m} = P_{s1} - \Delta P_s \tag{9.14}$$

It should be noted that ΔP_s is defined in a manner similar to ΔP_T.

The secondary loss coefficient can be obtained by subtracting the profile loss from the total loss, i.e.,

$$Y_s = Y_T - Y_p \tag{9.15}$$

The net secondary loss coefficient Y'_s is defined as:

$$Y'_s = Y_s - Y_1 \tag{9.16}$$

where Y_1 is the mass averaged inlet boundary layer loss

relative to the exit dynamic pressure.

9.7.1 Effect of the Exit Measuring Station Location

The effect of the exit measuring station position on the measured losses should be accounted for by estimating the mixing losses. Most of the cascade data reported in the literature included the mixing losses, in which case, the measurements were taken at some distance downstream from the cascade (generally of the same order of magnitude as the chord length). Came [40] in his preliminary tests noted a rising trend for both the profile and secondary losses with distances downstream from the cascade up to 1.2C. Further test data presented by the same author were obtained at a distance of 1.36 C downstream from the cascade. Wolf [55] found that the most favourable position for the exit test plane is in the range of 1.2C to 1.5C downstream from the trailing edge. The rise in the measured losses, in Wolf's results, over a distance ranging from 0.5C to 1.2C was of the order of 13%. Langston [44] measured the losses at different positions from the cascade inlet section to a downstream location of 0.75C from the exit section. The losses were found to rise by about 20% over the distance between 0.2C and 0.75C downstream of the exit plane.

In the present study, since the measuring plane is located at a streamwise distance of only 0.33C from the

trailing edge, it was estimated that the measured losses should be increased by about 15% to account for the effect of mixing.

9.7.2 Profile and Secondary Losses

Ideally the test results should be analysed to separate the profile loss, endwall boundary layer loss and the secondary loss associated with the vortex core. As mentioned earlier in this chapter, the differentiation between the profile loss and the secondary loss was not possible.

In order to calculate the secondary loss the profile loss therefore is to be estimated using existing correlations. The available correlations however do not yield accurate results. Denton [39] examined seven different correlations comparing them with 79 cascade results and found that none of them predicted the profile loss accurately. The author of [39] recommended the method of Balje and Binsely [57], having the least error according to his study.

For the present analysis, four different correlations were used to estimate the profile loss. A summary of the measured loss data in comparison with several correlations is given in Table 9.3. It can be seen that although the loss level is high, yet the measured overall total loss coefficient is less than that predicted by various correlations (with the exception of Soderberg [36]).

Table 9.3

A Comparison of the Measured and the Calculated Losses

a) Calculated Loss Coefficients

Profile Loss			Secondary Loss			Total Loss		
Y_p	Ainley [38]	0.095	Y_s	Ainley [38]	0.393	Y_T	Ainley [38]	0.488
Y_p	Hawthorne [56]	0.074	Y_s	Dunham [3]	0.265	Y_T	Hawthorne [56]	0.311
Y_p	Balje [57]	0.058	Y_s	Came [40]	0.334	Y_T	Soderberg	0.174
Y_p	Denton [39]	0.040	Y_s	Dunham & Came [41]	0.540			
			Y_s	Soderberg (as given by Ref. [37])	0.075			

b) Measured Loss Coefficients

Test Number		1	2	3	4	5	6
Y_T		0.239	0.205	0.204	0.191	0.195	0.270
Y_l		0.032	0.027	0.031	0.026	0.028	0.035
Y_s	Using Ainley's Y_p	0.144	0.110	0.109	0.096	0.100	0.175
Y'_s		0.112	0.083	0.078	0.070	0.072	0.140
$Y'_s/Y'_{s\ max}$		0.800	0.593	0.557	0.500	0.514	1.000
Y_s	Using Balje's Y_p	0.181	0.160	0.162	0.135	0.143	0.225
Y'_s		0.149	0.133	0.131	0.109	0.115	0.190
$Y'_s/Y'_{s\ max}$		0.780	0.700	0.690	0.570	0.610	1.000

The variation of the calculated secondary loss parameter with the relative upstream boundary layer is shown in Figure 9.32. The blade loading parameter Z in the loss parameter is defined as:

$$Z = \left(\frac{C_L}{C}\right)^2 \frac{\cos^2 a_2}{\cos^3 a_m} \qquad (9.17)$$

and

$$C_L = 2\frac{S}{C}(\tan a_1 - \tan a_2)\cos a_m \qquad (9.18)$$

Shown in Figure 9.32 are the Dunham [3] and Came [40] correlations as well as the nominal value of the secondary loss parameters used in turbine performance predictions. Other results shown in Figure 9.32 show a noticeable scatter. In many of these cases the secondary loss had to be calculated [40] and δ^*/C values were based on 1/7 power law inlet boundary layer profile. It is worth mentioning that the values of δ^*/C in turbine applications are within the lower half of the range shown. Came [40] mentioned that in this range the cascade loss is very much less than the indicated loss in turbines for the same δ^*/C. Commenting on Dunham and Came's correlation [41], Denton mentioned that their correlation considerably underestimates the efficiency when applied to low aspect ratio multi-stage steam turbines. He found that in order to obtain a correct prediction, the Dunham and Came secondary loss had to be multiplied by 0.35. The present results

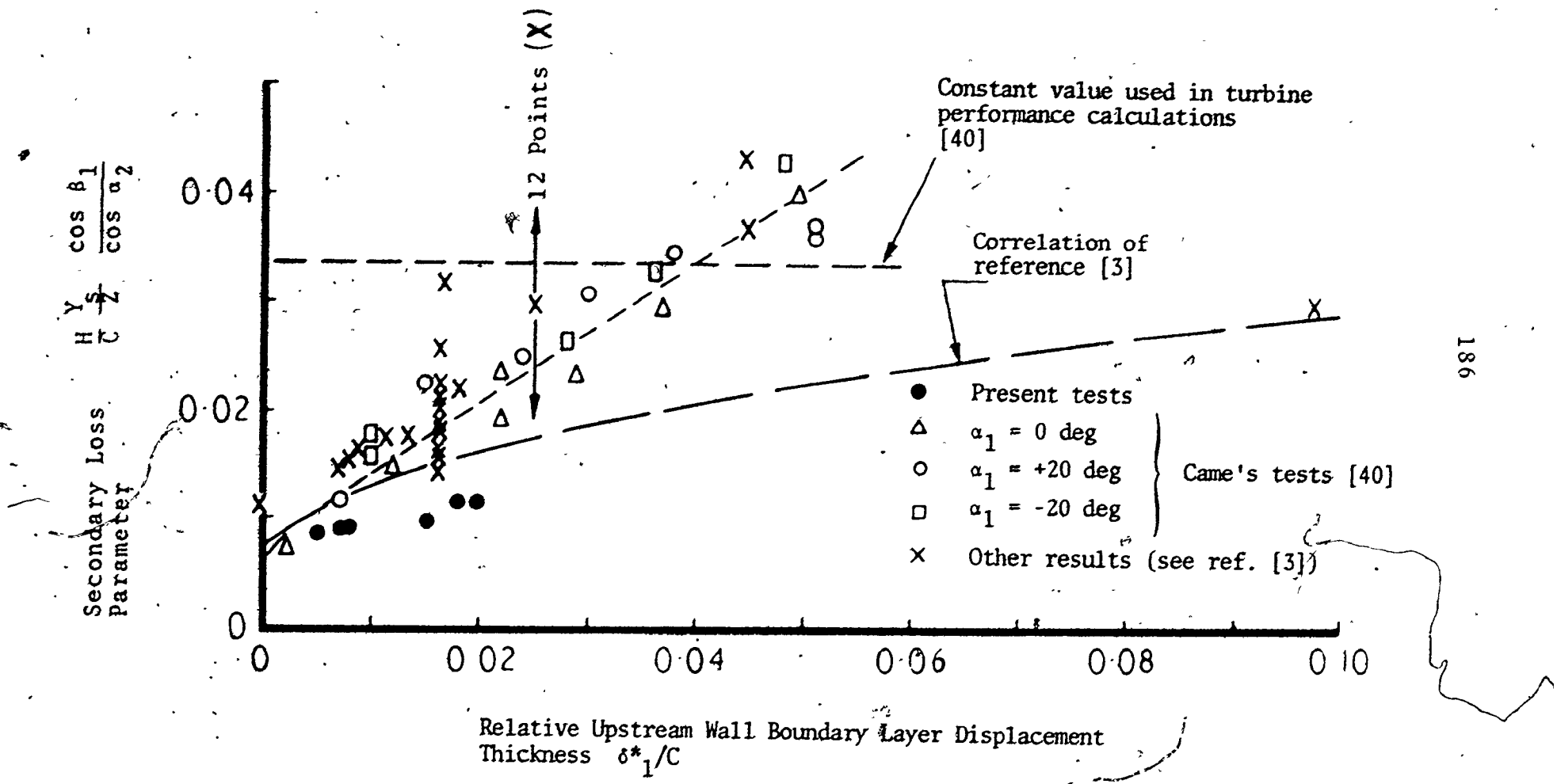

Figure 9.32 Variation of Gross Secondary Loss with the Inlet Displacement Thickness.

confirm Denton's point since it was found that the Came-Dunham prediction is about 3.5 times the measured loss.

It should be remembered that for the present results, the inlet boundary layer displacement thickness was averaged on both endwalls as indicated in Table 9.3. It should also be recalled that the secondary loss was calculated by subtracting the profile loss (obtained from correlations from the total loss.

Figure 9.33 shows the variation of the secondary loss coefficient Y'_s with δ^*/C in comparison with the results of Wolf [55], Klein [58] and Came [40]. In Klein's results no variation of Y'_s with δ^*_1/C was noticed over the entire range. Wolf's results indicated that a maximum Y'_s was reached at $\delta^*_1/C \simeq 0.03$ while Came's showed a rising trend. The present results also indicate a rising trend. However, it is not linear.

Wolf [55] suggested that δ^*_{1crit} at which Y'_s reaches a maximum must be related to the location at which the inlet boundary layer is deflected just enough to reach the suction surface of the blade. Came associated it with the main stream deflection rather than the boundary layer thickness.

A comparison of the secondary loss parameter with the inlet boundary layer loss is shown in Figure 9.34. The correlation of the gross secondary flow loss coefficient Y_s with the blade loading parameter does not seem to yield

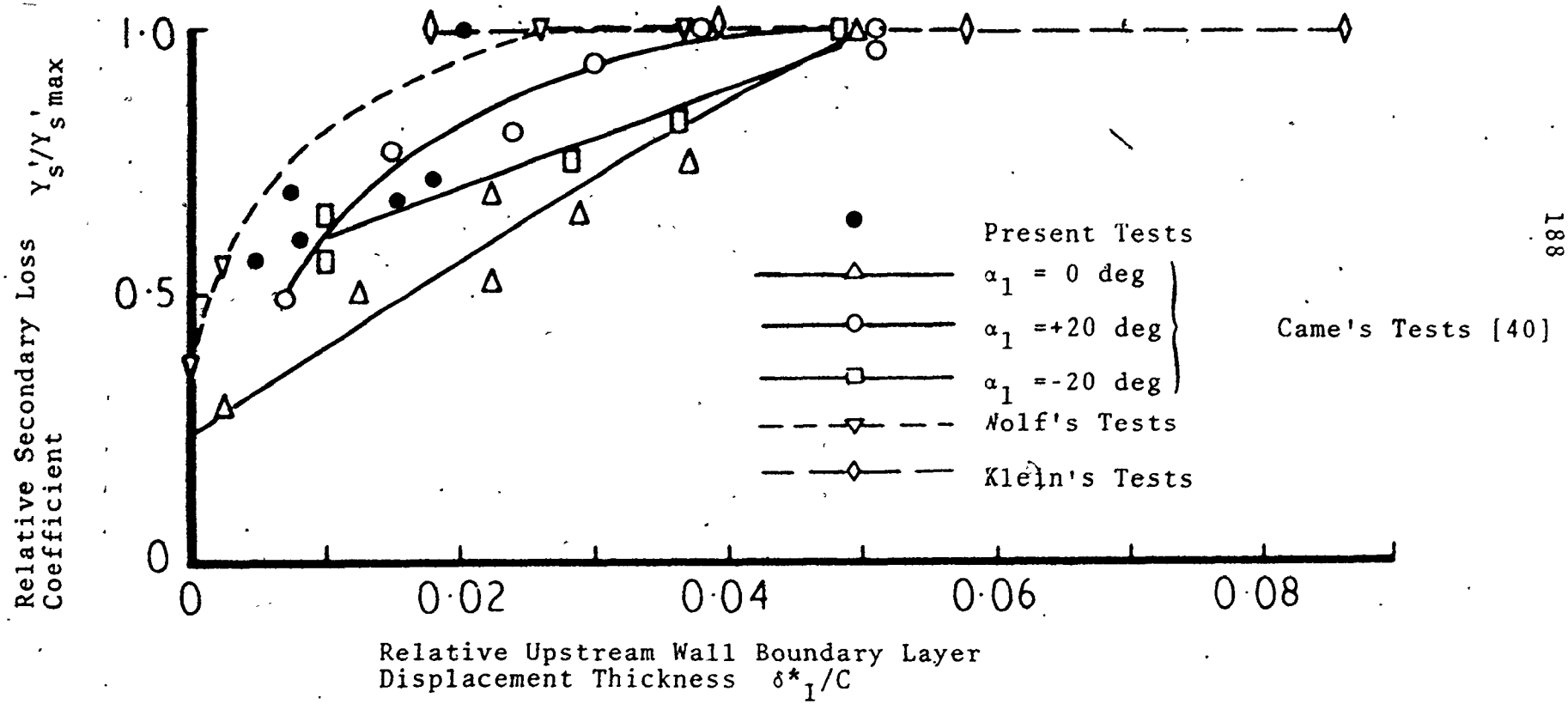

Figure 9.33 Variation of Secondary Loss Y_s' with Inlet Displacement Thickness.

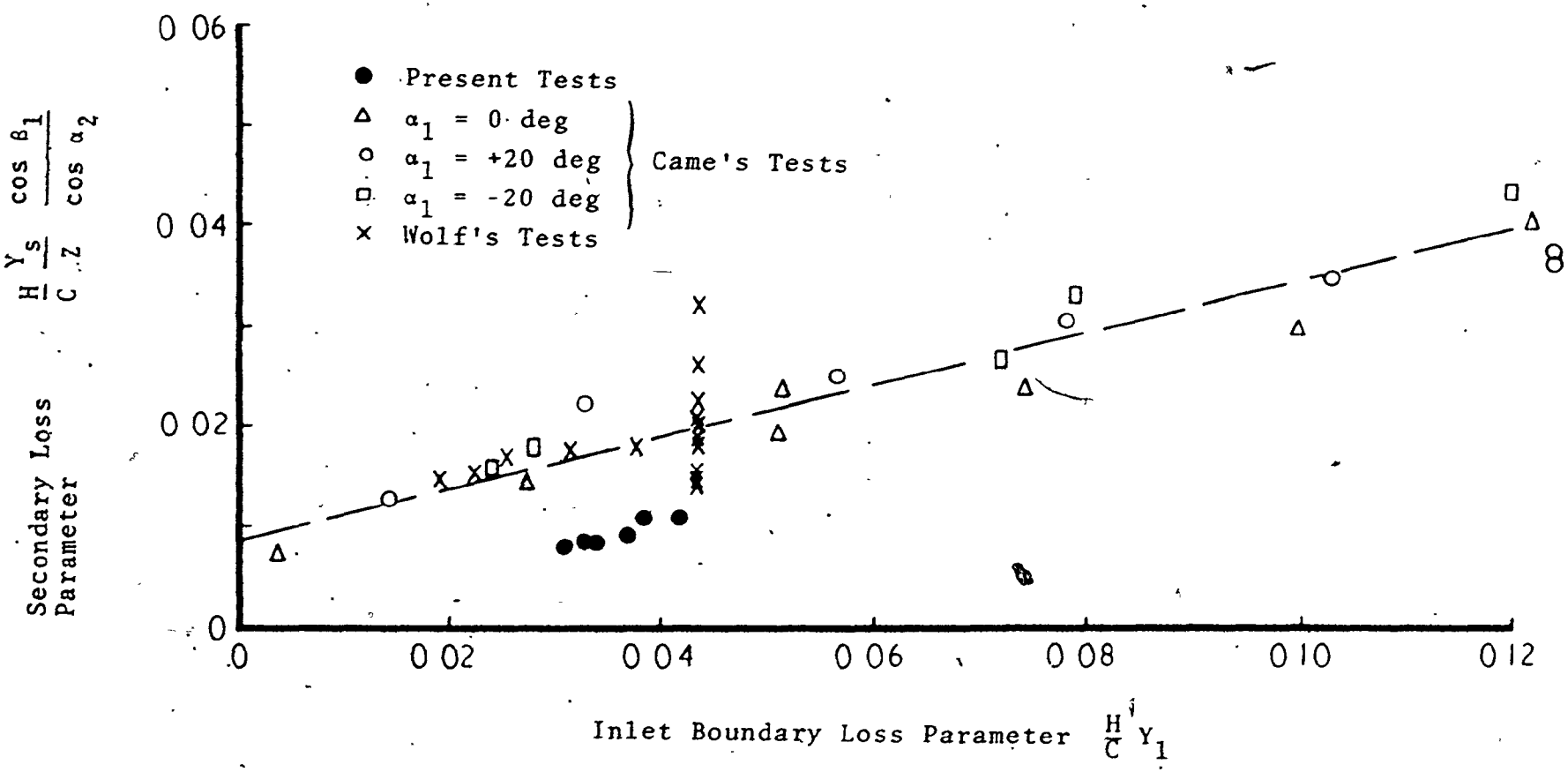

Figure 9.34 Variation of Gross Secondary Loss with Inlet.Boundary Layer Loss.

consistent results with respect to the actual losses as affected by the inlet boundary layer displacement thickness.

The general conclusion that can be drawn from comparing the secondary losses with correlations is that the correlations overestimate the losses.

9.8 Flow Visualization

In order to obtain more insight into the complex flow patterns within the blade passage a flow visualization study was conducted utilizing smoke injection and oil-film techniques.

9.8.1 Smoke Flow Visualization

Smoke was produced by mixing anhydrous ammonia and sulphur-dioxide using the smoke probe shown in Figure 5.14. The rates of smoke production and injection into the air stream were carefully controlled by means of pressure regulators to obtain close matching of the local smoke velocity and direction with that of the air stream. Difficulties were encountered with the smoke diffusion since the final trace was formed by the mixing of two jets. It was also found difficult to present the test results photographically. Since the photographs cannot show the three-dimensional path of the traces only projections on the passage endwalls and/or blade surfaces can therefore be envisaged. Moreover, in regions of low contrast clear

pictures are difficult to obtain.

The smoke was injected at different radial and circumferential locations at the passage inlet. A typical photograph of the smoke trace is shown in Figure 9.35. A summary of the smoke flow visualization test results can be given as follows:

1. Smoke injected within the endwall boundary layers was swept towards the suction surface of the blade shortly after the leading edge plane. The flow rolled up into a vortex climbing up the suction surface and was finally discharged near the middle of the passage with considerable diffusion.
2. The smoke injected near the outer part of the boundary layer close to the blade pressure surface was associated with larger envelopes of the vortex indicating that the outer part of the vortex is formed from the boundary layer fluid close to the pressure surface. On the other hand, smoke injected near the blade suction surface within the boundary layer formed spiral motions of smaller size indicating that such fluid formed the inner core of the passage vortices.
3. Smoke injected within the boundary layer near the blade leading edge was divided into two traces, one looping around the suction surface of the blade and the other was swept across the channel to the suction

Figure 9.35 A Typical Smoke Trace Within the Passage.

side of the next blade. The smoke thus visualized was considerably diffused, but it is believed that at this location the horse-shoe vortex was identified.

4. Smoke injected in the main stream near the edge of the boundary layers was directed towards the end-walls shortly beyond the leading edge plane. The flow had a tendency to migrate towards the blade suction surface.

5. Smoke injected near mid-span near the blade pressure surface followed the passage geometry reasonably well up to an axial location of about 0.7C and was then slightly displaced towards the pressure side.

6. Smoke injected in the main stream close to the suction surface was diffused rapidly beyond an axial distance of about 0.3C.

9.8.2 Surface Flow Visualization

A mixture of lamp-black and kerosene was used for the passage surface flow visualization. A thin layer of the mixture was spread as evenly as possible on the passage walls in order to obtain pictures of reasonable consistency. A typical illustration of an oil-film test run is shown in Figures 9.36 through 9.39. It should be noted that the general flow pattern depicted from these figures is compatible

with the static pressure contours on the passage walls discussed in Chapter 8.

The general features of the passage surface flow patterns can be summarized as follows.

i) Blade Pressure Surface

1. On the blade pressure surface (Figure 9.36) the stagnation line h-h is identified as a dark strip parallel to the leading edge.
2. In the lower region there is considerable radial flow towards the inner wall near the leading edge. The radial flow decreases gradually towards the trailing edge.
3. In the upper region of the blade surface the flow looks reasonably two-dimensional.

ii) Inner Wall

1. On the inner endwall (Figure 9.37) the inlet boundary layer is swept towards the suction side of the blade in the zone a i n.
2. A separation line h j can be identified across the channel.
3. The cross channel flow in the new endwall boundary layer is observed to be directed strongly towards the suction side in the region h i p k and gradually gains an axial component in the region k p o r.

4. The horse-shoe vortex leg looping around the suction side of blade A seemed to extend over the zone designated as a p d. The flow direction in the area c p d j was opposite to the cross flow indicating a vortex motion of an opposite direction to that of the passage vortex.

5. The flow direction in the zone b c g was found difficult to identify. The flow motion in this area was found to be chaotic. The flow direction in the area a b g was also vague.

6. The flow in the zone d e f followed the blade surface closely. Although a clear separation line d e can be identified it is not sure whether the flow in the zone d e f was a result of the corner vortices or the leg of the horse-shoe vortex associated with blade B (which could not be traced beyond the point i).

iii) Blade Suction Surface

1. The two-dimensional flow was limited to triangular-shaped area a b r (Figure 9.38) starting from the leading edge as a base and narrowing down to a point b.

2. The point b is likely the point at which the two passage vortices merge and depart from the blade suction surface into the passage. The traces of the

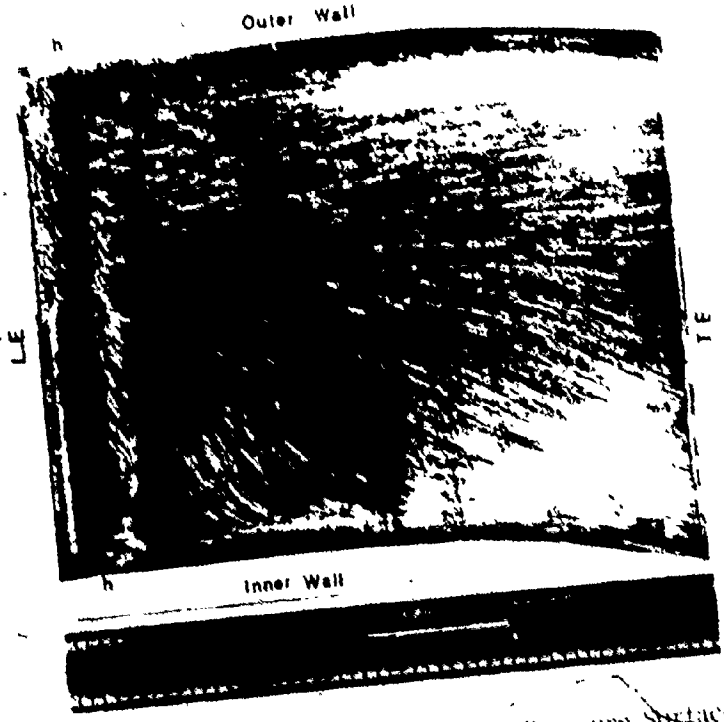

Figure 9.36 Flow Traces on the Blade Pressure Surface.

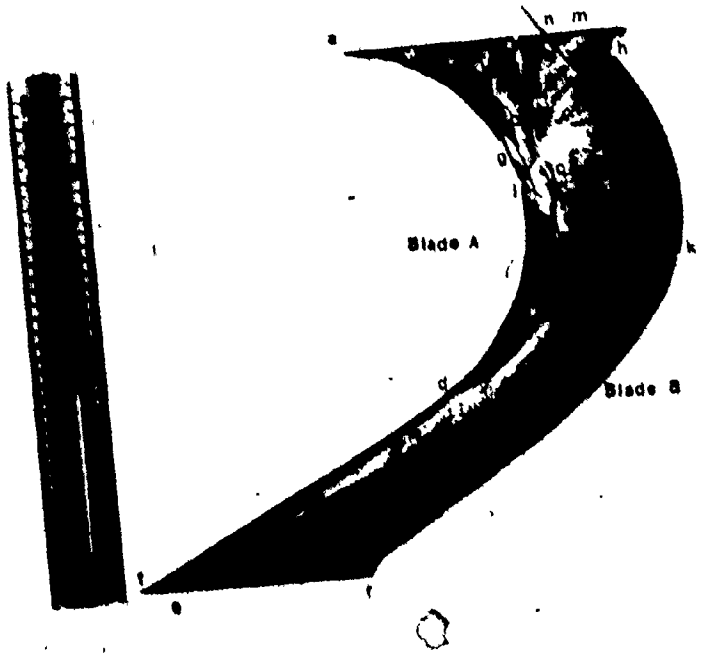

Figure 9.37 Flow Traces on the Inner Annular Wall.

outer edge of the passage-vortices are within the areas designated as a j h and r p w.

3. The radial flow emanating from the focal zone t j have a fan shape. The zone t j also shown in Figure 9.37 is associated with dense cross-channel flow. A similar pattern is observed near the outer wall.

iv) Outer Wall

The flow traces on the outer wall are shown in Figure 9.39. The pattern is seen to be similar to that on the inner wall. The inlet boundary layer however is noticed to separate at a distance further downstream than that on the inner wall.

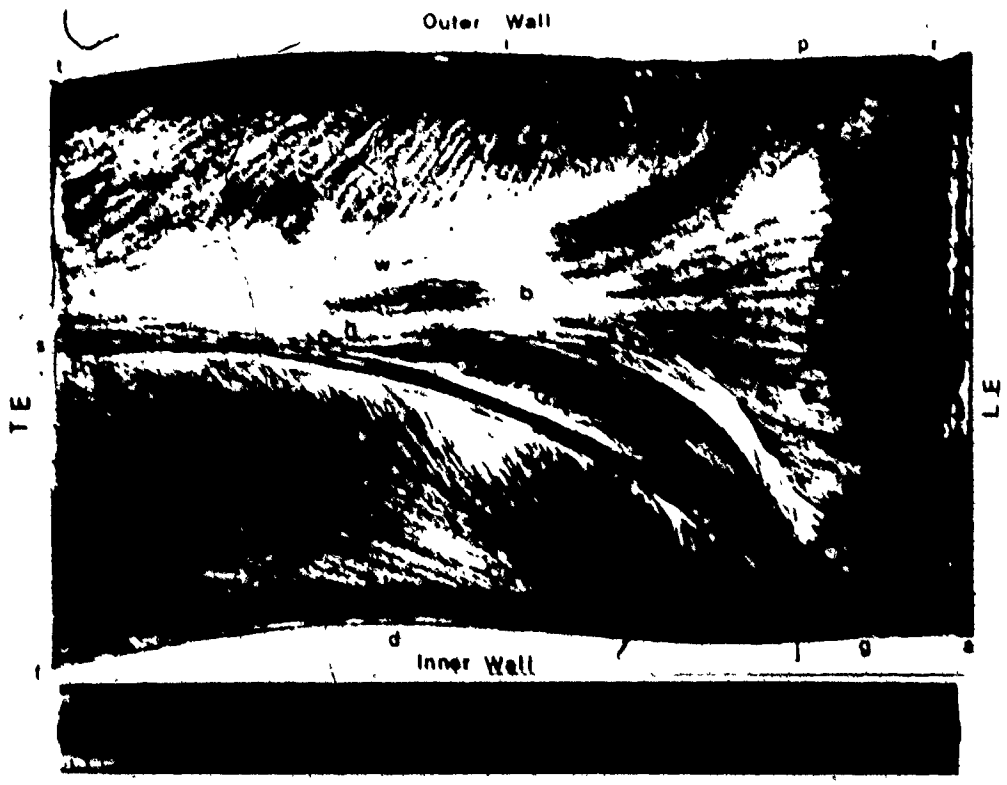

Figure 9.38 Flow Traces on the Blade Suction Surface.

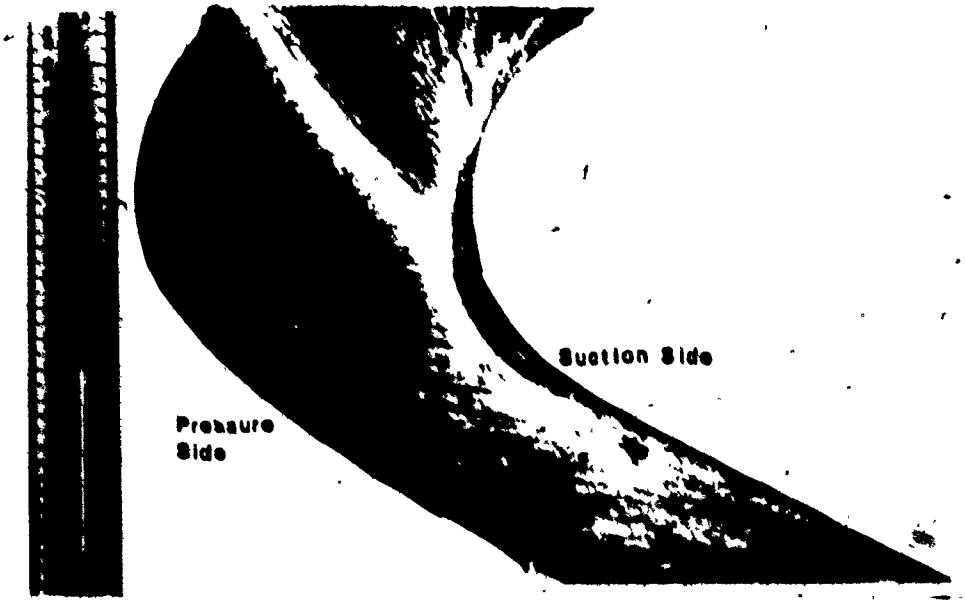

Figure 9.39 Flow Traces on the Outer Annular Wall.

CHAPTER 10

CONCLUSIONS AND RECOMMENDATIONS

In order to study the performance of a highly loaded annular cascade of turbine blades, a special test rig of hyperboloidal inlet and exit ducts was constructed and tested. The tests were carried out at a Reynolds number of 4.7×10^5 (based on the blade chord), varying the inlet boundary layer displacement thickness on both the inner and outer endwalls. The analysis of extensive test results obtained at the inlet to the cascade, center passage walls and exit from the cascade leads to the following general conclusions:

1. The inlet main flow traverses at several locations in both the radial and circumferential directions indicated that reasonable periodicity was established at the inlet measuring station. Adjustment of the inlet flow conditions was effected utilizing the experimental measures provided in the test rig design.
2. The data obtained for the inlet endwalls boundary layer indicated that the average displacement thickness could be controlled within the range

of practical interest for turbine applications.

3. The Reynolds number and the free stream turbulence level are compatible with most of the cascade data reported in the literature.

4. The analysis of the static pressure contour maps for the center passage walls and the results of the flow visualization study render a physical description of the flow behaviour within the cascade. Two large vortices were visible in the center of the passage at the cascade exit. The vortices were formed by the roll up of the endwall boundary layers on the suction surface of the blade.

5. The study of the total pressure loss contour, flow visualization results and the secondary flow patterns at the exit measuring station revealed some interesting features:

   i A high loss core was found in the middle of the blade passage with two peaks enclosed.

   ii Two large vortices were detected coinciding with the high-loss core, one vortex corresponding to each loss peak within the core.

   iii The two counter rotating vortices merged into a band of high underturning.

   iv Two low-loss zones were identified near the endwalls.

   v Two smaller areas of high loss were located at

the blade trailing edge junctions with the inner walls.

vi The control of the inlet endwall boundary layers indicated that each boundary layer had a direct contribution to the corresponding loss peak of the high loss core as well as the corresponding vortex.

vii The area of the high loss core and the associated high underturning were reduced with the reduction of the inlet endwall boundary layer displacement thickness.

6. Due to the merging of the two secondary vortices in the middle of the passage, the profile loss could not be distinguished from the secondary loss. The profile loss was, therefore, estimated using existing correlations.

7. The exit boundary layer measured at the exit from the cascade was found to be very small and the losses associated with it were found negligible.

8. Comparison of the overall and the secondary loss coefficients with existing prediction models indicated that most of the available correlations overestimate the losses.

Suggestions for Further Studies

1. The effect of the location of the exit measuring station requires further investigation in order to assess the losses due to mixing.
2. The effect of the flow incidence can be examined using different inlet ducts to provide various inlet flow angles.
3. The effect of the orientation of the blades in the annulus can be further studied. It is suggested to reposition the blades such that the trailing edges coincide with the radial direction.
4. Further measurements within the blade passage may lead to a better understanding of the vortex formation as well as the endwall boundary layer behaviour.
5. It is strongly recommended to construct a rectilinear counterpart to the present annular cascade test rig. The new test rig would serve several purposes:
   i Comparison of the general performance characteristics of the annular and rectilinear cascades. Since in annular cascades, the radial pressure gradient and the varying pitch/chord ratio undoubtedly influence the location of the secondary vortices at the exit from the cascade, the extent of such

effects can be assessed through the study of the difference in the performance of the two rigs.

ii The two-dimensional (profile) loss can be readily measured, since it is anticipated that the two passage vortices would be separated from each other in the rectilinear cascade.

iii Considering the flexibility of the rectilinear cascade rigs, the effect of various parameters can be studied (e.g., S/C, H/C, incidence, δ_1,...etc.) with the aim of obtaining a complete data record for the given blade profile.

BIBLIOGRAPHY

1. Lakshminarayana, B. and Horlock, J. H., "Review: Secondary Flows and Losses in Cascades and Axial Flow Turbomachines", Int. J. Mech. Sci., 5, 1963, p. 287.

2. Hawthorne, W. R. and Novak, R. A., "The Aerodynamics of Turbomachinery", Annual Review of Fluid Mechanics, Vol. 1, 1969, p. 341.

3. Dunham, J., "A Review of Cascade Data on Secondary Losses in Turbines", J. of Mech. Eng. Sci., Vol. 12, No. 1, 1970, p. 48.

4. Horlock, J. H. and Lakshminarayana, B., "Secondary Flow: Theory, Experiments and Applications in Turbomachinery Aerodynamics", Annual Review of Fluid Mechanics, Vol. 5, 1973, p. 247.

5. Lakshminarayana, B. and Horlock, J. H., "Generalized Expressions for Secondary Vorticity Using Intrinsic Coordinates", J. Fluid Mech., Vol. 59, Part 1, 1973, p. 97.

6. Hawthorne, W. R., "Secondary Circulation in Fluid Flow", Proc. Royal Society, 206 (Series A), 1951, p. 374.

7. Squire, H. B. and Winters, K. G., "The Secondary Flow in a Cascade of Airfoils in a Nonuniform Stream", J. of Aero Sci., April 1951, p. 271.

8. Hawthorne, W. R., "The Secondary Flow About Struts and Airfoils", J. of the Aero Sci., Sept. 1954, p. 588.

9. Preston, J. H., "A Simple Approach to the Theory of Secondary Flows", The Aero. Quarterly, Vol. 5, Sept. 1954, p.

10. Loos, H. G., "An Analysis of Secondary Flow in the Stator of an Axial Turbomachine", Guggenheim Jet Propulsion Centre, C.I.T., Tech. Report 3, Sept., 1953.

11. Lakshminarayana, B. and Horlock, J. H., "Effect of Shear Flows on Outlet Angle in Axial Compressor Cascades. Methods of Prediction and Correlation with Experiments", J. of Basic Eng., March 1964, p. 191.

12. Bardon, M. F., Moffatt, W. C., and Randall, J. L., "Secondary Flow Effects on Gas Exit Angles in Rectilinear Cascades", J. of Eng. for Power, Jan. 1975, p. 93.

13. Louis, J. F., "Rotational Viscous Flow", Proc. 9th Int. Conf. Appl. Mech., 3, 1956, p. 306.

14. Marris, A. W., "Secondary Flows in an Incompressible Fluid of Varying Density in a Rotating Reference Frame", Trans. ASME, D88, 1966, p. 533.

15. Hawthorne, W. R., "Rotational Flow Through Cascades, Part 1: The Components of Vorticity", Quarterly Jour., Mech. and Appl. Math., Vol. VII, Part 3, 1955, p. 267.

16. Erich, F. F., "Secondary Flows in Cascades of Twisted Blades", Jour. of the Aero. Sci., January 1955, p. 51.

17. Dixon, S. L., "Secondary Vorticity in Axial Compressor Blades", Fluid Mechanics and Design of Turbomachines, ed. B. Lakshminarayana, Britsch, W. R. and Gearhart, W., NASA SP 304, 1972.

18. Lighthill, M. J., "Drift", J. Fluid Mech., 1, 1956, p. 31.

19. Hawthorne, W. R. and Armstrong, W. D., "Rotational Flow Through Cascades, Part II: The Circulation About the Cascade", Quart., Jour. Mech. and Appl. Math., Vol. 8, Part 3, 1955, p. 281.

20. Smith, H. B., "Secondary Flow in Axial Flow Turbomachinery", Trans. ASME, 77, October 1955, p. 1065.

21. Johnston, J. P., "On the Three-Dimensional Turbulent Boundary Layer Generated by Secondary Flow", ASME, Jour. of Basic Eng., March 1960, p. 233.

22. Sjolander, S. A., "The Endwall Boundary Layer in an Annular Cascade of Turbine Nozzle Guide Vanes", Technical Report ME 1A75-4, Carleton University, Ottawa, December 1975.

23. Mayer, A., "Generalization of Boundary Layer Momentum Integral Equations to Three-Dimensional Flows Including Those of Rotating Systems", NACA R1067, 1952.

24. Railly, J. W., and Howard, J. H. G., "Velocity Profile Development in Axial Flow Compressors", J. Mech. Eng. Sci., Vol. 4, No. 2, 1962, p. 166.

25. Jansen, W., "The Application of Endwall Boundary Layer Effects in the Performance Analysis of Axial Compressors", ASME Paper No. 67 WA/GT 11, November 1957.

26. Stratford, B. S., "The Use of Boundary Layer Techniques to Calculate the Blockage from the Annulus Boundary Layer in a Compressor", ASME Paper No. 67 WA/GT 7, November 1967.

27. Mellor, G. L. and Wood, G. M., "An Axial Compressor Endwall Boundary Layer Theory", J. Basic Eng., June 1971, p. 300.

28. Horlock, J. H. and Hoadley, D., "Calculation of the Annulus Wall Boundary Layer in Axial Flow Turbomachines", British ARC G.P. 1196, March 1971.

29. Hirsch, Ch., "End-Wall Boundary Layers in Axial Compressors", ASME Paper No. 74-GT-72, 1974.

30. Marsh, H. and Horlock, J. H., "Wall Boundary Layers in Turbomachines", J. Mech. Eng. Sci., Vol. 14, No. 6, 1972, p. 411.

31. Horlock, J. H., "Cross-Flows in Bounded Three-Dimensional Turbulent Boundary Layers", J. Mech. Eng. Sci., Vol. 15, No. 4, 1973, p. 274.

32. Anand, A. K. and Lakshminarayana, B., "Three-Dimensional Turbulent Boundary Layer in a Rotating Helical Channel", Jour. of Fluids Eng., June 1975, p. 197.

33. Railly, J. W. and Sharma, P. B., "Treatment of the Annulus Wall Boundary Layer Using a Secondary Flow Hypothesis", Jour. of Eng. for Power, January 1977, p. 29.

34. Salvage, J. W., "Investigation of Secondary Flow Behavior and End-Wall Boundary Layer Development Through Compressor Cascades", Von Karman Institute for Fluid Dynamics, TN No. 107, 1974.

35. Louis, J. F., "Secondary Flow in Compressor Cascades", British ARC, R&M 3136, 1960.

36. Soderberg, O. E., "Secondary Flow and Losses in a Compressor Cascade", Gas Turbine Laboratory, Report No. 46, M.I.T., 1958.

37. Horlock, J. H., "Axial Flow Turbines, Fluid Mechanics and Thermodynamics", Butterworth Scientific Publications, London, 1966.

38. Ainely, D. G., and Mathieson, G. C. R., "A Method of Performance Estimation for Axial Flow Turbines", Aeronautical Research Council, R&M 2974, 1957.

39. Denton, J. D., "A Survey and Comparison of Methods for Predicting the Profile Loss of Turbine Blades", I. Mech. Eng., Conference Publication, 3, 1973, p. 204.

40. Came, P. M., "Secondary Loss Measurements in a Cascade of Turbine Blades", I. Mech. Eng. Conference Publication, 3, 1973, p. 75.

41. Dunham, J. and Came, P. M., "Improvements to the Ainely-Mathieson Method of Turbine Performance Prediction", Trans. ASME, Jour. of Eng. for Power, July 1970, p. 252.

42. Bown, R. L., "A Investigation of the Secondary Flow Phenomena in a Cascade of High Deflection Axial Flow Impulse Turbine Blades", M.Sc. Thesis, U.S. Naval Postgraduate School, Monterey, California, December 1966.

43. Woods, J. R., "An Investigation of Secondary-Flow Phenomena and Associated Losses in a High-Deflection Turbine Cascade", Ph.D Thesis, Naval Postgraduate School, Monterey, California, September 1972.

44. Langston, L. S., Nice, M. L., and Hooper, R. M., "Three-Dimensional Flow Within a Turbine Cascade Passage", Jour. of Eng. for Power, January 1977, p. 21.

45. Herzig, H. Z., and Hansen, A. G., "A Visualization Study of Secondary Flows in Cascades", NACA Report 1163, 1954.

46. Rohlik, H. E., Kofskey, M. G., Allen, H. W., and Herzig, H. Z., Secondary Flows and Boundary Layer Accummulations in Turbine Nozzles", NACA Report 1168, 1954.

47. Kofskey, M. G. and Allen, H. W., "Smoke Study of Nozzle Secondary Flows in a Low Speed Turbine", NACA TN 3260, 1954.

48. Allen, H. W. and Kofskey, M. G., "Visualization Study of Secondary Flows in Turbine Rotor Tip Regions", NACA, TN 3519, 1955.

49. Hansen, A. G. and Herzig, H. Z., "Cross Flows in Laminar Incompressible Boundary Layers", NACA, TN 3651, 1956.

50. Herzig, H. Z. and Hansen, A. G., "Visualization Studies of Secondary Flows with Applications to Turbomachines", Trans. ASME, 77, 1955, p. 249.

51. Myachin, E. V., "A Three-Dimensional Test Rig for the Investigation of the Secondary Flow in High Turning Turbine Blade Cascades", Mech. Eng. Dept. Report, McMaster University, 1973.

52. Molhotra, R. K., "The Two-Dimensional Development and Analysis of Blade Profiles Having Large Turning Angles", M.Eng. Thesis, Mech. Eng. Dept., McMaster University, March 1971.

53. Stannard, J. H., "The Aerodynamic Design and Testing of High Turning Angle Turbine Blades", Ph.D Thesis, Mech. Eng. Dept., McMaster University, April 1975.

54. Schlichting, H., "Boundary Layer Theory", McGraw-Hill Book Company Publication, Sixth Ed., 1968.

55. Wolf, H., "Die Randverluste In Geraden Schaufelgittern", Wissenschaftliche Zeitschrift der Technischen Hochschule, Dresden, 10, No. 2, 1961.

56. Hawthorne, W.R., "Thermodynamics of Cooled Turbines", Part I - "The Turbine Stage", Trans. ASME 78, 1956, p. 1765. Part II - "The Multistage Turbine", Trans. ASME, 78, 1956, p. 1781.

57. Balje, O. E. and Binsley, R. L., "Axial Turbine Performance Evaluation", Jour. of Eng. Power, Trans. ASME, October 1968, pp. 341-348.

58. Klein, A., "Investigation of the Effect of the Entry Wall Boundary Layers on the Secondary Flows of Axial Flow Turbines", Forsch. Geb. Ing.-Wes., 32, 1966, pp. 175-187.

APPENDIX 1

SUPPLEMENTARY DRAWINGS FOR THE TEST RIG

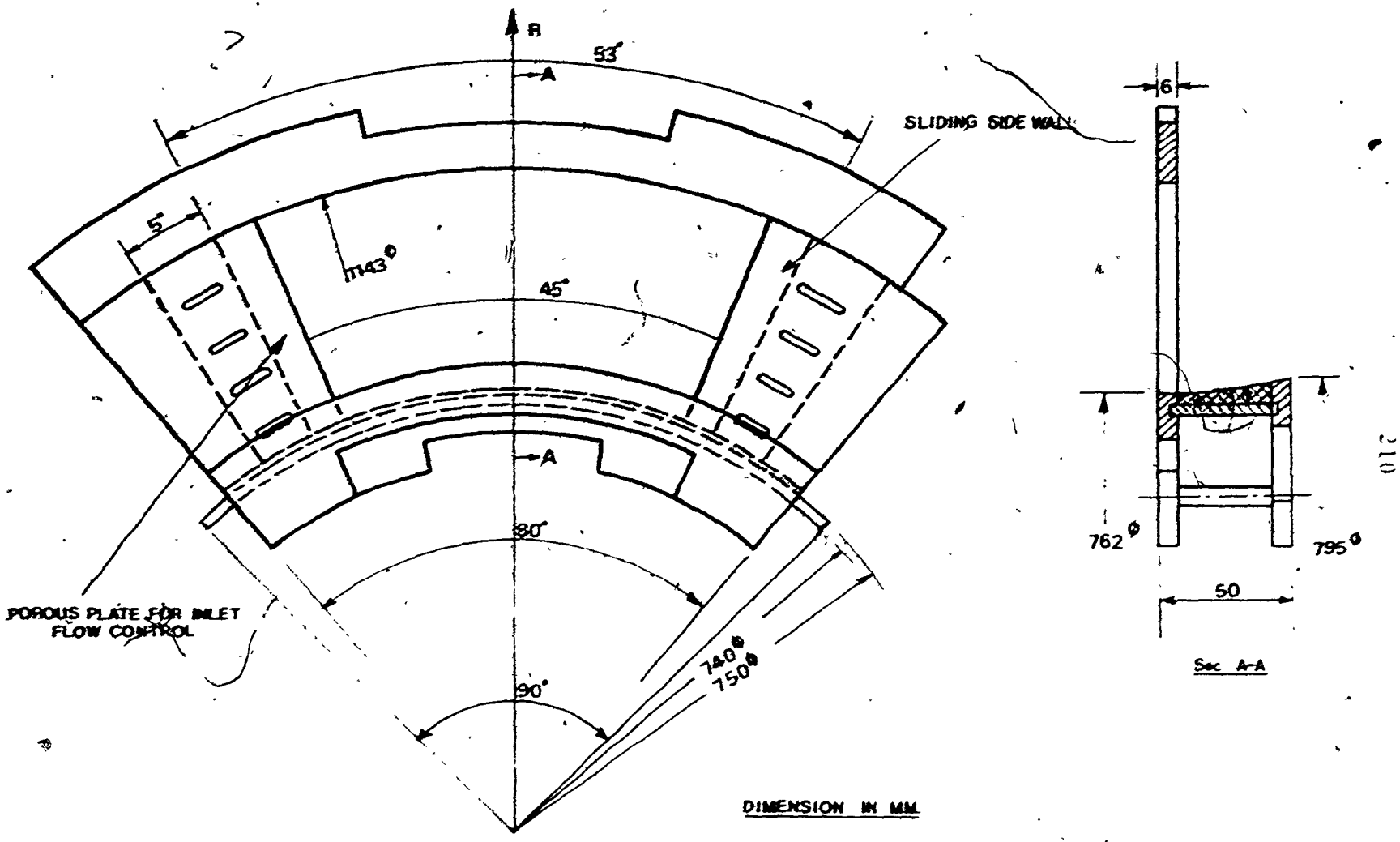

Figure A1.1 Sliding Annular Segment at the Inlet to the Cascade.

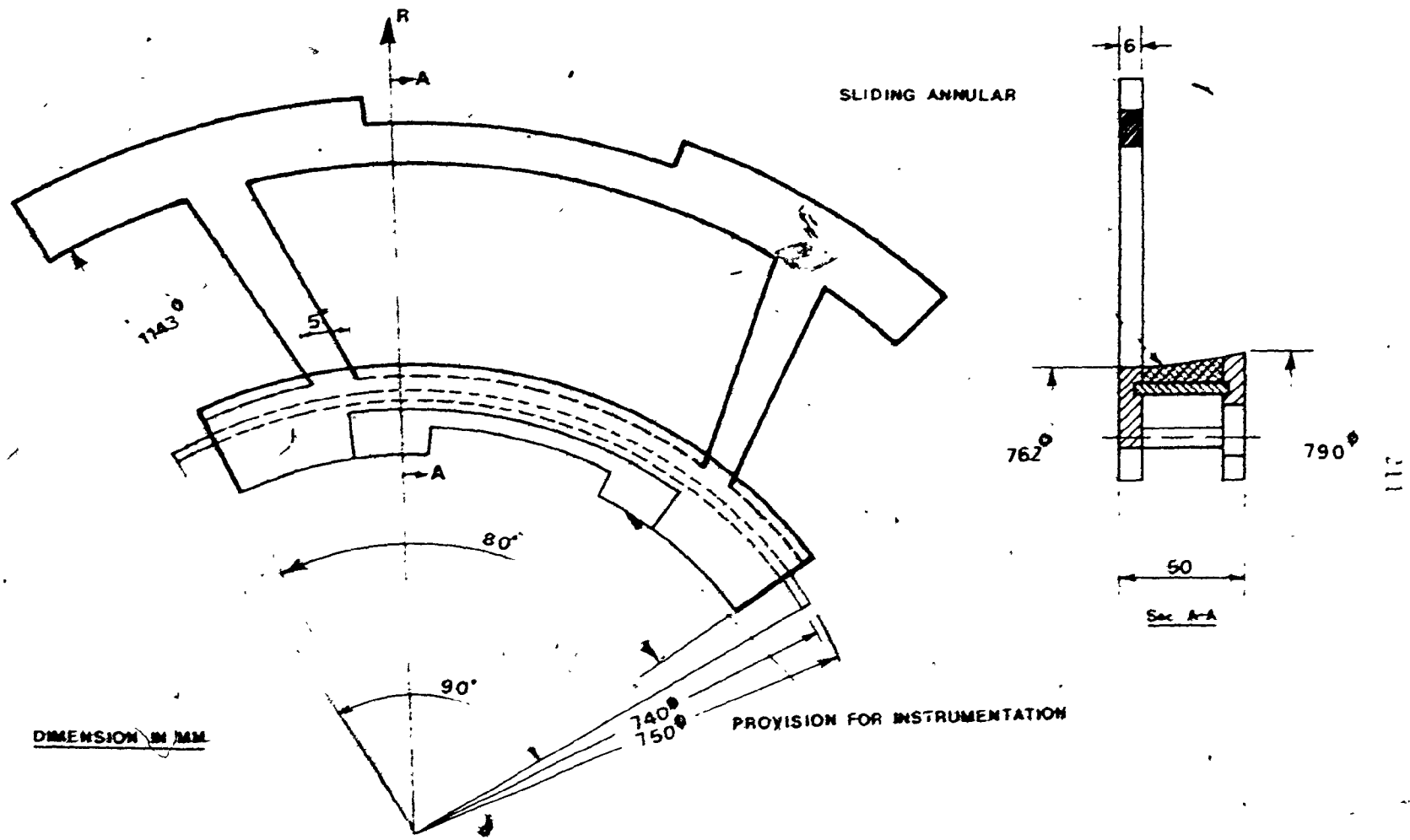

Figure A1.2 Sliding Annular Segment at the Exit From the Cascade.

APPENDIX 2

SUPPLEMENTARY INFORMATION FOR THE INSTRUMENTATION

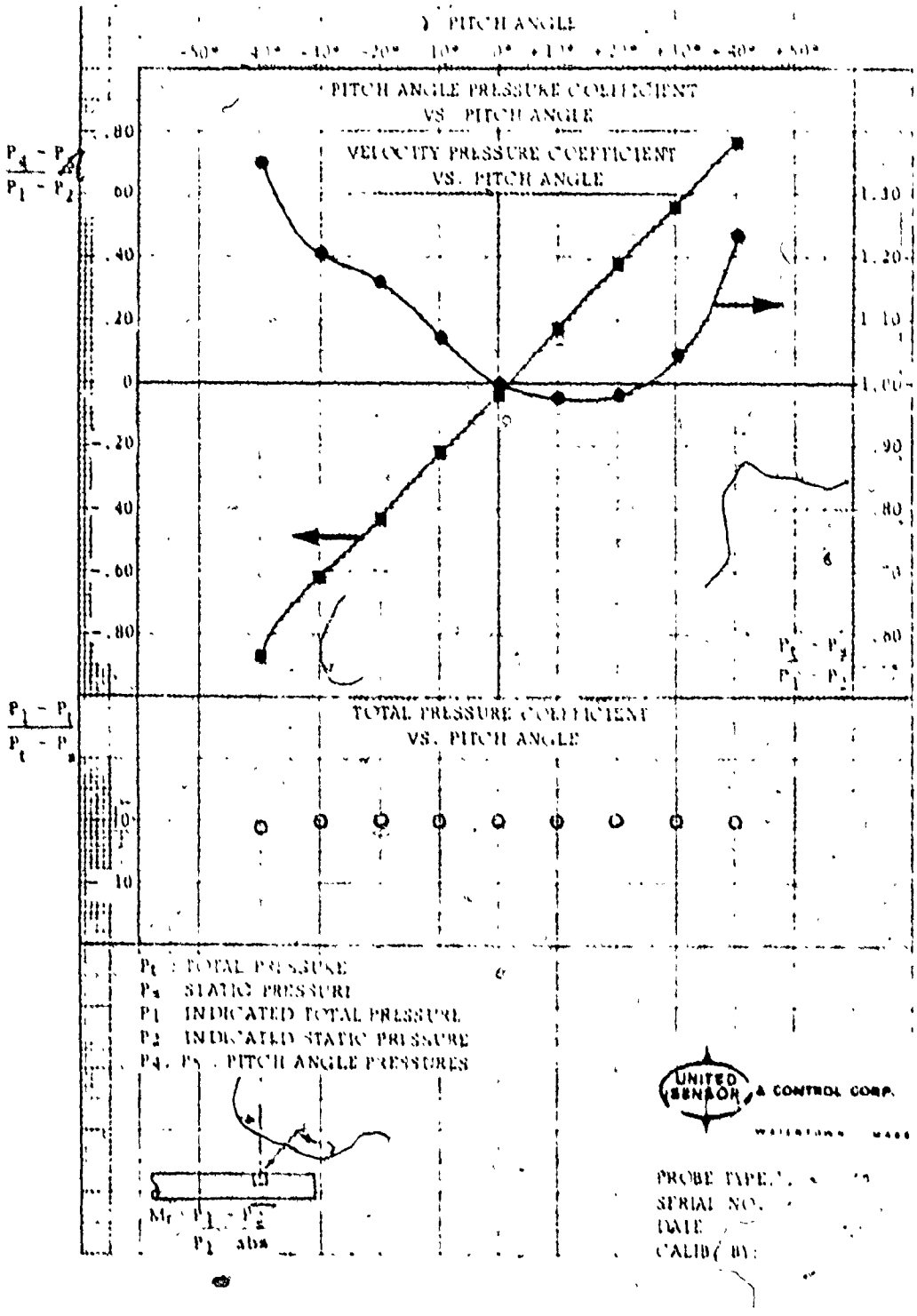

Figure A3.1 Calibration Data for the Three-Dimensional Probe (Type DA 125).

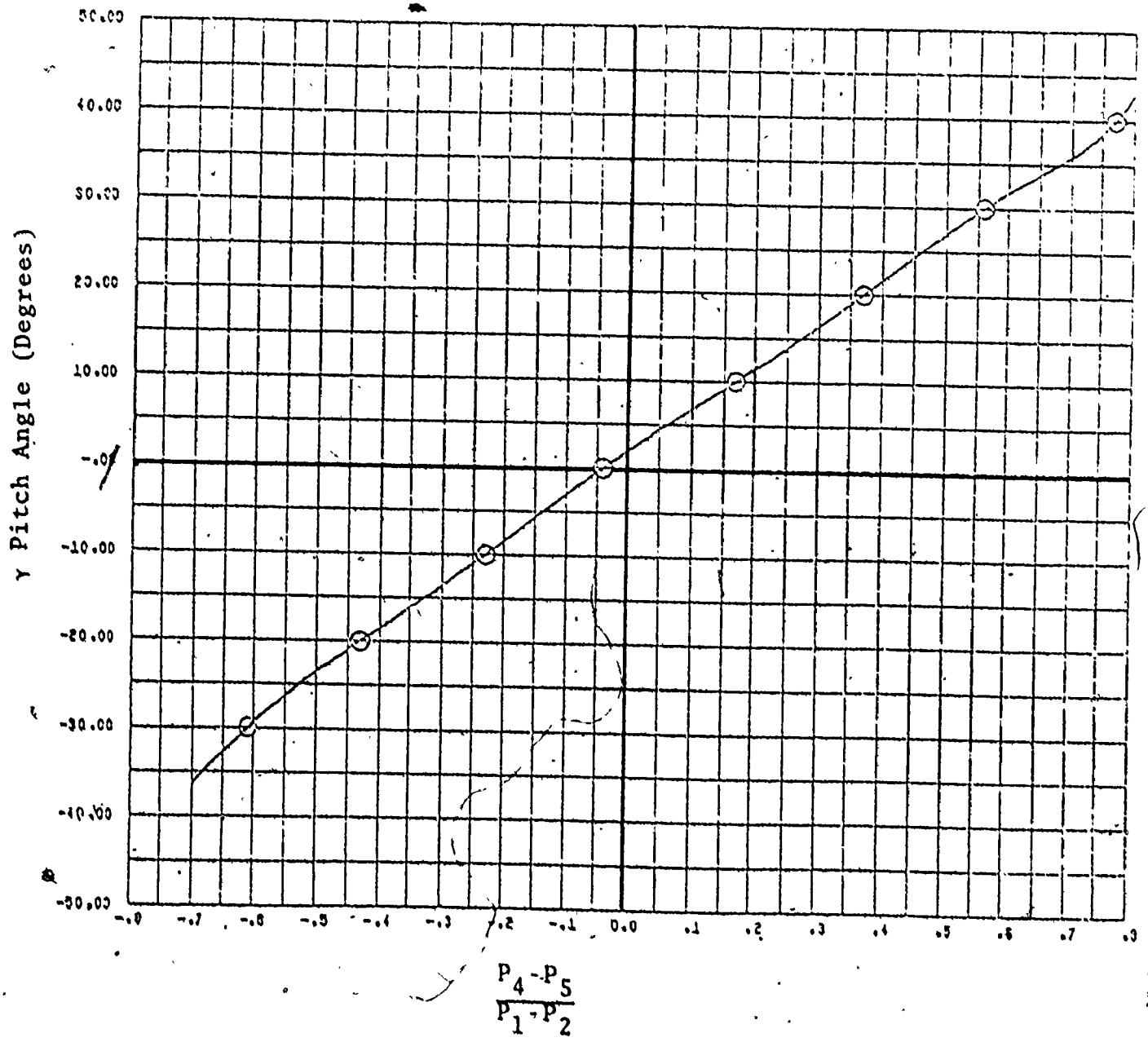

Figure A2.2 Polynomial Curve-Fit for the Pitch Angle Pressure Coefficient vs. Pitch Angle.

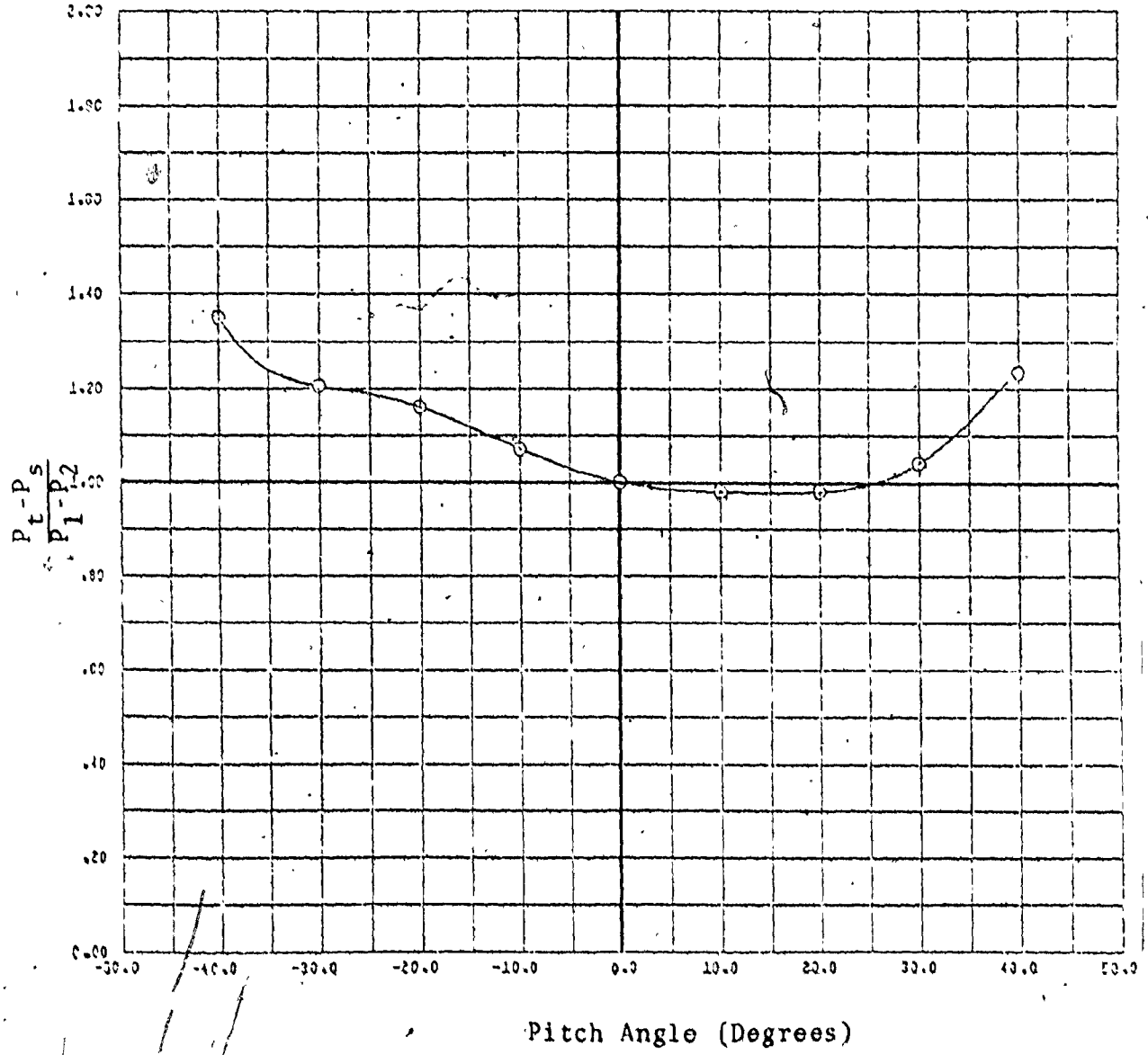

Figure A2.3 Polynomial Curve-Fit for the Velocity Pressure Coefficient vs. Pitch Angle.

Specifications of the Pressure Transducer

Model	Setra 237 low range pressure transducer (capacitance type sensor).
Range	± 05 psid (± 3447.878 Pa) bidirectional.
Maximum overload	100 psi, positive direction, 2.5 psi in negative direction.
Excitation	24 volts D.C., 25 ma, nominal.
Full range output	± 2.5 volts, nominal.
Zero output	< ± 100 mv at 77°F (-0.010 volts).
Non-linearity	< ± 0.25% of full range output, (best straight line method).
Hysteresis	< ± 0.1% of full range output, (infinite resolution).
Ambient operating temperature limits	0°F to 175°F
Compensated temperature range	30°F to 150°F
Thermal zero shift	< ± 0.015% full range 1°F, 30°F to 150°F.
Thermal coefficient of sensitivity	< ± 0.01% full range 1°F, 30°F to 150°F.
Acceleration response	< 0.0002 psi/g typical.
Volume increase due to F.R. pressure	1×10^{-5} cubic inches.
Natural frequency	-5000 Hz nominal.
Output noise	< 5 mv R.M.S.

APPENDIX 3

DATA REDUCTION PROGRAM

```
      PROGRAM TST (INPUT,OUTPUT,TAPE5=INPUT,TAPE6=OUTPUT)                MAI  10
      DIMENSION Z(20),DR(20),R(20),THETA1(20),THETA2(20),P1(20,20),      MAI  20
     *P2(20,20),P3(20,20),P4(20,20),P5(20,20),DIV(20,20),PT(20,20),      MAI  30
     *PS(20,20),PITCH(20,20),V(20,20),VA(20,30),CPO(20,20),CPS(20,20),   MAI  40
     *CPOY(20),CPSY(20),DIVY(20),CPON(20),CPSN(20),DIVN(20),VY(20),      MAI  50
     *VM(20)                                                            MAI  60
                                                                        MAI  70
                                                                        MAI  80
C     ************************************************************     MAI  90
C     *                                                          *     MAI 100
C     *                  DATA REDUCTION PROGRAM                  *     MAI 110
C     *                                                          *     MAI 120
C     *  INPUT DATA.....                                         *     MAI 130
C     *                                                          *     MAI 140
C     *  Z.......ARRAY OF THE RADIAL  LOCATIONS  MEASURED FROM  *     MAI 150
C     *          THE INNER WALL.                                 *     MAI 160
C     *                                                          *     MAI 170
C     *  DR......ARRAY OF THE RADIAL INCREMENTS.                 *     MAI 180
C     *                                                          *     MAI 190
C     *  R.......ARRAY OF THE  RADIAL LOCATIONS  MEASURED FROM  *     MAI 200
C     *          THE CENTER OF THE ANNULAR CASCADE.              *     MAI 210
C     *                                                          *     MAI 220
C     *  THETA1..ARRAY OF THE L.H.S. BOUNDARIES OF THE PASSAGE   *     MAI 230
C     *          TRAVERSED IN DEGREES MEASURED FROM THE DIREC-   *     MAI 240
C     *          TION  "R".                                      *     MAI 250
C     *                                                          *     MAI 260
C     *  THETA2..ARRAY OF THE R.H.S. BOUNDARIES OF THE PASSAGE   *     MAI 270
C     *          TRAVERSED IN DEGREES MEASURED FROM THE DIREC-   *     MAI 280
C     *          TION  "R".                                      *     MAI 290
C     *                                                          *     MAI 300
C     *  (P1,P2, ARRAYS OF THE PRESSURE READINGS OF  THE FIVE    *     MAI 310
C     *   P3,P4, HOLE  PROBE IN CHART UNITS.                     *     MAI 320
C     *   P5)....                                                *     MAI 330
C     *                                                          *     MAI 340
C     *  DIV.....ARRAY OF THE EXIT ANGLE  DEVIATION  (AIR EXIT   *     MAI 350
C     *          ANGLE-BLADE EXIT ANGLE)*                        *     MAI 360
C     *                                                          *     MAI 370
C     *  CALCULATED PARAMETERS.....                              *     MAI 380
C     *                                                          *     MAI 390
C     *  PT......TOTAL  PRESSURE IN MILLIMETERS OF WATER.        *     MAI 400
C     *                                                          *     MAI 410
C     *  PS......STATIC PRESSURE IN MILLIMETERS OF WATER.        *     MAI 420
C     *                                                          *     MAI 430
C     *  PITCH...PITCH ANGLE IN DEGREES.                         *     MAI 440
C     *                                                          *     MAI 450
C     *  V.......VELOCITY IN (M/SEC).                           *     MAI 460
C     *                                                          *     MAI 470
C     *  VA......AXIAL VELOCITY (M/SEC).                         *     MAI 480
C     *                                                          *     MAI 490
C     *  CP......LOCAL TOTAL-PRESSURE LOSS-COEFFICIENT.          *     MAI 500
C     *                                                          *     MAI 510
C     *  CPS.....LOCAL STATIC PRESSURE COEFFICIENT.              *     MAI 520
C     *                                                          *     MAI 530
C     *  CPOY....PITCHWISE MASS AVERAGED PRESSURE LOSS COEFFI-   *     MAI 540
C     *          CIENT.                                          *     MAI 550
C     *                                                          *     MAI 560
C     *  CPSY....PITCHWISE MASS AVERAGED STATIC  PRESSURE  CO-   *     MAI 570
C     *          EFFICIENT.                                      *     MAI 580
C     *                                                          *     MAI 590
C     *  DIVY....PITCHWISE MASS AVERAGED EXIT ANGLE DEVIATION.   *     MAI 600
C     *                                                          *     MAI 610
C     *  CPON....PITCHWISE  ARITHMATIC  AVERAGE TOTAL PRESSURE   *     MAI 620
C     *          LOSS COEFFICIENT.                               *     MAI 630
C     *                                                          *     MAI 640
C     *  CPSN....PITCHWISE ARITHMATIC AVERAGE STATIC  PRESSURE   *     MAI 650
C     *          COEFFICIENT.                                    *     MAI 660
C     *                                                          *     MAI 670
C     *  DIVM....PITCHWISE ARITHMATIC AVERAGE EXIT ANGLE DEVI-   *     MAI 680
C     *          ATION.                                          *     MAI 690
C     *                                                          *     MAI 700
C     *  VY......PITCHWISE MASS AVERAGED AXIAL VELOCITY,         *     MAI 710
C     *                                                          *     MAI 720
C     ************************************************************     MAI 730
                                                                        MAI 740
```

```
C     **********************                                          MAI 750
C     *                    *                                          MAI 760
C     *  PREPARE PLOTS.    *                                          MAI 770
C     *                    *                                          MAI 780
C     **********************                                          MAI 790
                                                                      MAI 800
                                                                      MAI 810
      CALL PLOT(X,Y,-20)                                              MAI 820
      CALL NAME                                                       MAI 830
      CALL PLOT(3.0,0.0,-3)                                           MAI 840
                                                                      MAI 850
                                                                      MAI 860
C     **********************                                          MAI 870
C     *                    *                                          MAI 880
C     *  READ INPUT DATA.  *                                          MAI 890
C     *                    *                                          MAI 900
C     **********************                                          MAI 910
                                                                      MAI 920
                                                                      MAI 930
C     ************************************************************  MAI 940
C     *                                                          *    MAI 950
C     *  PAT.....ATMOSPHERIC PRESSURE IN INCHES OF MERCURY.      *    MAI 960
C     *                                                          *    MAI 970
C     *  TAT.....ATMOSPHERIC  TEMPERATURE  IN DEGREES FAHREN--   *    MAI 980
C     *          HEIT.                                           *    MAI 990
C     *                                                          *    MAI1000
C     *  NR......NUMBER OF CIRCUMFERENTIAL LOCATIONS.            *    MAI1010
C     *                                                          *    MAI1020
C     *  NP......NUMBER OF RADIAL LOCATIONS.                     *    MAI1030
C     *                                                          *    MAI1040
C     *  PO1.....INLET STAGNATION PRESSURE IN  MILLIMETERS  OF   *    MAI1050
C     *          WATER                                           *    MAI1060
C     *                                                          *    MAI1070
C     *  PS1.....INLET  STATIC  PRESSURE IN MILLIMETERS OF WA-   *    MAI1080
C     *                                                          *    MAI1090
C     *          TER                                             *    MAI1100
C     *                                                          *    MAI1110
C     ************************************************************  MAI1120
                                                                      MAI1130
      READ(5,*)PAT,TAT,NR,NP,PO1,PS1                                  MAI1140
      READ(5,*)((Z(J),J=1,NR),(DR(J),J=1,NR),(THETA1(J),J=1,NR),      MAI1150
     *(THETA2(J),J=1,NR))                                             MAI1160
      DO 1 J=1,NR                                                     MAI1170
      R(J)=15.0+Z(J)                                                  MAI1180
1     READ(5,*)((P1(I,J),P2(I,J),P3(I,J),P4(I,J),P5(I,J),             MAI1190
     *DIV(I,J),I=1,NP),J=1,NR)                                        MAI1200
                                                                      MAI1210
                                                                      MAI1220
                                                                      MAI1230
C     ************************************************************  MAI1240
C     *                                                          *    MAI1250
C     *  USE THE  TRANSDUCER  CALIBRATION  DATA TO  OBTAIN THE   *    MAI1260
C     *                                                          *    MAI1270
C     *  PRESSURE READINGS IN MILLIMETERS OF WATER               *    MAI1280
C     *                                                          *    MAI1290
C     ************************************************************  MAI1300
                                                                      MAI1310
                                                                      MAI1320
      CALL MTRANS(P1,P2,P3,P4,P5,NP,NR)                               MAI1330
                                                                      MAI1340
                                                                      MAI1350
C     ************************************************************  MAI1360
C     *                                                          *    MAI1370
C     *  USE THE THREE-DIMENTIONAL PROBE  CALIBRATION DATA  TO   *    MAI1380
C     *                                                          *    MAI1390
C     *  OBTAIN THE TOTAL, STATIC  PRESSURE  AND THE PITCH AN-   *    MAI1400
C     *                                                          *    MAI1410
C     *  GLES.                                                   *    MAI1420
C     *                                                          *    MAI1430
C     ************************************************************  MAI1440
                                                                      MAI1450
                                                                      MAI1460
                                                                      MAI1470
                                                                      MAI1480
```

```
      CALL PR3D(P1,P2,P4,P5,PITCH,PT,PS,NP,NR)                          MA11490
                                                                        MA11500
                                                                        MA11510
                                                                        MA11520
C     ****************************************************************  MA11530
C     *                                                              *  MA11540
C     *  USE THE POTENTIOMETER CALIBRATION DATA TO OBTAIN  THE       *  MA11550
C     *                                                              *  MA11560
C     *  EXIT ANGLE DEVIATION IN DEGREES.                            *  MA11570
C     *                                                              *  MA11580
C     ****************************************************************  MA11590
                                                                        MA11600
                                                                        MA11610
      CALL POTN(DIV,NP,NR)                                              MA11620
                                                                        MA11630
                                                                        MA11640
C     ****************************************************************  MA11650
C     *                                                              *  MA11660
C     *  CALCULATE THE FLOW VELOCITY IN (FT/SEC).                    *  MA11670
C     *                                                              *  MA11680
C     ****************************************************************  MA11690
                                                                        MA11700
                                                                        MA11710
      CALL VEL(PAT,TAT,PS,PT,V,NP,NR)                                   MA11720
                                                                        MA11730
                                                                        MA11740
C     ****************************************************************  MA11750
C     *                                                              *  MA11760
C     *  CALCULATE THE AXIAL VELOCITY IN (FT/SEC).                   *  MA11770
C     *                                                              *  MA11780
C     ****************************************************************  MA11790
                                                                        MA11800
                                                                        MA11810
      CALL VELA(V,VA,PITCH,DIV,NP,NR)                                   MA11820
                                                                        MA11830
                                                                        MA11840
C     ****************************************************************  MA11850
C     *                                                              *  MA11860
C     *  CALCULATE THE LOCAL PARAMETERS CPO,CPS.                     *  MA11870
C     *                                                              *  MA11880
C     ****************************************************************  MA11890
                                                                        MA11900
                                                                        MA11910
      CALL LOCAL(PT,PS,P01,PS1,CPO,CPS,NP,NR)                           MA11920
                                                                        MA11930
                                                                        MA11940
C     ****************************************************************  MA11950
C     *                                                              *  MA11960
C     *  CALCULATE THE PITCHWISE MASS AVERAGED AND  ARITHMATIC       *  MA11970
C     *                                                              *  MA11980
C     *  AVERAGE PARAMETERS.                                         *  MA11990
C     *                                                              *  MA12000
C     ****************************************************************  MA12010
                                                                        MA12020
                                                                        MA12030
      CALL AVRAGE(CPO,CPS,DIV,VA,CPOY,CPOM,CPSY,CPSM,DIVY,             MA12040
     $DIVM,VY,VM,NP,NR)                                                 MA12050
                                                                        MA12060
                                                                        MA12070
C     ****************************************************************  MA12080
C     *                                                              *  MA12090
C     *  CALCULATE THE LOSS DATA.                                    *  MA12100
C     *                                                              *  MA12110
C     ****************************************************************  MA12120
                                                                        MA12130
                                                                        MA12140
      CALL LOSS(P01,PS1,PT,PS,DIV,VA,R,DR,DPT,DPS,P2ON,P2M,YT,NP,NR)    MA12150
                                                                        MA12160
                                                                        MA12170
C     ************************                                         MA12180
C     *                      *                                         MA12190
C     *  WRITE INPUT DATA.   *                                         MA12200
C     *                      *                                         MA12210
C     ************************                                         MA12220
```

```
      CALL WRITE1(PAT,TAT,NP,NR,PO1,PS1,THETA1,THETA2,Z,P1,P2,P3,
     *P4,P5,DIV,ZZ)                                                    NA12300
                                                                       NA12310
                                                                       NA12320
C     ****************************************************************NA12330
C     *                                                              *NA12340
C     *  OBTAIN THE DIMENSIONLESS VELOCITY VALUES.                   *NA12350
C     *                                                              *NA12360
C     ****************************************************************NA12370
                                                                       NA12380
      CALL DIMLSS(VM,ZZ,NR)                                            NA12390
                                                                       NA12400
C     ****************************************************************NA12410
C     *                                                              *NA12420
C     *  PREPARE THE PLOTTING FRAME.                                 *NA12430
C     *                                                              *NA12440
C     ****************************************************************NA12450
                                                                       NA12460
      CALL FRAME0                                                      NA12470
                                                                       NA12480
C     ****************************************************************NA12490
C     *                                                              *NA12500
C     *  PLOT THE EXPERIMENTAL POINTS.                               *NA12510
C     *                                                              *NA12520
C     ****************************************************************NA12530
                                                                       NA12540
      CALL GRAFN(  VM,ZZ,0.0,0.0,BIGTH,NR)                             NA12550
                                                                       NA12560
C     ****************************************************************NA12570
C     *                                                              *NA12580
C     *  JOIN THE POINTS WITH A CURVE.                               *NA12590
C     *                                                              *NA12600
C     ****************************************************************NA12610
                                                                       NA12620
      CALL CURVE(  VM,ZZ,NR)                                           NA12630
      CALL PLOT(20.0,0.0,-3)                                           NA12640
      CALL FRAME1                                                      NA12650
      CALL GRAFN(CPOY,ZZ,0.0,BIGTH,NR)                                 NA12660
      CALL CURVE(CPOY,ZZ,NR)                                           NA12670
      CALL PLOT(20.0,0.0,-3)                                           NA12680
      CALL FRAME2                                                      NA12690
      CALL GRAFN(DIVY,ZZ,0.0,BIGTH,NR)                                 NA12700
      CALL CURVE(DIVY,ZZ,NR)                                           NA12710
      CALL PLOT(20.0,0.0,-3)                                           NA12720
                                                                       NA12730
C     ****************************************************************NA12740
C     *                                                              *NA12750
C     *  WRITE OUTPUT INFORMATION.                                   *NA12760
C     *                                                              *NA12770
C     ****************************************************************NA12780
                                                                       NA12790
      CALL WRITE3(V,VA,PITCH,DIV,CPO,CPN,NP,NR)                        NA12800
      CALL WRITE5(CPOY,CPON,CPNY,CPNM,DIVY,DIVM,VY,VM,NP,NR)           NA12810
      CALL WRITE4(DPT,DPN,PSON,PSM,YT,NR)                              NA12820
      CALL FRAME4                                                      NA12830
      NCALE=0.005                                                      NA12840
                                                                       NA12850
                                                                       NA12860
```

```
C     ****************************************************************      MAIN2970
C     *                                                              *      MAIN2980
C     *   DRAW A MAP OF THE SECONDARY FLOW VELOCITY VECTORS.         *      MAIN2990
C     *                                                              *      MAIN3000
C     ****************************************************************      MAIN3010
                                                                             MAIN3020
                                                                             MAIN3030
      CALL DART(THETA1,R,V,DIV,PITCH,NP,NR,SCALE)                            MAIN3040
      CALL PLOT(35.0,0.0,-3)                                                 MAIN3050
      STOP                                                                   MAIN3060
      END                                                                    MAIN3070
                                                                             MAIN3080
                                                                             MAIN3090
                                                                             MAIN3100

      SUBROUTINE NAME                                                        NAM  10
C     ***************                                                        NAM  20
      CALL PLOT(0.0,0.0,-3)                                                  NAM  30
      CALL DATE(D1)                                                          NAM  40
      CALL LETTER(5.0,3.0,270.0,1.0,10.0,5HNEDKY)                            NAM  50
      CALL LETTER(10.0,0.0,270.0,2.0,10.0,D1)                                NAM  60
      RETURN                                                                 NAM  70
      END                                                                    NAM  80

      SUBROUTINE MTRANS(P1,P2,P3,P4,P5,NP,NR)                                MTR  10
C     ***************************************                                MTR  20
      DIMENSION P1(20,20),P2(20,20),P3(20,20),P4(20,20),P5(20,20)            MTR  30
      DO 1 J=1,NR                                                            MTR  40
      DO 1 I=1,NP                                                            MTR  50
      P1(I,J)=P1(I,J)*30.072                                                 MTR  60
      P2(I,J)=P2(I,J)*30.072                                                 MTR  70
      P3(I,J)=P3(I,J)*30.072                                                 MTR  80
      P4(I,J)=P4(I,J)*30.072                                                 MTR  90
      P5(I,J)=P5(I,J)*30.072                                                 MTR 100
1     CONTINUE                                                               MTR 110
      RETURN                                                                 MTR 120
      END                                                                    MTR 130

      SUBROUTINE PROD(P1,P2,P4,P3,PITCH,PT,PN,N,M)                           PRO  10
C     ********************************************                           PRO  20
      DIMENSION P1(20,20),P2(20,20),P3(20,20),P4(20,20),P5(20,20),           PRO  30
     *PITCH(20,20),PT(20,20),PN(20,20)                                       PRO  40
      DIMENSION X(9),Y(9),XX(9),YY(9),PP(20,20),PPP(20,20),WORK(50),         PRO  50
     *A(9),B(9)                                                             PRO  60
      DATA X/-0.07,-0.61,-0.40,-0.30,-0.04,0.17,0.07,0.56,0.77/              PRO  70
      DATA Y/-40.0,-30.0,-20.0,-10.0,0.0,10.0,20.0,30.0,40.0/                PRO  80
      DATAXX/-40.0,-30.0,-20.0,-10.0,0.0,10.0,20.0,30.0,40.0/                PRO  90
      DATAYY/1.00,1.205,1.16,1.07,1.00,0.90,0.98,1.04,1.200/                 PRO 100
      CALL LENQ(WORK,A,X,Y,8,0)                                              PRO 110
      CALL LENQ(WORK,B,XX,YY,8,0)                                            PRO 120
      DO 1 K=1,N                                                             PRO 130
      DO 1 I=1,N                                                             PRO 140
      PP(I,K)=ABS(P1(I,K)-P2(I,K))                                           PRO 150
      PP(I,K)=(P3(I,K)-P4(I,K))/PP(I,K)                                      PRO 160
      PITCH(I,K)=A(1)                                                        PRO 170
      DO 2 J=2,9                                                             PRO 180
2     PITCH(I,K)=A(J)*(PP(I,K)**(J-1))+PITCH(I,K)                            PRO 190
      PPP(I,K)=B(1)                                                          PRO 200
      DO 3 J=2,9                                                             PRO 210
3     PPP(I,K)=B(J)*(PITCH(I,K)**(J-1))+PPP(I,K)                             PRO 220
      PPP(I,K)= PPP(I,K)*ABS(P1(I,K)-P2(I,K))                                PRO 230
      PN(I,K)=ABS(P1(I,K)+PPP(I,K))                                          PRO 240
      PT(I,K)=P1(I,K)                                                        PRO 250
1     CONTINUE                                                               PRO 260
      RETURN                                                                 PRO 270
      END                                                                    PRO 280
```

```
      SUBROUTINE POTR(DIV,N,M)                                          POT  10
C     ************************
      DIMENSION DIV(20,20)                                              POT  20
      DO1 J=1,N                                                         POT  30
      DO11=1,N                                                          POT  40
      DIV(I,J)=DIV(I,J)-4.99                                            POT  50
      DIV(I,J)=DIV(I,J)*7.017                                           POT  60
1     CONTINUE                                                          POT  70
      RETURN                                                            POT  80
      END                                                               POT  90

      SUBROUTINE VEL(PAT,TAT,PS,PT,V,N,M)                               VEL  10
C     ***********************************
      DIMENSION PS(20,20),PT(20,20),V(20,20)                            VEL  20
      TS=TAT+460.0                                                      VEL  30
      DO 1 J=1,M                                                        VEL  40
      DO 1 I=1,N                                                        VEL  50
      RS=PAT-PS(I,J)/144.676                                            VEL  60
      RS=TS/RS                                                          VEL  70
      SX=ABS(PT(I,J)-PS(I,J))                                           VEL  80
      V(I,J)=0.156*SQRT(SX*RS)                                          VEL  90
1     CONTINUE                                                          VEL 100
      RETURN                                                            VEL 110
      END                                                               VEL 120

      SUBROUTINE VELA(V,VA,PITCH,DIV,N,M)                               VEL  10
C     ***********************************
      DIMENSION V(20,20),VA(20,20),PITCH(20,20),DIV(20,20)              VEL  20
      PI=4.0*ATAN(1.0)/180.0                                            VEL  30
      DO 1J=1,M                                                         VEL  40
      DO 11=1,N                                                         VEL  50
      A=PITCH(I,J)*PI                                                   VEL  60
      B=(DIV(I,J)+64.5)*PI                                              VEL  70
      VA(I,J)=V (I,J)*COS(A)*COS(B)                                     VEL  80
1     CONTINUE                                                          VEL  90
      RETURN                                                            VEL 100
      END                                                               VEL 110


      SUBROUTINE LOCAL(PT,PS,P01,P81,CPO,CPS,N,M)                       LOC  10
C     *******************************************
      DIMENSION PT(20,20),PN(20,20),CPO(20,20),CPS(20,20)               LOC  20
      DO 1J=1,N                                                         LOC  30
      DO 11=1,N                                                         LOC  40
      CPO(I,J)=ABS((PT(I,J)-P01)/(P81-P01))                             LOC  50
      CPN(I,J)=ABS((PN(I,J)-P81)/(P81-P01))                             LOC  60
1     CONTINUE                                                          LOC  70
      RETURN                                                            LOC  80
      END                                                               LOC  90


      SUBROUTINE AVRAGE(CPO,CPN,DIV,VA,CPOY, CPOM,CPSY,CPSN,DIVY,DIVM,  AVR  10
C     ****************************************************************
     *VY,VM,N,M)                                                        AVR  20
      DIMENSION CPO(20,20),CPN(20,20),DIV(20,20),VA(20,20),CPOY(20),    AVR  30
     *CPON(20),CPNY(20),CPNN(20),DIVY(20),DIVN(20),VY(20),VN(20)        AVR  40
      DO 2 J=1,M                                                        AVR  50
      CPOY(J)=0.0                                                       AVR  60
      CPNY(J)=0.0                                                       AVR  70
      DIVY(J)=0.0                                                       AVR  80
      VY(J)=0.0                                                         AVR  90
      CPON(J)=0.0                                                       AVR 100
      CPNN(J)=0.0                                                       AVR 110
      DIVN(J)=0.0                                                       AVR 120
      VN(J)=0.0                                                         AVR 130
      DO 11=1,N                                                         AVR 140
```

```
      CPOY(J)=CPOY(J)+CPO(I,J)*VA(I,J)                                  AVR 150
      CPSY(J)=CPSY(J)+CPS(I,J)*VA(I,J)                                  AVR 160
      DIVY(J)=DIVY(J)+DIV(I,J)*VA(I,J)                                  AVR 170
      VY(J)=VY(J)+VA(I,J)                                               AVR 180
      CPOM(J)=CPOM(J)+CPO(I,J)                                          AVR 190
      CPSM(J)=CPSM(J)+CPS(I,J)                                          AVR 200
      DIVM(J)=DIVM(J)+DIV(I,J)                                          AVR 210
      VM(J)=VM(J)+VA(I,J)                                               AVR 220
    1 CONTINUE                                                          AVR 230
      CPOY(J)=CPOY(J)/VY(J)                                             AVR 240
      CPSY(J)=CPSY(J)/VY(J)                                             AVR 250
      DIVY(J)=DIVY(J)/VY(J)                                             AVR 260
      CPOM(J)=CPOM(J)/FLOAT(N)                                          AVR 270
      CPSM(J)=CPSM(J)/FLOAT(N)                                          AVR 280
      DIVM(J)=DIVM(J)/FLOAT(N)                                          AVR 290
      VM(J)=VM(J)/FLOAT(N)                                              AVR 300
    2 CONTINUE                                                          AVR 310
      RETURN                                                            AVR 320
      END                                                               AVR 330


      SUBROUTINE LOSS(PO1,PS1,PT,PS,DIV,VA,R,DR,DPT,DPS,POSM,PSM,YT,N,M) LOS  10
C     ******************************************************************
      DIMENSION PT(20,20),PS(20,20),DIV(20,20),VA(20,20),R(20),DR(20),  LOS  20
     *STRT(20),STRS(20),STRD(20),STRV(20)                               LOS  30
      DO 2J=1,N                                                         LOS  40
      STRT(J)=0.0                                                       LOS  50
      STRS(J)=0.0                                                       LOS  60
      STRD(J)=0.0                                                       LOS  70
      STRV(J)=0.0                                                       LOS  80
      DO 1I=1,N                                                         LOS  90
      STRT(J)=STRT(J)+(PT(I,J)-PO1)*VA(I,J)                             LOS 100
      STRS(J)=STRS(J)+(PS(I,J)-PS1)*VA(I,J)                             LOS 110
      STRD(J)=STRD(J)+DIV(I,J)*VA(I,J)                                  LOS 120
      STRV(J)=STRV(J)+VA(I,J)                                           LOS 130
    1 CONTINUE                                                          LOS 140
      STRT(J)=STRT(J)*R(J)*DR(J)                                        LOS 150
      STRS(J)=STRS(J)*R(J)*DR(J)                                        LOS 160
      STRD(J)=STRD(J)*R(J)*DR(J)                                        LOS 170
      STRV(J)=STRV(J)*R(J)*DR(J)                                        LOS 180
    2 CONTINUE                                                          LOS 190
      A=0.0                                                             LOS 200
      B=0.0                                                             LOS 210
      C=0.0                                                             LOS 220
      D=0.0                                                             LOS 230
      DO 3J=1,N                                                         LOS 240
      A=A+STRT(J)                                                       LOS 250
      B=B+STRS(J)                                                       LOS 260
      C=C+STRD(J)                                                       LOS 270
      D=D+STRV(J)                                                       LOS 280
    3 CONTINUE                                                          LOS 290
      DPT=A/D                                                           LOS 300
      DPS=B/D                                                           LOS 310
      POSM=PO1+DPT                                                      LOS 320
      PSM=PS1+DPS                                                       LOS 330
      YT=DPT/AIM(POSM-PSM)                                              LOS 340
      RETURN                                                            LOS 350
      END                                                               LOS 360


      SUBROUTINE DIMLSN(VM,ZZ,NR)                                       DIM  10
C     ***************************
      DIMENSION VM(NR),ZZ(NR)                                           DIM  20
      DO 1 I=1,NR                                                       DIM  30
      VM(I)=VM(I)/110.0                                                 DIM  40
    1 CONTINUE                                                          DIM  50
      RETURN                                                            DIM  60
      END                                                               DIM  70
```

```
      SUBROUTINE WRITE1(PAT,TAT,NP,NR,PO1,PN1,THETA1,THETA2,Z,P1,P2,      WRI  10
C     ***************************************************************
     *P3,P4,P5,DIV,ZZ)                                                   WRI  20
      DIMENSION THETA1(20),THETA2(20),Z(20),ZZ(20),P1(20,20),P2(20,20),   WRI  30
     *P3(20,20),P4(20,20),P5(20,20),DIV(20,20),TH(20,20)                 WRI  40
      DIMENSION WO(20,20)                                                WRI  50
      DATA I1,I2,I3,I4,I5/1,2,3,4,5                                      WRI  60
      DO 1J=1,NR                                                         WRI  70
    1 ZZ(J)=Z(J)*7.5                                                     WRI  80
      A=-PO1                                                             WRI  90
      B=-PN1                                                             WRI 100
      DO 2J=1,NR                                                         WRI 110
      AA=THETA1(J)                                                       WRI 120
      DO 2I=1,NP                                                         WRI 130
      TH(I,J)=AA                                                         WRI 140
      AA=AA+2.0                                                          WRI 150
    2 CONTINUE                                                           WRI 160
      WRITE(6,11)PAT,TAT,B,A,NP,NR                                       WRI 170
      WRITE(6,22)                                                        WRI 180
      K=NP+1                                                             WRI 190
      WRITE(6,33)(NP,ZZ(J),(TH(I,J),I=1,NP),J=1,NP)                      WRI 200
      DO 10 I=1,NP                                                       WRI 210
      DO 10 J=1,NR                                                       WRI 220
   10 WO(I,J)=-P1(I,J)                                                   WRI 230
      WRITE(6,44) I1                                                     WRI 240
      WRITE(6,55) (NP,(WO(I,J),I=1,NP),J=1,NR)                           WRI 250
      DO 20 I=1,NP                                                       WRI 260
      DO 20 J=1,NR                                                       WRI 270
   20 WO(I,J)=-P2(I,J)                                                   WRI 280
      WRITE(6,44) I2                                                     WRI 290
      WRITE(6,55) (NP,(WO(I,J),I=1,NP),J=1,NR)                           WRI 300
      DO 30 I=1,NP                                                       WRI 310
      DO 30 J=1,NR                                                       WRI 320
   30 WO(I,J)= P3(I,J)                                                   WRI 330
      WRITE(6,44) I3                                                     WRI 340
      WRITE(6,55) (NP,(WO(I,J),I=1,NP),J=1,NR)                           WRI 350
      DO 40 I=1,NP                                                       WRI 360
      DO 40 J=1,NR                                                       WRI 370
   40 WO(I,J)=-P4(I,J)                                                   WRI 380
      WRITE(6,44) I4                                                     WRI 390
      WRITE(6,55) (NP,(WO(I,J),I=1,NP),J=1,NR)                           WRI 400
      DO 50 I=1,NP                                                       WRI 410
      DO 50 J=1,NR                                                       WRI 420
   50 WO(I,J)=-P5(I,J)                                                   WRI 430
      WRITE(6,44) I5                                                     WRI 440
      WRITE(6,55) (NP,(WO(I,J),I=1,NP),J=1,NR)                           WRI 450
      WRITE(6,66)                                                        WRI 460
      WRITE(6,55)(NP,  (DIV(I,J),I=1,NP),J=1,NR)                         WRI 470
      DO 3 K=1,NR                                                        WRI 480
    3 ZZ(K)=ZZ(K)*100.0                                                  WRI 490
   11 FORMAT(1H1///,5X,"EXIT FLOW DATA",5X,50(1H*)//,11X,"TEST NUMBER   WRI 500
     *(I)=",11X,I5(1H-)                                                  WRI 510
     111X,"ATMOSPHERIC PRESSURE.....=",F7.2," INCHES MERCURY"//,         WRI 520
     211X,"ATMOSPHERIC TEMPRATURE.....=",F7.2," DEGREES F"//,            WRI 530
     311X,"INLET STATIC GAUGE PRESSURE.....=",F7.2," MILLIMETERS WATER"  WRI 540
     4//,                                                                WRI 550
     411X,"INLET TOTAL  GAUGE PRESSURE.....=",F7.2," MILLIMETERS WATER"  WRI 560
     4//,                                                                WRI 570
     511X,"NUMBER OF RADIAL LOCATIONS.....=  ",I3,//,                    WRI 580
     611X,"NO. OF DATA POINTS (SAME RADIUS) =  ",I1,/)                   WRI 590
   22 FORMAT(1H1////,33X,"LOCATIONS OF DATA POINTS"/,30X,34(1H*)///,27X, WRI 600
     *"CIRCUMFERENTIAL LOCATIONS  (DEGREES)"/,27X,36(1H-)//,21X,"Z/H",10 WRI 610
     *X,"THETA"//)                                                       WRI 620
   33 FORMAT(20X,F5.3,*(F8.1,2X)//)                                      WRI 630
   44 FORMAT(1H1///,21X,"(P",I1,") IN MILLIMETERS OF WATER",21X,20(1H*)  WRI 640
     *//)                                                                WRI 650
   55 FORMAT(5X,*F9.3,//)                                                WRI 660
   66 FORMAT(1H1///,31X,"YAW ANGLE",/,31X,9(1H*)//)                      WRI 670
      RETURN                                                             WRI 680
      END                                                                WRI 690
```

```
      SUBROUTINE FRAME1                                                 FRA  10
C     *****************
      DIMENSION X(2),Y(2)                                               FRA  20
      N=2                                                               FRA  30
      XL=10.0                                                           FRA  40
      YL=10.0                                                           FRA  50
      XMARG=4.0                                                         FRA  60
      YMARG=4.0                                                         FRA  70
      XNDIV=10.0                                                        FRA  80
      YNDIV=10.0                                                        FRA  90
      HX=0.15                                                           FRA 100
      HY=0.15                                                           FRA 110
      XY=2.0                                                            FRA 120
      YX=0.7                                                            FRA 130
      X2=0.5                                                            FRA 140
      X(1)=0.0                                                          FRA 150
      X(2)=1.0                                                          FRA 160
      Y(1)=0.0                                                          FRA 170
      Y(2)=100.0                                                        FRA 180
      DATA FMTX,FMTY/6H(F5.1),6H(F7.2)/                                 FRA 190
      CALL FACTOR(N,X,Y,XL,YL,XMARG,YMARG)                              FRA 200
      CALL BRAKET(XL,YL,XMARG,YMARG)                                    FRA 210
      CALL DIVIDE(XL,YL,XMARG,YMARG,XNDIV,YNDIV,FMTX,FMTY,HX,HY,        FRA 220
     *XY,YX,X2)                                                         FRA 230
      CALL GRID(X,Y,XNDIV,YNDIV,N)                                      FRA 240
      CALL LETTER(4,0.25,0.0,0.5,0.0,4HCPOY)                            FRA 250
      CALL LETTER(3,0.25,90.0,0.1,7.0,3HZ/H)                            FRA 260
      RETURN                                                            FRA 270
      END                                                               FRA 280
```

```
      SUBROUTINE FRAME2                                                 FRA  10
C     *****************
      DIMENSION X(2),Y(2)                                               FRA  20
      N=2                                                               FRA  30
      XL=10.0                                                           FRA  40
      YL=10.0                                                           FRA  50
      XMARG=4.0                                                         FRA  60
      YMARG=4.0                                                         FRA  70
      XNDIV=5.0                                                         FRA  80
      YNDIV=10.0                                                        FRA  90
      HX=0.15                                                           FRA 100
      HY=0.15                                                           FRA 110
      XY=2.0                                                            FRA 120
      YX=0.7                                                            FRA 130
      X2=0.5                                                            FRA 140
      X(1)=-80.0                                                        FRA 150
      X(2)=10.0                                                         FRA 160
      Y(1)=0.0                                                          FRA 170
      Y(2)=100.0                                                        FRA 180
      DATA FMTX,FMTY/6H(F5.1),6H(F7.2)/                                 FRA 190
      CALL FACTOR(N,X,Y,XL,YL,XMARG,YMARG)                              FRA 200
      CALL BRAKET(XL,YL,XMARG,YMARG)                                    FRA 210
      CALL DIVIDE(XL,YL,XMARG,YMARG,XNDIV,YNDIV,FMTX,FMTY,HX,HY,        FRA 220
     *XY,YX,X2)                                                         FRA 230
      CALL GRID(X,Y,XNDIV,YNDIV,N)                                      FRA 240
      CALL LETTER(4,0.25,0.0,0.5,0.0,4HD1VY)                            FRA 250
      CALL LETTER(3,0.25,90.0,0.1,7.0,3HZ/H)                            FRA 260
      RETURN                                                            FRA 270
      END                                                               FRA 280
```

```
      SUBROUTINE FRAME0                                                 FRA  10
C     ****************
      DIMENSION X(2),Y(2)                                               FRA  20
      N=2                                                               FRA  30
      XL=10.0                                                           FRA  40
      YL=10.0                                                           FRA  50
      XMARG=4.0                                                         FRA  60
      YMARG=4.0                                                         FRA  70
      XNDIV=10.0                                                        FRA  80
      YNDIV=10.0                                                        FRA  90
      HX=0.15                                                           FRA 100
      HY=0.15                                                           FRA 110
      XY=2.0                                                            FRA 120
      YX=0.7                                                            FRA 130
      X2=0.5                                                            FRA 140
      X(1)=0.0                                                          FRA 150
      X(2)=1.0                                                          FRA 160
      Y(1)=0.0                                                          FRA 170
      Y(2)=100.0                                                        FRA 180
      DATA FMTX,FMTY/6H(F5.1),6H(F7.2)/                                 FRA 190
      CALL FACTOR(N,X,Y,XL,YL,XMARG,YMARG)                              FRA 200
      CALL BRAKET(XL,YL,XMARG,YMARG)                                    FRA 210
      CALL DIVIDE(XL,YL,XMARG,YMARG,XNDIV,YNDIV,FMTX,FMTY,HX,HY,        FRA 220
     *XY,YX,X2)                                                         FRA 230
      CALL GRIDC(X,Y,XNDIV,YNDIV,N)                                     FRA 240
      CALL LETTER(2,0.25,0.0,6.5,0.0,2HVM)                              FRA 250
      CALL LETTER(0,0.25,90.0,0.1,7.0,3HZ/H)                            FRA 260
      RETURN                                                            FRA 270
      END                                                               FRA 280
```

```
      SUBROUTINE FRAME4                                                 FRA  10
C     ****************
      DIMENSION X(2),Y(2)                                               FRA  20
      N=2                                                               FRA  30
      XL=24.0                                                           FRA  40
      YL=20.0                                                           FRA  50
      XMARG=10.0                                                        FRA  60
      YMARG=5.0                                                         FRA  70
      XNDIV=8.0                                                         FRA  80
      YNDIV=10.0                                                        FRA  90
      HX=0.2                                                            FRA 100
      HY=0.2                                                            FRA 110
      XY=0.0                                                            FRA 120
      YX=4.5                                                            FRA 130
      X2=0.5                                                            FRA 140
     /X(1)=-0.0                                                         FRA 150
      X(2)=8.0                                                          FRA 160
      Y(1)=0.0                                                          FRA 170
      Y(2)=10.0                                                         FRA 180
      DATA FMTX,FMTY/6H(F5.1),6H(F7.2)/                                 FRA 190
      CALL FACTOR(N,X,Y,XL,YL,XMARG,YMARG)                              FRA 200
      CALL BRAKET(XL,YL,XMARG,YMARG)                                    FRA 210
      CALL DIVIDE(XL,YL,XMARG,YMARG,XNDIV,YNDIV,FMTX,FMTY,HX,HY,        FRA 220
     *XY,YX,X2)                                                         FRA 230
      RETURN                                                            FRA 240
      END                                                               FRA 250
```

```
      SUBROUTINE GRAFN(X,Y,N,NN,N)                                      GRA  10
C     ****************************
      DIMENSION X(N),Y(N)                                               GRA  20
      DO 1 I=1,N                                                        GRA  30
      CALL UNITTO (X(I),Y(I),XX,YY)                                     GRA  40
1     CALL GRAF(XX,YY,N,NN)                                             GRA  50
      RETURN                                                            GRA  60
      END                                                               GRA  70
```

```
      SUBROUTINE CURVE(X,Y,M)                                          CUR  10
C     **********************
      DIMENSION X(M),Y(M)                                              CUR  20
      MM=M-1                                                           CUR  30
      X1=X(1)                                                          CUR  40
      Y1=Y(1)                                                          CUR  50
      CALL UNITTO(X1,Y1,XX,YY)                                         CUR  60
      CALL PLOT(XX,YY,3)                                               CUR  70
      DO 1 I=1,MM                                                      CUR  80
      CALL UNITTO (X(I+1),Y(I+1),XM,YM)                                CUR  90
      CALL PLOT(XM,YM,2)                                               CUR 100
1     CONTINUE                                                         CUR 110
      RETURN                                                           CUR 120
      END                                                              CUR 130
```

```
      SUBROUTINE WRITE2(V,VA,PITCH,DIV,CPO,CPS,NP,NR)                  WRI  10
C     ***********************************************
      DIMENSION V(20,20),VA(20,20),PITCH(20,20),DIV(20,20),CPO(20,20),  WRI  20
     *CPS(20,20)                                                       WRI  30
      DIMENSION WO(20,20)                                              WRI  40
      WRITE(6,11)                                                      WRI  50
      WRITE(6,22) (NP, (PITCH(I,J),I=1,NP ),J=1,NR)                    WRI  60
      DO 10 I=1,NP                                                     WRI  70
      DO 10 J=1,NR                                                     WRI  80
10    WO(I,J)=V(I,J)*.3048                                             WRI  90
      WRITE(6,12)                                                      WRI 100
      WRITE(6,22)(NP,(WO(I,J),I=1,NP),J=1,NR)                          WRI 110
      DO 20 I=1,NP                                                     WRI 120
      DO 20 J=1,NR                                                     WRI 130
20    WO(I,J)=VA(I,J)*.3048                                            WRI 140
      WRITE(6,13)                                                      WRI 150
      WRITE(6,22)(NP,(WO(I,J),I=1,NP),J=1,NR)                          WRI 160
      WRITE(6,14)                                                      WRI 170
      WRITE(6,22) (NP, (  CPO(I,J),I=1,NP ),J=1,NR)                    WRI 180
      WRITE(6,15)                                                      WRI 190
      WRITE(6,22) (NP, (  CPS(I,J),I=1,NP ),J=1,NR)                    WRI 200
11    FORMAT(1H1///,30X,"PITCH ANGLE"/,30X,11(1H*)//)                  WRI 210
12    FORMAT(1H1///,29X,"VELOCITY (M/SEC)"/,29X,15(1H*)//)             WRI 220
13    FORMAT(1H1///,25X,"AXIAL VELOCITY (M/SEC)"/,25X,15(1H*)//)       WRI 230
14    FORMAT(1H1////,17X,"TOTAL PRESSURE LOSS COEFFICIENT (CPO)"/,17X,  WRI 240
     *37(1H*)//)                                                       WRI 250
15    FORMAT(1H1////,19X,"STATIC PRESSURE COEFFICIENT (CPS)"/,19X,30(1H* WRI 260
     *)//)                                                             WRI 270
22    FORMAT(5X,*F9.3,//)                                              WRI 280
      RETURN                                                           WRI 290
      END                                                              WRI 300
```

```
      SUBROUTINE WRITE3(CPOY,CPOM,CPSY,CPSM,DIVY,DIVM,VY,VM,NP,NR)     WRI  10
C     ************************************************************
      DIMENSION CPOY(20),CPOM(20),CPSY(20),CPSM(20),DIVY(20),          WRI  20
     *DIVM(20),VY(20),VM(20)                                           WRI  30
      WRITE(6,11)                                                      WRI  40
      DO 10 I=1,NR                                                     WRI  50
      WRITE(6,22)(CPOY(I),CPOM(I),CPSY(I),CPSM(I),DIVY(I),DIVM(I),VY(I), WRI  60
     *VM(I))                                                           WRI  70
                                                                       WRI  80
10    CONTINUE                                                         WRI  90
11    FORMAT(1H1////,21X,"PITCHWISE AVERAGED PARAMETERS"/,21X,29(1H*)//, WRI 100
     *3X,"CPOY",5X"CPOM",5X,"CPSY",5X,"CPSM",5X,"DIVY",5X,"DIVM",5X,6X, WRI 110
     *"VY",7X,"VM",//)                                                 WRI 120
22    FORMAT(5X,8F9.3,//)                                              WRI 130
      RETURN                                                           WRI 140
      END
```

```
      SUBROUTINE WRITE4(DPT,DPS,P20M,P2M,YT,NR)                          WRI  10
C     ******************************************
      WRITE(6,22)DPT,DPS,P20M,P2M,YT                                     WRI  20
22    FORMAT(1H1///,5X,"DPT = ",F9.3//5X,"DPS = ",F8.3//,5X,"P20M= ",F8.3,/ WRI  30
     *,5X,"PIM = ",F8.3,//,5X,"YT  ",F8.3)                               WRI  40
      RETURN                                                             WRI  50
      END                                                                WRI  60


      SUBROUTINE DART(THETA1,R,V,DIV,PITCH,NP,NR,SCALE)                  DAR  10
C     *************************************************
      DIMENSION THETA1(20),R(20),V(20,20),DIV(20,20),PITCH(20,20)        DAR  20
      XR=6.9529                                                          DAR  30
      YR=14.266                                                          DAR  40
      PI=4.0*ATAN(1.0)/180.0                                             DAR  50
      E=64.5*PI                                                          DAR  60
      DO 1 J=1,NR                                                        DAR  70
      AA=THETA1(J)                                                       DAR  80
      DO 1 I=1,NP                                                        DAR  90
      A=AA*PI                                                            DAR 100
      B=DIV(I,J)*PI                                                      DAR 110
      DP=4.82+((R(J)-15.00)/7.5)*2.58                                    DAR 120
      C=(PITCH(I,J)+DP)*PI                                               DAR 130
      XX=R(J)*SIN(A)                                                     DAR 140
      YY=R(J)*COS(A)-YR                                                  DAR 150
      VR=V(I,J)*SIN(C)                                                   DAR 160
      VT=V(I,J)*COS(C)*SIN(B)/COS(E)                                     DAR 170
      DX=(VT*COS(A)-VR*SIN(A))*SCALE                                     DAR 180
      DY=(-VR*COS(A)-VT*SIN(A))*SCALE                                    DAR 190
      AA=AA+2.0                                                          DAR 200
      VX=XX+DX                                                           DAR 210
      VY=YY+DY                                                           DAR 220
      CALL UNITTO(XX,YY,XXX,YYY)                                         DAR 230
      CALL UNITTO(VX,VY,VXX,VYY)                                         DAR 240
      IF(XXX.EQ.VXX.AND.YYY.EQ.VYY)GOTO 1                                DAR 250
      CALL ARROW(XXX,YYY,VXX,VYY,3)                                      DAR 260
1     CONTINUE                                                           DAR 270
      RETURN                                                             DAR 280
      END                                                                DAR 290


      SUBROUTINE BRAKET(XL,YL,XMARG,YMARG)                               BRA  10
C     ************************************
      CALL PLOT(XMARG,YMARG,3)                                           BRA  20
      CALL PLOT(XL,YMARG,2)                                              BRA  30
      CALL PLOT(XL,YL,1)                                                 BRA  40
      CALL PLOT(XMARG,YL,1)                                              BRA  50
      CALL PLOT(XMARG,YMARG,1)                                           BRA  60
      CALL PLOT(XMARG,YMARG,3)                                           BRA  70
      RETURN                                                             BRA  80
      END                                                                BRA  90


      SUBROUTINE DIVIDE(XL,YL,XMARG,YMARG,XNDIV,YNDIV,FMTX,FMTY,HX,HY,   DIV  10
C     ***************************************************************
     *XY,YX,X2)                                                          DIV  20
      YSTEP=(YL-YMARG)/YNDIV                                             DIV  30
      XOR=XMARG                                                          DIV  40
      YOR=YMARG                                                          DIV  50
      NDIVX=IFIX(XNDIV)+1                                                DIV  60
      NDIVY=IFIX(YNDIV)+1                                                DIV  70
      DO 10 KY=1,NDIVY                                                   DIV  80
      CALL PLOT(XOR,YOR,3)                                               DIV  90
      CALL PLOT(XOR+0.1,YOR,2)                                           DIV 100
      CALL PLOT(XL-0.1,YOR,3)                                            DIV 110
      CALL PLOT(XL,YOR,2)                                                DIV 120
      CALL INCHTO(XMARG,YOR,XP,YP)                                       DIV 130
      ENCODE(10,FMTY,YD)YP                                               DIV 140
      CALL LETTER(10,HY,0.0,XY,YOR-HY/2.0,YD)                            DIV 150
      YOR=YOR+YSTEP                                                      DIV 160
10    CONTINUE                                                           DIV 170
```

```
      XSTEP=(XL-XMARG)/XNDIV                                          DIV 180
      DO 20 KK=1,NDIVX                                                DIV 190
      CALL PLOT(XOR,YMARG,3)                                          DIV 200
      CALL PLOT(XOR,YMARG+0.1,2)                                      DIV 210
      CALL PLOT(XOR,YL-0.1,3)                                         DIV 220
      CALL PLOT(XOR,YL,2)                                             DIV 230
      CALL INCHTO(XOR,YMARG,XH,YH)                                    DIV 240
      ENCODE(10,FMTX,KD)XH                                            DIV 250
      CALL LETTER(10,HX,0.0,XOR-X2,YX,KD)                             DIV 260
      XOR=XOR+XSTEP                                                   DIV 270
20    CONTINUE                                                        DIV 280
      RETURN                                                          DIV 290
      END                                                             DIV 300


      SUBROUTINE UNTAR(X,Y,WORK1,WORK2,M)                             UNT  10
C     **********************************
      DIMENSION X(M),Y(M),WORK1(M),WORK2(M)                           UNT  20
      DO 1 I=1,M                                                      UNT  30
1     CALL UNITTO(X(I),Y(I),WORK1(I),WORK2(I))                        UNT  40
      CALL PLOT(WORK1(1),WORK2(1),3)                                  UNT  50
      RETURN                                                          UNT  60
      END                                                             UNT  70


      SUBROUTINE STLIN(X1,Z1,X2,Z2)
C     *****************************                                   STL  10
      CALL UNITTO(X1,Z1,XX,ZZ)
      CALL PLOT(XX,ZZ,3)                                              STL  20
      CALL UNITTO(X2,Z2,XM,ZM)                                        STL  30
      CALL PLOT(XM,ZM,3)                                              STL  40
      RETURN                                                          STL  50
      END                                                             STL  60
                                                                      STL  70


      SUBROUTINE GRID(X,Y,XNDIV,YNDIV,M)                              GRI  10
C     **********************************
      DIMENSION X(M),Y(M)                                             GRI  20
      DELX=(X(2)-X(1))/(XNDIV*2.0)                                    GRI  30
      DELY=(Y(2)-Y(1))/(YNDIV*2.0)                                    GRI  40
      NN=IFIX(XNDIV)*2-1                                              GRI  50
      MM=IFIX(YNDIV)*2-1                                              GRI  60
      XX=X(1)                                                         GRI  70
      YY=Y(1)                                                         GRI  80
      DO 1 I=1,NN                                                     GRI  90
      XX=XX+DELX                                                      GRI 100
1     CALL STLIN(XX,Y(1),XX,Y(2))                                     GRI 110
      DO 2 I=1,MM                                                     GRI 120
      YY=YY+DELY                                                      GRI 130
2     CALL STLIN(X(1),YY,X(2),YY)                                     GRI 140
      RETURN                                                          GRI 150
      END                                                             GRI 160
```

EXIT FLOW DATA

TEST NUMBER (1)

ATMOSPHERIC PRESSURE.....= 29.94 INCHES MERCURY
ATMOSPHERIC TEMPRATURE.....= 82.00 DEGREES F
INLET STATIC GAUGE PRESSURE.....= -89.67 MILLIMETERS WATER
INLET TOTAL GAUGE PRESSURE.....= -13.43 MILLIMETERS WATER
NUMBER OF RADIAL LOCATIONS.....= 16
NO. OF DATA POINTS (SAME RADIUS) = 3

LOCATIONS OF DATA POINTS

CIRCUMFERENTIAL LOCATIONS (DEGREES)

Z/H	THETA							
.967	-8.0	-6.0	-4.0	-2.0	0.0	2.0	4.0	6.0
.933	-8.0	-6.0	-4.0	-2.0	0.0	2.0	4.0	6.0
.867	-6.0	-4.0	-2.0	0.0	2.0	4.0	6.0	8.0
.800	-6.0	-4.0	-2.0	0.0	2.0	4.0	6.0	8.0
.733	-6.0	-4.0	-2.0	0.0	2.0	4.0	6.0	8.0
.667	-4.0	-2.0	0.0	2.0	4.0	6.0	8.0	10.0
.600	-4.0	-2.0	0.0	2.0	4.0	6.0	8.0	10.0
.533	-4.0	-2.0	0.0	2.0	4.0	6.0	8.0	10.0
.467	-4.0	-2.0	0.0	2.0	4.0	6.0	8.0	10.0
.400	-2.0	0.0	2.0	4.0	6.0	8.0	10.0	12.0
.333	-2.0	0.0	2.0	4.0	6.0	8.0	10.0	12.0
.267	-2.0	0.0	2.0	4.0	6.0	8.0	10.0	12.0
.200	0.0	2.0	4.0	6.0	8.0	10.0	12.0	14.0
.133	0.0	2.0	4.0	6.0	8.0	10.0	12.0	14.0
.067	2.0	4.0	6.0	8.0	10.0	12.0	14.0	16.0
.033	2.0	4.0	6.0	8.0	10.0	12.0	14.0	16.0

(24) IN MILLIMETERS OF WATER

-19.715	-24.715	-17.715	-19.000	-20.715	-20.000	-20.858	-25.572
-31.715	-19.143	-20.000	-21.143	-22.572	-24.429	-24.286	-37.144
-26.858	-25.143	-19.572	-18.000	-23.000	-24.715	-26.001	-35.144
-22.715	-25.715	-18.858	-27.429	-42.715	-41.429	-30.715	-33.572
-21.000	-27.429	-56.144	-70.716	-65.144	-42.001	-32.572	-43.287
-22.000	-50.001	-67.144	-72.573	-60.001	-43.429	-38.572	-49.715
-32.572	-46.572	-63.716	-57.144	-51.430	-50.001	-37.429	-37.429
-42.001	-36.572	-59.144	-62.287	-72.859	-60.001	-35.429	-33.715
-33.001	-39.429	-49.144	-57.715	-47.144	-31.429	-29.429	-29.715
-25.001	-24.572	-25.715	-28.001	-22.858	-21.143	-25.143	-32.858
-22.572	-24.572	-19.143	-15.429	-15.715	-21.429	-24.000	-30.858
-22.572	-16.857	-12.286	-15.429	-20.000	-21.715	-25.143	-31.143
-22.858	-19.143	-13.143	-16.000	-18.286	-18.572	-19.715	-31.715
-23.143	-15.143	-12.286	-14.001	-15.429	-15.715	-25.429	-26.286
-34.858	-20.572	-12.857	-11.143	-11.715	-12.286	-15.429	-33.429
-52.858	-40.001	-23.143	-15.429	-12.286	-11.715	-15.715	-45.858

(22) IN MILLIMETERS OF WATER

-113.717	-113.717	-113.459	-113.717	-114.431	-116.145	-119.574	-122.288
-113.459	-112.574	-110.288	-116.717	-118.431	-119.002	-119.288	-119.288
-117.359	-112.717	-111.459	-111.288	-113.002	-119.431	-119.288	-119.145
-117.145	-115.574	-110.288	-114.361	-121.959	-125.145	-121.717	-121.145
-114.288	-116.459	-125.288	-130.288	-135.288	-123.861	-115.288	-117.431
-115.431	-121.431	-133.431	-135.717	-121.717	-121.145	-113.431	-114.002
-117.145	-118.359	-126.574	-123.431	-133.717	-114.859	-113.431	-112.002
-119.002	-121.717	-127.431	-141.145	-139.145	-121.431	-109.431	-106.574
-122.574	-129.431	-130.717	-132.002	-118.574	-106.288	-107.145	-112.288
-115.431	-124.002	-124.359	-121.145	-116.002	-111.145	-108.859	-113.431
-113.431	-119.145	-123.717	-122.859	-121.002	-116.574	-111.431	-112.002
-116.002	-123.717	-124.002	-123.859	-114.859	-113.145	-114.716	-116.288
-117.431	-123.145	-124.002	-121.859	-118.288	-114.288	-119.716	-117.717
-118.288	-119.431	-119.002	-115.431	-112.288	-106.574	-111.002	-111.574
-112.574	-113.145	-111.002	-108.288	-107.431	-106.002	-110.574	-107.145
-119.002	-117.145	-115.145	-111.717	-109.716	-108.002	-109.002	-112.288

(ZI) IN MILLIMETERS OF WATER

-115.812	-11-.+31	-112.-31	-117.-31	-117.863	-117.361	-117.145	-121.284
-116.717	-113.182	-117.1+5	-119.112	-119.717	-120.+31	-120.361	-121.145
-113.-7+	-115.-31	-112.1-5	-113.859	-117.717	-116.284	-121.1-5	-123.112
-113.361	-117.182	-11-.284	-115.1-5	-121.57+	-12-.-31	-125.361	-119.361
-114.-31	-11-.-31	-122.717	-126.-31	-13-.717	-129.1-5	-11-.57+	-113.717
-115.284	-122.812	-131.57+	-143.717	-131.-31	-121.1-5	-112.57+	-115.112
-118.284	-122.57-	-123.717	-12-.461	-128.288	-116.384	-117.-31	-112.859
-118.57-	-121.717	-123.57-	-131.57-	-1-1.1+3	-117.-31	-1-+.312	-107.71+
-123.868	-131.103	-1+2.283	-131.361	-117.1+5	-114.112	-115.57+	-112.859
-11+.57-	-122.57+	-124.284	-124.57-	-117.1+5	-111.-31	-119.-31	-113.717
-11-.312	-119.145	-126.57+	-12-.361	-114.717	-115.717	-11-.284	-112.57-
-115.234	-12-.284	-12-.112	-121.1-5	-115.284	-112.112	-111.-31	-115.717
-117.717	-123.-31	-123.-31	-12-.57+	-121.57+	-116.284	-119.1+5	-113.717
-115.717	-121.57-	-126.112	-11-.859	-113.57+	-107.-31	-111.1-5	-111.1+5
-11-.312	-112.859	-111.717	-114.-31	-105.716	-115.-31	-105.145	-107.143
-117.-31	-118.57-	-115.-31	-112.112	-113.512	-119.1+5	-109.716	-111.717

(P_w) IN MILLIMETERS OF WATER

-51.858	-52.572	-53.287	-53.858	-53.430	-51.572	-50.351	-55.144
-57.858	-52.287	-56.715	-55.301	-55.287	-53.144	-51.287	-61.573
-53.287	-53.430	-55.858	-56.144	-56.715	-54.715	-50.572	-57.573
-47.144	-53.287	-57.573	-63.287	-71.144	-76.144	-52.715	-54.573
-55.287	-65.287	-94.859	-101.287	-42.859	-55.301	-50.572	-73.430
-58.858	-85.716	-108.002	-103.430	-42.287	-61.715	-61.430	-83.430
-68.287	-81.716	-98.859	-80.002	-74.859	-76.002	-62.287	-76.002
-74.859	-66.573	-86.573	-81.144	-87.430	-85.287	-82.287	-75.430
-57.144	-62.573	-75.716	-85.430	-85.859	-74.859	-71.859	-65.573
-67.144	-73.715	-70.573	-58.287	-59.144	-61.301	-68.301	-67.716
-58.573	-61.858	-67.430	-67.144	-68.858	-57.715	-70.573	-71.287
-62.001	-69.429	-61.287	-69.144	-64.858	-62.858	-71.287	-65.430
-51.430	-51.001	-58.001	-66.001	-52.572	-57.144	-65.430	-59.144
-55.144	-62.001	-68.287	-65.715	-51.144	-57.144	-64.301	-57.430
-68.001	-69.715	-55.572	-53.429	-61.715	-66.301	-68.301	-61.858
-69.716	-53.431	-69.144	-59.144	-57.715	-58.858	-61.429	-63.144

[PSI] IN MILLIMETERS OF WATER

-36.881	-45.858	-52.144	-33.429	-34.715	-37.881	-58.286	-41.144
-49.715	-31.572	-31.143	-30.572	-35.429	-38.858	-43.429	-56.287
-46.858	-38.144	-28.429	-30.881	-36.429	-41.858	-43.001	-57.287
-47.431	-42.858	-25.001	-40.001	-56.430	-63.431	-57.858	-59.715
-35.429	-38.858	-52.144	-45.287	-38.859	-71.859	-59.001	-52.858
-35.429	-53.144	-70.859	-53.287	-41.144	-66.287	-60.001	-59.144
-44.858	-55.431	-72.287	-72.001	-68.859	-61.431	-44.858	-48.858
-54.858	-53.144	-76.859	-60.429	-44.573	-54.001	-38.715	-42.001
-58.144	-61.144	-72.859	-68.001	-54.287	-33.715	-35.858	-47.715
-43.429	-48.573	-50.572	-41.715	-34.858	-30.286	-32.286	-47.431
-36.001	-47.429	-41.715	-34.001	-31.429	-32.858	-31.143	-42.572
-38.858	-39.715	-36.001	-32.572	-32.001	-28.572	-34.286	-44.287
-45.858	-42.858	-39.144	-33.715	-32.001	-28.572	-26.001	-46.001
-43.715	-41.429	-34.286	-29.143	-26.001	-24.000	-26.858	-42.572
-52.287	-43.715	-36.572	-31.001	-25.572	-24.858	-25.715	-46.287
-53.287	-52.287	-44.572	-37.715	-32.001	-28.858	-34.001	-51.715

YAW ANGLE

.878	-3.173	-3.573	-.659	1.683	2.258	2.551	1.537
1.-53	-.878	-.235	1.683	2.788	2.789	1.244	-2.415
5.-83	1.612	1.611	2.781	-.682	-.683	1.756	.585
5.3-1	2.7[illegible]	2.707	6.111	8.454	6.219	3.268	.732
-.585	2.415	6.512	-.467	.732	-.756	-.146	.585
-6.[illegible]	-3.732	-8.732	-[illegible].512	-13.683	-14.3-1	-3.073	-1.171
-7.982	-8.927	-[illegible].927	-[illegible].197	-27.-39	-[illegible].391	-8.-39	-4.3-1
-5.293	-7.12-	-11.95-	-15.351	-11.258	-.756	-3.415	-6.658
-3.1-5	1.-53	6.293	11.787	5.854	1.683	-.585	-1.[illegible]
-.512	5.-88	11.[illegible]	11.402	7.12-	3.512	1.366	2.317
2.3-1	3.-39	-.2--	-.402	-.293	2.-13	.512	1.[illegible]
3.195	2.122	3.111	2.45-	2.122	1.[illegible]	.293	-.1-5
2.781	1.976	3.366	-.[illegible]	3.512	2.707	1.-63	1.111
2.733	3.512	5.-13	5.65-	-.-63	2.3-1	1.[illegible]	-.[illegible]
3.6[illegible]	2.927	5.63-	7.2--	6.732	5.561	-.[illegible]	2.781
-.643	2.-85	5.195	7.611	7.-53	6.21[illegible]	5.65-	3.366

238

PITCH ANGLE

-5.7--	-2.081	-7.811	-7.-5*	-6.696	-5.430	-4.353	-5.-6*
-3.153	-9.-30	-11.*36	-6.-95	-8.239	-5.503	-2.195	-.65*
-1.363	-11.187	-13.-7*	-11.007	-4.75-	-4.983	.427	1.830
2.1-6	47.391	-1-.737	-11.293	-7.663	1.576	-.723	-.82-
-8.375	-13.95*	-1-.245	-11.953	6.187	11.114	6.5-6	-1-.27-
-11.*44	-21.277	-26.-7*	-15.36-	1.203	-.433	1.152	-1-.-6-
-12.--*	-16.77-	-12.825	-3.661	-2.21-	-3.71-	-27.281	-15.79*
-11.732	-6.158	-.737	3.-1-	-3.191	-2-.649	-27.77*	-21.-1*
-.153	1.212	.31-	-11.2-3	-21.277	-25.-31	-21.356	-6.151
-11.33*	-.596	.262	-7.231	-11.6-*	-15.132	-1-.836	-11.1-1
-15.528	-7.57-	-.7--	-3.23-	-5.661	-11.65-	-13.7-*	-1-.695
-13.929	-.686	.163	-1.946	-12.15-	-17.337	-19.731	-4.-41
-9.341	-1.-67	1.116	-2.912	-3.716	-13.5--	-23.395	-12.715
-4.151	1.727	-.45-	-5.-61	-11.5-7	-15.435	-1-.673	-7.1-9
-3.251	.926	.377	-2.---	-6.185	-4.139	-11.1-8	-8.2**
.92--	3.796	3.617	1.263	-.951	-3.511	-2.581	.91-

VELOCITY (M/SEC)
****

-3.731	38.127	-1.378	+1.214	-3.662	-1.155	-1.355	-1.135
37.582	-1.279	-2.139	-1.583	-1.391	+1.724	-1.334	37.137
38.-13	38.86-	-1.5-3	-1.-02	-3.756	-1.132	38.711	37.103
38.3--	40.153	-1.53-	-1.35-	37.525	37.565	38.998	36.251
-1.169	-1.991	3-.-15	3-.141	3-.222	36.46-	37.107	34.246
-1.365	37.659	36.66-	3-.474	3-.412	3-.13-	35.53-	35.2--
37.596	37.289	3-.765	35.757	35.197	3-.253	3-.571	37.-63
37.-17	38.697	3-.149	3-.791	3-.-31	35.143	38.755	3-.111
38.623	36.982	37.-61	3-.77-	37.633	38.371	38.132	34.171
-3.61-	-1.113	-1.21-	-1.639	-1.755	-1.31-	-1.553	34.-17
-1.756	-1.182	-1.177	-3.143	-2.412	-1.4-7	-1.37	34.32-
-1.337	-2.029	-3.31-	-3.137	-2.765	-2.121	-1.75-	34.1--
-1.383	-2.13-	-3.331	-1.877	-2.-61	-2.324	-2.12-	34.124
-3.617	-1.913	-2.-.4	-3.264	-2.197	-1.745	38.971	34.62-
36.563	38.52-	-1.-7-	-1.357	-1.111	-1.96-	-1.378	36.249
38.265	39.93-	34.237	-1.242	-3.713	-1.719	38.72-	37.224

RADIAL VELOCITY (M/SEC)

16.752	18.224	19.603	18.614	16.314	16.111	16.177	16.631
15.241	14.192	17.944	20.252	19.921	19.046	16.561	17.344
13.483	15.795	16.361	15.063	14.134	14.765	15.249	15.532
13.721	15.426	15.375	15.429	12.454	12.394	15.331	15.464
14.321	15.594	11.316	12.179	14.256	14.327	15.446	14.436
21.211	17.124	18.377	23.134	24.682	23.144	16.293	15.192
21.266	21.154	24.548	24.749	24.166	23.427	19.615	21.187
19.341	21.683	21.242	24.147	21.414	16.181	16.797	19.371
19.934	15.476	12.454	9.029	11.146	14.159	16.131	17.295
17.423	14.164	11.119	14.141	12.451	14.433	15.542	15.441
15.744	15.265	15.249	15.117	15.551	16.171	16.514	15.507
16.457	16.924	16.451	16.564	16.452	16.573	16.333	16.714
15.741	16.411	16.278	15.425	15.677	15.541	16.143	16.291
15.642	15.681	14.361	14.372	14.441	15.773	15.795	16.443
13.472	15.171	13.781	13.742	13.119	13.413	14.461	17.447
11.795	14.117	13.536	13.371	12.511	13.421	13.347	12.513

TOTAL PRESSURE LOSS COEFFICIENT (CPD)

.382	.230	.056	.060	.096	.086	.097	.159
.240	.052	.086	.101	.120	.144	.142	.311
.176	.154	.081	.060	.126	.148	.155	.285
.122	.161	.071	.184	.384	.367	.227	.264
.335	.184	.560	.751	.678	.375	.251	.392
.112	.480	.735	.776	.611	.393	.330	.476
.251	.435	.661	.573	.494	.480	.315	.315
.375	.304	.600	.641	.779	.611	.233	.266
.217	.341	.468	.581	.442	.235	.210	.214
.165	.146	.161	.191	.124	.101	.154	.255
.120	.146	.075	.126	.080	.105	.139	.229
.120	.045	.015	.026	.046	.109	.154	.232
.124	.075	.054	.034	.064	.067	.042	.240
.127	.022	.015	.007	.026	.031	.157	.169
.241	.094	.008	.033	.023	.015	.026	.262
.517	.349	.127	.026	.015	.023	.030	.434

STATIC PRESSURE COEFFICIENT (CPS)
****

-.367	-.326	-.381	-.375	-.375	-.391	-.421	-.468
-.334	-.381	-.460	-.439	-.445	-.427	-.402	-.374
-.373	-.384	-.416	-.387	-.396	-.425	-.385	-.373
-.351	-.409	-.409	-.481	-.473	-.459	-.434	-.397
-.398	-.487	-.608	-.653	-.585	-.426	-.317	-.405
-.436	-.575	-.743	-.704	-.557	-.398	-.308	-.437
-.464	-.510	-.534	-.540	-.457	-.389	-.350	-.420
-.458	-.452	-.498	-.664	-.595	-.568	-.451	-.384
-.432	-.516	-.576	-.628	-.587	-.435	-.395	-.336
-.440	-.454	-.514	-.469	-.449	-.422	-.426	-.397
-.469	-.447	-.451	-.459	-.454	-.460	-.459	-.425
-.442	-.451	-.455	-.466	-.474	-.474	-.439	-.412
-.443	-.448	-.442	-.456	-.452	-.453	-.455	-.419
-.433	-.392	-.377	-.390	-.404	-.392	-.394	-.324
-.316	-.303	-.262	-.263	-.238	-.295	-.289	-.282
-.359	-.348	-.320	-.283	-.258	-.262	-.253	-.294

PITCHWISE AVERAGED PARAMETERS

CPCY	CPOM	CPSY	CPS1	DIVY	DIVM	VY	VM
.10-	.105	.387	.394	.126	.265	+52.179	.--87
.1+9	.151	.--39	.--83	.7--	.796	+37.361	.+7-
.1+9	.149	.393	.393	2.736	2.999	339.+-6	.+30
.2--	.223	.--26	.+23	-.350	-.35-	369.040	.394
.38-	.--10	.+7-	.--95	.670	1.125	334.--52	.+25
.492	.+85	.52+	.519	-10.552	-9.530	525.6+9	.566
.455	.---3	.--71	.--66	-17.--87	-16.706	607.327	.65-
.+90	.+83	.528	.522	-8.871	-9.--51	514.--40	.55-
.310	.339	.46-	.--92	1.911	3.073	373.314	.--02
.162	.152	.---3	.---6	-.266	-.902	366.358	.39-
.109	.109	.453	.+53	2.05-	2.893	410.605	.+-2
.098	.098	.--51	.+51	1.692	1.692	+34.263	.--63
.087	.066	.---6	.---6	2.--70	2.+94	421.7-7	.--5-
.072	.069	.331	.332	2.339	3.391	+35.215	.+37
.093	.392	.286	.285	4.541	-.747	363.352	.392
.187	.191	.299	.299	5.331	5.361	340.351	.366

DPT = 18.895
DPS = 33.552
P2OM= 32.325
PIM = 123.222
YT = .2 8